DEVELOPMENT OF PEPTIDE-MODIFIED GEMINI SURFACTANTS AS NON-VIRAL GENE DELIVERY SYSTEM

A Thesis Submitted to

the College of Graduate and Postdoctoral Studies

in Partial Fulfillment of the Requirements

for the Degree of Doctor of Philosophy

in the College of Pharmacy and Nutrition

University of Saskatchewan

Saskatoon, Saskatchewan

By

Mays Al-Dulaymi

PERMISION TO USE

In presenting this thesis/dissertation in partial fulfillment of the requirements for a postgraduate degree from the University of Saskatchewan, I agree that the Libraries of this University may make it freely available for inspection. I further agree that permission for copying of this thesis/dissertation in any manner, in whole or in part, for scholarly purposes may be granted by the professors who supervised my thesis/dissertation work (Drs. I. Badea or A. El-Aneed) or, in their absence, by the Head of the Department or the Dean of the College in which my thesis work was done. It is understood that any copying or publication or use of this thesis/dissertation or parts thereof for financial gain shall not be allowed without my written permission. It is also understood that due recognition shall be given to me and to the University of Saskatchewan in any scholarly use which may be made of any material in my thesis/dissertation.

Requests for permission to copy or to make other uses of materials in this thesis/dissertation in whole or part should be addressed to:

Dean of the College of Pharmacy and Nutrition
University of Saskatchewan
Saskatoon, Saskatchewan S7N 4L3
Canada

OR

Dean of the College of Graduate and Postdoctoral Studies
University of Saskatchewan
Room 116 Thorvaldson Building, 110 Science Place
Saskatoon, Saskatchewan S7N 5C9
Canada

ABSTRACT

Gene therapy is a promising therapeutic approach for the treatment of inherited and acquired genetic disorders. Gemini surfactants are an emerging class of cationic lipids that has shown promising results in delivering genetic materials, particularly to the skin. The unique structure of the gemini surfactants imparts a design flexibility that permit the modulation of their physicochemical properties toward the enhancement of transfection efficiency. The behavior of gemini surfactants in complex biological systems may ultimately determine their efficiency and cytotoxicity. Correlating the biodistribution and biological fate of the nanoparticles to their chemical structure and physicochemical properties will inform the rational design process, resulting in the production of compounds with higher efficiency and reduced toxicity. In this research, a series of 22 novel peptide-modified gemini surfactants was evaluated. The aim of my research is to elucidate their structure-activity relationship and to determine their skin penetration behaviour.

Transfection efficiency and cytotoxicity of the compounds were evaluated in murine keratinocytes and African green monkey kidney fibroblast cell lines. Physicochemical and structural properties of the nanoparticles were examined. Results revealed that the highest transfection efficiency and lowest cytotoxicity were associated with 16-7N(G-K)-16 gemini surfactant, showing an 8-fold increase in gene expression and a 20% increase in cell viability compared to the first-generation unsubstituted gemini surfactants. Furthermore, assessment of the contribution of the alkyl tail, in terms of length and saturation, indicated that compounds with hexadecyl tails were 5-10 fold more efficient than compounds with dodecyl and oleyl tails.

To track the level of localization of the gemini surfactants in the skin, mass spectrometric analytical strategies were developed. The tandem mass spectrometric (MS/MS) dissociation behavior of the compounds was evaluated. Diagnostic product ions were selected for accurate identification of the gemini surfactants in complex biological matrices. Such knowledge was utilized to develop rapid and simple flow injection analysis (FIA)-MS/MS method for the quantification of three peptide-modified gemini surfactants *ex vivo* in skin and phosphate buffered saline. Results showed a more than 11% deposition in the skin with minimum penetration into the saline compartment, suggesting the suitability of the delivery system to be used for topical application.

ACKNOWLEDGEMENTS

"In the Name of Allâh (God), the Most Gracious, the Most Merciful"
All my praises and thanks be to Allâh

I would like to express my sincere thanks and appreciation to my supervisors, Drs. Ildiko Badea and Anas El-Aneed for their guidance, encouragement, support and kindness. I consider myself very fortunate to have them as mentors.

I would also like to thank my advisory committee members Drs. Lee Wilson, Pawel Grochulski, Ed Krol and Azita Haddadi for their guidance, advices and scientific input. My gratitude is extended to Dr. Ronald E Verrall for his advice, encouragements and valuable scientific feedback. I would like to acknowledge Dr. J. Chitanda for the synthesis of the compounds utilized during my research.

It would have been difficult to complete the work associated with this document without the assistance and support of Ms. Deborah Michel. I am very grateful for her time and friendship.

My sincere gratitude is extended to Dr. Kishor Wasan, Dean of College of Pharmacy and Nutrition, for providing me with priceless professional development opportunities and supporting me during my studies.

I would like to thank College of Pharmacy and Nutrition, College of Graduate and Postdoctoral Studies, Canadian Institutes of Health Research-Training grant in Health Research Using Synchrotron Techniques (CIHR-THRUST), Apotex Inc and Graduate Students' Association for financial support during my program.

I appreciate and thank all my colleagues for their friendship and support: Mr. W. Mohammed-Saeid, Dr. M Donkuru, Dr. M Poorghorban, Mr. O. Alaidi, Ms. H. Elsayed, Ms. S. Alwani, Ms. A. Zagzoog, Ms. S. Fatani MS. F. Elessawy, Dr. A. Makhlouf, Mr. R. Rai, Ms. A. Poudel, Dr. and G. Gachumi. Special thanks to my friend Ms. M. Hamada, without whom this journey would have never been as pleasant.

Finally, I would like to thank Mrs. Darlene Figurski and her family for their kindness and great company.

Dedicated to

My parents, Aiyed Al-Dulaymi and Sahira Abood,

My brothers, Ahmed and Mustafa,

My sister-in-law, Rula,

&

My niece, Lara,

without whom love, care, support, generosity and patience I would not be the person I am

Table of Contents

LIST OF ABBREVIATIONS

BGSC	3P3[4N-(QN,8N-diguanidino spermidine)-carbamoyl] cholesterol
BGTC	3/3[N',N'-diguanidinoethyl-aminoethane) carbamoyl]cholesterol
PEG	Polyethylene glycol
CID	Collision-induced dissociation
CMC	Critical micelle concentration
COS-7	African green monkey kidney fibroblast
CXP	collision exit potential
Dc-chol	3ß-[N-(N',N'-dimethylaminoethane)-carbamoyl]cholesterol hydrochloride
DP	declustering potential
DiC14-amidine	N-t-butyl-N'-tetradecyl-3-tetradecylaminopropionamidine
D_m	diffusion coefficient
DMEM	Dulbecco's Modified Eagles Medium
DMRIE	1,2-dimyristyloxypropyl-3-dimethyl-hydroxy ethyl ammonium bromide
DOGS	Dioctadecyl-glycyl-carboxyspermine
DOPC	1,2-Dioleoyl-sn-Glycero-3-Phosphocholine
DOPE	1,2-di-(9Z-octadecenoyl)-sn-glycero-3-phosphoethanolamine
DORI	1,2-dioleoyloxypropyl-3-dimethyl-hydroxyethyl ammonium chloride
DORIE	1,2-dioleoyl-3-dimethyl-hydroxyethyl ammonium bromide
DOTAP	1,2-dioleoyl-3-trimethylammonium-propane
DOTIM	1 -[2-(9(Z)-Octadecenoyloxy)ethyl]-2-(8(Z)-heptadecenyl)-3-(2-hydroxyethyl) imidazolinium chloride
DOTMA	N-[1-(2,3-dioleyloxy)propyl]-N,N,N-trimethylammonium chloride

ELISA	Enzyme-linked immunosorbent assay
ESI	Electrospray ionization
FIA	Flow injection analysis
GFP	Green fluorescent protein
HER2	Human epidermal growth factor receptor-2
HPLC	High performance liquid chromatography
IFN-γ	Interferon gamma
$\mathbf{J_{ss}}$	Steady-state flux
$\mathbf{K_m}$	Partition coefficient
$\mathbf{K_p}$	Skin permeability coefficient
LC	Liquid chromatography
$\mathbf{MS^n}$	Multistage mass spectrometry
MRM	Multiple reaction monitoring
MS	Mass spectrometry
MS/MS	Tandem mass spectrometric
MTBE	Methyl-tert-butyl ether
m/z	Mass to charge
NLS	Nuclear localization signal
N/P	Nitrogen to phosphate charge ratios
OTC	Ornithine transcarbamylase
P	Lipid packing parameter
PAM212	Murine keratinocytes
PBS	Phosphate buffered saline

pDNA	plasmid DNA
SAINT	synthetic amphiphile interaction
SAR	Structure activity relationship
SAXS	Small-angle X-ray scattering
SC	Stratum corneum
SPE	Solid phase extraction
t_{lag}	lag-time
X-SCID	X-linked severe combined immunodeficiency

LIST OF FIGURES

Figure 3.7. SAXS scattering profile of the P/G/L lipoplexes of the peptide modified gemini surfactants at N/P ratios of 2.5, 5 and 10. Black arrows indicate the position of Bragg peaks. q values with ratio of 1: √3: √4 correspond to the inverted hexagonal (HII) phase.

Figure 3.8. *In vitro* transfection of PAM 212 cells comparing the level of IFN-γ expression across the different subfamilies of the peptide-modified gemini surfactants. Results are the average of three plates of quadruplicate wells, error bars represent standard deviation. * Indicates significant at $p < 0.05$.

Figure 3.9. Evaluation of PAM 212 cell viability of the peptide-modified gemini surfactants at three N/P ratios. Results are the average of three plates of quadruplicate wells, error bars represent standard deviation.

Figure 4.1. (A) Prototype of gemini surfactants showing the two ionic head groups, hydrocarbon tails and the spacer and (B) schematic representation of the general structure of the tested peptide modified gemini surfactants.

Figure 4.2. The ESI-QqLIT-MS/MS spectrum of 16-7N(C_{11}-K_3)-16 as a representative example of gemini surfactants with tri-terminal lysine moieties. Ions were labelled as designated in Figures 5-7. Strcture of the three initial product ions are shown as an insert (top).

Figure 4.3. The proposed mechanism for the formation of product ion (A) and (b_1): amide bond cleavage initiated by lysine side chain.

Figure 4.4. The proposed mechanism for the formation of product ion (B) and (a_1): cleavage of $C\alpha - C_{amide}$ bond through a_x - y_x fragmentation pathway.

Figure 4.5. Proposed MS/MS product ions generated form product ion (A) at *m/z* 538.54 of 16-7N(C11-K3)-16 gemini surfactant. Product ion 2* is a transient ion.

Figure 4.6. Proposed MS/MS product ions generated form product ion (B) at *m/z* 359.36 of 16-7N(C11-K3)-16 gemini surfactant.

Figure 4.7. Proposed MS/MS product ions generated form product ion (C) at *m/z* 396.38 of 16-7N(C11-K3)-16 gemini surfactant.

LIST OF TABLES

CHAPTER 1

Literature Review

1.1. Introduction

Gene therapy holds a promising future for the treatment of many acquired and inherited diseases. It is defined as the insertion of exogenous genetic material (DNA, RNA, mRNA) into cells in order to supplement a new gene, repair a defective gene or block gene overexpression [1]. The induced changes could be either transient or permanent in the targeted cells or tissues. The idea of using genes to modulate biochemical pathways was first introduced by Rogers in 1968 when genetic material was inserted into Turkish tobacco seed using Tobacco mosaic virus [2]. However, gene therapy was pioneered by Friedmann and Roblin when they described the possible use of viruses in transferring genes to humans in 1972 [3].

One of the key challenges for gene therapy is the development of effective and safe carrier systems. Since Friedmann and Roblin's initial work, the development of gene delivery systems has attracted a great deal of attention from many research groups. Two methods of gene delivery are currently available: viral and non-viral vectors. Viral vectors are more efficient in transferring genes to cells; it has resulted in a few marketed gene therapy products such as Gendicine™ used for the treatment of head and neck squamous cell carcinoma, Glybera® for lipoprotein lipase deficiency and Imlygic® (talimogene laherparepvec) approved by the FDA for the treatment of melanoma [4-6]. However, viral gene therapy suffers from major inherent drawbacks. In particular, safety concerns have been raised due to their propensity to generate a severe immune response. In 1999, the tragic death of an 18-year-old patient during clinical trials was the result of a massive immune response after the administration of adenovirus vector that encoded for the ornithine transcarbamylase gene [7]. In addition, viral vectors could cause

carcinogenesis such as the development of T-cell leukaemia in two patients who participated in a retrovirus-based gene therapy clinical trial to treat X-linked severe combined immunodeficiency syndrome (X-SCID) [8]. The cause of the adverse effect was the insertion of the retroviral vector that led to the deregulation of LMO-2 gene expression which in turn triggered T-cell proliferation [9, 10]. Another limitation of viral vectors is that they usually have a fixed size capsid so they are limited in the size of genes that can be encapsulated [7]. Non-viral methods, on the other hand, have the potential to address many of these limitations. They are considered safer alternatives since they tend to have lower immunogenicity than viral vectors. In addition, they have relatively unlimited DNA packaging capacity and are typically easier to produce than viral vectors. Non-viral methods employ diverse systems such as cationic lipids and polymers to compact the therapeutic DNA into nano-sized lipoplexes and polyplexes, respectively.

This review summarizes the different barriers that non-viral systems must overcome to efficiently deliver the genetic material into the targeted site. In addition, it underlines prominent non-viral gene delivery systems with a focus on the cationic lipid-based gene delivery vectors. Finally, it highlights the potential use of lipid-based nanocarriers for skin gene delivery.

1.2. Barriers to non-viral gene delivery systems

Non-viral gene delivery systems have emerged as a promising modality to address the limitations of viral gene delivery vectors, particularly safety [11]. However, the use of non-viral based strategies has poorly translated into clinical success mainly due to their lower efficiency in delivering the genetic material compared to viral vectors [12]. One of the greatest challenges that impede the success of non-viral vectors is the variety of extracellular and intracellular delivery barriers [13]. These barriers are essential components of the human defense system, which prevent the entrance of foreign materials. A deep understanding of the biological barriers is an essential

requirement for the design of effective vectors capable of overcoming these delivery hurdles. The following section describes the main biological barriers faced by the non-viral gene delivery approach and discusses potential strategies for circumventing each barrier.

1.2.1. Extracellular barriers

Extracellular barriers include all immunological and physical hurdles that face the delivery system from the site of administration until the arrival to the target cell. Thus, the type of extracellular barriers encountered by the delivery vectors mainly depends on the route of administration. For example, intravenously administered vectors encounter the reticuloendothelial system which could rapidly remove the delivery vehicle from the blood circulation [14, 15]. Design strategies such as the attachment of polyethylene glycol (PEG) to lipoplexes and polyplexes was adopted to shield the vector from the extracellular environment and prolong the circulation time [16, 17]. For example, intravenously administered lipoplexes grafted with 15-mol % PEG showed a higher blood circulating concentration after 6 hours of administration [16]. However, PEGylated lipoplexes exhibited significantly lower transfection efficiency compared to the unmodified lipoplexes [16]. This was attributed to the impaired membrane interaction and reduced cellular uptake that resulted from vectors PEGylation: "PEG dilemma" [18, 19]. Several attempts have been made to overcome this dilemma including the incorporation of a ceramide moiety into the PEGylated vectors [20]. Ceramide-PEG-coated vectors preferentially lose their shielding material near the desired delivery target, thus, they prolong the circulation time without reducing the transfection efficiency [20].

Another major rate-limiting step for intravenously administered delivery systems is the passage through the endothelium of the blood vessels. The endothelium is composed of a monolayer of endothelial cells separated by small interendothelial spaces [21]. The size of the

interendothelial spaces is largely affected by the endothelial layer disease condition [21]. For example, under certain pathological conditions such as inflammation or cancer, the size of the interendothelial spaces increases permitting the escape of nanoparticles from the blood vessels. In addition, the size of interendothelial gaps is influenced by their anatomical location within the body. For instance, interendothelial spaces of the brain blood capillaries are about hundred times smaller than those in the liver [22]. Such a variation could be utilized as a targeting strategy for specific organ or disease condition.

Once the delivery vectors have escaped the blood vessels, they must navigate through the dense extracellular matrix of the interstitial space. The extracellular matrix is a dynamic and complex milieu composed of a network of collagen, proteoglycans, glycosaminoglycans and microfibrilar elastins [23]. Similar to the endothelium, the integrity of the tissue varies depending on the disease condition and the anatomical location[23, 24]. Optimizing the physicochemical properties of the delivery system including particle size and surface charge could improve the passage through the extracellular matrix. For example, particle size of less than 200 nm was reported to show effective tumor accumulation [25].

1.2.2. Cellular uptake

The cell membrane represents the first barrier at the cellular level that hinders gene transfer. Typically, the cell internalizes macromolecules from the surrounding media by endocytosis [26]. The association of naked DNA with the cellular membrane is usually very low due to the electrostatic repulsion between the relatively high negative charge density of both the DNA and the cell membrane. Positively charged non-viral gene delivery vehicles can circumvent this problem by inducing electrostatic interaction with the negatively charged constituents of the plasma membrane such as heparan sulfate, proteoglycans and integrins [26-28]. Several studies

suggested that optimizing the surface charge of the non- viral gene delivery complexes enhances the efficiency of cellular entry [29, 30]. However, mainly non-specific interaction with cytoplasmic membranes was achieved.

Efforts have been made to achieve cell-specific gene delivery by incorporating targeting ligands into the delivery vehicle such as the addition of cell penetrating peptides, a "Trojan horse approach" [31]. These peptides consist of 5–40 amino acids that can bind to specific receptors on the cell membrane to induce receptor-mediated endocytosis which is believed to be a more efficient internalization pathway for targeted gene delivery [32]. Promising results were attained in utilizing peptides such as HIV-1 trans-activating transcriptional (TAT) protein and Drosophila homeobox protein Antennapedia in non-viral gene delivery systems [31].

Furthermore, the incorporation of monoclonal antibodies into the delivery vector has been used to promote cell-specific gene delivery [33, 34]. For example, Chiu *et al.* showed that polyethylenimine polyplexes conjugated with monoclonal antibody specific to human epidermal growth factor receptor-2 (HER2) showed up to a 20-fold increase in the level of gene expression compared to the non-derivatized polyplexes in the HER2 overexpressing cells. On the other hand, no significant difference was observed in the HER2 low-expressing cell line indicating the success of the targeting approach [33].

It is noteworthy that despite the success of techniques such as the coupling of cell penetrating peptides or monoclonal antibodies to the delivery vector *in vitro*, nonselective *in vivo* penetration has caused safety concerns [35]. Current focus is on the development of "smart" strategies to overcome such a problem [36].

1.2.3. Endosomal escape

Once inside the cell, the DNA must escape from the endosomes to avoid lysosomal degradation [37]. As such, the ability of the delivery vectors to escape from the endosomal compartments is an essential characteristic of efficient gene delivery systems. Different escape mechanisms have been suggested including direct or induced endosomal membrane rupture [38]. Direct endosomal membrane disruption typically occurs as a result of the electrostatic interactions between the anionic endosomal lipid membrane and the positively charged gene carrier [39, 40].

Several strategies have been adopted to facilitate the release of the DNA from the endosomal compartments. For instance, the incorporation of the fusogenic lipid 1, 2-dioleoyl-*sn*-glycero-3-phosphoethanolamine (DOPE) exhibited promising results in facilitating the endosomal escape due to its ability to undergo phase transition from the bilayer to the inverted hexagonal phase (H_{II}) [41, 42]. Another approach involves the use of cationic polymers such as polyethyleneimine to mediate the "proton sponge" mechanism [38, 43]. These polymers have a high buffering capacity owing to the presence of several amino nitrogen groups that can undergo protonation upon endosomal acidification [43]. Protonation induces an extensive influx of ions into the endosomal compartments resulting in osmotic swelling and rupture of the endosomal membrane [43].

Finally, the incorporation of pore-forming peptides is considered a common strategy to facilitate the release of DNA. Examples of these peptides are GALA and KALA; amphipathic peptides that were designed to mimic the membrane penetrating activity of viruses [44, 45]. They undergo conformational changes from a random coil to α-helix structure as a function of pH reduction, resulting in endosomal membrane disruption. Another common example is melittin, a

small cationic endosomolytic peptide that represents a major component of bee venom [46]. Melittin's α-helix structure interacts with the lipid membrane forming toroidal pores [47]. In fact, the incorporation of melittin into a polyethyleneimine delivery system showed up to a 700-fold increase in the level of luciferase gene transfer [46]. Unfortunately, the cytotoxicity profile of the pore-forming peptides has limited the translation of such a methodology for *in vivo* applications [48].

1.2.4. Nuclear localization

For successful gene expression, transport of the DNA into the nucleus is required in order to allow access to the transcriptional machinery. The nuclear envelope represents the most formidable barrier for non-viral gene delivery. In fact, a study suggested that less than 1% of the DNA injected into the cytoplasm was able to reach the nucleus [49]. The passage of the DNA across the nuclear envelope is believed to take place through three possible routes: i) passive entry during mitosis, ii) passive diffusion through nuclear pores and iii) active traverse across the nuclear membrane [50].

During mitosis, DNA can passively move into the nucleus due to the broken nuclear envelope. Thus, rapidly dividing cells are generally easier to transfect than quiescent cells [51]. Such attributes could be utilized as a targeting strategy for specific disease conditions like cancer. In fact, there are more than 1,415 ongoing clinical trials worldwide that are investigating the potential of cancer gene therapy [52]. Only small macromolecules with particle size of less than 50 kDa (~9 nm) can passively diffuse through the nuclear membrane, however, larger macromolecules containing nuclear localization signal (NLS) can cross via active translocation [53, 54].

NLS is a targeting sequence consisting of a short chain of positively charged basic amino acids such as lysines or arginines that enables nuclear entry by interacting with surface proteins namely importin-α and importin-β [55]. Incorporating NLS into the genetic material or the carriers has been successfully used as a strategy to improve the nuclear import of non-viral gene delivery systems [56, 57]. Nevertheless, the NLS approach suffers from limitations, particularly the possibility of burying their localized signal in the therapeutic DNA due to their electrostatic interaction with the negatively charged phosphate groups [58]. In addition, successful outcomes were attained with linear DNA but not circular pDNA which is a better vector for sustained gene expression [58, 59]. New generations of specific NLSs are needed to lift this barrier in the development of efficient non-viral gene delivery vectors.

1.3. Non-viral gene delivery systems

1.3.1. Naked DNA

The introduction of naked DNA into cells is considered the simplest and the safest non-viral gene delivery method. The first *in vivo* study to transfer genes dates back to the 1990s when Jon A. Wolff *et al* directly injected plasmid DNA into mouse skeletal muscle [60]. Though the main purpose of the study was to evaluate cationic lipids as delivery agents, the level of gene expression without a vector was sufficient to consider direct injection for genetic vaccination [60]. Following that a series of experiments were conducted targeting different tissues such as skin, liver, kidney, lung and heart [61-64]. Successful attempts to directly inject naked DNA to the tumours in order to express antigens (cancer vaccine) were also reported [65]. Currently there are about 18 % of all clinical trials worldwide that utilize naked DNA [52]. DNA direct injection method yields high gene expression within tissues that is easily accessible, such as skin and muscles cells. The method of injection could determine the level of gene expression. Levy *et al.*

detected 200-fold higher gene expression with the use of an injection guided by intense illumination along the longitudinal axis of the mouse quadriceps muscle and parallel to the myofibers than with a perpendicular injection[66].

Systemic injection of plasmid DNA showed a much lower level of gene expression compared to the viral or liposomal vectors [67, 68]. This is mainly due to the fact that naked DNA is more susceptible to degradation than encapsulated DNA. Unprotected DNA is degraded rapidly by the serum and the cytoplasmic nucleases which makes the technique not as effective for systemic applications as for targeting specific tissues[68]. The low level of gene expression and the need for a large amount of DNA are the main limitations for the use of naked DNA for gene therapy. To overcome these limitations, various physical methods such as electroporation, particle bombardment (gene gun), ultrasound induced pores (sonophoresis), magnetic field assisted transfection (magnetofection), and microinjection have been utilized to shuttle naked DNA into cells [69]. These methods circumvent extracellular and intracellular biological barriers and facilitate the transfer of genes leading to significant improvements in the delivery process (enhance the rate and the extent of gene delivery to targeted cells). However, the main drawback to all the physical methods is that they cause damage to the cell membrane. In addition, their efficiency in delivering genetic materials is still not adequate [69].

1.3.2. Lipid-based gene delivery system

Lipid-based drug delivery systems have received increasing attention because of their ability to deliver a wide variety of drugs ranging from small molecules to biotechnology products. The idea of using lipids as a carrier for genetic materials was first proposed by Felgner and his colleagues in 1987 when they used N-[1-(2,3-dioleyloxy)propyl]-N,N,N-trimethylammonium chloride (DOTMA) and 1,2-dioleoyl-sn-glycerol-3-phosphoethanolamine (DOPE) to perform a DNA-transfection protocol [70]. Since that time, various generations of cationic lipids have been developed resulting in significant improvements in the *in vitro* and *in vivo* transgene delivery [71-73].

Cationic lipids are self-assembling amphiphilic compounds that possess two essential characteristics for gene delivery. Firstly, they have a cationic head group that interacts with the DNA's anionic phosphate group condensing the DNA and shielding it from degradation by nucleases. Secondly, they have a lipid moiety as a fusogenic group that can facilitate penetration into the cell. Cationic lipids are responsible for the overall net positive charge of the lipoplex, which in turn will create an electrostatic interaction with the negative charge of the cell surface. Based on the chemical structure of the cationic head group, cationic lipids could be classified into the following categories: quaternary ammonium salt lipids, lipopolyamines, amidinium and guanidinium salt lipids and heterocyclic cationic lipids[71].

A) Quaternary ammonium salt-based lipids

Cationic lipids bearing quaternary ammonium are, by far, the most-studied class of cationic lipids. DOTMA (2,3-dioleyloxypropyl-1-trimethylammonium bromide) (Table 1.1) was the first compound in this family reported in Felgner's seminal paper [70]. Following that, a wide variety of structural modifications to the first compound increased exponentially resulting in

compounds that have higher transfection efficiency and/or lower toxicity. For example, replacement of the ether linkage with an ester linkage resulted in the formation of the biodegradable compound DOTAP (2-dioleoyl-3-trimethylammonium-propane) (Table 1.1) [74]. Furthermore, the replacement of the methyl group in DOTMA and DOTAP with a hydroxyethyl group producing DORIE (1,2-dioleoyl-3-dimethyl-hydroxyethyl ammonium bromide) and DORI (1,2-dioleoyloxypropyl-3-dimethyl-hydroxyethyl ammonium chloride) respectively, led to an improved transfection profile (Table 1.1) [75]. This indicates that the hydroxyl moiety plays an important role in the compound's activity. Two mechanisms were proposed: 1) the hydroxyl group will form hydrogen bonds with DNA or the cellular membrane which will lead to a better compaction and subsequently better delivery process and 2) when the hydroxyl group forms hydrogen bonds with the cellular membrane and/or the DNA, the compounds containing the hydroxyl group remain in contact with the aqueous phase, maintaining the integrity of the bilayer structure and the stability of the complexes [75].

In vitro transfection studies with COS-7 cells showed that DORIE has a higher transfection efficiency than DORI [75]. Felgner's group conducted further structure activity relationship (SAR) studies on DORIE by modifying the alkyl tail length and the degree of unsaturation. DORIE (with C18:1 alkyl tails where C18:1= mono-unsaturated oleyl chain) was compared with compounds that have C14, C16 and C18 hydrophobic tails. 1,2-dimyristyloxypropyl-3-dimethyl-hydroxy ethyl ammonium bromide (DMRIE) (Table 1.1) , a C14 compound, was the most efficient [75]. It was suggested that the decreasing length of the alkyl chain was accompanied by reducing phase transition temperature and bilayer stiffness which affects both fusion with the cell membrane as well as endosomal escape; both of which are critical for effective gene transfer [75]. Due to the high transfection efficiency and low

toxicity, DMRIE has been utilized in several clinical trials such as human basal cell carcinoma [76] , melanoma [77] and prostate cancer [78]; promising results were reported in terms of efficiency and safety profile. Numerous other quaternary ammonium salt-based lipids were developed over the past three decades making this group the most widely used lipids in gene delivery.

Table 1.1. Chemical structure of quaternary ammonium salt-based lipids

DOTMA [70]	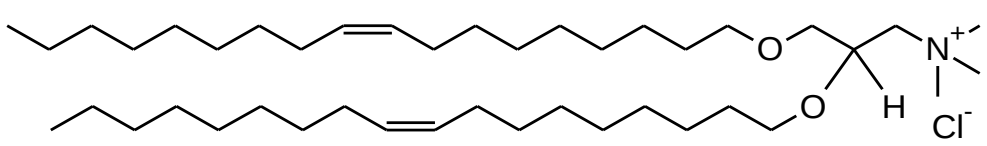
DOTAP [74]	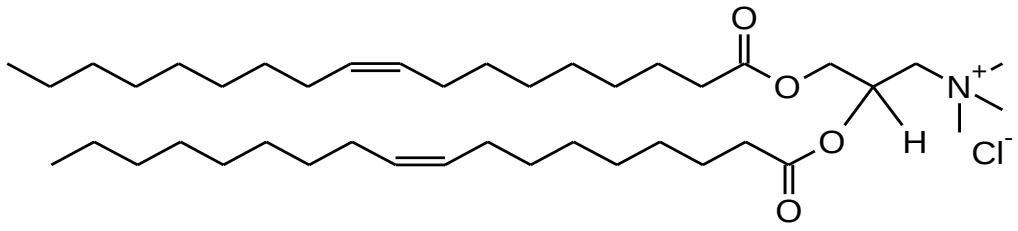
DORIE [75]	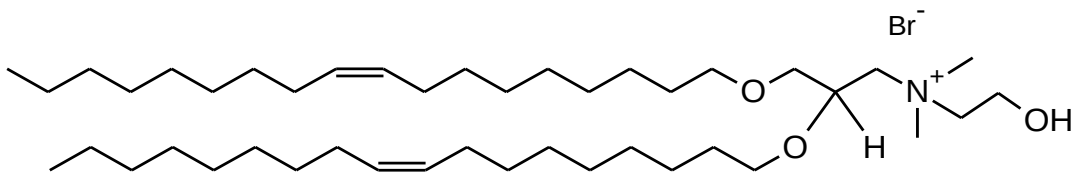
DORI [75]	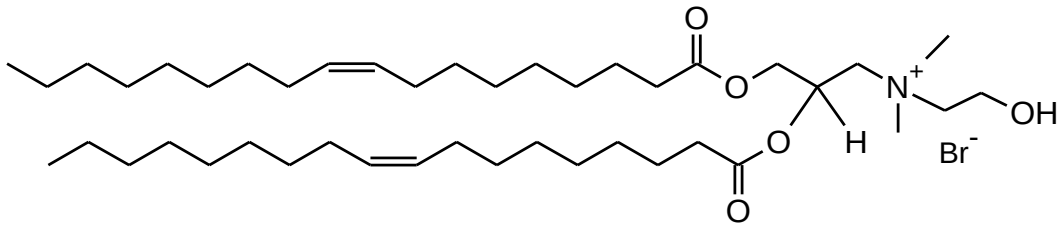
DMRIE [75]	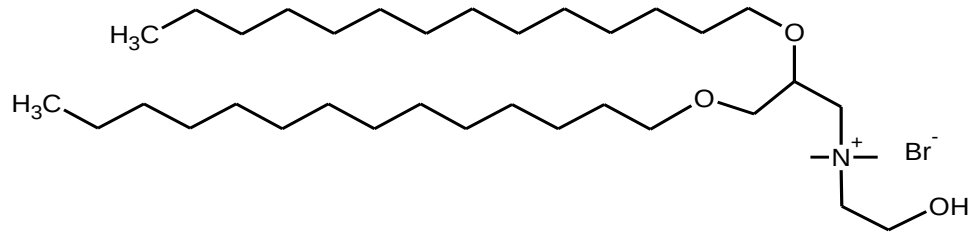

B) Lipopolyamines

The first attempt to introduce lipopolyamine compounds was pioneered by Behr, capitalizing on the ability of the naturally nucleus-occurring polyamines (spermine and spermidine) to efficiently compact DNA. Dioctadecyl-glycyl-carboxyspermine (DOGS) (Table 1.2) was synthesized by attaching hydrophobic tails to spermine through a glycyl spacer [79, 80]. DOGS showed a high level of *in vitro* and *in vivo* gene expression without the use of a helper lipid [80]. Lipopolyamines are pro-cationic compounds (protonated at physiological pH), are more efficient than quaternary ammonium lipids in neutralizing the polyanionic phosphate backbone of the DNA resulting in better compaction [81]. Byk and his colleagues conducted an extensive SAR evaluation by introducing step-by-step modification to the backbone of DOGS congeners [82]. The modifications included: using various geometrically differing polyamines; varying the geometry and the length of the linker; and changing the length of the lipid. Compound RPR-120535 showed the highest transfection efficiency among the entire tested series (Table 1.2) [82]. RPR-120535 had a linear polar head group configuration which showed superior transfection efficiency to the branched, T-shaped and the globular head groups. Further investigations on this lead compound revealed that varying the length of the linker resulted in the same level of gene expression. However, varying the length of the hydrophobic tail showed that 18 carbon atoms was optimal for achieving the highest transfection efficiency compared to compounds with 12,13 and 14 carbon atoms [82]. Enhanced transfection efficiency was justified by increasing the compound hydrophobicity, however, no conclusive explanation was provided [82].

The introduction of a class of lipopolyamines bearing a cholesterol moiety as a hydrophobic anchor was proposed by Gao *et al* introducing DC-Chol (3B [N-(N', N'-dirnethylaminoethane)-carbamoyl] cholesterol) (Table 1.2) [83]. DC-Chol was the first cationic

lipid to be used for clinical trials to treat cystic fibrosis [84]. In 1996 Lee *et al* introduced another polyamine cholesterol derivative named Lipid 67 (Table 1.2) by connecting cholesterol moiety to a spermine head group in a T-shape configuration [85]. Lipid 67 was tested *in vivo* for its ability to transfer a cystic fibrosis transmembrane conductance regulator (CFTR) cDNA as treatment of cystic fibrosis. The result showed that Lipid 67 was 100 times more active than previously used cationic lipids [85]. A series of studies were conducted to optimize the safety and the stability of this lipid during aerosolisation [86, 87]. It was co-formulated with DOPE to facilitate the endosomal escape of the genetic material and with a polyethylene glycol-containing lipid dimyristoyl phosphatidylethanolamine [(DMPE)-PEG5000] to stabilize the formulation [86]. The administration of a single dose of this formulation with DNA encoding for CFTR to 35 patients suffering from cystic fibrosis during a phase I clinical trial was successful in achieving a high level of gene expression and restoring CFTR normal function [88-90]. More recently, a Phase II clinical trial has been launched to assess the safety and the efficacy of the lipid-mediated vector in multi-dose administration [91]. Lipopolyamines are more efficient in compacting DNA and their pH buffering ability facilitates the endosomal escape of DNA.

Table 1.2. Chemical structure of Lipopolyamine

DOGS [79, 80]	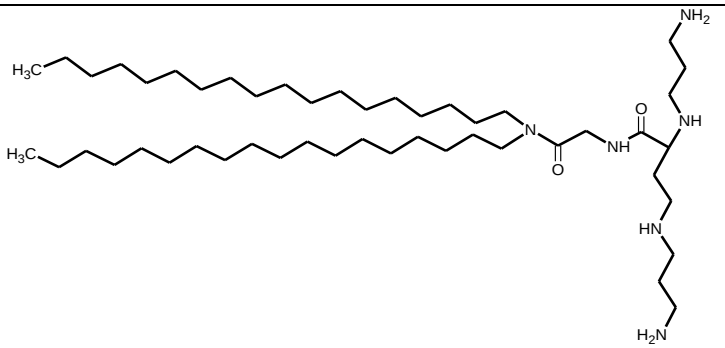
RPR-120535 [82]	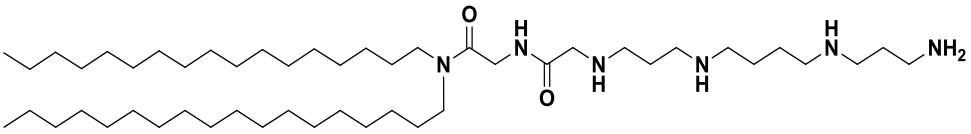
DC-Chol [83]	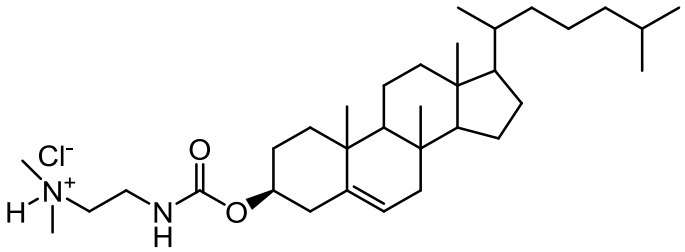
Lipid 67 [85]	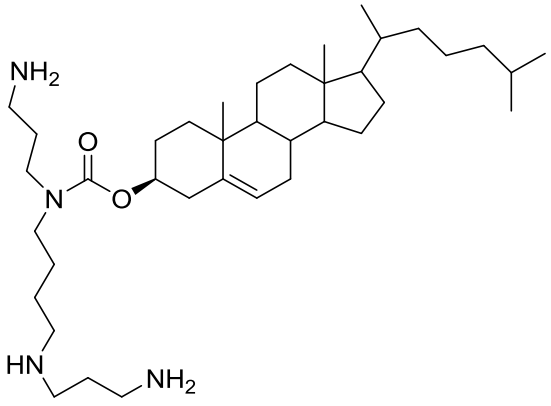

C) Amidinium and Guanidinium salts

Instead of ammonium groups, this family of cationic lipids bears amidinium or guanidinum groups (Table 1.3). Amidinium or guanidinum groups possess several advantages over the amines. Firstly, they have a higher pK_a, thus they protonate over a wide range of pH values. Secondly, they have higher affinity to bind to DNA because of their ability to form hydrogen bonds with the DNA phosphate group. Thirdly, they have good intrinsic biocompatibility [92]. Amidinium cationic lipids were first described by Ruysschaertet and his colleagues, when they introduced *N*-*t*-butyl-*N*'-tetradecyl-3-tetradecylaminopropionamidine (diC14-amidine) (Table 1.3) [93]. Transfection evaluation was conducted on Chinese hamster ovary cells and human erythroleukemic cells showing maximum gene level incorporation within the first hour of the treatment and low cytotoxicity was reported [93].

Lehn's group was the first to introduce guanidinum cationic lipids, when they attached bis-guanidinium to cholesterol producing the two guanidinium-cholesterol derivatives BGTC, (3/3[*N'*,*N'*-diguanidinoethyl-aminoethane) carbamoyl]cholesterol) and BGSC, (3P3[4N-(QN,8N-diguanidino spermidine)-carbamoyl] cholesterol) (Table 1.3) [92]. A variety of mammalian cell lines were used to assess the transection efficiency of BGTC and BGSC, both compounds showed higher gene expression levels than Lipofectin®.

Table 1.3. Chemical structure of amidinium and guanidinium salt lipids.

diC14-amidine[93]	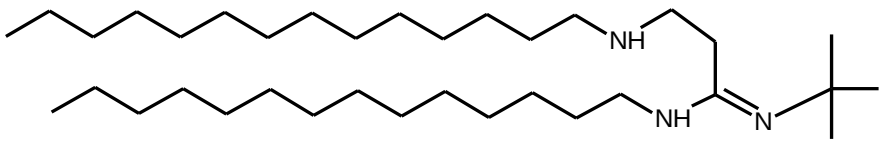
BGTC [92]	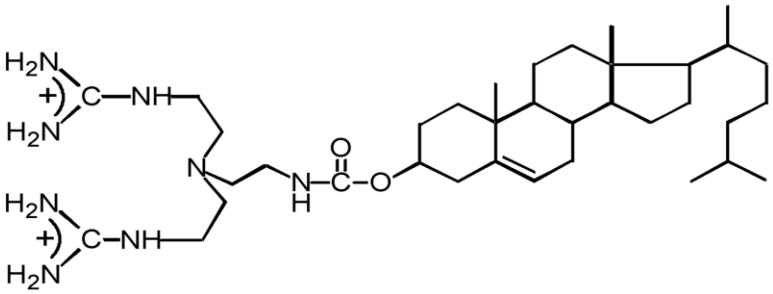
BGSC [92]	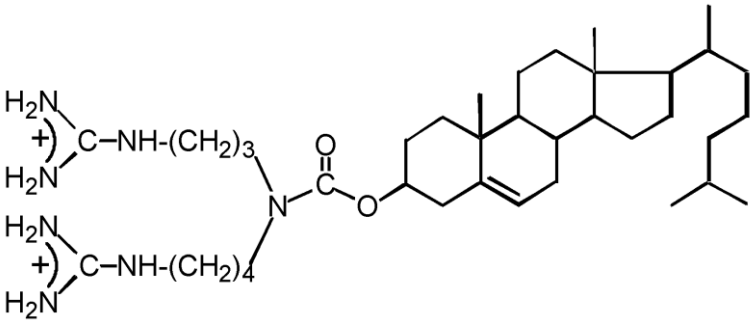

D) Heterocyclic Cationic Lipids

Heterocyclic cationic lipids have attracted the interest of several research groups since the type of the head group can profoundly affect the transfection efficiency. Different kinds of heterocyclic ring head groups have been utilized such as pyridinium [94-97], piperazine [98], morpholine [99] and imidazolinium [100]. However, compounds with pyridine, pyridinium head groups and their derivatives are the most widely used and their efficiency was comparable or even exceeds that of commercially available transfection agents [94-97]. Pyridinium cationic lipids were first introduced by Engberts and co-workers; they developed a series of compounds named synthetic amphiphile interaction (SAINT), (Table 1.4) [94-97]. Intensive SAR assessment showed that SAINT with mono-unsaturated alkyl chains had transfection efficiency higher than that of the commercially available transfection agents [94].

Another heterocyclic group is imidazolinium cationic lipids which were firstly discussed by Solodin *et al.,* synthesizing three compounds that differ only in the length of the hydrophobic chains and the degree of unsaturation (C12, C14 and C18:1) [100]. Highest *in vivo* transfection efficiency was associated with the compound bearing the oleoyl chain, 1-[2-(9(Z)-Octadecenoyloxy) ethyl]-2-(8(Z)-heptadecenyl)-3-(2-hydroxyethyl) midazolinium chloride (DOTIM), (Table 1.4). Currently, DOTIM is co-formulated with cholesterol and pDNA to be tested for its safety in a phase I clinical trial for the treatment of relapsed or refractory leukemia [101]. Heterocyclic cationic lipids in general show a potential of high transfection efficiency and low cytotoxicity due to delocalization of the positive charge on the aromatic ring that might improve the DNA compaction and facilitate endosomal escape.

Table 1.4. Chemical structure of Heterocyclic cationic lipids

SAINT [94-97]	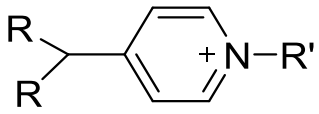 SAINT-1 R= $(CH_2)_{15}CH_3$, R'=CH_3 SAINT-2 R= $(CH_2)_8CH{=}CH(CH_2)_7CH_3$, R'=$CH_3$ SAINT-9 R= $(CH_2)_{15}CH_3$, R'= $(CH_2)_4N^+(CH_3)_3$ SAINT-21 R=$(CH_2)_8CH{=}CH(CH_2)_7CH_3$, R'= $(CH_2)_4N^+(CH_3)_3$
DOTIM [100]	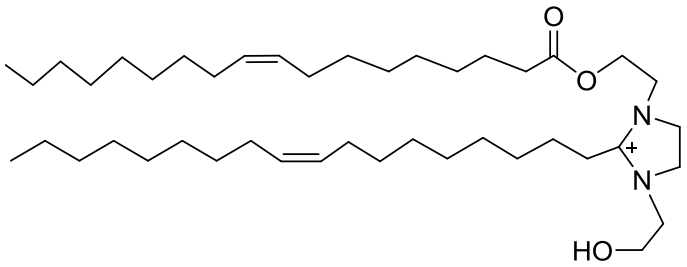

1.3.3. Dicationic gemini surfactants

The term "gemini surfactant" was coined by Menger in 1991 to describe a family of amphiphiles composed of two head groups (cationic, anionic, or neutral) and two hydrophobic tails covalently linked by a spacer (Figure 1.1) [102]. The unique molecular structure of gemini surfactants resulted in a number of superior properties compared to classical monomeric surfactants such as: 1) one or two orders of magnitude lower critical micelle concentrations (CMC) resulting in lower cytotoxicity, 2) lower Krafft temperature 3) higher efficiency in reducing surface tension and 4) enhanced wetting properties [102].

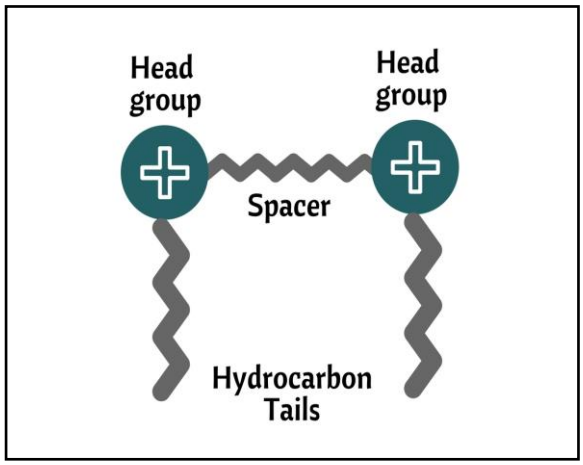

Figure 1.1. General structure of cationic gemini surfactant.

Cationic gemini surfactants are of particular interest in gene therapy due to their ability to interact with the negatively charged phosphate groups of the nucleic acids through electrostatic interaction resulting in neutralizing, condensing and encapsulating the pDNA into nano-sized particles (Figure 1.2) [103]. The hydrophobic domains of the gemini surfactants, on the other hand, engage in cooperative hydrophobic interactions which stabilize the complexes during the delivery process [104]. Hydrogen and van der Waals interactions also participate in the condensation of the pDNA [104]. Neutral lipid vesicles, such as DOPE, is usually added to the

pDNA-gemini surfactant complexes due to its fusogenic properties, which facilitate cell penetration and endosomal escape (Figure 1.2) [42].

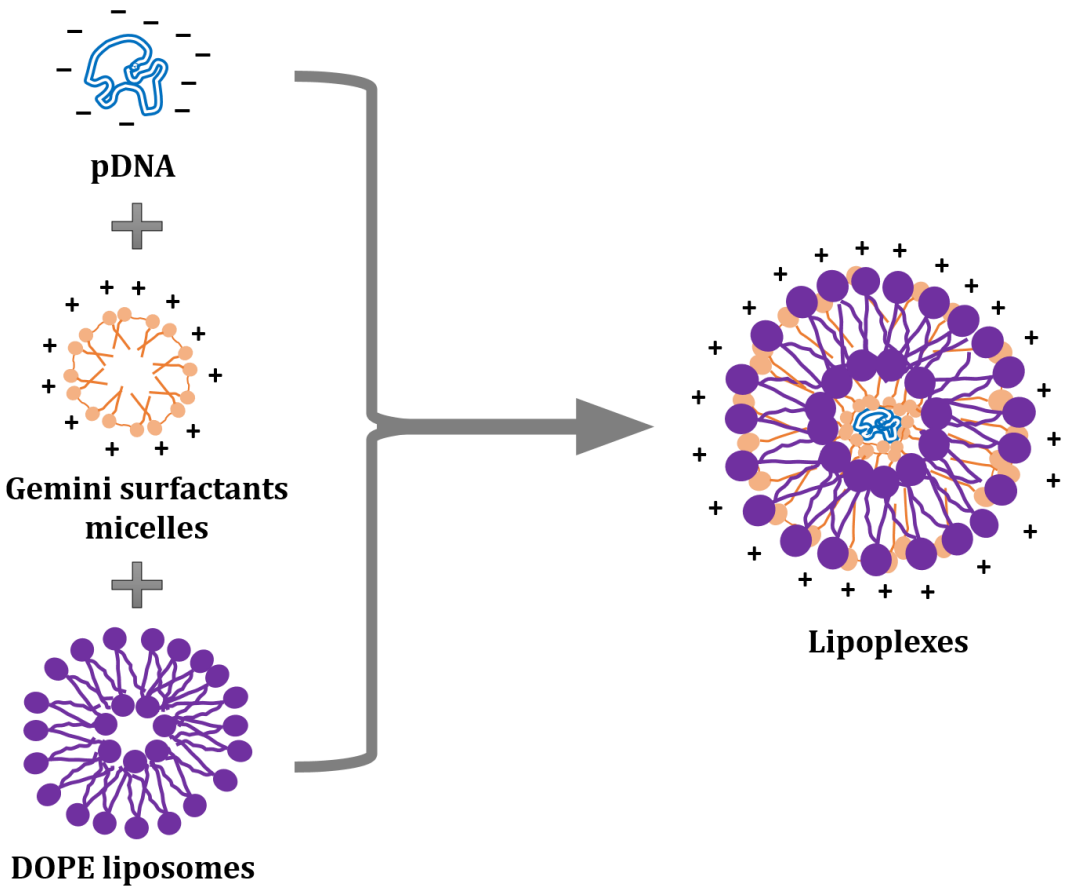

Figure 1.2. Schematic representation of the gemini surfactants-based gene delivery system shows the constituent part of the gemini surfactant-based lipoplexes. Cationic gemini surfactants interact with the negatively charged pDNA through electrostatic interaction and cooperative hydrophobic interaction of the alkyl tails. The complex is usually combined with a liposomal system such as DOPE to form lipoplexes.

The nature of the interaction between the nucleic acids and the gemini surfactants controls critical steps such as pDNA compaction and subsequent intracellular release [105]. The supramolecular arrangement of the gemini surfactants in a micellar dispersion will determine the structural arrangement of the pDNA-gemini surfactant complexes [106]. Gemini surfactants have the ability to self-assemble into a wide variety of aggregate structures depending on the proportion between the tail and head regions, depicted by the lipid packing parameter, *P* [107].

$$P = V/a_0 l$$

Where V is the volume of the hydrophobic chain, l the length of the hydrophobic chain and a_0 is the surface area occupied by the head group. The *P* value gives an insight about the preferred curvature of the structure. For example an *P* value of 0.3 is typical for spherical micelle structure, a bilayer structure forms when $P = 1$, and $P > 1$ gives an inverted micellar organization [108]. Thus, *P* values can be rationally modified to form various aggregate structures by varying one or more of the following: 1) the head group size and valence, 2) the tail length and its degree of unsaturation, and 3) and the spacer length.

1.3.3.1. Rational design

Gemini surfactants' unique structure offers virtually endless possibilities for structural modifications, allowing for a "fine-tuning" of their physicochemical characteristics which in turn can modulate transfection efficiency and cytotoxicity. Over the past quarter century, a large variety of gemini surfactants have been synthesized by combination of various head groups, spacer regions and hydrophobic domains. A detailed understanding of the role and impact of each structural modification is a fundamental step before any translation into clinical settings.

1.3.3.2. Effect of head group and spacer

The positively charged head group of the gemini surfactants is considered the main driving force for the electrostatic interaction with the negatively charged genetic material, which results in compacting the nucleic acid into nano-sized lipoplexes and shielding it from further degradation by enzymatic activity [108]. As such, the nature, size and charge density of the gemini surfactant head group greatly impacts the physicochemical characterization, toxicity and transfection efficiency of the delivery system [108-111].

The spacer region of the gemini surfactants also plays a crucial role in determining the efficiency of the delivery system. It impacts the shape and size of the gemini surfactants affecting the self-assembly process and the CMC value [108-111]. In addition, the length and composition of the spacer greatly influence the binding of the gemini surfactant with the DNA [108-111]. The following section will briefly highlight the most commonly used cationic gemini surfactants' head groups and spacer modifications, discussing their impact on the gene delivery process.

A) Quaternary ammoniums head groups

Cationic gemini surfactants bearing quaternary ammonium head groups are, by far, the most extensively studied class of gemini surfactants, mainly due to their ease of preparation and efficiency in compacting the genetic material [112]. They were first introduced in Menger's seminal paper in 1991[102], after which a series of compounds have been synthesised and utilized in delivering genetic materials both *in vitro* and *in vivo* [109].

In our lab, we built on the basic structures of gemini surfactants with quaternary ammonium head groups and adopted a rational design approach by conducting component-by-component testing, aimed at improving their ability to deliver DNA while minimizing toxicity.

The first generation is the cationic *N, N*-bis(dimethylalkyl)-α,ω-alkane-diammonium which is the simplest and the most frequently encountered family of gemini surfactants with the general formula [$C_mH_{2m+1}(CH_3)_2N^+(CH_2)_s N^+(CH_3)_2 C_mH_{2m+1}.2X^-$], abbreviated as *m-s-m*, where *m* = the number of carbon atoms in the alkyl tails, s = the number of carbon atoms in the spacer and X = the counter ion (Table 1.5, group 1) [113, 114]. In the *m-s-m* family, modifications to the gemini surfactants' architecture by varying the length of the spacer (s = 2-16) induced significant differences in the level of the transfection efficiency. An *in vitro* transfection study in murine keratinocytes (PAM 212) revealed that compounds with s = 3 exhibited the highest level of gene expression and had a lower toxicity profile than the commercially available transfection agent, Lipofectamine Plus™ [113]. This was attributed to the distance between the two amine groups (0.49 nm) which is suitable for optimal electrostatic interactions with the two adjacent phosphate groups in the DNA backbone that have a distance of 0.34 nm [113]. Further elongation in the spacer was accompanied by a decreasing trend in the transfection up to s = 8, after which the transfection efficiency increased gradually [113]. This was explained by the folding of the spacer into a U-shape as a function of spacer elongation resulting in a decrease in the distance between the two amine head groups especially with s = 12-16. *In vivo* topical application of the lead compound-based lipoplexes, 16-3-16, revealed a significant level of the transgene expression, demonstrating the promises of this family as effective non-viral gene delivery vectors [113, 115, 116].

In light of the apparent importance of the distance between the two amine head groups in the interaction with the DNA, a second generation of gemini surfactants was proposed by inserting secondary or tertiary amine functional groups in the spacer region in an attempt to improve transfection. The gemini surfactants 12–7NH–12 ,12–7N(CH_3)–12 , 12–5N(CH_3)–12 and 12-8N(CH_3)-12 (Table 1.5, group 2) were evaluated in COS-7 cell-line [117]. Experimental

data showed that compounds with a three methylene (CH_2- CH_2- CH_2) separation between adjacent nitrogen centers, such as 12–7NH–12 and 12–7N(CH_3)–12 exhibited higher level of transfection compared to compounds separated with merely two methylene (CH_2- CH_2) moieties, 12–5N(CH_3)–12 and 12-8N(CH_3)-12 [117]. The findings demonstrate the significance of optimal spacing between the nitrogen atoms within the spacer region [117]. In addition, 12–7NH–12 exhibited higher level of gene expression with 9-fold increase compared to an unsubstituted gemini surfactant 12-3-12 and a 3-fold increase compared to the aza analog, 12–7N(CH_3)–12. This was explained by the pH-dependent change in morphology arising from the protonated secondary amine functional group [117].

In an attempt to enhance the transfection of the second generation gemini surfactants and reduce their cytotoxicity, a third generation of structures were designed in our laboratory, by coupling amino acids onto the N position of the spacer region of the 12-7NH-12 gemini surfactant [118]. Novel compounds with the general chemical formula $C_{12}H_{25}(CH_3)_2N^+(CH_2)_3$-N(AA)-$(CH_2)_3$-$N^+(CH_3)_2$-$C_{12}H_{25}$ where AA= glycine, lysine, glycyl-lysine or, lysyl-lysine (Table 1.5, group 3) were evaluated in three different cell-lines, namely monkey kidney fibroblasts (COS-7), rabbit epithelial cells, and murine keratinocyte cells [118]. Results showed that the compounds substituted with either glycine or glycyl–lysine moieties had higher transfection efficiency compared to the unsubstituted compound, 12-7NH-12, in all the tested cell lines [118]. The insertion of amino acids provides additional terminal amino groups that contribute to: (i) enhanced binding to the cell membrane by forming additional hydrogen bonding, (ii) improved gemini surfactant-DNA electrostatic interactions due to the high pK_a value of the terminal amines and (iii) induced liposomal fusion through a flip-flop mechanism due to the strong electrostatic interaction between the nanoparticles and the cell membrane [118, 119]. Additionally, cytotoxicity

of the third generation compounds was as low as the parent unsubstituted compound and significantly lower than commercial Lipofectamine Plus™ demonstrating the intrinsic biocompatibility of amino acids [119]. In order to assess their *in vivo* behavior, the glycyl-lysine substituted gemini surfactant-based lipoplexes was topically applied onto rabbit vaginal cavities, exhibiting higher transgene efficiency compared to the parent compound without visible toxicity [120].

In order to capitalize on the potential of amino acid modified gemini surfactants as effective and safe gene delivery vectors, further modification to the third generation gemini surfactant structure is needed to augment their performance. This research evaluates a new family of peptide-modified gemini surfactants having various structural modifications, hoping to establish a comprehensive structure-activity relationship. The long-term goal is to develop a model that could predict transfection efficiency of the gene delivery nanoparticles from the structural characterization/organization of these particles. This model might become a design tool for new delivery materials that have optimal delivery characteristics beyond existing gemini surfactants

B) Heterocyclic head group

Heterocyclic chemical groups such as pyridinium, pyrolidinium and imidazolium were incorporated into the gemini surfactants as 'softer' charged systems than quaternary amines. This was attributed to the delocalization of the positive charge on several atoms of the heterocyclic head group [121]. As such, heterocyclic head groups can mediate for a balanced interaction with the nucleic acid accommodating for both processes of genetic material compaction and subsequent release [121, 122]. In addition, the lower charge density of the heterocyclic-based gemini surfactants minimized the repulsion between the adjacent gemini surfactants, resulting in lower

CMC compared to the ammonium-based gemini surfactants [121]. A low CMC value in gemini surfactants usually translates into higher transfection efficiency owing to the enhanced stability of the lipoplexes during the delivery process [123].

Several generations of gemini surfactants with heterocyclic head-groups were introduced over the last two decades showing promising results [95, 121, 124, 125]. The impact of varying the spacer length on the transfection efficiency was more pronounced compared to the gemini surfactants bearing quaternary ammonium head groups. This was linked to the larger steric demand of the heterocyclic head groups relative to quaternary ammonium head groups. Engberts *et al* were the first to synthesize pyridinium gemini surfactants with four hydrophobic chains varying the length of the aliphatic spacer (*s* = 3, 4 and 5) (Table 1.5, group 4) [95]. Transfection studies conducted on the COS-7 cell-line revealed that the compound with spacing s = 4 exhibited the highest transfection efficiency compared with the shorter s = 3 or longer s = 5 spacers, however, no clear explanation was presented [95]. In another study, pyridinium cationic gemini surfactants having two aliphatic chains and various spacer lengths (*s* = 3, 4, 8 and 12) (Table 1.5, group 5) were evaluated in a human rhabdomyosarcoma cell line [124]. Similar to past observations [95], gemini surfactants with s = 4 exhibited the highest transfection efficiency among the tested compounds [124]. It was suggested that a spacer of 4 carbons allowed the compound to act like molecular tongs gripping the basic groups near each other, resulting in efficient compaction of the DNA [124].

Unlike quaternary ammonium head group gemini surfactants,[117] the insertion of secondary amine functional groups in the spacer region did not translate into an increase in the transfection efficiency (Table 1.5, group 6) [126]. This was explained by the strong interaction with the DNA that impedes its release upon cellular entry. The authors tested this theory by

assessing the transfection activity of the gemini surfactants' Boc-protected synthetic precursors (Table 1.5, group 7) [126]. Results supported the hypothesis revealing a five-fold increase in the transfection efficiency in the Boc-protected precursor-based lipoplexes [126].

C) Glycosylated head groups

The replacement of the head group region with acyclic carbohydrate moieties such as glucose and mannose resulted in the production of what is known as the sugar-based gemini surfactants [127]. Since sugars are nontoxic, biodegradable materials, less cytotoxicity is expected for sugar-based gemini surfactants. In addition, some mono-carbohydrates, such as mannose and galactose have been used as a targeting ligand for specific tissues and cells. For example, mannose-containing lipoplexes were efficiently recognized by mannose receptors expressed in the liver and macrophages exhibiting higher gene expression both *in vitro* and *in vivo* [128].

Engberts *et al.* were the first to synthesize sugar-based gemini surfactants and explore their structure activity relationship by examining the effects of the head group size, carbohydrate stereochemistry as well as the length and nature of the spacer region (Table 1.5, group 8) [129, 130]. Results suggested that neither variations in the head group nor the spacer significantly impacted the level of transfection efficiency [130]. However, the use of an aliphatic chain spacer was remarkably more toxic than the use of a more hydrophilic spacer such as ethylene oxide [130].

Sugar-based gemini surfactants adopted a pH-dependent aggregation behavior in an endosome simulated environment [131-133]. Upon gradual acidification, sugar-based gemini surfactant lipoplexes exhibited different phase behaviors, namely lamellar phase and inverted hexagonal phase [131, 133]. Adopting such a phase transition can assist in the escape of the vector from the late endosomal compartment and the possible release of the DNA cargo.

D) Amino acids head groups

The incorporation of amino acids into the gemini surfactant head groups was aimed at producing lipoamino acids mimicking compounds with biocompatible and biodegradable features [134, 135]. Both basic (e.g. lysine) and aromatic (e.g. serine) amino acids were successfully utilized in delivering genetic materials showing a reduced cytotoxicity [134-137]. In addition to the fact that amino acids are naturally-occurring non-toxic compounds, they possess multifunctional properties, such as the presence of a chiral center in the amino acid. The chirality induces changes in the molecular orientation, allowing the formation of a wide variety of aggregate structures [138]. Furthermore, amino acids are pH sensitive motifs that respond to the pH drop in the endosomal compartment resulting in the release of the encapsulated genetic material, resulting in higher transfection efficiency [139].

Varying the spacer length and the nature of the amino acid head group-gemini surfactants did not translate into major differences in transfection efficiency. For example, experimental data of gemini surfactants composed of two *N*-acyl-lysines linked through a di-amine spacer (Table 1.5, group 9) revealed no changes in the transfection efficiency upon changing the spacer length [134]. This could be attributed to the distance between the cationic charges and the spacer which led to a negligible role for the spacer (Table 1.5, group 9) [134].

The nature of the linkage (amine, amide and ester) between the spacer and the head groups was also evaluated in a series of serine-based gemini surfactants (Table 1.5, group 10) [137]. Transfection studies exhibited contradicting results between the tested cell-lines: human embryonic kidney cells and human epithelial cervical carcinoma cell line, which prevent drawing a solid conclusion [137]. However, it was suggested that the C–O bond in the ester series made the

spacer more flexible which resulted in optimized interaction with the DNA and lowered cytotoxicity [137].

Table 1.5. Chemical structure of gemini surfactants used as gene delivery vectors

1. Quaternary ammonium gemini surfactants (1st generation)	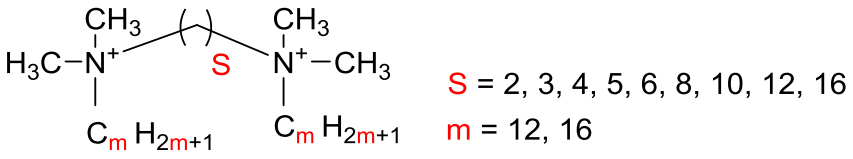
2. Quaternary ammonium gemini surfactants (2nd generation)	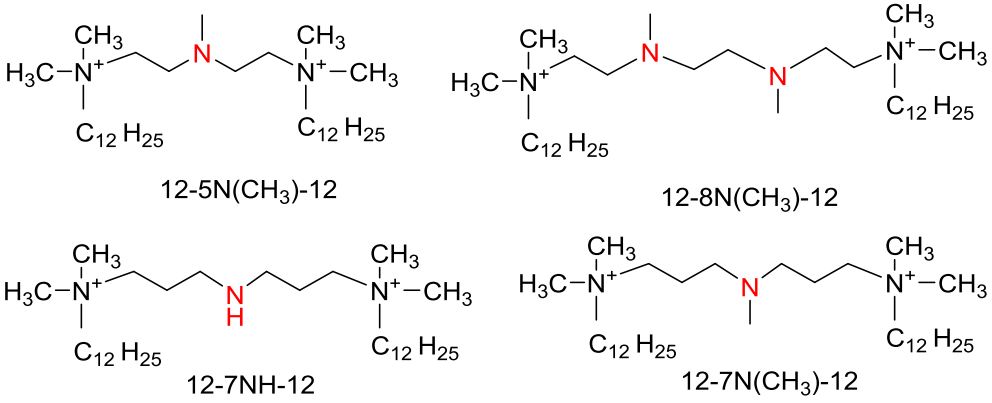
3. Quaternary ammonium gemini surfactants (3rd generation)	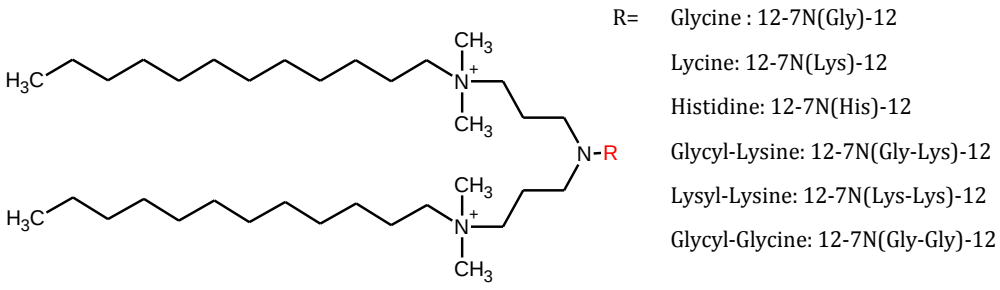
4. Pyridinium gemini surfactants	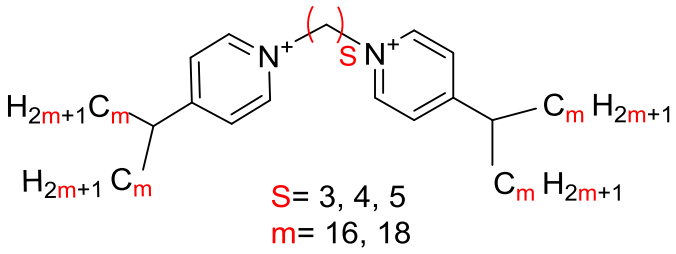

5. Pyridinium gemini surfactants	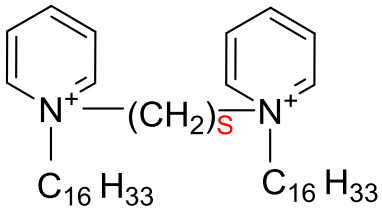 S= 3, 4, 8, 12
6. Pyridinium gemini surfactants	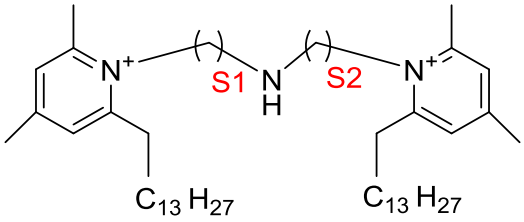 Spacer compinations : $(CH_2)_2NH(CH_2)_2$ $(CH_2)_3NH(CH_2)_3$ $(CH_2)_3NH(CH2)_4$ $(CH_2)_3NH(CH_2)_4NH(CH_2)_3$
7. Pyridinium gemini surfactants	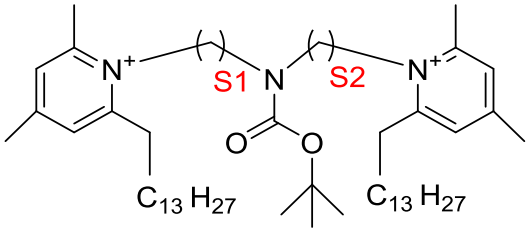 Spacer compinations : $(CH_2)_2NBoc\ (CH_2)_2$ $(CH_2)_3NBoc\ (CH_2)_3$ $(CH_2)_3NBoc\ (CH_2)_4$ $(CH_2)_3NBoc(CH_2)_4NBoc(CH_2)_3$

8. Carbohydrate based gemini surfactants	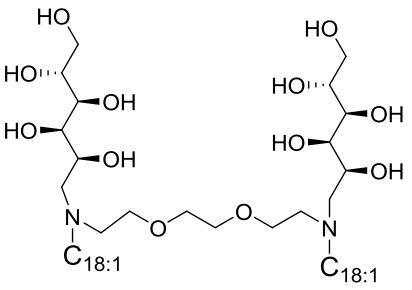 **GS1** 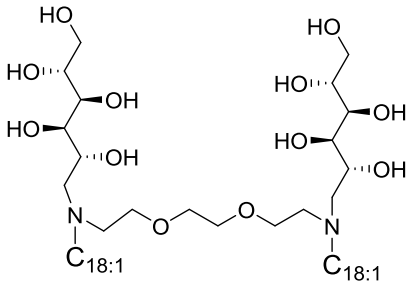 **GS2** 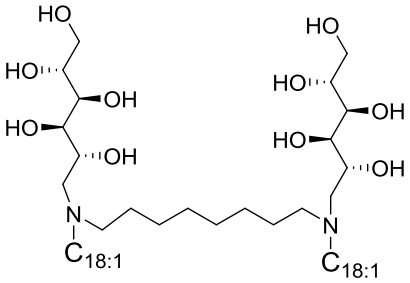 **GS3** 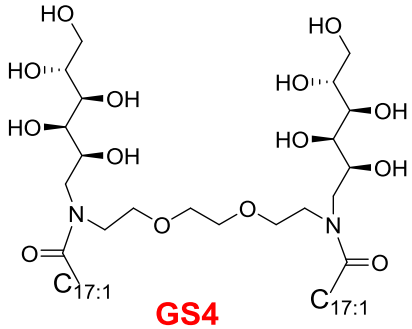 **GS4** 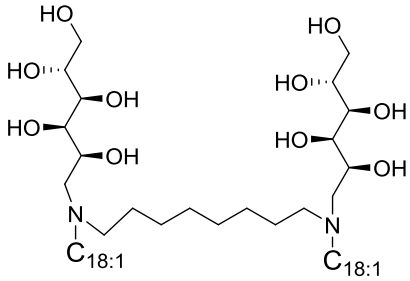 **GS5**
9. Amino acid gemini surfactants	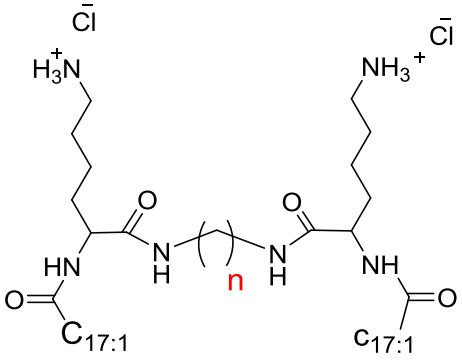 **n=4,6 or 8**

10. Amino acid gemini surfactants	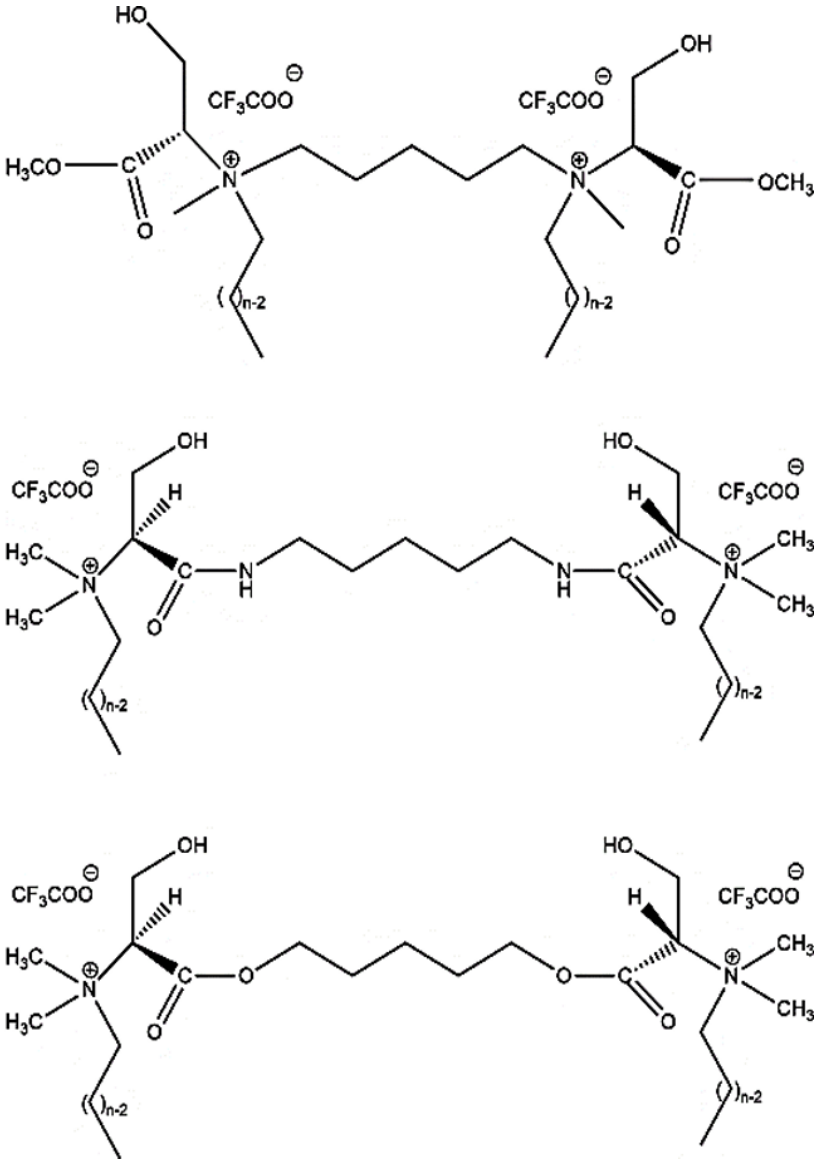

1.3.3.3. Effect of the hydrophobic tail

The hydrophobic domain of gemini surfactants impacts their interactions with the hydrophobic domain of the DNA. It also affects the aggregation behaviour, shape of the supramolecular assembly and membrane fluidity. The following section briefly explores the most common structural variation of the hydrophobic domain of gemini surfactants and their influence on biological activity.

A) Aliphatic Tail length

An aliphatic tail is, by far, the most widely used hydrophobic domain in gemini surfactant-based gene carriers. The length of the alkyl tail was found to significantly alter the physicochemical characteristics of gemini surfactants, affecting their efficacy to deliver the genetic material [113, 136, 140, 141]. Several studies have suggested that an increase in the tail length could be translated into superior transfection efficiency [136, 140]. Since the cooperative hydrophobic interaction between the tail groups plays a key role in the interaction with the nucleic acid, increasing the alkyl tail length (higher hydrophobicity) produced a stronger DNA interaction [142, 143]. In fact, Matulis *et al* revealed that the addition of a methylene group in the aliphatic lipid chain led to an increase of the lipid-DNA binding constant by 4 fold [144]. In addition, alkyl tail elongation is associated with decrease in the aggregation properties and the CMC [145], resulting in a higher tendency of gemini surfactants to self-assemble with enhanced stability [146].

It should be noted that increasing the alkyl tail length may have negative consequences. Longer chains will elevate the micelles critical temperature (Krafft temperature) which cause the supramolecular assemblies to become stiffer at physiological temperature [147]. This will

eventually interfere with the lipid mixing at the cellular membrane affecting both cellular uptake and endosomal escape. In addition, further elongation in the alkyl tail might produce a larger particle size which could affect critical steps, such as the route of cellular entry, rate of cellular uptake, and intracellular fate [121, 148, 149].

Although several studies have attempted to identify the optimal alkyl tail length, a definitive conclusion is rarely obtained due to the complex interplay between the head group, the spacer region and the nature of the tail that is specific to each series of gemini surfactants. Nevertheless, high transfection efficacy was usually achieved when the tail length falls within the range of 12 to 18C [109].

B) Degree of unsaturation and stereochemistry

The use of unsaturated hydrocarbon tails is a common structural modification that has been extensively assessed in the literature to optimize the transfection efficiency of gemini surfactants. The the introduction of unsaturation (double and triple bond) in the surfactants tails resulted in an increased CMC compared to the saturated equivalents [150]. In addition, it lowered the Krafft temperature below the physiological temperature resulting in enhanced susceptibility of the nano-assemblies to morphological changes at physiological temperature, which in turn will ease the process of lipid mixing (membrane fusion) during endocytoses [151]. Thus, unsaturation of the alkyl tail can be used as a strategy to overcome the stiffness of the supramolecular assemblies that occurs at physiological temperature with tail elongation.

Membrane fluidity is an essential requirement for successful gene transfer as it greatly impacts critical steps such as membrane fusion and endosomal escape [152]. Unsaturated hydrophobic tails are known to have higher membrane fluidity than saturated ones [153, 154]. This

is mainly linked to the geometrical characteristics of the unsaturated bond that hamper the packing of lipids at the molecular level inducing a looser packing arrangement.

The stereochemical arrangement of the unsaturated hydrophobic tails is another important factor in determining the transfection efficiency of the lipid-based gene delivery systems [155]. There is an apparent debate in the literature on whether trans or cis configuration is more favorable for higher transfection, however, the overwhelming majority of evidence showed that cis orientation is a better choice for higher transfection [129, 140]. A cis-configured double bond is expected to hamper the lipid packing more than a trans-configured bond, resulting in a higher CMC value [150].

The position of the double bond or the triple bond in the alkyl chain is an additional parameter that should be considered when the effect of unsaturation is evaluated. The position of the double bond can affect the CMC and the lipid packing arrangement within the supramolecular assembly [150]. For example, unsaturation adjacent to the head group or at the end of the alkyl chain has a smaller effect on the aggregation properties than a double or triple bond in the middle of the alkyl tail. This could be attributed to the lesser impact in hampering the packing of the lipids when the unsaturation is positioned around the extremities [150]. Despite the added advantages of unsaturation via decreasing the compounds' melting point and increasing solubility, the existence of unsaturation makes the compound more susceptible to oxidation reducing stability during storage [156].

C) Asymmetry

The above sections focused on the most commonly used gemini surfactants, namely symmetrical compounds. The last decade, however, has witnessed a growing interest in the use of asymmetrical gemini surfactants, *m-s-n* where m ≠ n [157-159]. Thermodynamic studies reported no major differences in the aggregation behaviour when the number of m + n is equal to the total carbons number in the tails of the corresponding symmetrical analogs [157, 158]. However, in compounds where m was fixed but n varied, resulting in different degrees of asymmetry, the CMC was decreased and the micellization process was significantly altered [160]. In order to assess how such results could affect the DNA complexation, a series of gemini surfactants with different degrees of asymmetry have been synthesized. A weaker interaction with the nucleic acid and gemini surfactants was attained with higher degree of asymmetry due to disruption in the intermolecular hydrophobic interactions [159].

1.4. Topical lipid-based gene therapy

1.4.1. Skin as target organ for gene delivery

Topical application of genetic materials into the skin is an attractive method for gene delivery because of the numerous advantages over other routes of delivery. It is a pain-free, convenient and easy to administer method, which could enhance patient compliance and reduce the need for costly health care services. The skin is a highly accessible organ that provides an ideal site for gene administration due to the potential for visual monitoring of the treated area and timely intervention if unwanted side effects appeared [161]. In addition, skin represents an excellent site for the induction of adaptive immune responses since it is rich in potent antigen presenting cells [162]. As such, DNA-immunization is a highly promising application of topical gene delivery. Despite all the advantages associated with the use of skin as a target organ, it

represents a formidable barrier to the penetration of drugs. Thus understanding the skin structure is a fundamental step toward the design of efficient delivery system.

Skin is the largest organ of the human body with a surface area of about 1.7 m^2 corresponding to 10% of the total body weight of an average adult. It consists of three anatomically distinct layers: the epidermis, dermis and hypodermis in addition to a number of additional features such as hair follicles, sweat glands and sebaceous glands [163] (Figure 1.3). More than 90 % of the epidermis is keratinocytes alongside other cell types such as melanocytes, Langerhans cells and Merkel cells [163]. It is comprised of four distinct layers: the stratum corneum, stratum granulosum, stratum spinosum and stratum germinativum [163]. The stratum corneum (SC) (or horny layer) is the outermost layer of the epidermis and it represents the rate-limiting step for the penetration of drugs through the skin [164]. It consists of protein-rich corneocytes packed within an extracellular lipid matrix forming a "brick and mortar" arrangement. The thickness of the SC is dependent on the anatomical site, age, sex and disease status [165]. The stratum granulosum is the layer below the SC; it is also referred to as the granular layer due to the presence of three layers of granular cells which are characterized by the presence of intracellular keratohyalin granules in the cytoplasm [163]. Below the stratum granulosum is the stratum spinosum or prickle cell layer which consists of two to six rows of polygonal shaped keratinocytes [163]. The stratum germinativum (basal layer) is the innermost layer of the epidermis that is the main residence of melanocytes, Langerhans cells and Merkel cells within the epidermis in addition to mitotically active columnar shape keratinocytes [163].

The epidermis binds tightly to the dermis through the dermal-epidermal junction membrane which provides adequate mechanical support to the epidermis and serves as selective barrier to regulate molecular and cellular exchanges between the two layers. The dermis is the

connective tissue bulk component of the skin; it is comprised of cells (mainly fibroblasts), fibrous proteins (75% collagen) and aqueous ground substances [163]. The thickness of the dermal layer is mainly dependent on the body region providing the required pliability, elasticity, and tensile strength to the skin and protecting the body from external mechanical injuries. The hypodermis (subcutis) is a fatty tissue that represents the innermost layer of the skin [163]. It is composed mainly of adiopocytes and plays an important role in maintaining body temperature.

Drug molecules penetrate the skin layers through two main routes: transepidermal and transappendageal [166]. The permeating molecule can cross the skin by either one of the routes or a combination of both pathways, depending on its physicochemical properties. Transepidermal routes transport drug molecules across the SC using transcellular (through the corneocytes) and/or intracellular pathways (through intercellular lipid domains) [164] (Figure 1.3). On the other hand, transappendageal routes (shunt routes), transport drugs via sweat gland ducts, hair follicles and associated sebaceous glands [164]. In theory, the relatively large size of the sweat glands pores and hair follicles opening can make the penetration of large genetic material possible. However, the appendages cover only 0.1% – 1% of the total skin surface indicating the insignificance of this route. In addition, natural secretions (sweat and sebum) can hamper drug penetration. As such, it is important to understand the particularities of these routes in the drug design and delivery process. It is also critical to recognize the limitations of dermal drug delivery in order to tailor delivery systems that can overcome these limitations.

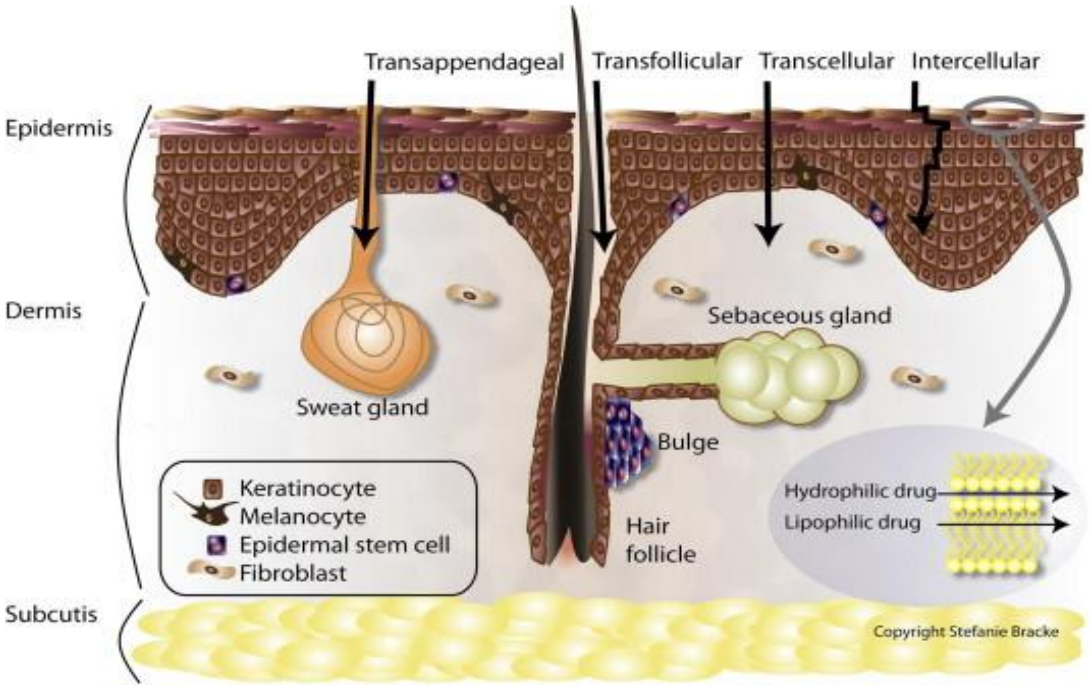

Figure 1.3. Diagrammatic cross section of human skin showing the different cell layers, appendages and possible routes of particle penetration. *Reprinted from the European Journal of Pharmaceutical Sciences, Vol 43, Lipid-mediated gene delivery to the skin, P 199-211, ©2011, with permission from Elsevier.*

1.4.2. Barriers for topical gene therapy

The stratum corneum (SC) is the main physical barrier of the skin that hinders both topical and transdermal drug delivery. This could be attributed to its lipid-rich nature and unique chemical arrangement embodied by the brick and mortar model. In addition, the SC high turn-over rate, acidity and the presence of enzymatic activity provide additional restriction to the delivery process [165]. The physicochemical properties of the candidate drug such as lipophilicity, size, surface charge, pKa and partitioning coefficient govern the diffusion into or through the skin [164]. For example, uncharged lipophilic drugs with a molecular weight less than 500 Dalton are believed to penetrate the skin passively [167]. Furthermore, the concentration of the drug, site

of application, disease state of the skin, age and the application method can determine the amount of the drugs that penetrate the SC. Macromolecules, such as the high molecular weight negatively charged DNA do not pass the epidermis layer. Thus, active strategies as efficient delivery systems need to be employed.

1.4.3. Lipid-based carriers for skin gene delivery

In recent years, there has been an increased interest in examining the potential of lipid vesicles as carriers for skin gene delivery. Several types of lipid vesicles have emerged such as classical liposomes, cationic liposomes, niosomes, Transfersomes®, and others. Phospholipids are the main constituent of classical liposomes that offer numerous advantages for skin gene delivery. The chemical composition of phospholipids is similar to the composition of skin lipids and cell membrane [168]. As such, phospholipid-based liposomes can fuse with the epidermal lipids, destabilizing the lipid matrix and enhancing drug penetration[169]. In addition, most phospholipids are non-toxic and biodegradable minimizing the possibility of side effects [170]. Cholesterol might be added to classical liposomes to enhance bilayer characteristics. It increases the membrane microviscosity, reducing permeability to water soluble molecules [171]. This in turn enhances the rigidity and stability of the vesicles [171].

The transappendageal follicular pathway is the main route of gene delivery with classical liposomes; however, conflicting results have suggested that the transepidermal pathway may also be significantly involved [172]. Although classical liposomes have been widely investigated for their potential application in topical gene therapy [173], the level of gene delivery has not been satisfactory. Combinations with other delivery enhancing strategies that disturb the SC are needed. Thus, the emergence of new delivery systems that achieve a high level of gene expression is necessary, as outlined below.

The addition of an edge activator to phospholipids led to the formation of highly elastic deformable vesicles named Transfersomes® [174]. An edge activator is a single chain surfactant that is capable of destabilizing the lipid bilayer. It increases the vesicle deformability and elasticity by decreasing the interfacial tension [175]. Therefore, improved penetration through the intercellular lipids of the SC is achieved. Different types of edge activators have been introduced such as sodium cholate, sodium deoxycholate, Tween 80, Tween 20 and Span 80[173]. The type of the edge activator plays a crucial part in determining the extent of transdermal absorption. For example the use of cholate-based Transfersomes® showed the best results in topical DNA delivery compared to other edge activators [173].

In order to ameliorate the efficiency of the previously described vascular systems, niosomes vascular system was first introduced by L'Oreal as a drug carrier for cosmetic applications[176]. Niosomes are composed of single-chain synthetic non-ionic surfactants such as diacylglycerides, saccharose diesters, polyoxyethylene alkyl ethers or polyoxyethylene alkyl esters with cholesterol [173]. Although niosomes appear to have the same physical properties as liposomes, niosomes showed better chemical stability and enhanced penetration into the skin. The surfactants' solubilization properties improve the mixing of niosomes with skin lipids causing an alteration in the structure of the SC in the intercellular layers which in turn enhances the penetration through the skin [177].

Cationic lipids are another category of lipid-based carriers that has been widely investigated as a non-viral gene delivery system for skin gene therapy. Through their positive charge, they induce an electrostatic interaction with negatively charged DNA leading to the formation of nano-sized lipoplexes that shield the DNA from enzymatic degradation. In addition, charge-mediated interactions with the skin surface have a crucial role in the passive delivery

across the skin [178]. Cationic lipids have the ability to passively target tumors taking advantage of the leaky tumor vasculature, hence increasing gene delivery to the target cancerous tissue. Furthermore, cationic lipids can act as an adjuvant for immunotherapy as they are preferentially taken up by immune cells [179]. The first *in vivo* lipid-mediated gene transfer study into the skin of a living animal model was conducted by Alexander and Akhurst in 1995 [180]. The cationic lipid DOTAP was complexed with pDNA encoding for β-galactosidase at a ratio of 1:1.6 (w/w). Rapid gene expression was achieved (after 6 h) in the hair follicle, epidermis and also in the deeper layers of the dermis and lasted up to 48 hours [180]. The level of gene expression was dependent on the phase of hair cycle growth indicating the importance of transfollicular routes in lipid-based DNA delivery [180]. Since then, the use of cationic lipids has captured increased interest as an important component in topical gene delivery.

The incorporation of cationic lipids into other vascular systems such as niosomes or Transfersomes® alters the charge of these vascular systems resulting in the formation of cationic niosomes and cationic Transfersomes® vesicles. Cationic niosomes or Transfersomes® take advantage of both systems producing carriers that are more efficient and more tailored for gene delivery. Kim *et al.* investigated the ability of cationic Transfersomes® constructed from DOTAP and sodium cholate to transfect intact hair-removed dorsal skin of mice with pDNA encoding for green fluorescent protein (GFP) [181]. GFP expression was detected in some organs such as the liver and the lungs up to 6 days, demonstrating a promising approach for non-invasive gene delivery. In addition, cationic Transfersomes® composed of the cationic lipid DOTMA and sodium deoxycholate were employed for topical vaccination against hepatitis B in Balb/c mice [182]. A high immune response was provoked producing a serum antibody titer and endogenous cytokine levels comparable with those produced by intramuscular injection of

recombinant hepatitis B surface antigen (HBsAg) [182]. More recently, cationic niosomes made of dimethyl dioctadecyl ammonium bromide (DDAB), Tween 61 and cholesterol were loaded with pDNA encoding human tyrosinase and evaluated for their potential as drug carriers for topical vitiligo therapy [183]. Transdermal absorption through rat skin was conducted using Franz diffusion cells demonstrating four-fold higher tyrosinase activity than the free plasmid [183].

The use of cationic gemini surfactant-based lipoplexes for skin gene delivery was firstly conducted by Badea et al. to treat scleroderma [115]. Cationic gemini surfactants *N, N′*-bis(dimethylhexadecyl)-1,3-propanediammonium dibromide (designated as 16-3-16) was formulated with pDNA encoding for IFN-γ in the presence of DOPE, DPPC and penetration enhancer and administrated into IFN-γ-deficient mice. A three-fold increase in transgene expression was achieved in the animals treated with gemini surfactant-based lipoplexes compared to animals treated with a plasmid DNA solution indicating the promise associated with the use of gemini surfactants [115]. This research will capitalize on the use of a new generation of dicationic gemini surfactants: peptide-modified gemini surfactants as potential carriers for skin gene delivery.

1.5. Biological fate of topical lipid-based gene carrier

Upon topical application, lipid-based nanoparticles distribute within various tissues and cellular components [115, 180, 181]. As of yet, the ultimate fate of the building constituents of the lipid-based nanoparticles has not been fully understood. Many questions remain unanswered regarding the degradation profile of nanoparticles after releasing their therapeutic cargo including the formation of metabolic breakdown by-products, some of which may be toxic. Correlating the biodistribution and the biological fate of the nanoparticles to their chemical structure and physicochemical properties will provide insights into the rational design process to produce lipid-based gene carriers with higher efficiency and reduced toxicity.

Fluorescently labeled and radiolabeled carriers have been widely utilized in tracking the fate and distribution of lipid-based nanoparticles [174, 184, 185] . For example, Cevc and Blume used radioactive ^{3}H-DPPC to follow the fate of dermally applied lipids after both occlusive and non-occlusive application [174]. Two kinds of vesicles systems; classical liposomes and transfersomes, were applied onto intact mouse skin to investigate the influence of lipid composition on biodistribution. Results showed that with the use of liposomes or occluded transfersomes, up to 25% of the total dose was associated with the SC and a few percent was localized in the deeper epidermal layers [174]. However, the use of transfersomes under non-occlusive conditions resulted in the detection of 30±10% of the applied lipids in the subdermis and up to 6–8% in the blood [174]. These results indicate the importance of both the method of the application and the liposomal composition on the nanoparticles biodistribution. Similar to radiolabeling, fluorescently labeled lipid-vesicle biodistribution was monitored using confocal laser scanning microscopy after topical application onto intact murine skin [185]. Results confirm the penetration

of the liposomes through the skin to the systemic circulation, indicting the feasibility of using fluorescent labelling in tracking lipid based carriers [185].

Despite promising results, the use of fluorescent and radioactive labeling could have a considerable effect on the pharmacokinetic profile by altering the physicochemical properties of the delivery system [186]. A research group in Belgium has recently conducted a detailed study on the effect of fluorescent labeling density on the intracellular trafficking of lipid-based DNA delivery systems. It was shown that with higher labeling densities, the affinity of pDNA for lipids increased, influencing the dissociation of DNA from lipoplexes which may alter the endosomal escape and consequently reduce the transfection efficiency [186]. In addition, labeling strategies are limited to qualitative and semi-quantitative assessment of the biodistribution of lipid-based nanoparticles [184, 187]. As such, there is a sense of urgency to use more reliable techniques to monitor the fate and biodistribution of the gene carriers within biological matrices.

Mass spectrometry (MS) is a powerful analytical tool that is used for both quantitative and qualitative applications [188-191]. It is widely applied in the field of pharmaceutical research due to its sensitivity, accuracy, and high throughput capability [192-194]. The presence of two permanently charged quaternary ammonium groups and the lack of a chromophore or fluorophore on the gemini surfactants make MS the technique of choice for the identification and quantification of gemini surfactants. In our lab, MS was used to study the fragmentation mechanism of different families of diquaternary ammonium gemini surfactants and to establish universal tandem mass spectrometric (MS/MS) fingerprints for accurate identification of gemini surfactants within complex biological matrices [195-198]. Furthermore, liquid chromatography tandem mass spectrometry (LC–MS/MS) methods were developed for the quantification of first and second generations gemini surfactants within PAM212 murine keratinocytes to determine

the rate of cellular uptake and removal [199-201]. Ongoing research includes the identification and quantification of two structurally distinct gemini surfactants within transfected PAM212 keratinocytes that possess distinct cytotoxicity profiles. MS will be employed to investigate the subcellular localization and to detect and quantify any potential metabolites in order to establish structure–toxicity correlations, which will give insights into the rational design process.

In this research, MS will be utilized to detect and quantify topically applied diquaternary ammonium gemini surfactants in an ex-vivo skin model of CD1 mice and a biologically relevant buffer to assess their cutaneous deposition and penetration behaviour. Understanding the MS/MS fragmentation behavior will be required for the development of multiple reaction monitoring (MRM) FIA–MS/MS method. The method can be used in the future to track the fate and biodistribution of gemini surfactants. Such knowledge is needed to guide the development of effective gene delivery system.

1.6. Rationale

Gene therapy is a promising therapeutic approach predicated on the intentional modulation of gene expression in cells to treat genetic disorders, both inherited and acquired. Current focus is on the design of "intelligent" nanoparticles that respond to stimuli and carry their cargo to the targeted site, increasing gene transfer into the cells and promoting gene expression – the ultimate goal of gene therapy. However, one of the major hurdles for the successful application of gene therapy is the effective delivery of genetic material into the targeted cells. Gemini surfactants are a group of cationic lipids able to form nanoparticles with nucleic acids of a certain size and morphology and deliver the encapsulated materials to target tissues. They are composed of two head groups attached to their hydrocarbon tails and connected by a spacer. Altering the chemical structure of the gemini surfactants was shown to have a dramatic impact on the physicochemical properties of the gene-gemini surfactant lipoplexes, affecting the transfection efficiency of the delivery vector. As such, a series of 22 new derivatives have been synthesized having 12-18:1C hydrocarbon tails and spacer group substitutions ranging from dipeptide-substituted compounds to oligo-peptides. *This research evaluates the impact of the structural variations of the peptide-modified gemini surfactant nanoparticles on their physicochemical properties and transfection efficiency.*

A major application of gemini surfactants is topical gene delivery. Topical gene delivery is a convenient and easy to administer route, particularly for wound healing, DNA-immunization, melanoma treatment and vitiligo. In this research, topical formulation of peptide modified gemini surfactants is assessed *ex vivo* for their dermal penetration ability. The aim beyond this project is to develop targeted delivery for the treatment of melanoma.

While extensive research is being done to monitor the biodistribution of the active

therapeutic agent, the ultimate fate of lipid-based carriers has not been fully understood. Many questions remain unanswered regarding the degradation profile of the building constituents of nanoparticles after releasing their therapeutic cargo including the formation of breakdown by-products, some of which may be toxic. Correlating the biodistribution and the biological fate of the nanoparticles to their chemical structure and physicochemical properties will guide future formulation decision, resulting in the production of lipid-based gene carriers with higher efficiency and reduced toxicity. Herein, mass spectrometry (MS) is employed to detect and quantify topically applied gemini surfactants in skin tissue of an animal model in order to determine their behavior in complex biological environment.

The long-term possible outcomes of this research are to develop a model that could be used to predict the *in vivo* distribution and transfection efficiency of the gene delivery nanoparticles. Such a model might become a design tool for new delivery materials that have optimal bio-distribution and delivery characteristics beyond gemini surfactants.

1.7. Research Hypothesis

1.7.1. Optimization of the DNA binding properties of novel peptide-modified gemini surfactant- based gene delivery systems will result in more efficient and less toxic dermal gene delivery system compared to the unsubstituted gemini surfactants.

1.7.2. The distribution of diquaternary ammonium gemini surfactants will be confined to the skin layers.

1.8. Research Objectives

1.8.1. Hypothesis #1:

- To develop and characterize novel peptide-modified gemini surfactant-based gene delivery systems for *in vitro* and *ex vivo* applications.

Specific aims:

- To assess the physicochemical and structural properties of novel peptide-modified gemini surfactant-based gene delivery systems.
    A. To study the MS/MS fragmentation behavior of the peptide-modified gemini surfactants (hydrocarbon-peptide-substituted).
    B. To identify the supramolecular arrangement of peptide-modified lipoplex formulations using small angle X-ray scattering technique.
    C. To conduct size and zeta potential measurements for the lipoplex formulations.
- To evaluate the efficiency of peptide-modified gemini surfactants lipoplex formulations in delivering genetic materials *in vitro*.
- To determine the *in vitro* cytotoxicity of the peptide-modified gemini surfactants lipoplex formulations.

- To evaluate the skin permeation efficiency of the lead compounds of peptide-modified gemini surfactants lipoplex formulations *ex vivo*.
- To examine the relationship between the physicochemical properties of the delivery agent and their *in vitro* transfection efficiency and *ex vivo* permeation efficiency (structure activity relationship).

1.8.2. Hypothesis #2:

- To develop flow injection analysis -tandem mass spectrometry (FIA–MS/MS) methods for the determination of novel peptide-modified gemini surfactants within complex biological matrices.
- To detect and quantify the lead compounds of peptide-modified gemini surfactants in skin tissues as well as in phosphate buffered saline (PBS): a biologically relevant buffer.

1.9. Bibliography

1 Friedmann T. The Development of Human Gene Therapy. (Cold Spring Harbor Laboratory Press, 1999).

2 Rogers S, Pfuderer P. Use of viruses as carriers of added genetic information. Nature 1968; 219: 749-51.

3 Friedmann T, Roblin R. Gene therapy for human genetic disease? Science 1972; 175: 949-55.

4 Wilson JM. Gendicine: The First Commercial Gene Therapy Product; Chinese Translation of Editorial. Human gene therapy 2005; 16: 1014-5.

5 Ylä-Herttuala S. Endgame: glybera finally recommended for approval as the first gene therapy drug in the European union. Molecular Therapy 2012; 20: 1831-2.

6 DiGiulio S. FDA Approves First Oncolytic Virus Therapy—Imlygic for Melanoma. Oncology Times 2015.

7 Thomas CE, Ehrhardt A, Kay MA. Progress and problems with the use of viral vectors for gene therapy. Nature Reviews Genetics 2003; 4: 346-58.

8 Hacein-Bey-Abina S, von Kalle C, Schmidt M, Le Deist F, Wulffraat N, McIntyre E, *et al*. A serious adverse event after successful gene therapy for X-linked severe combined immunodeficiency. New England Journal of Medicine 2003; 348: 255-6.

9 Hacein-Bey-Abina S, Von Kalle C, Schmidt M, McCormack M, Wulffraat N, Leboulch P, *et al*. LMO2-associated clonal T cell proliferation in two patients after gene therapy for SCID-X1. Science 2003; 302: 415-9.

10 Hacein-Bey-Abina S, Garrigue A, Wang GP, Soulier J, Lim A, Morillon E, *et al*. Insertional oncogenesis in 4 patients after retrovirus-mediated gene therapy of SCID-X1. The Journal of clinical investigation 2008; 118: 3132.

11 Yin H, Kanasty RL, Eltoukhy AA, Vegas AJ, Dorkin JR, Anderson DG. Non-viral vectors for gene-based therapy. Nature Reviews Genetics 2014; 15: 541-55.

12 Oliveira C, Ribeiro AJ, Veiga F, Silveira I. Recent Advances in Nucleic Acid-Based Delivery: From Bench to Clinical Trials in Genetic Diseases. Journal of Biomedical Nanotechnology 2016; 12: 841-62.

13 Gottfried LF, Dean DA. Extracellular and intracellular barriers to non-viral gene transfer. (INTECH Open Access Publisher, 2013).

14 Yoo J-W, Chambers E, Mitragotri S. Factors that control the circulation time of nanoparticles in blood: challenges, solutions and future prospects. Current pharmaceutical design 2010; 16: 2298-307.

15 Ward CM, Read ML, Seymour LW. Systemic circulation of poly (L-lysine)/DNA vectors is influenced by polycation molecular weight and type of DNA: differential circulation in mice and rats and the implications for human gene therapy. Blood 2001; 97: 2221-9.

16 Ikeda Y, Nagasaki Y. Impacts of PEGylation on the gene and oligonucleotide delivery system. Journal of Applied Polymer Science 2014; 131.

17 Suk JS, Xu Q, Kim N, Hanes J, Ensign LM. PEGylation as a strategy for improving nanoparticle-based drug and gene delivery. Advanced drug delivery reviews 2016; 99: 28-51.

18 Mishra S, Webster P, Davis ME. PEGylation significantly affects cellular uptake and intracellular trafficking of non-viral gene delivery particles. European journal of cell biology 2004; 83: 97-111.

19 Deshpande MC, Davies MC, Garnett MC, Williams PM, Armitage D, Bailey L*, et al*. The effect of poly (ethylene glycol) molecular architecture on cellular interaction and uptake of DNA complexes. Journal of controlled release 2004; 97: 143-56.

20 Rejman J, Wagenaar A, Engberts JB, Hoekstra D. Characterization and transfection properties of lipoplexes stabilized with novel exchangeable polyethylene glycol–lipid conjugates. Biochimica et Biophysica Acta (BBA)-Biomembranes 2004; 1660: 41-52.

21 Galley H, Webster N. Physiology of the endothelium. British journal of anaesthesia 2004; 93: 105-13.

22 Sarin H. Physiologic upper limits of pore size of different blood capillary types and another perspective on the dual pore theory of microvascular permeability. Journal of angiogenesis research 2010; 2: 1.

23 Frantz C, Stewart KM, Weaver VM. The extracellular matrix at a glance. J Cell Sci 2010; 123: 4195-200.

24 Netti PA, Berk DA, Swartz MA, Grodzinsky AJ, Jain RK. Role of extracellular matrix assembly in interstitial transport in solid tumors. Cancer research 2000; 60: 2497-503.

25 Miyata K, Nishiyama N, Kataoka K. Rational design of smart supramolecular assemblies for gene delivery: chemical challenges in the creation of artificial viruses. Chemical Society Reviews 2012; 41: 2562-74.

26 El-Sayed A, Harashima H. Endocytosis of gene delivery vectors: from clathrin-dependent to lipid raft-mediated endocytosis. Molecular Therapy 2013; 21: 1118-30.

27 Payne CK, Jones SA, Chen C, Zhuang X. Internalization and Trafficking of Cell Surface Proteoglycans and Proteoglycan-Binding Ligands. Traffic 2007; 8: 389-401.

28 Erbacher P, Remy J, Behr J. Gene transfer with synthetic virus-like particles via the integrin-mediated endocytosis pathway. Gene Therapy 1999; 6: 138-45.

29 He C, Hu Y, Yin L, Tang C, Yin C. Effects of particle size and surface charge on cellular uptake and biodistribution of polymeric nanoparticles. Biomaterials 2010; 31: 3657-66.

30 Fröhlich E. The role of surface charge in cellular uptake and cytotoxicity of medical nanoparticles. International journal of nanomedicine 2012; 7: 5577.

31 Järver P, Langel Ü. The use of cell-penetrating peptides as a tool for gene regulation. Drug discovery today 2004; 9: 395-402.

32 Wang F, Wang Y, Zhang X, Zhang W, Guo S, Jin F. Recent progress of cell-penetrating peptides as new carriers for intracellular cargo delivery. Journal of Controlled Release 2014; 174: 126-36.

33 Chiu S-J, Ueno NT, Lee RJ. Tumor-targeted gene delivery via anti-HER2 antibody (trastuzumab, Herceptin®) conjugated polyethylenimine. Journal of controlled release 2004; 97: 357-69.

34 Ikegami S, Yamakami K, Ono T, Sato M, Suzuki S, Yoshimura I, *et al*. Targeting gene therapy for prostate cancer cells by liposomes complexed with anti-prostate-specific membrane antigen monoclonal antibody. Human gene therapy 2006; 17: 997-1005.

35 Vives E. Present and future of cell-penetrating peptide mediated delivery systems:“is the Trojan horse too wild to go only to Troy?”. Journal of controlled release 2005; 109: 77-85.

36 Huang Y, Jiang Y, Wang H, Wang J, Shin MC, Byun Y, *et al*. Curb challenges of the “Trojan Horse” approach: smart strategies in achieving effective yet safe cell-penetrating peptide-based drug delivery. Advanced drug delivery reviews 2013; 65: 1299-315.

37 Minchin RF, Yang S. Endosomal disruptors in non-viral gene delivery. Expert opinion on drug delivery 2010; 7: 331-9.

38 Liang W, Lam JK. Endosomal escape pathways for non-viral nucleic acid delivery systems. (INTECH Open Access Publisher, 2012).

39 Xu Y, Szoka FC. Mechanism of DNA release from cationic liposome/DNA complexes used in cell transfection. Biochemistry 1996; 35: 5616-23.

40 Zelphati O, Szoka Jr FC. Intracellular distribution and mechanism of delivery of oligonucleotides mediated by cationic lipids. Pharmaceutical research 1996; 13: 1367-72.

41 Hoekstra D, Rejman J, Wasungu L, Shi F, Zuhorn I. Gene delivery by cationic lipids: in and out of an endosome. Biochemical Society Transactions 2007; 35: 68-71.

42 Zuhorn IS, Bakowsky U, Polushkin E, Visser WH, Stuart MC, Engberts JB, *et al*. Nonbilayer phase of lipoplex–membrane mixture determines endosomal escape of genetic cargo and transfection efficiency. Molecular therapy 2005; 11: 801-10.

43 Akinc A, Thomas M, Klibanov AM, Langer R. Exploring polyethylenimine-mediated DNA transfection and the proton sponge hypothesis. The journal of gene medicine 2005; 7: 657-63.

44 Li W, Nicol F, Szoka FC. GALA: a designed synthetic pH-responsive amphipathic peptide with applications in drug and gene delivery. Advanced drug delivery reviews 2004; 56: 967-85.

45 Wyman TB, Nicol F, Zelphati O, Scaria P, Plank C, Szoka FC. Design, synthesis, and characterization of a cationic peptide that binds to nucleic acids and permeabilizes bilayers. Biochemistry 1997; 36: 3008-17.

46 Ogris M, Carlisle RC, Bettinger T, Seymour LW. Melittin enables efficient vesicular escape and enhanced nuclear access of nonviral gene delivery vectors. Journal of Biological Chemistry 2001; 276: 47550-5.

47 Yang L, Harroun TA, Weiss TM, Ding L, Huang HW. Barrel-stave model or toroidal model? A case study on melittin pores. Biophysical journal 2001; 81: 1475-85.

48 Hassane FS, Saleh A, Abes R, Gait M, Lebleu B. Cell penetrating peptides: overview and applications to the delivery of oligonucleotides. Cellular and molecular life sciences 2010; 67: 715-26.

49 Pollard H, Remy J-S, Loussouarn G, Demolombe S, Behr J-P, Escande D. Polyethylenimine but not cationic lipids promotes transgene delivery to the nucleus in mammalian cells. Journal of Biological Chemistry 1998; 273: 7507-11.

50 Belting M, Sandgren S, Wittrup A. Nuclear delivery of macromolecules: barriers and carriers. Advanced drug delivery reviews 2005; 57: 505-27.

51 Miller AM, Dean DA. Tissue-specific and transcription factor-mediated nuclear entry of DNA. Advanced drug delivery reviews 2009; 61: 603-13.

52 Gene Therapy Clinical Trials Worldwide John Wiley and Sons Ltd., <http://www.wiley.com/legacy/wileychi/genmed/clinical/>. Accesed Jan 2018

53 Lukacs GL, Haggie P, Seksek O, Lechardeur D, Freedman N, Verkman A. Size-dependent DNA mobility in cytoplasm and nucleus. Journal of Biological Chemistry 2000; 275: 1625-9.

54 Macara IG. Transport into and out of the nucleus. Microbiology and molecular biology reviews 2001; 65: 570-94.

55 Lange A, Mills RE, Lange CJ, Stewart M, Devine SE, Corbett AH. Classical nuclear localization signals: definition, function, and interaction with importin α. Journal of Biological Chemistry 2007; 282: 5101-5.

56 Chan C-K, Jans DA. Using nuclear targeting signals to enhance non-viral gene transfer. Immunology and cell biology 2002; 80: 119-30.

57 Brandén LJ, Mohamed AJ, Smith CE. A peptide nucleic acid–nuclear localization signal fusion that mediates nuclear transport of DNA. Nature biotechnology 1999; 17: 784-7.

58 Nagasaki T, Myohoji T, Tachibana T, Futaki S, Tamagaki S. Can nuclear localization signals enhance nuclear localization of plasmid DNA? Bioconjugate chemistry 2003; 14: 282-6.

59 Tanimoto M, Kamiya H, Minakawa N, Matsuda A, Harashima H. No enhancement of nuclear entry by direct conjugation of a nuclear localization signal peptide to linearized DNA. Bioconjugate chemistry 2003; 14: 1197-202.

60 Wolff JA, Malone RW, Williams P, Chong W, Acsadi G, Jani Aa, *et al*. Direct gene transfer into mouse muscle in vivo. Science 1990; 247: 1465-8.

61 Maruyama H, Higuchi N, Nishikawa Y, Kameda S, Iino N, Kazama J, *et al*. High-level expression of naked DNA delivered to rat liver via tail vein injection. The journal of gene medicine 2002; 4: 333-41.

62 Maruyama H, Higuchi N, Nishikawa Y, Hirahara H, Iino N, Kameda S, *et al*. Kidney-targeted naked DNA transfer by retrograde renal vein injection in rats. Human gene therapy 2002; 13: 455-68.

63 Tsan M, White JE, Shepard B. Lung-specific direct in vivo gene transfer with recombinant plasmid DNA. American Journal of Physiology-Lung Cellular and Molecular Physiology 1995; 268: L1052-L6.

64 Lin H, Parmacek M, Morle G, Bolling S, Leiden J. Expression of recombinant genes in myocardium in vivo after direct injection of DNA. Circulation 1990; 82: 2217-21.

65 Rice J, Ottensmeier CH, Stevenson FK. DNA vaccines: precision tools for activating effective immunity against cancer. Nature Reviews Cancer 2008; 8: 108-20.

66 Levy M, Barron L, Meyer K, Szoka Jr F. Characterization of plasmid DNA transfer into mouse skeletal muscle: evaluation of uptake mechanism, expression and secretion of gene products into blood. Gene therapy 1996; 3: 201.

67 Liu Y, Liggitt D, Zhong W, Tu G, Gaensler K, Debs R. Cationic liposome-mediated intravenous gene delivery. Journal of Biological Chemistry 1995; 270: 24864-70.

68 Misra A. Challenges in Delivery of Therapeutic Genomics and Proteomics. (Elsevier Science, 2010).

69 Niidome T, Huang L. Gene therapy progress and prospects: nonviral vectors. Gene therapy 2002; 9: 1647-52.

70 Felgner PL, Gadek TR, Holm M, Roman R, Chan HW, Wenz M, *et al*. Lipofection: a highly efficient, lipid-mediated DNA-transfection procedure. Proceedings of the National Academy of Sciences 1987; 84: 7413-7.

71 Ilies M, Seitz WA, Balaban AT. Cationic lipids in gene delivery: principles, vector design and therapeutical applications. Current pharmaceutical design 2002; 8: 2441-73.

72 Singh J, Mohammed-Saied W, Kaur R, Badea I. Nanoparticles in Gene Therapy: From Design to Clinical Applications. Reviews in Nanoscience and Nanotechnology 2013; 2: 275-99.

73 Zhi D, Zhang S, Cui S, Zhao Y, Wang Y, Zhao D. The Headgroup Evolution of Cationic Lipids for Gene Delivery. Bioconjugate chemistry 2013; 24: 487-519.

74 Leventis R, Silvius JR. Interactions of mammalian cells with lipid dispersions containing novel metabolizable cationic amphiphiles. Biochimica et Biophysica Acta (BBA)-Biomembranes 1990; 1023: 124-32.

75 Felgner JH, Kumar R, Sridhar C, Wheeler CJ, Tsai YJ, Border R, *et al*. Enhanced gene delivery and mechanism studies with a novel series of cationic lipid formulations. Journal of Biological Chemistry 1994; 269: 2550-61.

76 Hottiger M, Dam T, Nickoloff B, Johnson T, Nabel G. Liposome-mediated gene transfer into human basal cell carcinoma. Gene therapy 1999; 6: 1929-35.

77 Bergen M, Chen R, Gonzalez R. Efficacy and safety of HLA-B7/β-2 microglobulin plasmid DNA/lipid complex (Allovectin-7®) in patients with metastatic melanoma. Expert opinion on biological therapy 2003; 3: 377-84.

78 Belldegrun A, Tso C-L, Zisman A, Naitoh J, Said J, Pantuck AJ, *et al*. Interleukin 2 gene therapy for prostate cancer: phase I clinical trial and basic biology. Human gene therapy 2001; 12: 883-92.

79 Behr J-P. DNA strongly binds to micelles and vesicles containing lipopolyamines or lipointercalants. Tetrahedron letters 1986; 27: 5861-4.

80 Behr J-P, Demeneix B, Loeffler J-P, Perez-Mutul J. Efficient gene transfer into mammalian primary endocrine cells with lipopolyamine-coated DNA. Proceedings of the National Academy of Sciences 1989; 86: 6982-6.

81 Remy J-S, Sirlin C, Vierling P, Behr J-P. Gene transfer with a series of lipophilic DNA-binding molecules. Bioconjugate chemistry 1994; 5: 647-54.

82 Byk G, Dubertret C, Escriou V, Frederic M, Jaslin G, Rangara R, *et al*. Synthesis, activity, and structure-activity relationship studies of novel cationic lipids for DNA transfer. Journal of medicinal chemistry 1998; 41: 224-35.

83 Gao X, Huang L. A novel cationic liposome reagent for efficient transfection of mammalian cells. Biochemical and biophysical research communications 1991; 179: 280-5.

84 Gill D, Southern K, Mofford K, Seddon T, Huang L, Sorgi F, *et al*. A placebo-controlled study of liposome-mediated gene transfer to the nasal epithelium of patients with cystic fibrosis. Gene therapy 1997; 4: 199-209.

85 Lee ER, Marshall J, Siegel CS, Jiang C, Yew NS, Nichols MR, *et al*. Detailed analysis of structures and formulations of cationic lipids for efficient gene transfer to the lung. Human gene therapy 1996; 7: 1701-17.

86 Eastman SJ, Lukason MJ, Tousignant JD, Murray H, Lane MD, George JAS, *et al*. A concentrated and stable aerosol formulation of cationic lipid: DNA complexes giving high-level gene expression in mouse lung. Human gene therapy 1997; 8: 765-73.

87 Eastman SJ, Tousignant JD, Lukason MJ, Chu Q, Cheng SH, Scheule RK. Aerosolization of cationic lipid: pDNA complexes-in vitro optimization of nebulizer parameters for human clinical studies. Human gene therapy 1998; 9: 43-52.

88 Alton E, Stern M, Farley R, Jaffe A, Chadwick S, Phillips J, *et al*. Cationic lipid-mediated< i> CFTR</i> gene transfer to the lungs and nose of patients with cystic fibrosis: a double-blind placebo-controlled trial. The Lancet 1999; 353: 947-54.

89 Ruiz F, Clancy J, Perricone M, Bebok Z, Hong J, Cheng S, *et al*. A clinical inflammatory syndrome attributable to aerosolized lipid-DNA administration in cystic fibrosis. Human gene therapy 2001; 12: 751-61.

90 ClinicalTrials.gov, Identifier: NCT00789867.ed

91 ClinicalTrials.gov Identifier: NCT01621867.ed

92 Vigneron J-P, Oudrhiri N, Fauquet M, Vergely L, Bradley J-C, Basseville M, *et al*. Guanidinium-cholesterol cationic lipids: efficient vectors for the transfection of eukaryotic cells. Proceedings of the National Academy of Sciences 1996; 93: 9682-6.

93 Ruysschaert J-M, Elouahabi A, Willeaume V, Huez G, Fuks R, Vandenbranden M, *et al*. A novel cationic amphiphile for transfection of mammalian cells. Biochemical and biophysical research communications 1994; 203: 1622-8.

94 Van Der Woude I, Wagenaar A, Meekel AA, Ter Beest MB, Ruiters MH, Engberts JB, *et al*. Novel pyridinium surfactants for efficient, nontoxic in vitro gene delivery. Proceedings of the National Academy of Sciences 1997; 94: 1160-5.

95 Meekel AA, Wagenaar A, S˘misterová J, Kroeze JE, Haadsma P, Bosgraaf B, *et al*. Synthesis of pyridinium amphiphiles used for transfection and some characteristics of

amphiphile/DNA complex formation. European Journal of Organic Chemistry 2000; 2000: 665-73.

96 Smisterová J, Wagenaar A, Stuart MC, Polushkin E, ten Brinke G, Hulst R, *et al*. Molecular shape of the cationic lipid controls the structure of cationic lipid/dioleylphosphatidylethanolamine-DNA complexes and the efficiency of gene delivery. Journal of Biological Chemistry 2001; 276: 47615-22.

97 Roosjen A, Šmisterová J, Driessen C, Anders JT, Wagenaar A, Hoekstra D, *et al*. Synthesis and characteristics of biodegradable pyridinium amphiphiles used for in vitro DNA delivery. European Journal of Organic Chemistry 2002; 2002: 1271-7.

98 Islam RU, Hean J, van Otterlo WA, de Koning CB, Arbuthnot P. Efficient nucleic acid transduction with lipoplexes containing novel piperazine-and polyamine-conjugated cholesterol derivatives. Bioorganic & medicinal chemistry letters 2009; 19: 100-3.

99 Gao M, Wang M, Miller KD, Sledge GW, Hutchins GD, Zheng Q-H. Facile synthesis of carbon-11-labeled cholesterol-based cationic lipids as new potential PET probes for imaging of gene delivery in cancer. Steroids 2010; 75: 715-20.

100 Solodin I, Brown CS, Bruno MS, Chow C-Y, Jang E-H, Debs RJ, *et al*. A novel series of amphiphilic imidazolinium compounds for in vitro and in vivo gene delivery. Biochemistry 1995; 34: 13537-44.

101 ClinicalTrials.gov, Identifier: NCT00860522.ed

102 Menger FM, Littau C. Gemini-surfactants: synthesis and properties. Journal of the American Chemical Society 1991; 113: 1451-2.

103 Rosenzweig HS, Rakhmanova VA, MacDonald RC. Diquaternary ammonium compounds as transfection agents. Bioconjugate chemistry 2001; 12: 258-63.

104 Ahmed T, Kamel AO, Wettig SD. Interactions between DNA and Gemini surfactant: impact on gene therapy: part I. Nanomedicine 2016; 11: 289-306.

105 Uhríková D, Zajac I, Dubničková M, Pisárčik M, Funari SS, Rapp G, *et al*. Interaction of gemini surfactants butane-1, 4-diyl-bis (alkyldimethylammonium bromide) with DNA. 2005; 42: 59-68.

106 Wang C, Li X, Wettig SD, Badea I, Foldvari M, Verrall REJPCCP. Investigation of complexes formed by interaction of cationic gemini surfactants with deoxyribonucleic acid. 2007; 9: 1616-28.

107 Cullis PR, Hope MJ, Tilcock CP. Lipid polymorphism and the roles of lipids in membranes. Chemistry and physics of lipids 1986; 40: 127-44.

108 Karlsson L, van Eijk MC, Söderman O. Compaction of DNA by gemini surfactants: effects of surfactant architecture. Journal of colloid and interface science 2002; 252: 290-6.

109 Ahmed T, Kamel AO, Wettig SD. Interactions between DNA and Gemini surfactant: impact on gene therapy: part I. Nanomedicine 2016.

110 Ahmed T, Kamel AO, Wettig SD. Interactions between DNA and gemini surfactant: impact on gene therapy: part II. Nanomedicine 2016; 11: 403-20.

111 Wettig SD, Verrall RE, Foldvari M. Gemini surfactants: a new family of building blocks for non-viral gene delivery systems. Current gene therapy 2008; 8: 9-23.

112 Elsabahy M, Badea I, Verrall R, Donkuru M, Foldvari M. Dicationic gemini nanoparticle design for gene therapy. Organic nanomaterials. Wiley 2014: 509-28.

113 Badea I, Verrall R, Baca-Estrada M, Tikoo S, Rosenberg A, Kumar P, *et al*. In vivo cutaneous interferon-γ gene delivery using novel dicationic (gemini) surfactant–plasmid complexes. The journal of gene medicine 2005; 7: 1200-14.

114 Wettig S, Verrall R. Thermodynamic studies of aqueous m–s–m gemini surfactant systems. Journal of colloid and interface science 2001; 235: 310-6.

115 Badea I, Wettig S, Verrall R, Foldvari M. Topical non-invasive gene delivery using gemini nanoparticles in interferon-γ-deficient mice. European journal of pharmaceutics and biopharmaceutics 2007; 65: 414-22.

116 Badea I, Virtanen C, Verrall R, Rosenberg A, Foldvari M. Effect of topical interferon-γ gene therapy using gemini nanoparticles on pathophysiological markers of cutaneous scleroderma in Tsk/+ mice. Gene Therapy 2011; 19: 978-87.

117 Wettig SD, Badea I, Donkuru M, Verrall RE, Foldvari M. Structural and transfection properties of amine-substituted gemini surfactant-based nanoparticles. The journal of gene medicine 2007; 9: 649-58.

118 Yang P, Singh J, Wettig S, Foldvari M, Verrall RE, Badea I. Enhanced gene expression in epithelial cells transfected with amino acid-substituted gemini nanoparticles. European Journal of Pharmaceutics and Biopharmaceutics 2010; 75: 311-20.

119 Singh J, Yang P, Michel D, E Verrall R, Foldvari M, Badea I. Amino Acid-Substituted Gemini Surfactant-Based Nanoparticles as Safe and Versatile Gene Delivery Agents. Current Drug Delivery 2011; 8: 299-306.

120 Singh J, Michel D, Getson HM, Chitanda JM, Verrall RE, Badea I. Development of amino acid substituted gemini surfactant-based mucoadhesive gene delivery systems for potential use as noninvasive vaginal genetic vaccination. Nanomedicine 2015; 10: 405-17.

121 Sharma VD, Ilies MA. Heterocyclic Cationic Gemini Surfactants: A Comparative Overview of Their Synthesis, Self-assembling, Physicochemical, and Biological Properties. Medicinal research reviews 2014; 34: 1-44.

122 Sharma VD, Lees J, Hoffman NE, Brailoiu E, Madesh M, Wunder SL, *et al*. Modulation of pyridinium cationic lipid–DNA complex properties by pyridinium gemini surfactants and its impact on lipoplex transfection properties. Molecular pharmaceutics 2014; 11: 545-59.

123 Dauty E, Remy J-S, Blessing T, Behr J-P. Dimerizable cationic detergents with a low cmc condense plasmid DNA into nanometric particles and transfect cells in culture. Journal of the American Chemical Society 2001; 123: 9227-34.

124 Fisicaro E, Compari C, Bacciottini F, Contardi L, Barbero N, Viscardi G, *et al*. Nonviral gene delivery: gemini bispyridinium surfactant-based DNA nanoparticles. The Journal of Physical Chemistry B 2014; 118: 13183-91.

125 Ilies MA, Johnson BH, Makori F, Miller A, Seitz WA, Thompson EB, *et al*. Pyridinium cationic lipids in gene delivery: an in vitro and in vivo comparison of transfection efficiency versus a tetraalkylammonium congener. Archives of biochemistry and biophysics 2005; 435: 217-26.

126 Ilies MA, Seitz WA, Johnson BH, Ezell EL, Miller AL, Thompson EB, *et al*. Lipophilic pyrylium salts in the synthesis of efficient pyridinium-based cationic lipids, gemini surfactants, and lipophilic oligomers for gene delivery. Journal of medicinal chemistry 2006; 49: 3872-87.

127 Johnsson M, Engberts JB. Novel sugar-based gemini surfactants: aggregation properties in aqueous solution. Journal of physical organic chemistry 2004; 17: 934-44.

128 Kawakami S, Sato A, Nishikawa M, Yamashita F, Hashida M. Mannose receptor-mediated gene transfer into macrophages using novel mannosylated cationic liposomes. Gene therapy 2000; 7: 292-9.

129 Fielden ML, Perrin C, Kremer A, Bergsma M, Stuart MC, Camilleri P, *et al*. Sugar-based tertiary amino gemini surfactants with a vesicle-to-micelle transition in the endosomal pH range mediate efficient transfection in vitro. European Journal of Biochemistry 2001; 268: 1269-79.

130 Wasungu L, Scarzello M, van Dam G, Molema G, Wagenaar A, Engberts JB, *et al*. Transfection mediated by pH-sensitive sugar-based gemini surfactants; potential for in vivo gene therapy applications. Journal of molecular medicine 2006; 84: 774-84.

131 Bell PC, Bergsma M, Dolbnya IP, Bras W, Stuart MC, Rowan AE, *et al*. Transfection mediated by gemini surfactants: engineered escape from the endosomal compartment. Journal of the American Chemical Society 2003; 125: 1551-8.

132 Johnsson M, Wagenaar A, Stuart MC, Engberts JB. Sugar-based gemini surfactants with pH-dependent aggregation behavior: vesicle-to-micelle transition, critical micelle concentration, and vesicle surface charge reversal. Langmuir 2003; 19: 4609-18.

133 Wasungu L, Stuart MC, Scarzello M, Engberts JB, Hoekstra D. Lipoplexes formed from sugar-based gemini surfactants undergo a lamellar-to-micellar phase transition at acidic pH. Evidence for a non-inverted membrane-destabilizing hexagonal phase of lipoplexes. Biochimica et Biophysica Acta (BBA)-Biomembranes 2006; 1758: 1677-84.

134 Pérez L, Pinazo A, Pons R, Infante M. Gemini surfactants from natural amino acids. Advances in colloid and interface science 2014; 205: 134-55.

135 Morán MC, Pinazo A, Pérez L, Clapés P, Angelet M, García MT, *et al*. "Green" amino acid-based surfactants. Green Chemistry 2004; 6: 233-40.

136 Castro M, Griffiths D, Patel A, Pattrick N, Kitson C, Ladlow M. Effect of chain length on transfection properties of spermine-based gemini surfactants. Organic & biomolecular chemistry 2004; 2: 2814-20.

137 Cardoso AM, Morais CM, Cruz AR, Silva SG, do Vale ML, Marques EF, *et al*. New serine-derived gemini surfactants as gene delivery systems. European Journal of Pharmaceutics and Biopharmaceutics 2015; 89: 347-56.

138 Brito RO, Oliveira IS, Araújo MJ, Marques EF. Morphology, thermal behavior, and stability of self-assembled supramolecular tubules from lysine-based surfactants. The Journal of Physical Chemistry B 2013; 117: 9400-11.

139 Xu R, Wang X-L, Lu Z-R. New amphiphilic carriers forming pH-sensitive nanoparticles for nucleic acid delivery. Langmuir 2010; 26: 13874-82.

140 McGregor C, Perrin C, Monck M, Camilleri P, Kirby AJ. Rational approaches to the design of cationic gemini surfactants for gene delivery. Journal of the American Chemical Society 2001; 123: 6215-20.

141 Nagarajan R. Molecular packing parameter and surfactant self-assembly: the neglected role of the surfactant tail. Langmuir 2002; 18: 31-8.

142 Hayakawa K, Santerre JP, Kwak JC. The binding of cationic surfactants by DNA. Biophysical chemistry 1983; 17: 175-81.

143 Rudiuk S, Yoshikawa K, Baigl D. Enhancement of DNA compaction by negatively charged nanoparticles: Effect of nanoparticle size and surfactant chain length. Journal of colloid and interface science 2012; 368: 372-7.

144 Matulis D, Rouzina I, Bloomfield VA. Thermodynamics of cationic lipid binding to DNA and DNA condensation: roles of electrostatics and hydrophobicity. Journal of the American Chemical Society 2002; 124: 7331-42.

145 Donkuru M, Wettig SD, Verrall RE, Badea I, Foldvari M. Designing pH-sensitive gemini nanoparticles for non-viral gene delivery into keratinocytes. Journal of Materials Chemistry 2012; 22: 6232-44.

146 Menger FM, Keiper JS. Gemini surfactants. Angewandte Chemie International Edition 2000; 39: 1906-20.

147 Chu Z, Feng Y. Empirical correlations between Krafft temperature and tail length for amidosulfobetaine surfactants in the presence of inorganic salt. Langmuir 2011; 28: 1175-81.

148 Prabha S, Arya G, Chandra R, Ahmed B, Nimesh S. Effect of size on biological properties of nanoparticles employed in gene delivery. Artificial cells, nanomedicine, and biotechnology 2014: 1-9.

149 Prabha S, Zhou W-Z, Panyam J, Labhasetwar V. Size-dependency of nanoparticle-mediated gene transfection: studies with fractionated nanoparticles. International Journal of Pharmaceutics 2002; 244: 105-15.

150 Kuiper JM, Buwalda RT, Hulst R, Engberts JB. Novel pyridinium surfactants with unsaturated alkyl chains: aggregation behavior and interactions with methyl orange in aqueous solution. Langmuir 2001; 17: 5216-24.

151 Kirby AJ, Camilleri P, Engberts JB, Feiters MC, Nolte RJ, Söderman O, *et al*. Gemini surfactants: new synthetic vectors for gene transfection. Angewandte Chemie International Edition 2003; 42: 1448-57.

152 Ramezani M, Khoshhamdam M, Dehshahri A, Malaekeh-Nikouei B. The influence of size, lipid composition and bilayer fluidity of cationic liposomes on the transfection efficiency of nanolipoplexes. Colloids and Surfaces B: Biointerfaces 2009; 72: 1-5.

153 Róg T, Murzyn K, Gurbiel R, Takaoka Y, Kusumi A, Pasenkiewicz-Gierula M. Effects of phospholipid unsaturation on the bilayer nonpolar region a molecular simulation study. Journal of lipid research 2004; 45: 326-36.

154 Deinum G, Van Langen H, Van Ginkel G, Levine YK. Molecular order and dynamics in planar lipid bilayers: effects of unsaturation and sterols. Biochemistry 1988; 27: 852-60.

155 Kudsiova L, Ho J, Fridrich B, Harvey R, Keppler M, Ng T, *et al*. Lipid chain geometry of C14 glycerol-based lipids: effect on lipoplex structure and transfection. Molecular BioSystems 2011; 7: 422-36.

156 Fujiwara T, Hasegawa S, Hirashima N, Nakanishi M, Ohwada T. Gene transfection activities of amphiphilic steroid–polyamine conjugates. Biochimica et Biophysica Acta (BBA)-Biomembranes 2000; 1468: 396-402.

157 Bai G, Wang J, Wang Y, Yan H, Thomas RK. Thermodynamics of hydrophobic interaction of dissymmetric gemini surfactants in aqueous solutions. The Journal of Physical Chemistry B 2002; 106: 6614-6.

158 Wang X, Wang J, Wang Y, Ye J, Yan H, Thomas RK. Micellization of a series of dissymmetric gemini surfactants in aqueous solution. The Journal of Physical Chemistry B 2003; 107: 11428-32.

159 Jiang N, Wang J, Wang Y, Yan H, Thomas RK. Microcalorimetric study on the interaction of dissymmetric gemini surfactants with DNA. Journal of colloid and interface science 2005; 284: 759-64.

160 Fan Y, Li Y, Cao M, Wang J, Wang Y, Thomas RK. Micellization of dissymmetric cationic gemini surfactants and their interaction with dimyristoylphosphatidylcholine vesicles. Langmuir 2007; 23: 11458-64.

161 Greenhalgh DA, Rothnagel JA, Roop DR. Epidermis: an attractive target tissue for gene therapy. Journal of investigative dermatology 1994; 103: 63S-9S.

162 Banchereau J, Steinman RM. Dendritic cells and the control of immunity. Nature 1998; 392: 245-52.

163 Freinkel RK, Woodley DT. The Biology of the Skin. (Taylor & Francis, 2001).

164 Benson HAE, Watkinson AC. Topical and Transdermal Drug Delivery: Principles and Practice. (Wiley, 2012).

165 Williams A. Transdermal and Topical Drug Delivery: From Theory to Clinical Practice. (Pharmaceutical Press, 2003).

166 Prasanthi D, Lakshmi P. Vesicles-mechanism of transdermal permeation: a review. Asian J Pharm Clin Res 2012; 5: 18-25.

167 Brown MB, Martin GP, Jones SA, Akomeah FK. Dermal and transdermal drug delivery systems: current and future prospects. Drug delivery 2006; 13: 175-87.

168 Sperelakis N. Cell physiology source book: essentials of membrane biophysics. (Elsevier, 2012).

169 Vanić Ž. Phospholipid vesicles for enhanced drug delivery in dermatology. Journal of Drug Discovery, Development and Delivery 2015; 2: 1-9.

170 Egbaria K, Weiner N. Liposomes as a topical drug delivery system. Advanced Drug Delivery Reviews 1990; 5: 287-300.

171 Vemuri S, Rhodes C. Preparation and characterization of liposomes as therapeutic delivery systems: a review. Pharmaceutica Acta Helvetiae 1995; 70: 95-111.

172 Pierre MBR, Costa IdSM. Liposomal systems as drug delivery vehicles for dermal and transdermal applications. Archives of dermatological research 2011; 303: 607-21.

173 Geusens B, Strobbe T, Bracke S, Dynoodt P, Sanders N, Gele MV, *et al*. Lipid-mediated gene delivery to the skin. European Journal of Pharmaceutical Sciences 2011; 43: 199-211.

174 Cevc G, Blume G. Lipid vesicles penetrate into intact skin owing to the transdermal osmotic gradients and hydration force. Biochimica et Biophysica Acta (BBA)-Biomembranes 1992; 1104: 226-32.

175 Cevc G, Gebauer D, Stieber J, Schätzlein A, Blume G. Ultraflexible vesicles, Transfersomes, have an extremely low pore penetration resistance and transport therapeutic amounts of insulin across the intact mammalian skin. Biochimica et Biophysica Acta (BBA)-Biomembranes 1998; 1368: 201-15.

176 Chandu VP, Arunachalam A, Jeganath S, Yamini K, Tharangini K, Chaitanya G. Niosomes: a novel drug delivery system. International journal of novel trends in pharmaceutical sciences 2012; 2: 25-31.

177 Manosroi A, Khositsuntiwong N, Götz F, Werner RG, Manosroi J. Transdermal enhancement through rat skin of luciferase plasmid DNA loaded in elastic nanovesicles: Biological recognition and interactions of liposomes. Journal of liposome research 2009; 19: 91-8.

178 Gonzalez-Rodriguez M, Rabasco A. Charged liposomes as carriers to enhance the permeation through the skin. Expert opinion on drug delivery 2011; 8: 857-71.

179 Foged C, Brodin B, Frokjaer S, Sundblad A. Particle size and surface charge affect particle uptake by human dendritic cells in an in vitro model. International journal of pharmaceutics 2005; 298: 315-22.

180 Alexander MY, Akhurst RJ. Liposome-mediated gene transfer and expression via the skin. Human molecular genetics 1995; 4: 2279-85.

181 Kim A, Lee EH, Choi S-H, Kim C-K. In vitro and in vivo transfection efficiency of a novel ultradeformable cationic liposome. Biomaterials 2004; 25: 305-13.

182 Mahor S, Rawat A, Dubey PK, Gupta PN, Khatri K, Goyal AK, *et al*. Cationic transfersomes based topical genetic vaccine against hepatitis B. International journal of pharmaceutics 2007; 340: 13-9.

183 Manosroi J, Khositsuntiwong N, Manosroi W, Götz F, Werner RG, Manosroi A. Enhancement of transdermal absorption, gene expression and stability of tyrosinase

plasmid (pMEL34)-loaded elastic cationic niosomes: Potential application in vitiligo treatment. Journal of pharmaceutical sciences 2010; 99: 3533-41.

184 Uyechi L, Gagne L, Thurston G, Szoka Jr F. Mechanism of lipoplex gene delivery in mouse lung: binding and internalization of fluorescent lipid and DNA components. Gene therapy 2001; 8: 828-36.

185 Cevc G, Schätzlein A, Richardsen H. Ultradeformable lipid vesicles can penetrate the skin and other semi-permeable barriers unfragmented. Evidence from double label CLSM experiments and direct size measurements. Biochimica et Biophysica Acta (BBA)-Biomembranes 2002; 1564: 21-30.

186 Rombouts K, Martens TF, Zagato E, Demeester J, De Smedt SC, Braeckmans K, *et al*. Effect of Covalent Fluorescence Labeling of Plasmid DNA on Its Intracellular Processing and Transfection with Lipid-Based Carriers. Molecular pharmaceutics 2014; 11: 1359-68.

187 Mignet N, De Chermont QLM, Randrianarivelo T, Seguin J, Richard C, Bessodes M, *et al*. Liposome biodistribution by time resolved fluorimetry of lipophilic europium complexes. European Biophysics Journal 2006; 35: 155-61.

188 Aceña J, Stampachiacchiere S, Pérez S, Barceló D. Advances in liquid chromatography–high-resolution mass spectrometry for quantitative and qualitative environmental analysis. Analytical and bioanalytical chemistry 2015; 407: 6289-99.

189 Lyubarskaya Y, Kobayashi K, Swann P. Application of mass spectrometry to facilitate advanced process controls of biopharmaceutical manufacture. Pharmaceutical Bioprocessing 2015; 3: 313-21.

190 Lietz CB, Gemperline E, Li L. Qualitative and quantitative mass spectrometry imaging of drugs and metabolites. Advanced drug delivery reviews 2013; 65: 1074-85.

191 Pacholarz KJ, Garlish RA, Taylor RJ, Barran PE. Mass spectrometry based tools to investigate protein–ligand interactions for drug discovery. Chemical Society Reviews 2012; 41: 4335-55.

192 Gross JH, Roepstorff P. Mass Spectrometry: A Textbook. (Springer, 2011).

193 Korfmacher WA. Mass Spectrometry for Drug Discovery and Drug Development. (Wiley, 2012).

194 Korfmacher WA. Using Mass Spectrometry for Drug Metabolism Studies, Second Edition. (Taylor & Francis, 2010).

195 Buse J, Badea I, Verrall RE, El-Aneed A. Tandem mass spectrometric analysis of the novel gemini surfactant nanoparticle families G12-s and G18: 1-s. Spectroscopy Letters 2010; 43: 447-57.

196 Buse J, Badea I, Verrall RE, El-Aneed A. Tandem mass spectrometric analysis of novel diquaternary ammonium gemini surfactants and their bromide adducts in electrospray-positive ion mode ionization. Journal of Mass Spectrometry 2011; 46: 1060-70.

197 Mohammed-Saeid W, Buse J, Badea I, Verrall R, El-Aneed A. Mass spectrometric analysis of amino acid/di-peptide modified gemini surfactants used as gene delivery agents: Establishment of a universal mass spectrometric fingerprint. International Journal of Mass Spectrometry 2012; 309: 182-91.

198 Donkuru M, Chitanda JM, Verrall RE, El-Aneed A. Multi-stage tandem mass spectrometric analysis of novel β-cyclodextrin-substituted and novel bis-pyridinium gemini surfactants designed as nanomedical drug delivery agents. Rapid Communications in Mass Spectrometry 2014; 28: 757-72.

199 Buse J, Badea I, Verrall RE, El-Aneed A. A general liquid chromatography tandem mass spectrometry method for the quantitative determination of diquaternary ammonium gemini surfactant drug delivery agents in mouse keratinocytes' cellular lysate. Journal of Chromatography A 2013; 1294: 98-105.

200 Buse J PR, Verrall RE, Badea I, Zhang H, Mulligan CC, Peru KM, Bailey J, Headley JV, El-Aneed A.*. The Development and assessment of high-throughput mass spectrometry-based methods for the quantification of a nanoparticle drug delivery agent in cellular lysate. Journal of Mass Spectrometry. 2014.

201 Donkuru M, Michel D, Awad H, Katselis G, El-Aneed A. Hydrophilic interaction liquid chromatography–tandem mass spectrometry quantitative method for the cellular analysis of varying structures of gemini surfactants designed as nanomaterial drug carriers. Journal of Chromatography A 2016; 1446: 114-24.

CHAPTER 2

Di-Peptide-Modified Gemini Surfactants as Gene Delivery Vectors: Exploring the Role of the Alkyl Tail in Their Physicochemical Behaviour and Biological Activity

Mays A. Al-Dulaymi[1], Jackson M. Chitanda[2], Waleed Mohammed-Saeid[1], Hessamaddin Younesi Araghi[3], Ronald E. Verrall[3], Pawel Grochulski[1, 4], Ildiko Badea[1*]

1. College of Pharmacy and Nutrition, University of Saskatchewan, Saskatoon, SK, Canada.
2. Department of Chemical and Biological Engineering, University of Saskatchewan, Saskatoon, SK, Canada
3. Department of Chemistry, University of Saskatchewan, Saskatoon, SK, Canada
4. Canadian Light Source, Saskatoon, SK, Canada

---

*This chapter is published in The AAPS Journal, 2016, 18(5):1168-81.

Transitioning rationale:

Literature review provided evidence about the potential of gemini surfactants as a gene delivery vector. Modifications to the gemini surfactants' molecular structure may significantly affect the efficiency of the delivery system. Previous research revealed that the insertion of amino acids into the gemini surfactants' spacer resulted in the production of compounds with enhanced transfection efficiency and reduced cytotoxicity. This chapter aims at evaluating the impact of altering the hydrophobic tails of gemini surfactants on the physicochemical characteristics and biological activity.

Contribution statement:

Mays Al-Dulaymi contributed to this manuscript by designing the study, performing experiments, data acquisition, data analysis and manuscript writing except the chemical synthesis part. Dr. Jackson Chitanda synthesized the gemini surfactants used in this work. Drs. Grochulski and Badea performed the onsite SAXS measurements.

2.1. Abstract

The aim of this work was to elucidate the structure-activity relationship of new peptide-modified gemini surfactant-based carriers. Glycyl-lysine modified gemini surfactants that differ in the length and degree of unsaturation of their alkyl tail were used to engineer DNA nano-assemblies. To probe the optimal nitrogen to phosphate (N/P) ratio in the presence of helper lipid, *in vitro* gene expression and cell toxicity measurements were carried out. Characterization of the nano-assemblies was accomplished by measuring the particle size and surface charge. Morphological characteristics and lipid organization were studied by small angle X-ray scattering technique. Lipid monolayers were studied using a Langmuir-Blodgett trough. The highest activity of glycyl-lysine modified gemini surfactants was observed with the 16-carbon tail compound at 2.5 N/P ratio, showing a 5 to 10-fold increase in the level of reporter protein compared to the 12 and 18:1 carbon-tail compounds. This ratio is significantly lower compared to the previously studied gemini surfactants with alkyl or amino- spacers. In addition, the 16-carbon tail compound exhibited the highest cell viability (85%). This high efficiency is attributed to the lowest critical micelle concentration of the 16-tail gemini surfactant and a balanced packing of the nanoparticles by mixing a saturated and unsaturated lipid together. At the optimal N/P ratio, all nanoparticles exhibited an inverted hexagonal lipid assembly. The results showed that the length and nature of the tail of the gemini surfactants play an important role in determining the transgene efficiency of the delivery system. Moreover, the interplay between the head group and the nature of tail is specific to each series, thus in the process of rational design the contribution of the latter should be assessed in the appropriate context.

2.2. Introduction

Over the past quarter century, gene delivery has attracted significant interest due to the potential of gene therapy to treat both genetic and acquired diseases. However, one of the major hurdles for the successful application remains the effective delivery of genetic material into the targeted cells. Currently, there are two main categories of gene therapy vectors: viral and non-viral. Viruses are the most effective vectors for gene therapy; however, they suffer from major drawbacks particularly their propensity to trigger immune response and mutagenic toxicity [1]. Non-viral methods, on the other hand, are considered safer alternatives, which can be prepared, easily in large quantities and at lower cost. Although numerous non-viral methods of delivery are currently available, the use of cationic lipids is the most prominent[2]. They have the ability to compact the negatively charged DNA through electrostatic interaction forming nano-sized lipoplexes as a delivery vehicle [3-5]. One special family of cationic lipids is the quaternary ammonium gemini surfactants [6], which have shown promising results in delivering DNA. Gemini surfactants are composed of two head groups attached to their hydrocarbon tails and connected by a spacer. Compared to classic monomeric surfactants, gemini surfactants possess a number of superior properties such as one to two orders of magnitude lower critical micelle concentration (CMC), lower Krafft temperature, and greater ability to reduce surface tension.

The structure of the gemini surfactants plays an essential role in determining the supramolecular arrangement into nanoparticles; hence, will have direct effects on the cytotoxicity and the gene delivery efficiency. Our research strategy follows a rational design approach to develop novel families of gemini surfactants and conduct component-by-component tests aimed at producing compounds with superior transgene efficiency and minimum cytotoxicity. As a starting point, the simplest family of gemini surfactants with aliphatic spacer,

was extensively studied [7-11]. Modifications to the gemini surfactants' architecture by varying the length of the hydrophobic tail and/or the spacer were found to have a significant impact on the morphology of the lipid/DNA nanoparticles (lipoplexes) and their transfection efficiency [8, 9]. In an attempt to form intelligent nanoparticles that respond to environmental stimuli, pH-sensitive gemini surfactants were also synthesized by inserting an amino group into the spacer [12]. Among the series, 12-7NH-12 showed superior transfection efficiency and adopted various morphologies which may have facilitated membrane fusion, aiding the release of the DNA within the cell. In order to achieve a more balanced binding and release of the genetic material, a third generation was conceived by coupling amino acids or peptides into the N position of the spacer of 12-7NH-12. The insertion of amino acids that provided additional terminal amino groups resulted in: (i) enhanced binding to the cell membrane by forming hydrogen bonds, (ii) improved gemini surfactant-DNA electrostatic interaction due to the high pK_a value of the terminal amines and (iii) induced liposomal fusion through a flip-flop mechanism due to the strong electrostatic interaction between the nanoparticles and the cell membrane [13, 14]. The glycyl-lysine substituted gemini surfactant yielded lipoplexes with enhanced transfection efficiency showing a significantly higher gene expression compared to the unsubstituted parent compound without increasing cytotoxicity [13, 14].

In this work, further investigations of the glycyl-lysine substituted gemini surfactants was carried out by examining the effect of the length of the alkyl tail and the degree of unsaturation on the assembly of the nanoparticles and, subsequently, the impact on their transfection efficiency and cytotoxicity. Three glycyl-lysine substituted compounds having dodecyl, hexadecyl and oleyl tails (Figure 2.1A) were complexed with pDNA and the transfection efficiency of the lipoplexes was tested *in vitro*. Small-angle X-ray scattering (SAXS)

measurements were carried out in order to probe the morphology of the lipoplexes and to correlate with their transfection efficiency. The ultimate goal of this study is to enrich the understanding of the structure-activity relationship of the gemini surfactants and to provide fundamental information for the bottom-up design of gemini surfactant-based gene delivery systems.

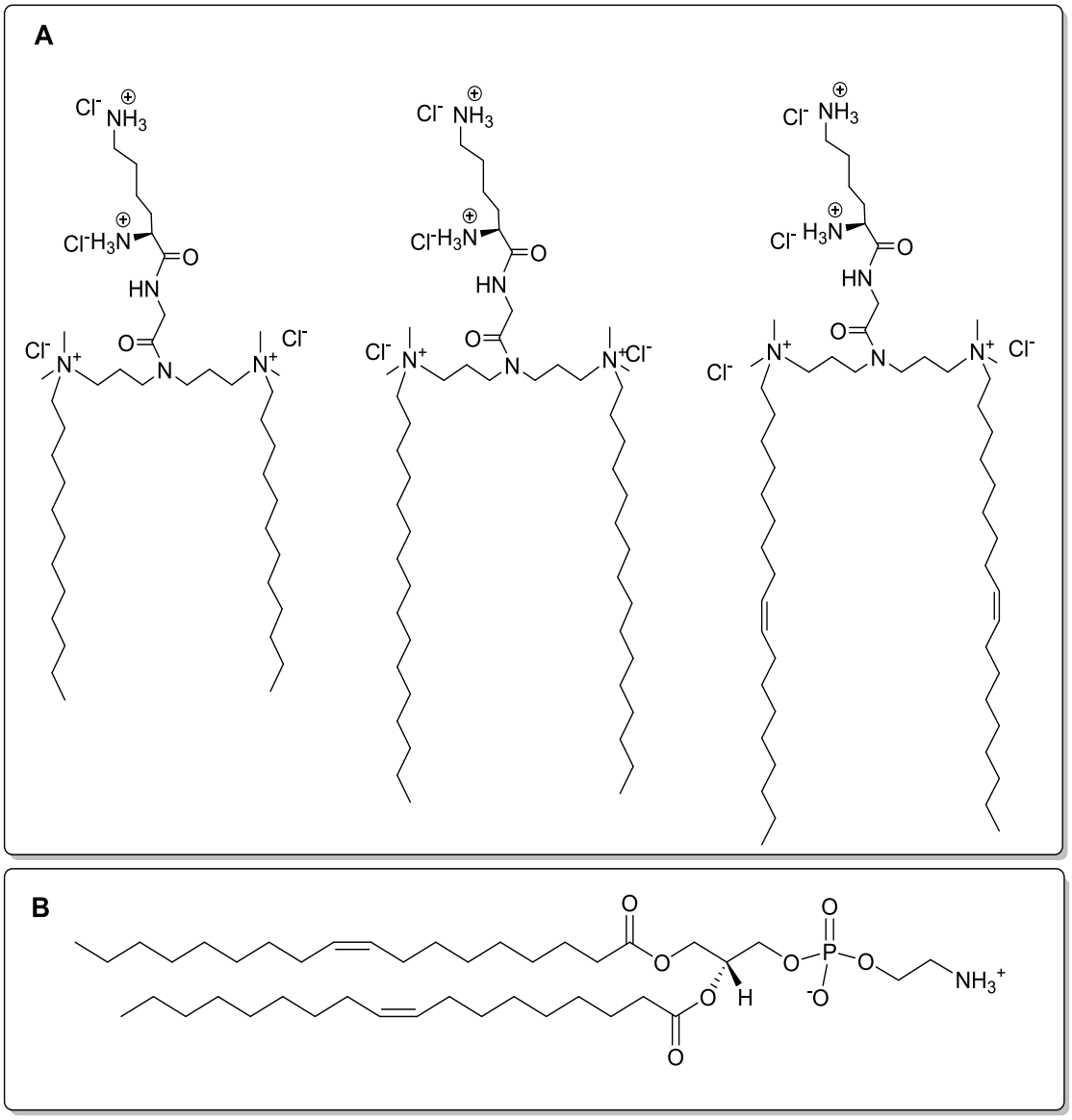

Figure 2.1. Chemical structure of (A) the tested cationic gemini surfactants and (B) helper lipid DOPE

2.3. Materials and methods

2.3.1. Synthesis of glycyl-lysine modified gemini surfactants

The synthesis of three dipeptide cationic gemini lipids, designated as m-7N(G-K)-m (G = glycine and K = lysine) where m is the alkyl tail carbon chain length, m = 12, 16 and 18:1 (18:1 = mono-unsaturated oleyl chain), is illustrated in Scheme 1. Unless otherwise stated, all reactions were performed under N_2 atmosphere using standard Schlenk techniques. Boc-gly-OH (99%), *O*-(7-azabenzotriazol-1-yl)-1,1,3,3-tetramethyluronium hexafluorophosphate (HATU, 98%), bis-boc-lysine (99%),and *N*-diisopropylethylamine (DIPEA, 99.8%) were obtained from Chem-Impex International Inc. Dry dimethylformamide (DMF, ≥99.5%, kept over molecular sieves), *3,3'*-iminobis(*N*,*N*-dimethyl-propylamine) (97%), iodohexadecane (95%, stabilized with copper) and 4M HCl (in dioxane) were purchased from Sigma-Aldrich. HPLC grade methanol and iododododecane (98%, stabilized with copper) were purchased from Alfa Aesar, while anhydrous ACS grade granular Na_2SO_4 and ACS grade $NaHCO_3$ powder were acquired from EMD chemical company. Oleylbromide was prepared from oleyl alcohol (97%, Acros Organics) using triphenylphosphine dibromide (96%, Aldrich) as previously described [15]. All chemicals were used without any further purification. Mass Spectra were obtained by using a QSTAR^{XL} MS/MS System. ^{1}H NMR spectra, in either $CDCl_3$ or dimethylsulfoxide (DMSO)-d_6, were recorded by using a Bruker 500 MHz Avance spectrometer. Chemical shifts, δ, are reported in ppm, referenced to the residual ^{1}H and ^{13}C ($CDCl_3$ at 7.26, 77.23 and DMSO-d_6 at 2.50, 39.58), respectively.

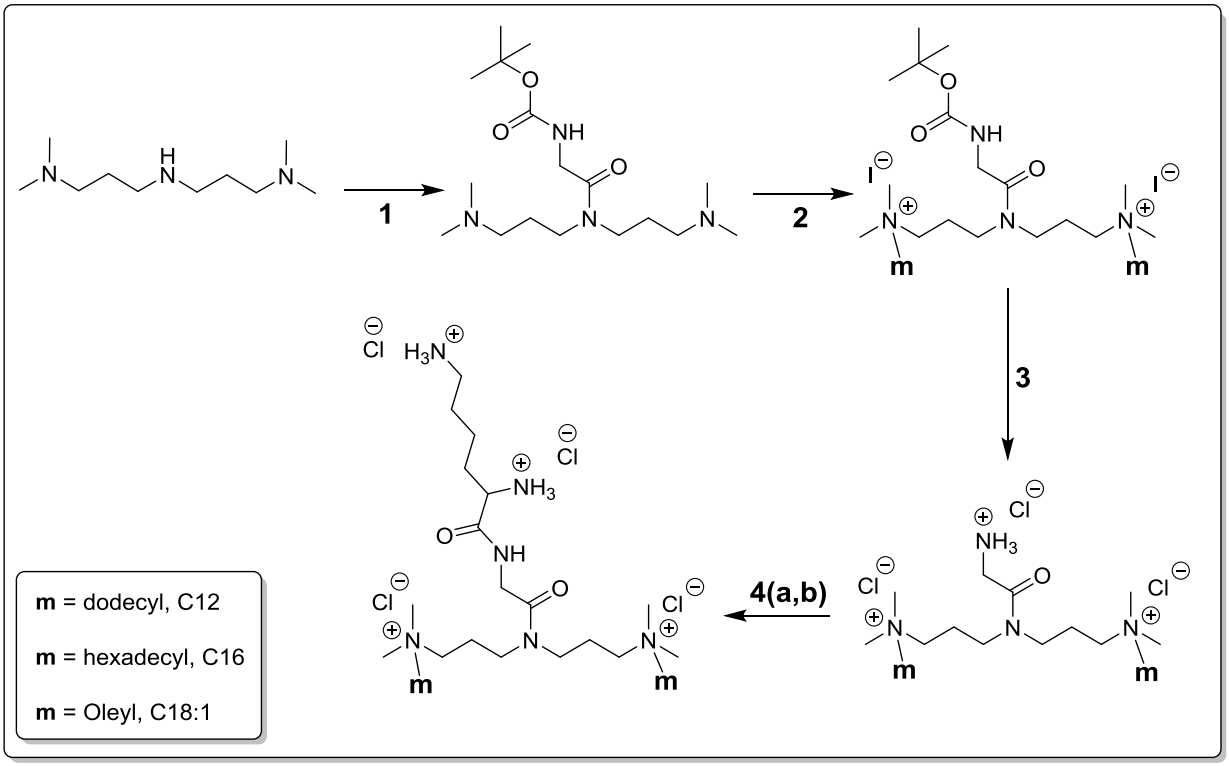

Scheme 2.1. Synthesis of glycyl-lysine gemini surfactants having different carbon tail lengths and functionalities. Step (**1**): Boc-glycine, HATU, DIPEA, DMF, 18 h. Step (**2**): iododododecane, iodohexadecane or oleybromide, DMF, 18 h. Step (**3**): 4M HCl, dichloromethane, 2 h. Step (**4a**): bis-boc-lysine, HATU, DIPEA, DMF, 18 h (**4b**) 4M HCl, dichloromethane, 2 h.

Briefly, in step (**1)** boc-glycine (1.00 g, 0.0457 mmol), HATU (2.480 g, 6.54 x 10^{-3} mol) and DIPEA (2.1 mL, 5.944 x 10^{-3} mol, 2eq.) were sequentially placed in a 100 mL Schlenk flask containing 20 mL DMF and stirred under an inert atmosphere for 15 min to give a pale-yellow and later a dark-red mixture. 3,3'-iminobis (*N*, *N*-dimethyl-propylamine (4.00 g, 0.0467 mmol, 1 eq.) was then added and the reaction mixture was stirred for 18 h. DMF was removed under high vacuum. To the residue, 100 mL dichloromethane (DCM) was added and then solvent extracted with saturated sodium bicarbonate (5 x 100 mL). The combined aqueous layers were further extracted with DCM (5 x 100 mL). Organic layers were combined and dried over anhydrous sodium sulfate. Excess DCM was removed under vacuum to give a reddish oily desired

compound that was confirmed by ^{1}H-NMR. This was further purified by washing with chloroform; the desired compound is soluble in chloroform (69%).

In step (**2**), the product of step (**1**) was reacted with the respective alkyl and alkene halide compounds (C12, C16 or C18:1) in a 1 to 2 ratio, respectively. For C12 and C16 alkyl tails, the mixture was stirred at ambient temperature overnight in DMF and the C18:1 tail was stirred at 80 °C for 2 days in DMF. After the removal of excess solvent; the residue was washed by decantation using diethyl ether and thereafter with pentane. The red substance was dried under high vacuum. Proton NMR was consistent with the expected spectra of the desired compounds.

In step (**3**), Boc de-protection was carried out by dissolving the boc containing products of step (**2)** in 20 mL dry DCM and adding 10 mole equivalents of HCl (4M in dioxane). After stirring for 2 h, excess solvent was removed and the residue was washed by decantation with diethyl ether. Finally, DCM was added to dissolve the compound and then it was precipitated by using diethyl ether. This was repeated three times before the sample was dried under high vacuum.

In Step (**4a**), bis-boc-lysine, HATU and DIPEA were sequentially placed in a 100 mL Schlenk flask containing 20 ml DMF at inert atmosphere to give a pale-yellow and later to a dark-red mixture. After stirring for 15 min, the product from step (**3**) was added. DMF was removed under high vacuum after stirring for 18 h. To the residue, 100 mL DCM was added and then extracted with saturated sodium bicarbonate (5 x 100 mL). The extracted organic layer were dried over anhydrous sodium sulfate, and then concentrated under vacuum to give the reddish oily compound. The final step (step (**4b**)) is the boc deprotection step as described in step (**3**). The final products had a yellowish to orange color. The counter ion exchange reaction, from

either bromide or iodide to chloride counter ion, was achieved during the two de-protection steps (addition of excess HCl).

All steps were verified by ^{1}H NMR spectroscopy and were consistent with the expected spectrum for desired compounds.

12-N(GK)-12: ^{1}H NMR (500 MHz, DMSO-d_6): δ 8.97 (m) 1H (NH_3-CH(-CH_2-)-C=O; 8.46 (m) 3H (-NH_3), 8.30 (m) 3H (-NH_3); 4.12 (d) 1H; 4.04 (d) 1H (-NH-CH_2-C=O-); 3.90 (m) 1H (-NH-CH_2-C=O-); 3.33 (m) 12H; 3.07 (s) 6H (-N(CH_3)$_2$); 3.04 (s) 6H (-N(CH_3)$_2$); 2.71 (m) 2H; 2.01 (m) 2H; 1.91 (m) 2H, 1.70 (m) 2H; 1.65-1.60 (m) 6H; 1.45 (m) 2H; 1.24 (m) 36H; 0.84 (t) 6H (-CH_3). MS-TOF (m/z); Calculated for $C_{42}H_{90}N_6O_2^{2+}$; expected 355.3557, found 355.3571

16-N(GK)-16: ^{1}H NMR (500 MHz, DMSO-d_6): δ = 8.93 (m) 1H (NH_3-CH(-CH_2-)-C=O-); 8.44 (m) 3H (-NH_3), 8.27 (m) 3H (-NH_3); 4.15 (d) 1H (-NH-CH_2-C=O-); 4.04 (d) 1H (-NH-CH_2-C=O-); 3.90 (m) 1H; 3.33 (m) 12H; 3.04(s) 6H (-N(CH_3)$_2$); 3.04 (s) 6H (-N(CH_3)$_2$); 2.72 (m) 4H; 2.01 (m) 2H; 1.91 (m) 2H, 1.77 (m) 2H; 1.68-1.59 (m) 6H; 1.45 (m) 2H; 1.23 (m) 50H; 0.84 (t) 6H (-CH_3). MS-TOF (m/z); Calculated for $C_{50}H_{106}N_6O_2^{2+}$; expected 411.4183, found 411.4094

18-N(GK)-18: ^{1}H NMR (500 MHz, DMSO-d_6): δ 8.88 (m) 1H (NH_3-CH(-CH_2-)-C=O-); 8.37 (m) 3H (-NH_3), 8.17 (m) 3H (-NH_3); 5.32 (m) 4H (-CH=CH-); 4.12 (d) 1H (-NH-CH_2-C=O-); 4.05 (d) 1H (-NH-CH_2-C=O-), 3.90 (m) 1H; 3.40-3.25 (m) 12H; 3.04(s) 6H (-N(CH_3)$_2$); 3.02 (s) 6H (-N(CH_3)$_2$); 2.72 (m) 4H; 1.94 (m) 8H; 1.91 (m) 2H, 1.77 (m) 2H; 1.68-1.59 (m) 8H; 1.45 (m) 2H; 1.23 (m) 42H; 0.84 (t) 6H (-CH_3). MS-TOF (m/z); Calculated for $C_{54}H_{110}N_6O_2^{2+}$; expected 437.4340, found 437.4334.

2.3.2. Formulations

The plasmid pGT.IFN-GFP (pDNA), encoding for murine interferon gamma (IFN-γ) and green fluorescent protein (GFP) was utilized in this work [8]. QIAGEN Plasmid Giga Kit (Mississauga, ON, Canada) was used to isolate and purify the plasmid DNA according to the manufacturer's instructions. The gemini lipids were combined with pDNA at six different nitrogen (cationic) to phosphate (anionic) charge ratios (N/P) of 1, 2.5, 5, 10, 15 and 20 in the presence of a fixed amount of a helper lipid, 1,2-dioleoyl-*sn*-glycerol-3-phosphoethanolamine (DOPE) (Avanti Polar Lipids Inc., Alabaster, USA). (Figure 2.1B), at a final concentration of 1mM to create pDNA / gemini lipid / helper lipid (P/G/L) nanoparticles. An appropriate amount of 3mM aqueous solutions of gemini was added to 200 µg/mL pDNA and incubated for 20 minutes at room temperature (P/G complex). 1 mM DOPE was prepared as described previously [9] and added to P/G complexes to form the final nanoparticles (P/G/L).

2.3.3. Cell culture and in vitro transfection study

COS-7 African green monkey kidney fibroblasts cell line (ATCC, CRL-1651) were grown to 80% confluency in 75-cm^2 tissue culture flasks in Dulbecco's modified Eagle's medium (DMEM) obtained from ATCC (Manassas, VA USA) supplemented with 10% (vol/vol) fetal bovine serum and 1% (vol/vol) antibiotic antimycotic agents and incubated at 37 °C with 5% CO_2. One day prior to transfection, 96-well tissue culture plates (Falcon, BD Mississauga, ON, Canada) were seeded with the cells at a density of 1×10^4 cells/well. The supplemented DMEM was replaced with DMEM one hour prior to transfection. Cells were transfected with 0.2 µg/well pDNA and incubated at 37 °C in CO_2 for 5 h. Lipofectamine Plus reagent (Invitrogen Life Technologies) was used as a positive control according to the manufacturer's protocol. The transfection mixture was replaced by supplemented DMEM after 5 h. Supernatants were collected at 24 and 48 h and replaced with fresh medium. The collected supernatants were stored

at - 20 °C. The results presented are the average of three plates of quadruplicate wells.

2.3.4. Enzyme-linked immunosorbent assay (ELISA)

ELISA was carried out to measure the level of interferon gamma using flat bottom 96-well plates (Immulon 2, Greiner Labortechnik, Germany) according to the BD Pharmingen protocol. A standard IFN-γ curve was created using recombinant mouse IFN-γ standard (BD Biosciences, Mississauga, ON, Canada) to calculate the concentration of the secreted IFN-γ.

2.3.5. 3-(4,5-Dimethylthiazol-2-yl)-2,5-diphenyltetrazolium bromide (MTT) assay

MTT assay was performed to examine the cytotoxicity of the peptide-substituted gemini surfactants in the COS-7 cell-line. Three 96-well cell culture plates were seeded with cells at a density of 1×10^4 cells/well and treated with the P/G/L nanoparticles. Plates were incubated for 5 h at 37 °C with 5% CO_2 before replacing the old media with fresh media as described in the transfection section. Cell toxicity was evaluated 48 h after treatment. Lipofectamine, a commercial transfection agent, was used as a positive control. A sterile solution of 5 mg/mL of MTT (Invitrogen, U.S.A.) in phosphate buffered saline (PBS) was prepared, mixed with supplemented media, then added to the cells and incubated for 3 h. The supplemented media was removed and the formed, purple formazan crystal was dissolved in dimethyl sulfoxide (spectroscopy grade, Sigma-Aldrich, ON, Canada) and the plates incubated at 37 °C for 10 m. Absorbance was measured at 550 nm using a microplate reader (BioTek® Microplate Synergy HT, VT, U.S.A.). The results are the average of three plates (treated with individually prepared formulations of quadruplicate wells) and the cytotoxicity is expressed as a percentage of the non-transfected control cells ± standard deviation.

2.3.6. Size and ζ-potential measurements

Size and ζ-potential measurements for the three lipids at six N/P ratios were performed by using a Zetasizer Nano ZS instrument (Malvern Instruments, Worcestershire, UK). An MPT-2 autotitrator was connected to the Zetasizer Nano ZS to measure size and ζ-potential of 16-7N(G-K)-16 at N/P =10 as a function of pH. A 9 mL aliquot of sample was placed in the titration cell of the autotitrator and titrated with 0.1 M HCl over the desired pH range using 0.2–0.5 pH unit increments. Samples were prepared as described in the formulation section and each sample was measured three times and the results reported are the average of the three readings ± standard deviation.

2.3.7. SAXS measurements

The formulations were prepared as for the transfection study using ten times higher concentrations. The SAXS experiments were performed at the BL4-2 beam line at Stanford Synchrotron Radiation Lightsource (SSRL, Stanford, USA) using a wavelength of 1.1271 Å (11KeV energy). The scattered X-ray was detected on MAR225-HE (225 mm x 225 mm (3072 x 3072 pixels, pixel size 73.24 μm) at 20s exposure time and at sample to detector distance of 1.1m. The SAXS detector was calibrated with silver behenate. GSASII software was used to plot diffraction intensity versus 2θ (where θ is the diffraction angle) or the scattering vector ($q = \frac{4\pi}{\lambda}\sin\theta$) by radial integration of the 2D patterns.

2.3.8. Langmuir Studies

The Langmuir-Blodgett technique was utilized to determine the surface area occupied by the gemini surfactant head group. Surface pressure-mean molecular area isotherms were collected using a Langmuir minitrough (KSV, Helsinki, Finland) equipped with a Wilhelmy plate balance. The trough was filled with ultrapure water (Millipore, resistivity 18 MΩ·cm) as a

subphase and the temperature was maintained at 22 °C. Stock solutions of the three gemini lipids or DOPE were prepared at a concentration of 1 mM of lipid in chloroform. 30 μL of the stock solution was spread dropwise on the surface of the subphase with a Hamilton syringe. The solvent was allowed to evaporate for 10 min before the monolayer was compressed at a speed of 20 $mm \cdot min^{-1}$.

2.3.9. Structure calculations

An estimate of the length of the hydrocarbon tails was attained by using Avogadro software [16]. Volume calculations were conducted with Gaussian09 software, revision C.01 [17]. The geometry was optimized on the B3LYP level of theory with 6-311+G(d,p) basis set. Optimized structures were confirmed using harmonic frequency calculations. Volumes for the optimized structure were calculated using united atom radii.

2.3.10. Statistical analysis

Statistical analyses were performed using SPSS software (Version 23.0). Results expressed as the average of $n \geq 3 \pm SD$. One-way analysis of variance (ANOVA, Scheffé/Dunnett's post hoc tests) were used for statistical analyses. Significant differences were considered at $p<0.05$ level.

2.4. Results and Discussion

2.4.1. Evaluation of the *in vitro* transfection activity

One of the purposes of the study was to investigate the effect of structure on the level of gene expression. The tested compounds, 12-7N(G-K)-12, 16-7N(G-K)-16 and 18:1-7N(G-K)-18:1 varied in the length of their hydrophobic tails and the degree of unsaturation within the carbon tails. P/G/Ls of the gemini lipid 16-7N(G-K)-16 showed the highest transfection efficiency compared to 12-7N(G-K)-12 and 18:1-7N(G-K)-18:1 at all N/P ratios (Figure 2.2). The interaction of pDNA with cationic amphiphiles plays a key role in the delivery of genetic material. Lipoplex formation results mainly from the electrostatic interaction between the negative phosphate group in the DNA backbone and the positive cationic lipid head group(s), in addition to the cooperative hydrophobic interaction between the tail groups of the cationic lipid [18]. By increasing the length of the alkyl tail, there is an increase in the compound's hydrophobicity resulting in better interaction with the DNA [19, 20]. Matulis *et al* showed that addition of a methylene group in the aliphatic lipid chain increases the lipid-DNA binding constant by 4 fold [18].

At N/P of 1 (Figure 2.2), a low level of protein expression was detected in cells treated with 16-7N(G-K)-16 nanoparticles (1.6 ±1 ng INF-γ /10^4 cells) while none was detected for 12-7N(G-K)-12 and 18:1-7N(G-K)-18:1 nanoparticles. For all three gemini surfactants, increasing the N/P ratio was associated with an elevation in the level of protein expression reaching a maximum at an N/P value of 2.5 followed by a decreasing trend illustrating a bell-shaped disposition, especially for 16-7N(G-K)-16 (Figure 2.2). At the most efficient charge ratio (2.5 N/P), 16-7N(G-K)-16 gemini lipid showed the highest transfection efficiency (11.7± 0.8 ng INF-γ /10^4

cells) with more than a 10 fold and 5 fold increase in the level of INF-γ compared to 18:1-7N(G-K)-18:1 and 12-7N(G-K)-12, respectively. A significant decrease in the level of protein expression was observed at N/P ratios above 5 becoming undetectable for all the tested compounds at a charge ratio of 20. This could be explained by the very strong DNA compaction that could hinder the release of the DNA from the carrier.

Interestingly, the optimal N/P ratio of 2.5 was considerably lower compared to previous generations of gemini lipids, which showed maximum efficiency at N/P = 10 [8, 21]. This can be attributed to the fact that the glycyl-lysine substituted gemini surfactants have a greater number of terminal amino groups that can undergo protonation with decreasing pH, leading to an increase in the positive charge of the glycyl-lysine substituted compounds. As a result, fewer gemini surfactant molecules are required to neutralize and compact the DNA compared to the previous generations of gemini surfactants. Furthermore, the substitution with glycyl-lysine moieties in the spacer renders a conformational flexibility to the gemini surfactants and offers a balanced binding with the DNA, adequate to avoid enzymatic degradation and to maintain intracellular release [14]. Moreover, in the previously studied m-3-m series, there was only a 50% increase in gene delivery efficiency from the 12-tail to the 16-tail gemini [8], while in this new series there was a 5-fold increase between the 12 and the 16-tail peptide substituted gemini surfactants, demonstrating significantly better efficiency.

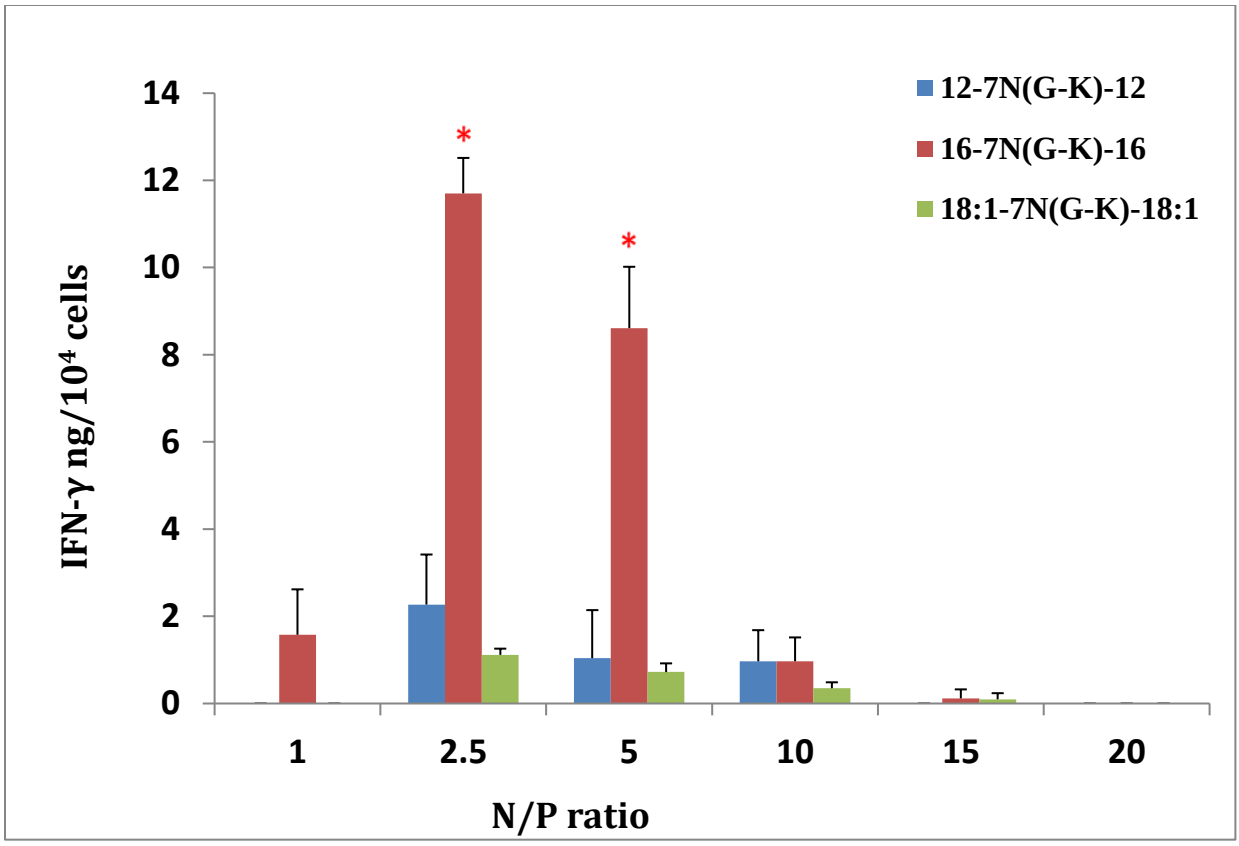

Figure 2.2. *In vitro* transfection of COS-7 cells comparing the level of IFN-γ expression of the three gemini surfactants after 48 h of treatment. Results are the average of three plates of quadruplicate wells, error bars represent standard deviation. * Indicates significant at $p < 0.05$.

2.4.2. Assessment of cell viability

The toxicity of the P/G/L nanoparticles prepared with the three gemini surfactants was evaluated in COS-7 cell line after 48 h of treatment (Figure 2.3). P/G/Ls of the 16-7N(G-K)-16 exhibited the highest cell viability, 67-85%, at all the N/P ratios studied followed by 12-7N(G-K)-12, 36-77%, and 18:1-7N(G-K)-18:1 with 23-67% of the cells being viable (Figure 2.3). It is worth noting that at the optimal ratio, P/G/Ls of the 16-7N(G-K)-16 showed a significantly lower toxicity (more than 80% cell viability, $p<0.05$) compared to a commercially available transfection agent (approximately 50 % viability) (Figure S1, Appendix I). Above the optimal N/P ratios there was a trend of dose-dependent increase of cytotoxicity for all compounds. Since at lower N/P ratios the concentration of gemini surfactants was lower, it was expected to show less toxicity. It was reported that after the neutralization of DNA with cationic surfactant, no more surfactant will bind to the lipoplex. As such, excess surfactant will remain in the supernatant as free micelles [22, 23]. Thus at higher N/P ratios, the toxicity could be triggered by the excess free surfactant.

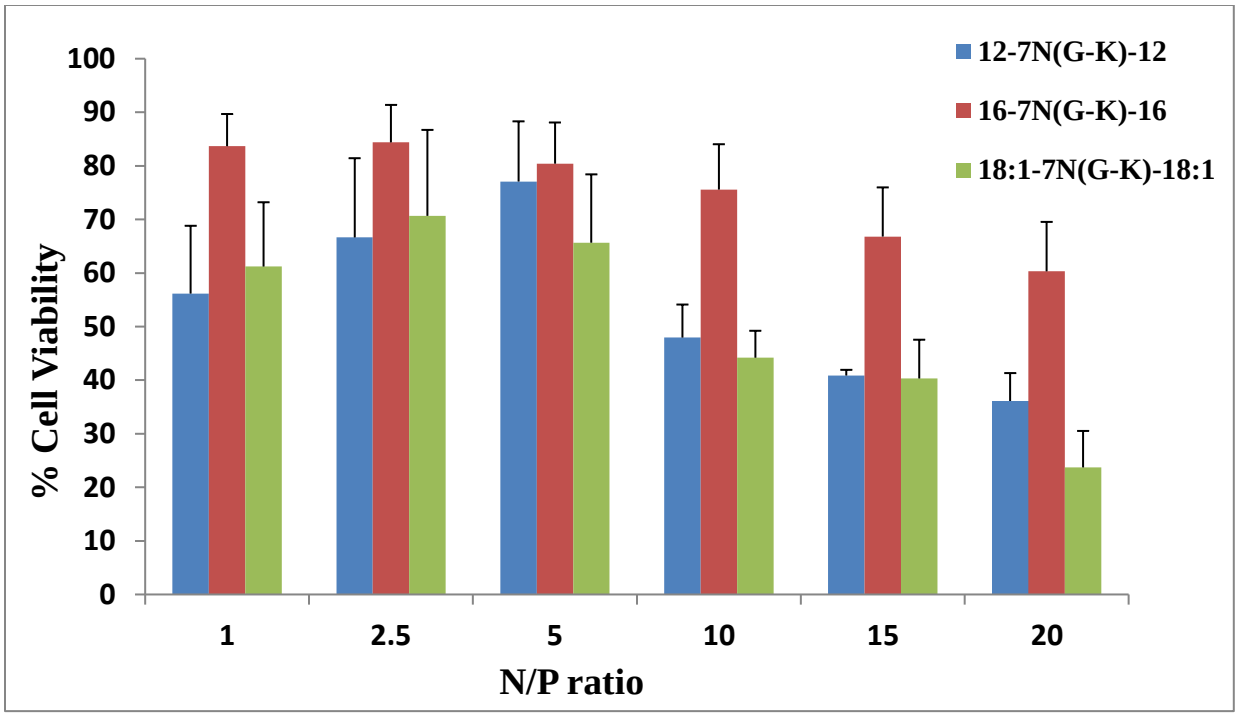

Figure 2.3. Evaluation of COS-7 cell viability at six different N/P ratios of the three gemini surfactants using MTT assay after 48 h of treatment. Results are the average of three plates of quadruplicate wells, error bars represent standard deviation.

2.4.3. Physicochemical characterization of the lipid-based gene delivery system

2.4.3.1. Determination of the critical micelle concentration (CMC)

Increasing the length of the alkyl chain from C12 to C16 was accompanied by a significant decrease in the critical micelle concentration (CMC) from 3.72 to 0.155 mM, while the compound with mono-unsaturated oleyl chains exhibited a slight but definite increase in CMC value (0.178 mM) compared to the C16 gemini. The behaviour of the C16 and C12 gemini is in agreement with previously observed behaviour of the diquaternary ammonium gemini surfactants [24]. Kuiper *et al.* showed that the introduction of a double bond, especially cis-oriented, increases the CMC of the compound compared to the corresponding saturated analogue [25]. This was attributed to (i) decrease in hydrophobicity as the hydrophobic fragmental constant

for the double bond is 0.63 while for the single bond it is 1.476, (ii) decrease in the tail length as the carbon-carbon double bond is shorter than the single bond, and (iii) the hindered ability of the alkyl chain to pack in the core of the micelle due to the less flexible unsaturated tails [25]. In addition, cis-oriented bond drives the carbon chain to turn back on itself, making the extension shorter compared to the fully extended tail. The lowest CMC for the 16-7NGK-16 surfactant indicates that this surfactant has the highest propensity for supramolecular assembly.

The CMC has been shown to correlate with transfection efficiency. Dauty *et al.* found that in dimerized surfactants, a low CMC was accompanied by higher transfection efficiency compared to monovalent counterparts as they increased the stability of the lipoplexes during the delivery process [26]. Similarly, the P/L/G nanoparticles of the 16-7N(G-K)-16 gemini surfactant having the lowest CMC showed the highest transfection ability in the series studied in this work. Based on this hypothesis, the 18:1-7N(G-K)-18:1 should show higher transfection efficiency compared to 12-7N(G-K)-12 as it has a lower CMC (0.178 mM). However, the 18:1-7N(G-K)-18:1 showed the lowest transfection efficiency at all charge ratios (Figure 2.2). This is in agreement with our previous results for the parent compound m-7NH-m [21], which can be attributed to the loose packing arrangement that might result from mixing two unsaturated lipids (18:1-7N(G-K)-18:1 and DOPE) to form the P/G/L nanoparticles.[27] The looser packing might be due to the presence of the double bond that confers less flexibility to the molecule compared to the fully saturated tails of 12-7N(G-K)-12 and 16-7N(G-K)-16. Formulations prepared by mixing a saturated and unsaturated lipid together resulted in the highest transfection efficiency compared to formulations prepared from mixing either two saturated lipids or two unsaturated lipids together [27].

2.4.3.2. Determination of size and ζ-potential

In order to correlate the gene delivery efficiency to the physicochemical properties of the P/L/G nanoparticles, size and zeta potential measurements of the three compounds at six N/P ratios were carried out. The nanoparticles showed a range of particle sizes between 70 and 900 nm. At the optimal N/P ratios of 2.5, no significant differences were observed between nanoparticles containing gemini compounds with the 12 carbon tail or the 16 carbon tail (77±2 nm and 81±3 nm, respectively), whereas the P/L/Gs with the 18-carbon mono-unsaturated oleyl tails showed a relatively larger particle size of 206±6 nm. This trend is in agreement with size measurements of previous generations of gemini surfactants [21] and correlates with the loose packing theory[27].

Similar to previous generations [28], the particle size of the lipoplexes decreased with increasing N/P ratio, implying the importance of charge ratio in determining the particle size. For example, at N/P=1 the particle size of all tested compounds was either very large [650 nm for 16-7N(G-K)-16 and 900 nm for 18:1-7N(G-K)-18:1] or outside of the measurable range of 10-6000nm for the 12-7N (G-K)-12, showing visible precipitation, while at a N/P ratio of 20 the particle size of the investigated compounds ranged between 54 and 61 nm (Figure 2.4A). Increasing the N/P ratio results in increased electrostatic interaction events between the gemini surfactants and the DNA, thus a better DNA compaction.

The size of the DNA lipoplexes impacts the route of cellular entry, efficiency of cellular uptake, cytotoxicity, and intracellular fate [29, 30]. Mammalian cells adopt a variety of endocytic pathways, the most common being clathrin-mediated endocytosis, caveolae-mediated endocytosis and clathrin- and caveolin-independent endocytosis [31, 32]. The size of endocytic vesicles formed during the endocytic processes varies with the specific pathway. For example,

the size of vesicles involved in clathrin-mediated endocytosis is in the rage of 120-200 nm, while in caveolae mediated endocytosis it is about 60–80 nm [31, 32]. The particle size of the lipoplexes of the best performing gemini surfactant, 16-7N(G-K)-16 at its optimal N/P ratio, N/P = 2.5, was 81 ± 3 nm which was suitable for efficient cellular uptake. In previous work, we showed that the uptake of lipoplexes formulated with 12-7N(G-K)-12 in cotton tail rabbit epithelial cells took place *via* both clathrin- and caveolae-mediated endocytosis [33]. Prabha *et al.* investigated the effect of particle size of nanoparticles formulated from poly (D, L-lactide-co-glycolide) on the level of gene expression in COS-7 cells. Small nanoparticles of 70 nm showed a 27-fold higher transfection than the large-sized nanoparticles of 200 nm [30]. This result could be one of the reasons in the present work for the low level of protein expression found with lipoplexes formulated with 18:1-7N(G-K)-18:1 having particle size of 206 ± 6 nm at N/P = 2.5, compared to lipoplexes formulated with 16-7N(G-K)-16 having particle size of 81 ± 3 nm, despite their close CMC values.

The nanoparticles reported herein also showed a wide range in zeta potential values, -8 to +94 mV (Figure 2.4B). All three compounds at N/P ratio of 1 exhibited negative zeta potentials (-8 to -0.64 mV), suggesting insufficient DNA charge neutralization and possibly inefficient compaction, indicated by the large particle size. All these factors explain the low level of gene expression at an N/P ratio of 1. The charge neutralization of the particles occurred at N/P ratios <2.5. For all three compounds, the zeta potential increased upon increasing the N/P ratio reaching their maximum value at N/P= 20; +25 mV for 12-7N(G-K)-12, +50 mV for 16-7N (GK)-16 and +37 mV for 18:1-7N (GK)-18:1 (Figure 2.4B). The zeta potential of the formulation with the highest transfection efficiency, 16-7N(G-K)-16 at N/P= 2.5, was +21 mV which is optimal for efficient cellular uptake and endosomal release.

Zeta potential is a pivotal parameter that influences the delivery of genetic materials both *in vitro* and *in vivo*. Similar to particle size, it affects cellular uptake, intracellular localization and cytotoxicity [34]. While positive charge is conducive to electrostatic interaction with anionic proteoglycans on the cell surface, a high charge density could cause cell membrane rupturing[34]. Thus the optimal surface charge needs to be determined for nanoparticle systems. All P/G/L nanoparticles showed a positive zeta potential of 10-21mV at the highest transfection efficiency, N/P of 2.5. Further increase of N/P ratios led to an increase in zeta potential, but did not translate into a higher transgene expression. From a pharmaceutical formulation development perspective, zeta potential is an important marker of the stability of a colloidal system indicating the net balance between the attractive and the repulsive forces among the nanoparticles, DLVO theory [35]. For example, having a large positive or negative zeta potential indicates high repulsive forces between particles in the system; as a result, the probability for flocculation to occur is minimal. Conversely, if the particles have low zeta potential values, the attractive forces due to van der Waals interactions dominate and cause particles to cluster and flocculate [35].

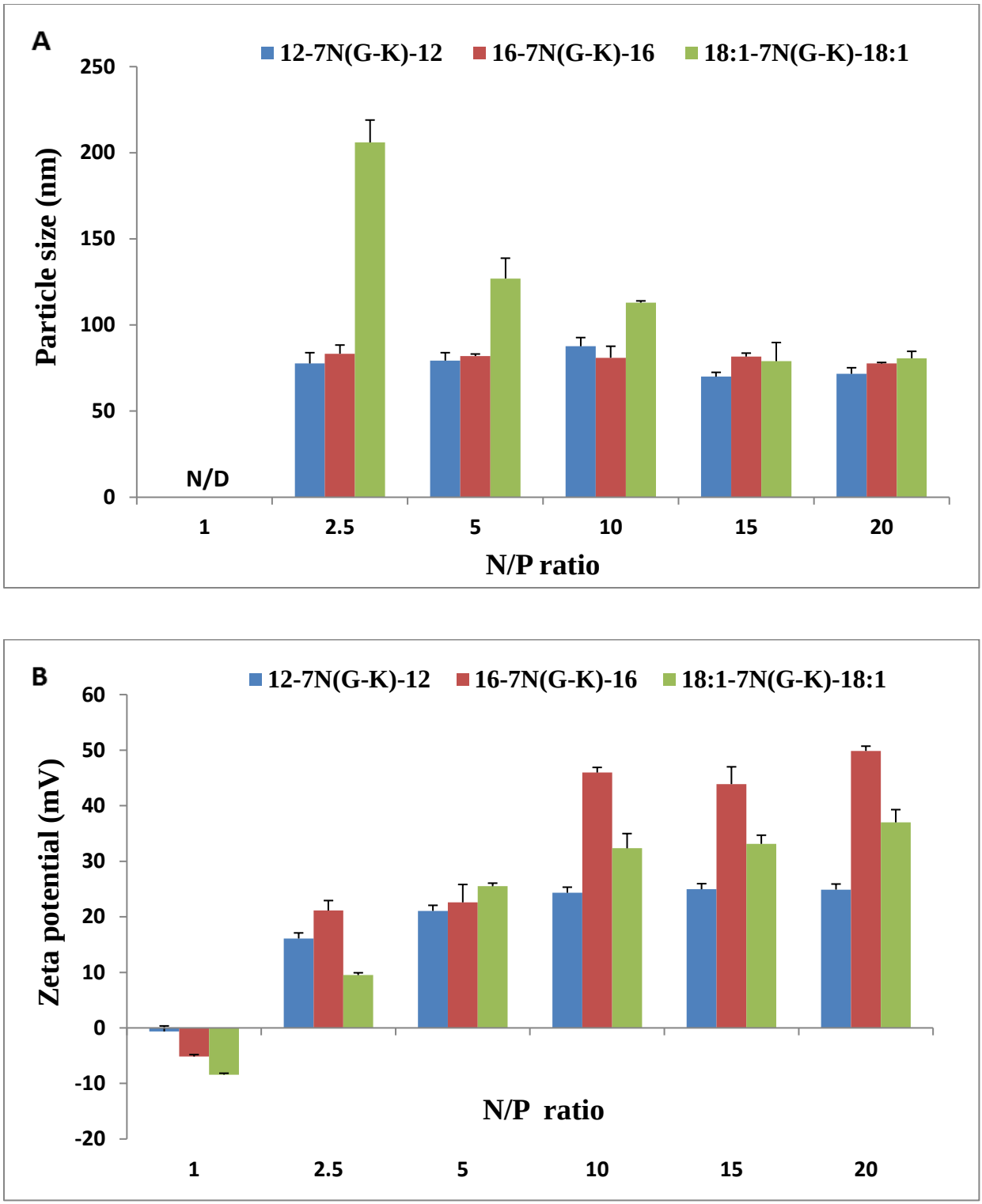

Figure 2.4. (A) Particle size and (B) Zeta potential results comparing the three different P/G/L nanoparticles vary in their tail length and degree of saturation at six N/P ratios. Results are shown as mean (n=3) ± standard deviation. N/D: not detectable; outside the measurable range.

2.4.3.3. Influence of pH on size and ζ-potential

pH sensitivity can be utilized to design intelligent nanoparticles that respond to variation in pH of the environment in order to avoid intracellular degradation. In order to examine the impact of pH, size and zeta measurements were performed over a range of pH from the intrinsic pH of the formulation to acidic pH on the nanoparticles formulated with the best performing lipid, 16-7N(G-K)-16 . The particle size of the nanoparticles showed an increase from 91 nm at pH= 6 to a maximum of 104 nm at pH 4, followed by a decrease at lower pH (Figure 2.5A). Zeta potential measurements showed a positive increase as a function of pH reduction from +48 to +65 mV (Figure 2.5B). This pH-induced particle size and zeta potential change indicates increased protonation of the terminal amines leads to an electrostatically induced expansion. The enlargement of the lipoplexes ruptures the membrane of the endocytotic vesicles releasing the cargo into the cytoplasm (proton sponge effect) [36]. In previous work, we found that both clathrin-mediated and caveolae-mediated pathways were utilized for the cellular uptake of lipoplexes formulated with 12-7N(G-K)-12[33]. In clathrin-mediated endocytosis, nanoparticles inside the endosomes experience a drop in pH before merging with lysosomes where they can undergo degradation[37]. Thus, adopting a pH-induced structural change enables the nanoparticles to escape from endosomes, avoiding lysosomal degradation, and resulting in increased gene delivery. No significant differences were observed between formulations with 16-7N(G-K)-16 and the previously studied 12-7N(G-K)-12, which also showed an expansion in size from 130 nm at pH 6 to a maximum size of 140 nm at pH= 4 [33].

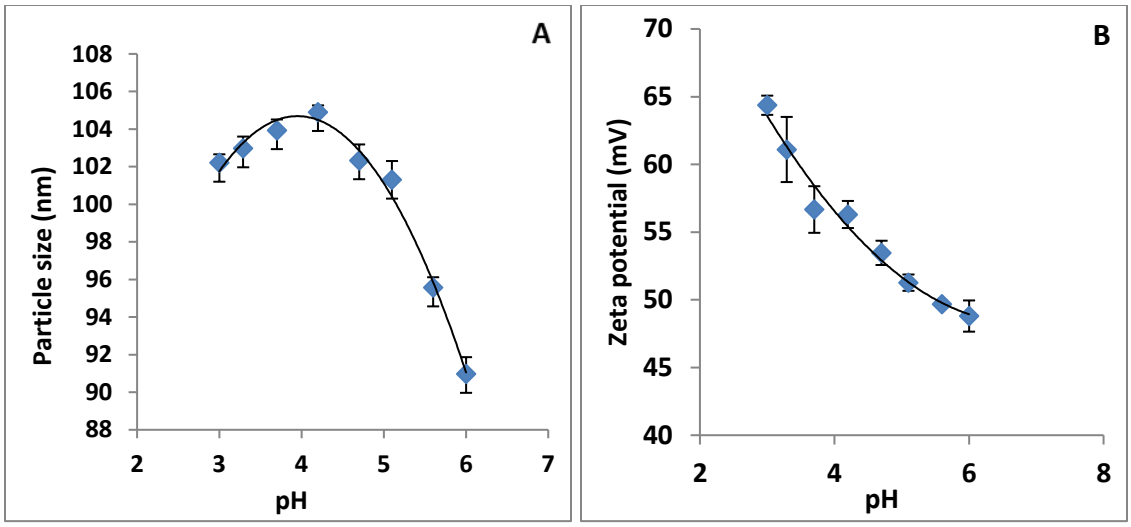

Figure 2.5. pH dependence of (A) particle size and (B) zeta potential of the P/16-7N(G-K)-16/L nanoparticles at N/P ratio of 10.

2.4.3.4. Determination of the lipid organization

SAXS was employed to study the effect of the nature of the hydrocarbon tail of the glycyl-lysine modified gemini surfactants on the supramolecular assembly of the nanoparticles at six N/P ratios. In the first stage, the scattering profile of each component was evaluated. The diffraction pattern of the plasmid DNA was featureless, indicating no liquid crystalline structure. The helper lipid, DOPE showed Bragg peaks at q values of 0.1039, 0.178 and 0.206 with ratio of 1:√3:√4 corresponding to the inverted hexagonal (H_{II}) phase [38]. The gemini surfactants alone showed diffused scattering at low q values of 0.12-0.18 indicating micellar organization (Figure 2.6). The diffraction pattern resulted from the shell-like structure of the chloride counter-ion cloud around the micelles corresponding to a micellar diameter of 5.2-3.4 nm, in agreement with values for a similar micelle solution of gemini surfactant [39]. Mixing the three components: DNA, gemini lipid and DOPE (P/G/L) led to a marked increase of the intensity at low q suggesting the formation of larger scattering objects in the solution and the appearance of Bragg peaks at higher q indicating internal ordering of the newly formed aggregates.

An inverted hexagonal phase was adopted in all P/G/Ls at their lower N/P ratios (Figure 2.7). Inverted hexagonal phase (H_{II}) is known to be responsible for high transfection efficiency due to its ability to facilitate fusion with the cell membrane and cytoplasmic release of the DNA into the cytosol [40]. The position of the scattering peaks and the corresponding unit cell spacings ($a = 4\pi/\sqrt{3}\ q_{10}$) (where q_{10} is the first Bragg peak) are listed in Table SI, Apendix I. The best performing formulation, 16-7N(G-K)-16 at 2.5 N/P, revealed an inverted hexagonal morphology with peak positions at q = 0.102, 0.177 and 0.203 corresponding to a unit cell spacing a = 71.129 Å. At the same N/P ratio, the repeat distance increased by increasing the length of the hydrophobic tail, in agreement with previously reported behaviour of cationic surfactant-nucleic acid lipoplexes [41-43]. Langevin *et al.* reported a linear relationship between the number of carbons in the surfactant tails and the d-spacing [43].

Upon increasing the N/P ratios from 1 up to 5, there was a slight shift in peaks towards lower q values, indicating a slight increase in the size of the unit cell as the interacting components are less closely packed and the system is more hydrated [41]. Interestingly, further increase of the N/P ratio between 10 and 20 (increasing the amount of gemini surfactant) was accompanied by significant changes in the scattering pattern. In P/G/Ls formulated with 12-7N(G-K)-12 and 16-7N(G-K)-16, there was a sign of interaction between the helper lipid and the excess gemini surfactants at N/P ratios of 5 (red arrows Figure 2.7) which led to the increase in the diffuse scattering that eventually overshadowed the Bragg peaks above the N/P ratio of 5.

In order to evaluate the possible interaction between the helper lipid and the free gemini surfactants micelles, SAXS measurements for formulations containing helper lipid and gemini surfactants in the absence of DNA were conducted. The scattering profile of the DOPE/gemini surfactants was similar to that of the corresponding P/G/L lipoplexes above the N/P ratio of 5

(Figure 2.8). These results are in accord with other studies [22, 23] suggesting that after neutralizing the DNA with cationic surfactants no more surfactant will bind to the lipoplexes and the excess surfactant will remain in the supernatant as free micelles, explaining the high toxicity trend above N/P ratios of 5 (Figure 2.3). It is worth noting that nanoparticles formulated with 18:1-7N(G-K)-18:1 gemini surfactant did not follow that trend and the inverted hexagonal phase was preserved upon increasing the gemini surfactant content and even this was the case when no DNA was added (Figure 2.7C and 2.8). This difference in behaviour could be attributed to the presence of the double bond (cis isomer) that might bring the compound's geometry closer to the shape of the DOPE compound (Figure 2.1). Further discussion on this issue is provided below in the lipid packing parameter section.

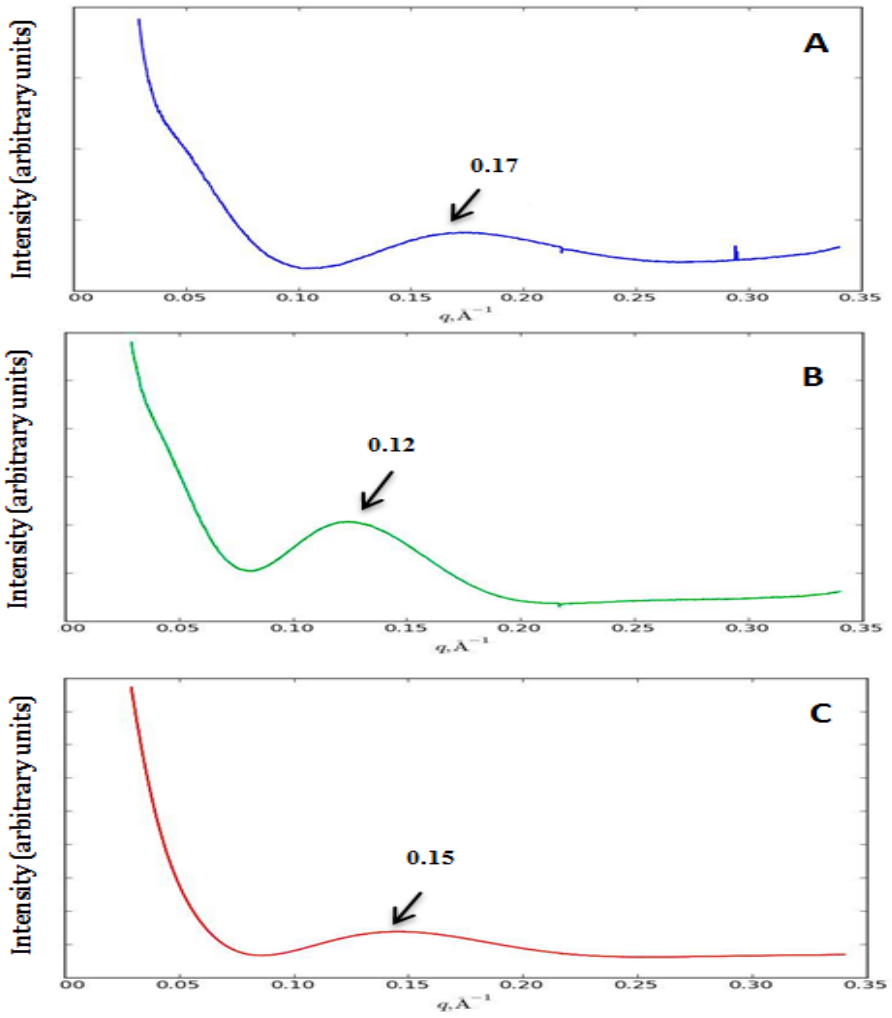

Figure 2.6. SAXS scattering profile of gemini surfactant solutions of (A) 12-7N(G-K)-12 ,(B) 16-7N(G-K)-16 and (C) 18:1-7N(G-K)-18:1.

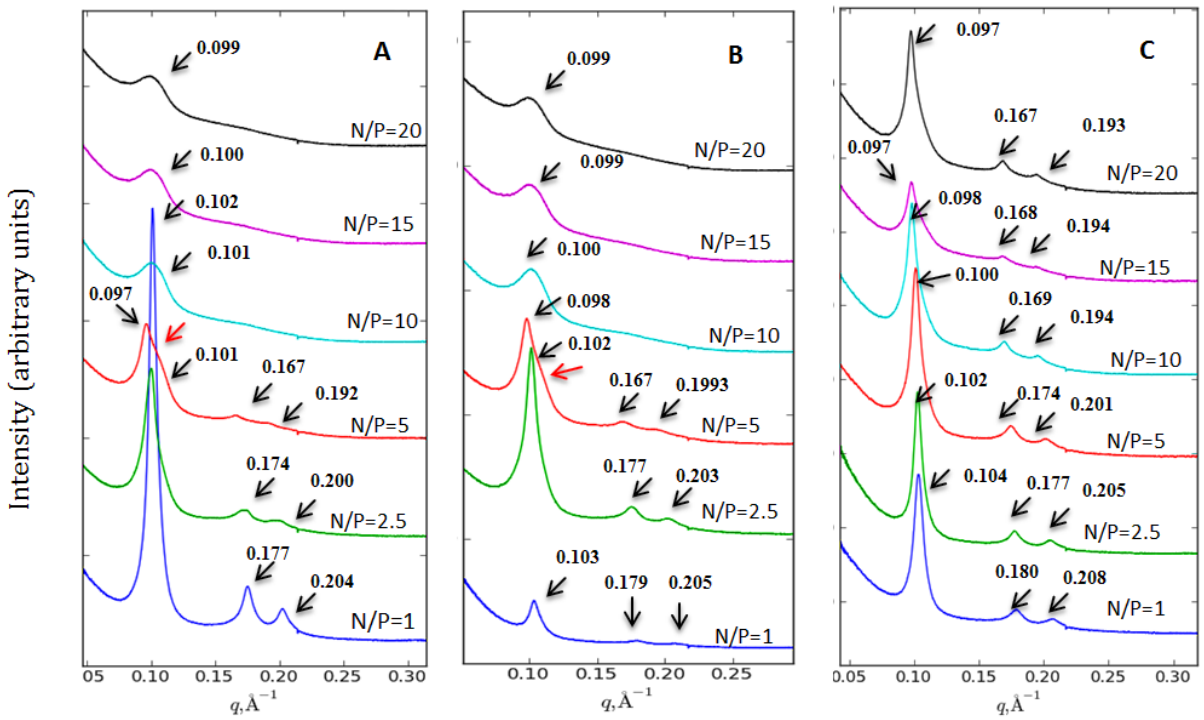

Figure 2.7. SAXS scattering profile of nanoparticles prepared with (A) P/12-7N(G-K)-12/L ,(B) P/16-7N(G-K)-16/L and (C) P/18:1-7N(G-K)-18:1/L.

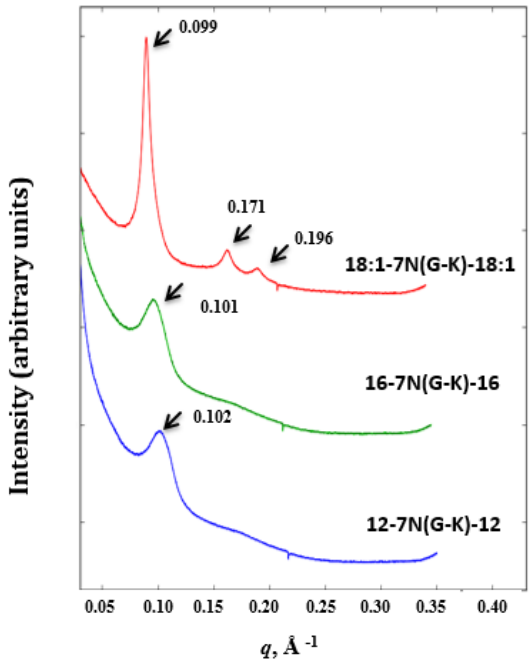

Figure 2.8. SAXS scattering profile of DOPE and gemini surfactant mixtures at quantities corresponding to an N/P ratio of 10.

2.4.3.5. Determination of the molecular packaging parameter of the lipids

In order to investigate the effect of structural differences on the preferred curvature of self-aggregates of the three gemini surfactants, the molecular packing parameter was estimated using values of parameters based on the behaviour of the gemini surfactant at the air-water interface. The molecular packing parameter P is a concept developed by Israelachvili *et al.* to describe the shape of aggregates formed by surface active compounds in aqueous solution [44]. It is defined as

$$P = V/a_0 l \quad (1)$$

where V is the volume of the hydrophobic tails, l is the length of the hydrocarbon tails, and a_0 is the head group area per molecule at the aggregate surface.

A specific value of P can be translated into a particular geometrical shape [44, 45]. It has been stated in the literature that the a_0 value is the main determinant of the P value since V/l ratio is fixed for common surfactants regardless of the tail length [46, 47]. However, Nagarajan showed that the tail has an explicit or an implicit impact on the P values[47]. While the volume and the length of hydrocarbon chains are simple geometrical properties which can be calculated from the chemical structure, evaluation of the head group area is more complicated [47]. It is an equilibrium parameter that is determined by a balance between both the attractive forces of the hydrophobic chains and the repulsive force of the adjacent head groups [48]. This work aims at exploring the effect of tail length and geometry on the head group area and the packing parameter.

The gemini surfactant 12-7N(G-K)-12 showed the smallest mean molecular area of a_0 = 52 Å^2, as a result, the largest molecular packing parameter (1.17). In agreement with previously reported trend of cationic gemini surfactants [49], the mean molecular area expanded with

increasing length of the alkyl tail. The gemini surfactant having hexadecyl tails showed a mean molecular area of 60 $Å^2$ and a P value of 0.84. The 18:1-7N(G-K)-18:1 gemini surfactant had an a_0 = 70 $Å^2$ and a P value of 0.67 which were the closest to the value of the DOPE head group area a_0 = 75 $Å^2$ and P of 0.63. The pressure-area isotherms are shown in Figure S2, Apendix I. The similarity in the head group area between the 18:1-7N(G-K)-18:1 gemini surfactant and DOPE might be the reason for the preservation of the hexagonal arrangement of the P/G/Ls at all N/P ratios (Figure 2.7C), while the other two gemini surfactants, with head group areas markedly different from DOPE induced structural changes in the P/G/Ls at high N/Ps (Figure 2.7A and 7B). Based on these findings, we constructed a model of hexagonal arrangement of all P/G/Ls (Figure 2.9A) and a schematic representation of the lipid assembly (Figure 2.9B). As mentioned earlier, the presence of the double bond in the 18:1-7N(G-K)-18:1 confers this gemini surfactant similar nature to the helper lipid, DOPE amenable to maintain the organization through a wide range of molar ratios, whereas, the 12-7N(G-K)-12 and 16-7N(G-K)-16 are disruptive for organization. The variation in the mean molecular area among the gemini surfactants, with the same chemical composition of the head group, underlines the role of the alkyl tail in the interaction among the different molecules of the delivery system and genetic material, ultimately impacting on the condensation of the DNA.

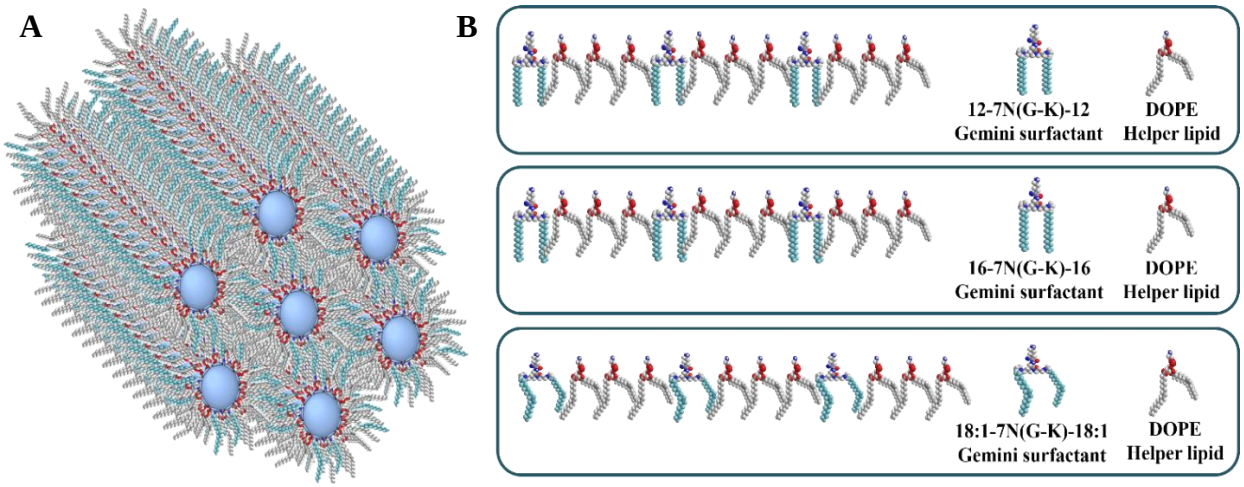

Figure 2.9. Schematic representation of (A) inverted hexagonal phase adopted by all lipoplexes at their optimal N/P ratios and (B) the variation in the lipid packing resulted from the variation in the gemini surfactants geometry.

2.5. Conclusion

A new generation of peptide-substituted gemini surfactants was synthesized to evaluate the impact of varying the length of the hydophobic tail on the lipoplex morphology, transfection efficiency and cytotoxicity. Three glycyl-lysine substituted compounds having dodecyl, hexadecyl and oleyl tails were tested. The results indicated that the transfection efficiency was highly dependent on both the length of the alkyl tail and gemini surfactant to plasmid DNA (N/P) charge ratio, moreover, it correlated with physicochemical properties of the lipoplexes. By selecting a suitable alkyl tail length, the level of gene expression could increase 5 to10 folds. On balance, the results indicate that the structure of the gemini surfactants play an important role in determining the transgene efficiency of the delivery system and suggests that it is an essential factor in the rational design of effective gemini vectors for gene delivery systems.

2.6. Bibliography

1 Thomas CE, Ehrhardt A, Kay MA. Progress and problems with the use of viral vectors for gene therapy. Nature Reviews Genetics 2003; 4: 346-58.

2 Gene Therapy Clinical Trials Worldwide John Wiley and Sons Ltd., <http://www.wiley.com/legacy/wileychi/genmed/clinical/> Accessed January 2018.

3 Ilies M, Seitz WA, Balaban AT. Cationic lipids in gene delivery: principles, vector design and therapeutical applications. Current pharmaceutical design 2002; 8: 2441-73.

4 Karmali PP, Chaudhuri A. Cationic liposomes as non-viral carriers of gene medicines: Resolved issues, open questions, and future promises. Medicinal research reviews 2007; 27: 696-722.

5 Felgner PL, Gadek TR, Holm M, Roman R, Chan HW, Wenz M, *et al*. Lipofection: a highly efficient, lipid-mediated DNA-transfection procedure. Proceedings of the National Academy of Sciences 1987; 84: 7413-7.

6 Menger FM, Littau C. Gemini-surfactants: synthesis and properties. Journal of the American Chemical Society 1991; 113: 1451-2.

7 Wettig S, Verrall R. Thermodynamic Studies of Aqueous m–s–m Gemini Surfactant Systems. Journal of colloid and interface science 2001; 235: 310-6.

8 Badea I, Verrall R, Baca-Estrada M, Tikoo S, Rosenberg A, Kumar P, *et al*. In vivo cutaneous interferon-γ gene delivery using novel dicationic (gemini) surfactant–plasmid complexes. The journal of gene medicine 2005; 7: 1200-14.

9 Foldvari M, Badea I, Wettig S, Verrall R, Bagonluri M. Structural characterization of novel gemini non-viral DNA delivery systems for cutaneous gene therapy. Journal of Experimental Nanoscience 2006; 1: 165-76.

10 Wang C, Li X, Wettig SD, Badea I, Foldvari M, Verrall RE. Investigation of complexes formed by interaction of cationic gemini surfactants with deoxyribonucleic acid. Physical Chemistry Chemical Physics 2007; 9: 1616-28.

11 Buse J, Badea I, Verrall RE, El-Aneed A. Tandem mass spectrometric analysis of the novel gemini surfactant nanoparticle families G12-s and G18: 1-s. Spectroscopy Letters 2010; 43: 447-57.

12 Wettig SD, Badea I, Donkuru M, Verrall RE, Foldvari M. Structural and transfection properties of amine-substituted gemini surfactant-based nanoparticles. The journal of gene medicine 2007; 9: 649-58.

13 Yang P, Singh J, Wettig S, Foldvari M, Verrall RE, Badea I. Enhanced gene expression in epithelial cells transfected with amino acid-substituted gemini nanoparticles. European Journal of Pharmaceutics and Biopharmaceutics 2010; 75: 311-20.

14 Singh J, Yang P, Michel D, E Verrall R, Foldvari M, Badea I. Amino Acid-Substituted Gemini Surfactant-Based Nanoparticles as Safe and Versatile Gene Delivery Agents. Current Drug Delivery 2011; 8: 299-306.

15 Sandri J, Viala J. Convenient Conversion of cis-Homoallylic Alcohols into Corresponding Bromides with Ph3PBr2. Synthetic communications 1992; 22: 2945-8.

16 Hanwell MD, Curtis DE, Lonie DC, Vandermeersch T, Zurek E, Hutchison GR. Avogadro: An advanced semantic chemical editor, visualization, and analysis platform. J. Cheminformatics 2012; 4: 17.

17 M. J. Frisch GWT, H. B. Schlegel, G. E., Scuseria MAR, J. R. Cheeseman, G. Scalmani, V. Barone, B. Mennucci,, G. A. Petersson HN, M. Caricato, X. Li, H. P. Hratchian,, A. F. Izmaylov JB, G. Zheng, J. L. Sonnenberg, M. Hada, M. Ehara,, K. Toyota RF, J. Hasegawa, M. Ishida, T. Nakajima, Y. Honda, O., Kitao HN, T. Vreven, J. A. Montgomery, Jr., J. E. Peralta, F. Ogliaro,, *et al*. (Gaussian, Inc., Wallingford CT, 2013).

18 Matulis D, Rouzina I, Bloomfield VA. Thermodynamics of cationic lipid binding to DNA and DNA condensation: roles of electrostatics and hydrophobicity. J Am Chem Soc 2002; 124: 7331-42.

19 Hayakawa K, Santerre JP, Kwak JC. The binding of cationic surfactants by DNA. Biophysical chemistry 1983; 17: 175-81.

20 Rudiuk S, Yoshikawa K, Baigl D. Enhancement of DNA compaction by negatively charged nanoparticles: Effect of nanoparticle size and surfactant chain length. Journal of colloid and interface science 2012; 368: 372-7.

21 Donkuru M, Wettig SD, Verrall RE, Badea I, Foldvari M. Designing pH-sensitive gemini nanoparticles for non-viral gene delivery into keratinocytes. Journal of Materials Chemistry 2012; 22: 6232-44.

22 Dias RS, Svingen R, Gustavsson B, Lindman B, Miguel MG, Åkerman B. Electrophoretic properties of complexes between DNA and the cationic surfactant cetyltrimethylammonium bromide. Electrophoresis 2005; 26: 2908-17.

23 Dias R, Mel'nikov S, Lindman B, Miguel MG. DNA phase behavior in the presence of oppositely charged surfactants. Langmuir 2000; 16: 9577-83.

24 Zana R, Benrraou M, Rueff R. Alkanediyl-. alpha.,. omega.-bis (dimethylalkylammonium bromide) surfactants. 1. Effect of the spacer chain length on the critical micelle concentration and micelle ionization degree. Langmuir 1991; 7: 1072-5.

25 Kuiper JM, Buwalda RT, Hulst R, Engberts JB. Novel pyridinium surfactants with unsaturated alkyl chains: aggregation behavior and interactions with methyl orange in aqueous solution. Langmuir 2001; 17: 5216-24.

26 Dauty E, Remy J-S, Blessing T, Behr J-P. Dimerizable cationic detergents with a low cmc condense plasmid DNA into nanometric particles and transfect cells in culture. J Am Chem Soc 2001; 123: 9227-34.

27 Moghaddam B, McNeil SE, Zheng Q, Mohammed AR, Perrie Y. Exploring the correlation between lipid packaging in lipoplexes and their transfection efficacy. Pharmaceutics 2011; 3: 848-64.

28 Brgles M, Šantak M, Halassy B, Forcic D, Tomašić J. Influence of charge ratio of liposome/DNA complexes on their size after extrusion and transfection efficiency. International journal of nanomedicine 2012; 7: 393.

29 Prabha S, Arya G, Chandra R, Ahmed B, Nimesh S. Effect of size on biological properties of nanoparticles employed in gene delivery. Artificial cells, nanomedicine, and biotechnology 2014: 1-9.

30 Prabha S, Zhou W-Z, Panyam J, Labhasetwar V. Size-dependency of nanoparticle-mediated gene transfection: studies with fractionated nanoparticles. International Journal of Pharmaceutics 2002; 244: 105-15.

31 El-Sayed A, Harashima H. Endocytosis of gene delivery vectors: from clathrin-dependent to lipid raft-mediated endocytosis. Molecular Therapy 2013; 21: 1118-30.

32 Conner SD, Schmid SL. Regulated portals of entry into the cell. Nature 2003; 422: 37-44.

33 Singh J, Michel D, Chitanda JM, Verrall RE, Badea I. Evaluation of cellular uptake and intracellular trafficking as determining factors of gene expression for amino acid-substituted gemini surfactant-based DNA nanoparticles. J Nanobiotechnology 2012; 10.

34 Fröhlich E. The role of surface charge in cellular uptake and cytotoxicity of medical nanoparticles. International journal of nanomedicine 2012; 7: 5577.

35 Myers D. Surfaces, interfaces and colloids. (Wiley-Vch New York etc., 1990).

36 Behr J-P. The proton sponge: a trick to enter cells the viruses did not exploit. CHIMIA International Journal for Chemistry 1997; 51: 34-6.

37 Maxfield FR, McGraw TE. Endocytic recycling. Nature reviews Molecular cell biology 2004; 5: 121-32.

38 Turner DC, Gruner SM. X-ray diffraction reconstruction of the inverted hexagonal (HII) phase in lipid-water systems. Biochemistry 1992; 31: 1340-55.

39 Aswal V, Goyal P, De S, Bhattacharya S, Amenitsch H, Bernstorff S. Small-angle X-ray scattering from micellar solutions of gemini surfactants. Chem Phys Lett 2000; 329: 336-40.

40 Ma B, Zhang S, Jiang H, Zhao B, Lv H. Lipoplex morphologies and their influences on transfection efficiency in gene delivery. Journal of Controlled Release 2007; 123: 184-94.

41 Ristori S, Ciani L, Candiani G, Battistini C, Frati A, Grillo I, *et al*. Complexing a small interfering RNA with divalent cationic surfactants. Soft Matter 2012; 8: 749-56.

42 Falsini S, Ristori S, Ciani L, Di Cola E, Supuran CT, Arcangeli A, *et al*. Time resolved SAXS to study the complexation of siRNA with cationic micelles of divalent surfactants. Soft matter 2014; 10: 2226-33.

43 MCLoughlin § D, Delsanti M, Albouy P, Langevin* D. Aggregates formation between short DNA fragments and cationic surfactants. Molecular Physics 2005; 103: 3125-39.

44 Israelachvili JN, Mitchell DJ, Ninham BW. Theory of self-assembly of hydrocarbon amphiphiles into micelles and bilayers. J. Chem. Soc., Faraday Trans. 2 1976; 72: 1525-68.

45 Kumar V. Complementary molecular shapes and additivity of the packing parameter of lipids. Proceedings of the National Academy of Sciences 1991; 88: 444-8.

46 Tanford C. The Hydrophobic Effect: Formation of Micelles and Biological Membranes 2d Ed. (J. Wiley., 1980).

47 Nagarajan R. Molecular packing parameter and surfactant self-assembly: the neglected role of the surfactant tail. Langmuir 2002; 18: 31-8.

48 Hiemenz PC, Rajagopalan R. Principles of Colloid and Surface Chemistry, Third Edition, Revised and Expanded. (Taylor & Francis, 1997).

49 Wang H, Wettig SD. Synthesis and aggregation properties of dissymmetric phytanyl-gemini surfactants for use as improved DNA transfection vectors. Physical Chemistry Chemical Physics 2011; 13: 637-42.

CHAPTER 3

Molecular Engineering as an Approach to Modulate Gene Delivery Efficiency of Peptide-Modified Gemini Surfactants

Mays Al-Dulaymi[1], Deborah Michel[1], Jackson M. Chitanda[2], Anas El-Aneed[1], Ronald E. Verrall [3], Pawel Grochulski[1, 4], Ildiko Badea[1*]

1. College of Pharmacy and Nutrition, University of Saskatchewan, Saskatoon, SK, Canada.
2. Department of Chemical and Biological Engineering, University of Saskatchewan, Saskatoon, SK, Canada
3. Department of Chemistry, University of Saskatchewan, Saskatoon, SK, Canada
4. Canadian Light Source, Saskatoon, SK, Canada

*This chapter is accepted in Bioconjugate Chemistry.

Transitioning rationale:

The incorporation of the amino acids into the gemini surfactants' spacer region caused a significant increase in their transfection efficiency and reduced cytotoxicity. In the previous chapter, we assessed the impact of altering the alkyl tails on the efficiency of the delivery system. In this chapter, we introduce a new series of peptide-modified gemini surfactants with various alkyl tails and peptides spacer modifications. The aim is to elucidate their structure activity relationship and to identify the fundamental architectural requirements for efficient gene delivery systems.

Contribution statement:

Mays Al-Dulaymi contributed to this manuscript by designing the study, performing experiments, data acquisition, data analysis and manuscript writing. Dr. Jackson Chitanda synthesized the gemini surfactants utilized in this work. Ms. Deborah Michel and Dr. Ildiko Badea performed the onsite SAXS measurements. Surface tension data acquisition was conducted by Dr. Shawn Wettig lab.

3.1. Abstract

Diquaternary ammonium gemini surfactants are an emerging class of non-viral gene delivery vectors. Their unique molecular structure impart preferable characteristics such as enhanced nucleic acid complexation ability, bottom-up design flexibility and relatively low cytotoxicity. To capitalize on the potential of gemini surfactants as effective gene delivery vectors, novel structural modifications should be explored. In this work, a series of novel 22 peptide-modified gemini surfactants was introduced with various alkyl tails and peptide spacer modifications. To the best of our knowledge, this work represents the first report of dendrimer-like gemini surfactants and first evaluation of the impact of incorporating a hydrocarbon linker into the peptide chain. The aim of this work was to assess the structure activity relationship of the novel peptide modified gemini surfactants and to identify the fundamental architectural requirements needed in designing the ultimate gene delivery systems.

Transfection efficiency and cytotoxicity were evaluated in PAM 212 murine keratinocyte and COS-7 African green monkey kidney fibroblast cell lines. Physicochemical properties of the nanoparticles were systematically investigated by evaluating the particle size and surface charge using dynamic light scattering and laser Doppler velocimetry, respectively. In addition, surface tension measurements were used to assess the critical micelle concentration (CMC) and lipid packing parameters. Morphological characteristics were studied by small-angle X-ray scattering (SAXS).

Results revealed that the highest transfection efficiency and the lowest cytotoxicity were associated with the glycyl-lysine modified gemini surfactants having the hexadecyl tail, 16-7N(G-K)-16. In fact, it showed an 8-fold increase in secreted protein with 20% increase in cell

viability relative to the first-generation unsubstituted gemini surfactants. Further increase in the size of the attached peptides resulted in a decrease in the transfection efficiency and cell viability. Whereas the incorporation of a hydrocarbon linker into the peptide chain decreased the transfection efficiency of compounds with di-peptides, it increased the transfection efficiency of compounds with larger peptide chains. Such an increase was more prominent with incorporation of a longer hydrocarbon linker. We conclude that a balance between the hydrophilic and hydrophobic characteristics of the compound is necessary since it results in physicochemical parameters conducive to the gene delivery process.

Keywords: structure activity relationship; non-viral vectors; cationic surfactants; dendrimer-like; small angle x-ray scattering

3.2. Introduction

The wealth of information gained upon completion of the human genome project has accelerated the discovery of the genetic basis of many disorders and the development of novel gene-editing technologies, presenting gene therapy as an approach that could revolutionize medicine [1, 2]. However, the success in delivering genes into the target site has not kept pace with the advancements in gene discovery and editing. This is mainly due to the lack of delivery vectors capable of overcoming various biological barriers and delivering the therapeutic DNA into the target site efficiently and safely. Over the past 30 years, both viral and non-viral vectors have been evaluated for their efficiency to deliver genetic material in clinical trials [3, 4]. While viruses have naturally evolved to deliver their genetic materials into the cells, they suffer from several inherent shortcomings such as immunogenicity, tumorigenicity, limited DNA packaging capacity and high cost [5]. Non-viral methods, on the other hand, have the potential to address many of these limitations, particularly safety concerns.

Among the various non-viral gene delivery modalities currently being explored, lipid-based delivery vectors are at the forefront [6]. In fact, there are more than 115 clinical trials that have investigated the feasibility of lipid-mediated transfection [7]. Diquaternary ammonium gemini surfactants are a unique class of the lipid-based delivery vectors that show promising results in delivering genetic materials [8]. They are composed of dimeric surfactants that retain positively charged head groups and hydrocarbon tails linked by a spacer chain [9]. The dicationic head groups and the hydrocarbon chains collectively offer a preferable nucleic acid complexation ability, resulting in the formation of nano-sized lipoplexes that favor cellular internalization [10]. In addition, the unique structure of gemini surfactants has imparted superior characteristics compared to their monomeric counterparts, particularly lower critical micelle concentration

(CMC) and Krafft temperature, which encourage the spontaneous formation of nanoparticles at very low concentrations [9]. Most importantly, the structural versatility of gemini surfactants have allowed for bottom-up design flexibility to modulate the physicochemical properties of the delivery system toward the enhancement of transfection efficiency [10].

Research efforts have focused on the design and advancement of novel gemini surfactants aiming at improving their transfection efficiency and reducing cytotoxicity [11-13]. The most extensively studied group is the classical *N*, *N*-bis(dimethylalkyl)-α, ω-alkane-diammonium gemini surfactants represented as *m*-*s*-*m* where *m* is the number of carbon atoms in the alkyl tails and s is the number of carbon atoms in the spacer. They have showed promising results in delivering genetic material both *in vitro* and *in vivo* [14, 15]. The potential of lipoplexes composed of N,N'-bis(dimethylhexadecyl)-1,3-propanediammonium dibromide gemini surfactant, designated as 16-3-16, was evaluated as a non-invasive topical gene delivery system for the treatment of localized scleroderma in normal, knock out and diseased animal models [14-16]. A significant elevation was observed in the level of transgene expression in both normal and knock out animal models upon treatment with gemini surfactant-based lipoplexes compared to treatment with naked DNA[14, 15]. Moreover, collagen production in diseased mice was decreased by 70%, suggesting the efficiency of the non-invasive delivery system [16].

Despite the success of the classical gemini surfactants, translation into clinical applications is delayed, mainly because their transfection efficiencies still lag behind those of viral vectors. In addition, some concerns regarding their toxicity profile have recently arisen [17]. Thus, the incorporation of biofunctional and biodegradable structural motifs were explored in an attempt to ameliorate their transfection efficiency and safety profile [18, 19]. For instance, amino acids are naturally occurring biocompatible and biodegradable materials that can be incorporated

into the gemini surfactants at low cost [20, 21]. They possess different functionalities, particularly pH sensitivity and chirality, which allow for the formation of a wide variety of aggregate structures. Furthermore, they mimic cell penetrating peptides located on viral capsids that are believed to be responsible for the viruses' high infection capacity [22]. Accordingly, a new series of gemini surfactants was introduced by coupling mono and di- amino acids moieties into their spacer region [23-25]. They demonstrated a superior *in vitro* transfection efficiency and safety compared to the previously developed classical gemini surfactants [23-25]. In addition, topical application of lipoplexes composed of glycyl-lysine modified gemini surfactants, designated as 12-7N(G-K)-12, into rabbit vaginal cavities exhibited higher gene expression compared to the unsubstituted parent compound without evidence of visible toxicity [26].

The enhanced activity associated with the incorporation of amino acids into the gemini surfactants spacer region was attributed to the balanced binding with the nucleic acid facilitating both processes of genetic material compaction and subsequent release [24]. In addition, the amino acids high buffering capacity endowed a pH-dependent increase in particle size and zeta potential which gave rise to "intelligent" nanoparticles that respond to endosomal acidification to avoid lysosomal degradation [25, 27]. The conjugation of amino acids also resulted in decreasing the amount of gemini surfactant required to neutralize and compact the DNA due to the presence of terminal amino groups that imparted a higher positive charge [25].

Further modification of the lead compound, 12-7N(G-K)-12, resulted in more than 5-fold increase in the level of gene expression only by optimizing its hydrophobic domain, emphasizing the importance additional structural modification in augmenting the efficiency of the delivery system [25]. In light of the apparent importance of fine-tuning, this work introduces a new series of peptide modified gemini surfactants and evaluates for the first time the impact of inserting a

hydrocarbon linker within the peptide chain (Figure 3.1). The transfection efficiency, cytotoxicity and physicochemical properties of these compounds were systematically investigated aiming at elucidating their structure activity relationship. Such knowledge will address fundamental questions about the architectural requirements needed for efficient gene delivery systems and it will feed into the design of novel carriers with higher activity and reduced toxicity.

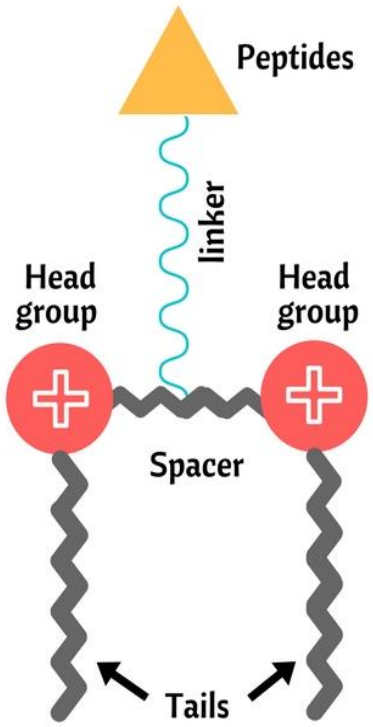

Figure 3.1. Schematic representation of gemini surfactants showing the two ionic head groups, hydrocarbon tails, spacer, hydrocarbon linker and the attached peptides.

3.3. Materials and methods

3.3.1. Materials

Twenty two peptide-modified cationic gemini surfactants, designated as m-7N(R)-m where m is the alkyl tail carbon chain length, m= 12, 16 or 18:1 (18:1 is a mono-unsaturated oleyl chain), and R is the peptide chain: R = glycyl-lysine, glycyl-trilysine, glycyl-heptalysine, glycyl-hexyl-lysine, glycyl-hexyl-trilysine, glycyl-undecyl-lysine, glycyl-undecyl-trilysine, hexyl-trilysine, undecyl-trilysine, hexyl-heptalysine and undecyl-heptalysine (Figure 3.2), were synthesized similar to previously reported procedures [25]. The plasmid pGThCMV.IFNGFP (pDNA), encoding for murine interferon gamma (IFN-γ) and green fluorescent protein (GFP) was utilized in this work [14]. QIAGEN Plasmid Giga Kit (Mississauga, ON, Canada) was used to isolate and purify the plasmid DNA according to the manufacturer's instructions. 1,2-dioleoyl-sn-glycerol-3-phosphoethanolamine (DOPE), used as a helper lipid, was purchased from Avanti Polar Lipids Inc. (Alabaster, AL, USA). Sucrose, used as a stabilizing, agent was purchased from Sigma Aldrich (Oakville, ON, Canada).

Minimal Eagle's Medium (MEM) and Dulbecco's modified Eagle's medium (DMEM) were obtained from ATCC (Manassas, VA, USA). Tissue culture plates were purchased from Falcon, BD (Mississauga, ON, Canada). Lipofectamine Plus ™ reagent and MTT (3-(4,5-Dimethylthiazol-2-yl)-2,5-Diphenyltetrazolium Bromide) were obtained from Invitrogen (Mississauga, ON, Canada). Recombinant mouse IFN-γ standard was attained from BD Biosciences (Mississauga, ON, Canada). Dimethyl sulfoxide (DMSO), ACS spectrophotometric grade, was purchased from Sigma-Aldrich (Mississauga, ON, Canada)

3.3.2. Formulations

The gemini surfactants were combined with pDNA at three different nitrogen (cationic) to phosphate (anionic) charge ratios (N/P) of 2.5, 5, and 10 in the presence of a fixed amount of a helper lipid, DOPE, to create pDNA / gemini surfactants / helper lipid (P/G/L) nanoparticles. An appropriate amount of 3mM aqueous solution of gemini surfactant was added to 200 µg/mL pDNA and incubated for 20 minutes at room temperature (P/G complex). DOPE at a final concentration of 1mM was prepared as described previously [28] and added to P/G complexes to form the final nanoparticles (P/G/L).

3.3.3. Cell culture and *in vitro* transfection study

PAM 212 murine keratinocyte and COS-7 african green monkey kidney fibroblast cell lines (ATCC, CRL-1651) were grown to 80% confluency in 75-cm^2 tissue culture flasks in MEM and DMEM supplemented with 10% (vol/vol) fetal bovine serum and 1% (vol/vol) antibiotic/antimycotic agents and incubated at 37 °C with 5% CO_2. One day prior to transfection, 96-well tissue culture plates were seeded with the cells at a density of 15×10^3 and 1×10^4 cells/well for PAM 212 and COS-7 cell lines, respectively. The supplemented medium was replaced with FBS-free medium one hour prior to transfection. Cells were transfected with 0.2 µg/well pDNA and incubated at 37 °C in CO_2 for 5 h. Lipofectamine Plus reagent ™ was used as a positive control according to the manufacturer's protocol. The transfection mixture was replaced by supplemented medium after 5 h. Supernatants were collected and replaced with fresh medium at 24, 48 and 72 h. The collected supernatants were stored at - 20 °C. The results presented are the average of three independent plates of quadruplicate wells.

3.3.4. Enzyme-linked immunosorbent assay (ELISA)

ELISA was carried out to measure the level of secreted interferon gamma using flat bottom 96-well plates according to the BD Pharmingen protocol. A standard IFN-γ curve was created using recombinant mouse IFN-γ standard to calculate the concentration of the secreted IFN-γ.

3.3.5. 3-(4,5-Dimethylthiazol-2-yl)-2,5-diphenyltetrazolium bromide (MTT) assay

MTT assay was performed to examine the cytotoxicity of the peptide-modified gemini surfactants in both PAM 212 and COS-7 cell-lines. Three 96-well cell culture plates were seeded with the optimal cell density for each cell line and treated with the P/G/L nanoparticles. Plates were incubated for 5 h at 37 °C with 5% CO_2 before replacing the old media with fresh media as described in the transfection section. Cell toxicity was evaluated 72 h after treatment in PAM212 and 48 h in Cos-7. Lipofectamine, a commercial transfection agent, was used as a positive control. A sterile solution of 5 mg/mL of MTT (Invitrogen, U.S.A.) in phosphate buffered saline (PBS) was prepared, mixed with supplemented media, then added to the cells and incubated for 3 h. The supplemented media was removed, then the formed, purple formazan crystal was dissolved in dimethyl sulfoxide and the plates incubated at 37 °C for 10 m. Absorbance was measured at 550 nm using a microplate reader (BioTek® Microplate Synergy HT, VT, U.S.A.). The results are the average of three plates (treated with individually prepared formulations of quadruplicate wells) and the cytotoxicity is expressed as a percentage of the non-transfected control cells ± standard deviation.

3.3.6. Size and ζ-potential measurements

Size and ζ-potential measurements for the tested lipids at three N/P ratios were performed by using a Zetasizer Nano ZS instrument (Malvern Instruments, Worcestershire, UK). Samples were prepared as described in the formulation section and each sample was measured three times and the results reported are the average of the three readings ± standard deviation.

3.3.7. Small-angle X-ray scattering measurements (SAXS)

The formulations were prepared as in the transfection study using ten times higher concentrations. The SAXS experiments were performed at the BL4-2 beam line at Stanford Synchrotron Radiation Lightsource (SSRL, Stanford, USA) using a wavelength of 1.1271 Å (11KeV energy). The scattered X-ray was detected on MAR225-HE (225 mm x 225 mm (3072 x 3072 pixels, pixel size 73.24 μm) at sample to detector distance of 1.1m with exposure time of 20s. The SAXS detector was calibrated with silver behenate. GSASII software was used to plot diffraction intensity versus 2θ (where θ is the diffraction angle) or the scattering vector ($q = \frac{4\pi}{\lambda}\sin\theta$) by radial integration of the 2D patterns.

3.3.8. Surface Tension Measurements

Surface tension measurements were performed using a Lauda model TE3 automated tensiometer (Lauda, Germany) by applying the du Nouy ring technique. The measured surface tension values (γ) were corrected using the method of Harkins and Jordan [29]. Experimental temperatures were maintained at 45.0 ºC using a circulating water bath. The stock gemini surfactant solutions were titrated into 15 mL of water and the surface tension was measured after each addition. The critical micelle concentration (CMC) values were obtained from the linear

fitting of the pre-micellar and post-micellar regions of the surface tension vs. logarithmic concentration plot.

3.3.9. Molecular packing parameter

Molecular packing parameter (P) was obtained according to the following equation.

$$P = \mathrm{V}/\mathrm{a}_0 \mathrm{l} \qquad (1)$$

where V is the volume of the hydrophobic tails, l is the length of the hydrocarbon tails, and a_0 is the head group area per molecule at the aggregate surface. The volume and length of the hydrophobic tail can be estimated from knowledge about the gemini surfactant's structure as will be discussed in the structure calculation section. Estimation of the head group area is rather complex since it is an equilibrium parameter that is determined by a balance between the several attractive and repulsive forces acting simultaneously to determine the preferred curvature of the gemini aggregates. As such, it was obtained from calculating the surface excess concentration according to the relation:

$$a_0 = (N_A \Gamma)^{-1} \qquad (2)$$

where N_A is the Avogadro number, and Γ is surface excess concentration derived from the Gibbs adsorption isotherm as shown in the equation below:

$$\Gamma = -\frac{1}{2.303 n\,\mathrm{RT}} \left(\frac{\mathrm{d}\gamma}{\mathrm{d}\,\log \mathrm{C}}\right)_{\mathrm{T}} \qquad (3)$$

where R is the gas constant ,T is the absolute temperature and *n* is the number of species at the interface resulting from the dissociation of the surfactants, which for gemini surfactants it is

equal to 3 [30]. The value for the premicellar slope, $(d\gamma/ d \log C)_T$, is obtained from the surface tension measurements.

3.3.10. Structure calculations

An estimate of the length of the hydrocarbon tails was attained by using Avogadro software [31]. Volume calculations were conducted with Gaussian09 software, revision C.01 [32]. The geometry was optimized on the B3LYP level of theory with 6-311+G(d,p) basis set. Optimized structures were confirmed using harmonic frequency calculations. Volumes for the optimized structure were calculated using united atom radii.

Calculated partition coefficient ($_c$log P) values were estimated using ACD/Physchem Profiler 2016 [33] (Advanced Chemistry Development, Inc., Toronto, ON, Canada).

3.3.11. Statistical analysis

Statistical analyses were performed using SPSS software (Version 23.0). Results expressed as the average of $n \geq 3 \pm SD$. One-way analysis of variance (ANOVA, Scheffé/Dunnett's post hoc tests) and Pearson's correlation were used for statistical analyses. Significant differences were considered at $p<0.05$ level.

3.4. Results and discussion

3.4.1. Molecular design of peptide-modified gemini surfactants

The high performance and low cytotoxicity of the previously evaluated amino acid-conjugated gemini surfactants have motivated the design of a novel series of 22 peptide-modified gemini surfactants (Figure 3.2) [23-25]. The aim of this work was (i) to produce compounds with higher transfection efficiencies, (ii) lower toxicity and (iii) to develop a better understanding of the impact of structural modification on the physicochemical characteristics and biological activity of the newly developed peptide-modified gemini surfactants, i.e., structure-activity relationship. The designed compounds are based on the *m*-7N(R)-*m* general structure, where *m* = the number of carbon atoms in the alkyl tails, *R* = the amino acid group coupled onto the N position of the spacer region as shown in Figure 3.2. The structural modification focused on altering the conjugated amino acid group grafted into the spacer and varying the hydrophobic tails.

In light of the important role of the terminal lysine moiety in the interaction with the nucleic acid and the production of intelligent nanoparticles that respond to environmental stimuli [24, 25, 27], we investigated the impact of increasing the number of terminal lysine moieties on the efficiency of the delivery system. Accordingly, compounds with tri- and hepta- lysine residues were designed to create dendrimer-like gemini surfactants (Figure 3.2, compounds 2-3). Furthermore, the impact of incorporating an hydrocarbon linker between the amino acids and spacer group was evaluated. The rationale was that a distance between the quaternary ammonium head group and the amino acid substituent might be required for efficient gene delivery. Hexyl and undecyl chains were tested to assess the effect of linker length on the gene delivery system (Figure 3.2, compounds 4-7). Eliminating the glycine residue and coupling of the hydrocarbon

linker directly into the spacer was also investigated to evaluate the role of the glycine in determining the transgene efficiency and physicochemical characteristics (Figure 3.2, compounds 8-11).

In addition to the assessment of various structural substituents into the spacer region, modifications to the hydrophobic tails were also conducted. In earlier studies, it was found that the length and the degree of unsaturation of the alkyl tail have a significant effect on the physicochemical properties of gemini surfactants, thereby affecting their efficiency to deliver the genetic material [25]. As such, this work evaluates three types of hydrophobic tails that are commonly reported in the literature for their high efficiency, namely dodecyl, hexadecyl and oleyl (Figure 3.2). Generally, compounds with hexadecyl tails demonstrated higher or very similar transfection efficiency compared to their structural analogues with dodecyl and oleyl chain in all compounds. This was in alignment with our previous report that specifically assessed the role of the alkyl tail on the transfection efficiency of di-amino acid-modified gemini surfactants [25]. Therefore, this manuscript focuses on compounds with hexadecyl alkyl tails with less emphasis on the dodecyl and oleyl chains.

To the best of our knowledge, this is the first report that describes the design of dendrimer-like gemini surfactants and incorporation of hydrocarbon linkers into the spacer region. By evaluating the structure-activity relationship of such model compounds, we believe that this study could provide a framework for the future development of peptide-based gemini surfactants.

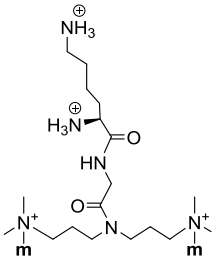

m-7N(G-K)-m

1A: **m**= dodecyl,C12
1B: **m**= hexadecyl, C16
1C: **m**= oleyl, C18:1

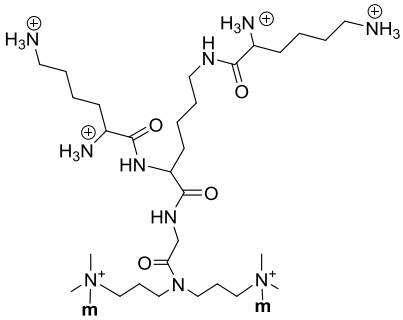

m-7N(G-K$_3$)-m

2A: **m**= dodecyl,C12
2B: **m**= hexadecyl, C16
2C: **m**= oleyl, C18:1

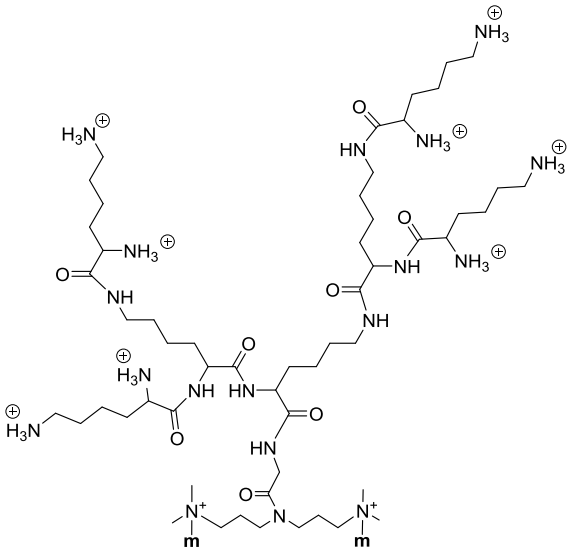

m-7N(G-K$_7$)-m

3A: **m**= dodecyl,C12
3B: **m**= hexadecyl, C16
3C: **m**= oleyl, C18:1

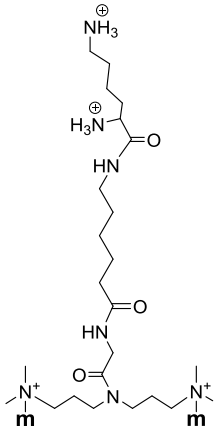

m-7N(G-C$_6$-K)-m

4: **m**= hexadecyl, C16

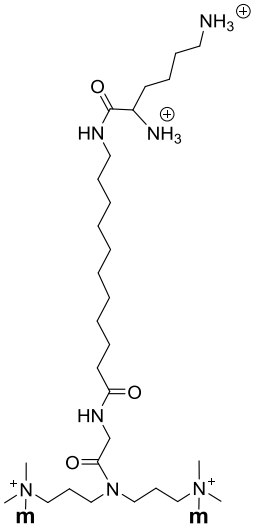

m-7N(G-C$_{11}$-K)-m

5A: **m**= dodecyl,C12
5B: **m**= hexadecyl, C16

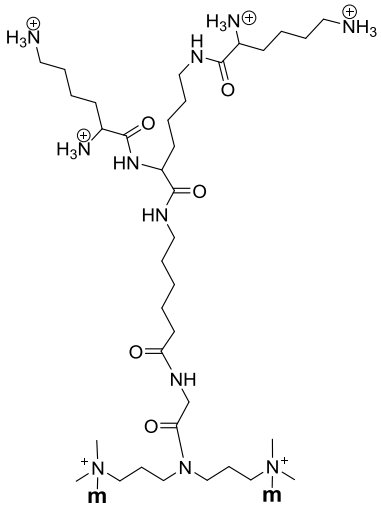

m-7N(G-C$_6$-K$_3$)-m

6A: **m**= dodecyl,C12
6B: **m**= hexadecyl, C16

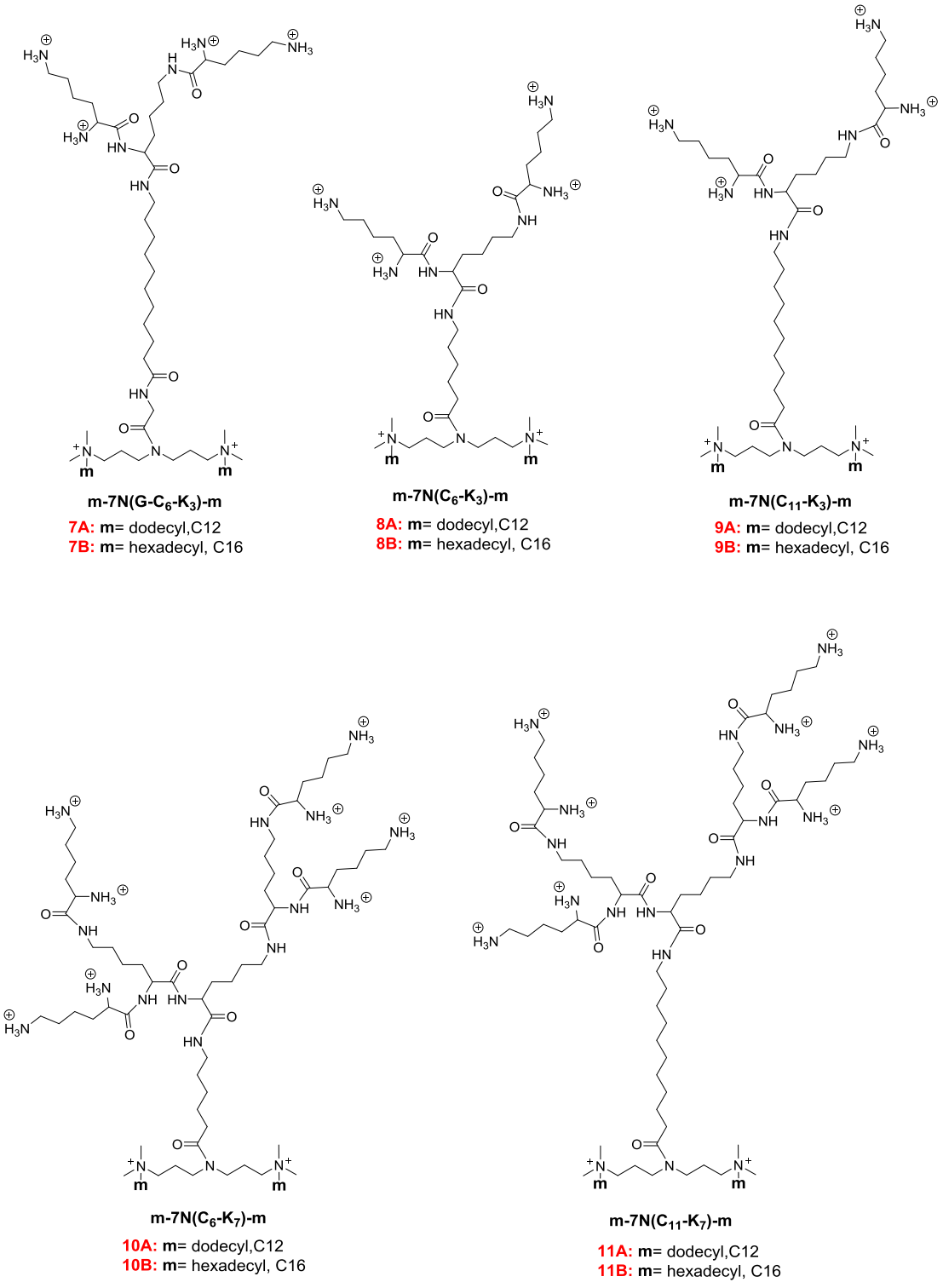

Figure 3.2. Chemical structure of the evaluated peptide-modified gemini surfactants where m is the alkyl tail carbon chain length, G is a glycine and K is a lysine residue.

3.4.2. Physicochemical characterization of the lipid-based gene delivery system

3.4.2.1. Determination of critical micelle concentration

The critical micelle concentration (CMC) is an important interfacial property that quantitatively describes the propensity of an amphiphile to assemble. It could give an indication of the ability of gemini surfactants to form stable complexes with the nucleic acid [34]. The self-assembly process is governed by a balance between attractive forces resulting from both hydrophobic interactions as well as hydrogen bonding, and repulsive forces caused by the electrostatic repulsion [35]. As such, all the structural elements of the gemini surfactants act simultaneously to determine micelle formation.

Peptide-modified gemini surfactants displayed a wide range of CMC values between 35 to 106 µM (Table 3.1). This could be rationalised by the diverse molecular structure of the peptides incorporated into the spacer region. In general, increasing the number of terminal lysine moieties within the structure was associated with an increase in the CMC value (Table 3.1). For example, CMC values increased from 83 to 93 then to 107 µM when the number of lysine moieties increased from one in 16-7N(G-K)-16 to three in 16-7N(G-K_3)-16 then to a sequence of seven residues in 16-7N(G-K_7)-16. This was negatively correlated (Pearson's correlation coefficient = -0.997, $p<0.05$) with the compounds lipophilicity where $_c$log p values decreased from 2.80, to 0.98 then to -2.04 for 16-7N(G-K)-16, 16-7N(G-K_3)-16 and 16-7N(G-K_7)-16, respectively (Table 3.1). The same trend was followed across all evaluated structural analogs such as 16-7N(G-C_6-K)-16 compared to 16-7N(C_6-K_3)-16 and 16-7N(G-C_{11}-K)-16 relative to 16-7N(G-C_{11}-K_3)-16 as shown in Table 3.1. Such a trend is in agreement with the reported pattern in the literature that the CMC in aqueous solution usually decreases upon increasing

hydrophobicity of the amphiphile as a result of strong hydrophobic interactions that induce micelle formation [36]. In addition, increasing the number of lysine moieties causes an increase of the charge density due to the high pK_a (≈ 10.5) value of the primary amines of the terminal lysine residues, which is 99% ionized at the formulation intrinsic pH (≈ 6). Increasing the charge density will contribute to the Coulombic repulsion between the adjacent molecules of gemini surfactants [37]. Consequently, more surfactants are needed to form micelles.

Furthermore, the incorporation of a hydrophobic linker into the spacer region resulted in a significant decrease in the CMC values (Table 3.1). This was also attributed to the overall increase in the compounds' hydrophobicity which ultimately impacted the self-assembly process [36]. For example, while the attachment of an hexyl linker into 16-7N(G-K)-16 resulted in decreasing the CMC from 83 to 45 µM as in 16-7N(G-C_6-K)-16, the incorporation of undecyl linker lowered CMC to 36 for 16-7N(G-C_{11}-K)-16. Moreover, incorporation of the hydrophobic linker increased the distance between the quaternary ammonium and the charged atoms on the peptide chain which could minimize the repulsive forces, favoring surfactant aggregation at lower concentrations. As such, longer linkers (i.e., undecyl linker over hexyl linker) imparted lower CMC values (Table 3.1).

Conversely, removing the glycine residue and coupling the hydrocarbon linker directly into the spacer region, 16-7N(C_{11}-K_3)-16 and 16-7N(C_6-K_3)-16, resulted in higher CMC values compared to the compounds that contained glycine (16-7N(G-C_{11}-K_3)-16 and 16-7N(G-C_6-K_3)-16) despite the higher lipophilicity of the former compared to the latter. For instance, although compound 16-7N(G-C_6-K_3)-16 had lower lipophilicity than 16-7N(C_6-K_3)-16 ($_c$log P values of 1.28 and 1.98, respectively), it exhibited a lower CMC value of 67 µM compared to 86 µM for the latter (Table 3.1). This could be explained by the tendency of the glycine moiety to form

hydrogen bonding with the neighbouring head groups which could minimize the electrostatic repulsion. As a result, fewer building blocks are needed to form a micelle. These findings are consistent with reports that the incorporation of a small hydrophilic moiety into the spacer provides a more water-compatible interface that results in a lower CMC compared to an unsubstituted compound [38].

Table 3.1. Hydrophobicity and micellization parameters of the peptide-modified gemini surfactants.

Gemini surfactants	^{c}log P	CMC (μM)	Head group area (Å^2)	Molecular packing parameter	Molecule shape	Micelle shape
16-7N(G-K)-16	2.80	83	40	1.26	Inverted truncated cone	Inverted micelles
16-7N(G-K$_3$)-16	0.98	93	123	0.41	Truncated cone	Cylindrical micelles
16-7N(G-K$_7$)-16	-2.04	107	190	0.27	Cone	Spherical micelles
16-7N(G-C$_6$-K)-16	3.77	45	115	0.44	Truncated cone	Cylindrical micelles
16-7N(G-C$_{11}$-K)-16	4.81	36	241	0.21	Cone	Spherical micelles
16-7N(G-C$_6$-K$_3$)-16	1.28	67	151	0.33	Truncated cone	Cylindrical micelles
16-7N(G-C$_{11}$-K$_3$)-16	3.27	57	257	0.20	Cone	Spherical micelles
16-7N(C$_6$-K$_3$)-16	1.98	86	79	0.64	Truncated cone	Flexible bilayers, vesicles
16-7N(C$_{11}$-K$_3$)-16	3.98	63	102	0.50	Truncated cone	Flexible bilayers, vesicles
16-7N(C$_6$-K$_7$)-16	-1.45	98	178	0.29	Cone	Spherical micelles
16-7N(C$_{11}$-K$_7$)-16	0.58	81	130	0.39	Truncated cone	Cylindrical micelles

3.4.2.2. Determination of the molecular packaging parameter

The shape of the gemini surfactant molecules plays an important role in determining their ability to form a supramolecular assembly with the DNA; hence, it impacts the performance of the gene delivery system [39]. Accordingly, understanding how the molecular structure of the gemini surfactant controls the shape of the resulting aggregate is an essential step in the rational design process. The shape of the aggregates can be obtained from estimating the molecular packing parameter (P) based on the behaviour of the gemini surfactant at the air-water interface [40]. This concept was introduced by Israelachvili *et al.* to relate the geometrical shape of the surfactants to the preferred curvature of its aggregates [40].

A specific value of P can be connected via geometrical relationship to a particular micelle shape [40, 41]. For example, a P values of less than 0.33 tend to form spherical micelles, whereas cylindrical or rod-like aggregates are observed with P values between 0.33 and 0.5. The formation of vesicles occurs for P values between 0.5 and 1.0. When P =1 bilayers with zero curvature are formed and a P value greater than 1 favours the formation of reversed structures.

Increasing number of the lysine moieties in compounds 16-7N(G-K)-16, 16-7N(G-K_3)-16 and 16-7N(G-K_7)-16 resulted in a significant enlargement in the head group areas from 40 to 123 to 190 $Å^2$, respectively (Table 3.1 and Figure 3.3). Such an increase was expected due to the bulkiness of the functional groups incorporated into the spacer (Figure 3.3). This in turn gave rise to diverse aggregate shapes across the three compounds, namely the 16-7N(G-K)-16 compound favoured the formation of inverted micelles, 16-7N(G-K_3)-16 formed cylindrical micelles while 16-7N(G-K_7)-16 gemini surfactants resulted in spherical micelles (Table 3.1).

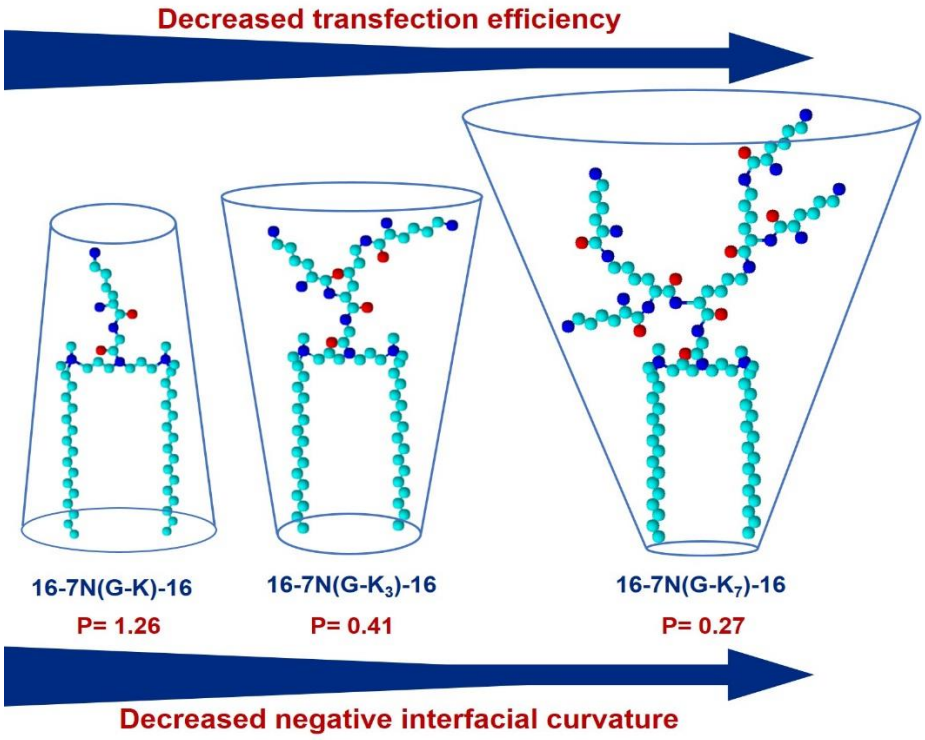

Figure 3.3. Schematic representation of peptide-modified gemini surfactant molecular shapes shows the impact of increasing the number of terminal lysine moieties on the molecular packing parameter (P), preferred curvature and transfection efficiency.

The incorporation of an hydrocarbon linker between the glycine and lysine residue(s) in compound 16-7N(G-K)-16 also induced a significant increase in the gemini surfactant head group areas (Table 3.1). For example, attachment of an undecyl linker in compound 16-7N(G-C_{11}-K)-16 gave rise to a head group areas twice as large as that of the hexyl linker in 16-7N(G-C_6-K)-16 (241 and 115 $Å^2$, respectively) (Table 3.1). In fact, the head group area resulting from the incorporation of undecyl linker in 16-7N(G-C_{11}-K)-16 was greater than that of compound 16-7N(G-K_7)-16 (241 and 190 $Å^2$, respectively) (Table 3.1). This could be explained by the greater tendency of 16-7N(G-K_7)-16 to form intramolecular hydrogen bonding than in 16-7N(G-C_{11}-K)-16 causing compaction of the head group. The insertion of chemical motifs that permit

intramolecular hydrogen bonding encourages interaction within the head group area, giving rise to a smaller cross sectional area and larger packing parameter [42, 43].

A similar trend was observed in compounds coupled with three lysine residues where the addition of the undecyl linker (16-7N(G-C_{11}-K_3)-16) resulted in an head group area 1.6-fold larger than that of the hexyl linker (16-7N(G-C_6-K_3)-16, Table 3.1). Contrary to the expectation that the addition of the hydrophobic linker (hexyl or undecyl) leads to a linear increase in the head group areas of gemini surfactants, regardless of the number of terminal lysine moieties, we observed that the expansion in the head group area was more prominent in the series that contained only one terminal lysine moiety. For example, while there was a 6-fold increase in the head group area of 16-7N(G-C_{11}-K)-16 compared to 16-7N(G-K)-16, the head group area of 16-7N(G-C_{11}-K_3)-16 increased by only 2-fold relative to 16-7N(G-K_3)-16 compound (Table 3.1). We also attribute this to the stronger intramolecular bonding in the dendrimer-like modified surfactants that minimize the cross sectional area [42, 43].

Removing the glycine moiety and conjugating the hexyl and undecyl linker directly into the spacer resulted in smaller head group areas compared to their analogs having the glycine. For example, 16-7N(C_6-K_3)-16 exhibited an head group area of 79 $Å^2$ whereas the 16-7N(G-C_6-K_3)-16 head group area is 151 $Å^2$ (Table 3.1). Surprisingly, the head group areas of compounds that had the linker directly incorporated into the spacer were even smaller than the compound without the linker as illustrated by compounds 16-7N(C_6-K_3)-16, 16-7N(C_{11}-K_3)-16 and 16-7N(G-K_3)-16 with head group areas of 79, 102 and 123 $Å^2$, respectively. A similar trend was observed for compounds with seven lysine moieties where compound 16-7N(G-K_7)-16 had a head group area of 190 $Å^2$ while compounds 16-7N(C_6-K_7)-16 and 16-7N(C_{11}-K_7)-16 exhibited areas of 178 and 130 $Å^2$, respectively (Table 3.1). This could be attributed to the increased distance between the

positively charged quaternary ammonium head group and the charged functional groups in lysine residues induced upon the incorporation of the linkers, which could minimize the repulsion between the positively charged entities within the molecules (Figure 3.4). In fact, unlike compounds having tri-lysine moieties, compounds with an hexyl linker had a larger head group than the undecyl linker analogues in series with hepta lysine residues (Table 3.1 and Figure 3.4). The higher charge density of the hepta-lysine moieties compared to the tri-lysine moieties probably requires a longer distance to be separated from the positively charged quaternary amine head groups, hence, smaller head group area. Finally, the alternation of hydrophobic and hydrophilic regions of the compounds containing the hydrophobic linker imparted a complexity to their aggregation behaviours. This is caused by the several intramolecular forces, i.e., attractive forces and repulsive forces, which are acting simultaneously on different parts of the molecule to determine their preferred curvature at the air-water interface.

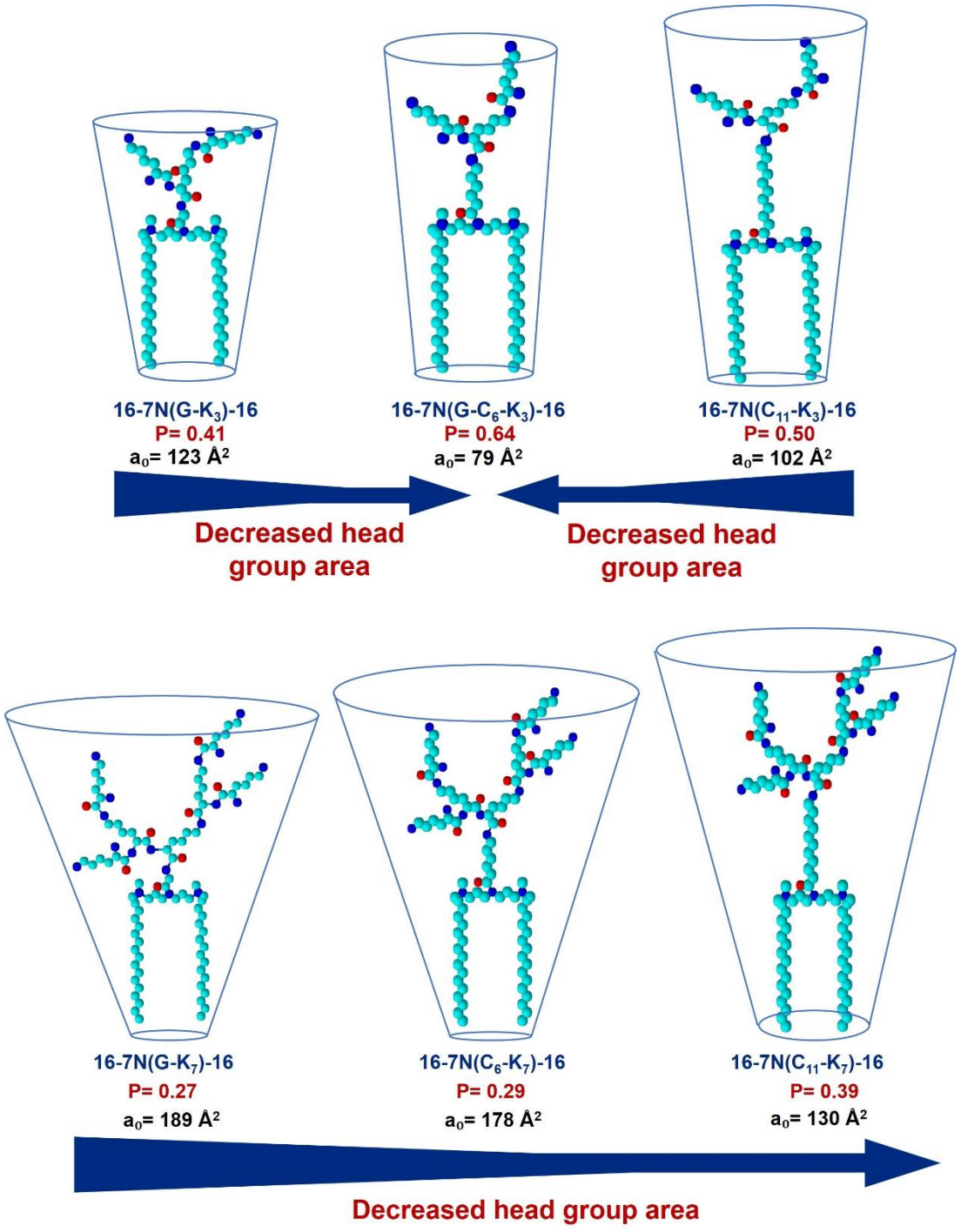

Figure 3.4. Schematic representation of peptide-modified gemini surfactant molecular shapes shows the impact of removing the glycine and incorporating an hydrocarbon linker on the molecular packing parameter (P) and head group area (a_0) of 16-7N(G-K_3)-16 and 16-7N(G-K_7)-16 series.

3.4.2.3. Determination of size and ζ-potential

Size and surface charge of gene delivery nanoparticles are important parameters that can affect the efficiency of the delivery system by impacting their stability, efficiency of cellular uptake, route of cellular entry, intracellular fate, and cytotoxicity [44-46]. Therefore, size and zeta potential measurements of the peptide-modified gemini surfactants P/L/G lipoplexes at three N/P ratios of 2.5, 5 and 10 were evaluated and correlated with the transgene efficiency of the delivery system. In agreement with our previous results, increasing the N/P ratio caused a gradual decrease in particle size and increase in zeta potential [25]. In addition, the impact of varying the alkyl tail on the particle size and zeta potential was also in alignment with our recent report that investigated the role of the alkyl tail [25]. As such, this section only discusses the average particle size and zeta potential of P/L/G lipoplexes with hexadecyl tails at N/P of 2.5, so that the impact of the peptides modifications is evaluated.

Lipoplexes at an N/P ratio of 2.5 showed a range of particle sizes between 72 and 107 nm. In general, increasing the number of lysine residues resulted in an enlargement in the average particle size of lipoplexes (Table 3.2). For compounds 16-7N(G-K)-16, 16-7N(G-K_3)-16 and 16-7N(G-K_7)-16, the particle size increased from 80 ± 1 to 95 ± 4 to 107 ± 3 nm, respectively. A similar trend was also observed within the structural analogues that contain the hydrophobic linker e.g., 16-7N(G-C_6-K)-16 compared to 16-7N(G-C_6-K_3)-16 and 16-7N(C_{11}-K_3)-16 compared to 16-7N(C_{11}-K_7)-16 (Table 3.2). The increase in size was expected since increasing the number of lysine moieties from mono- to di- then to hepta-conjugates added a larger steric demand onto the compounds, hence, increased the overall size of the aggregates. However, the increase in particle size was not as significant as the increase in the head group area as shown in Table 3.2. This could be attributed to the tighter compaction of the DNA molecule by the hepta-derivatives, due to the involvement of the terminal lysine residues in the

interaction with the phosphate groups. In fact, several reports indicated that amino acids such as lysine can interact with the DNA by forming hydrogen bonds and by van der Waals forces [47, 48].

Table 3.2. Particle size and zeta potential measurements of the peptide modified gemini surfactant lipoplexes with C16 tails at N/P of 2.5. Results are shown as mean (n=3) ± standard deviation. PDI is the polydispersity index.

Gemini surfactants	**Average size (nm) ± STD**	**PDI**	**Average zeta (mV) ± STD**
16-7N(G-K)-16	80 ± 1	0.23	24 ± 2
16-7N(G-K_3)-16	95± 4	0.25	38 ± 0.5
16-7N(G-K_7)-16	107 ± 3	0.24	48 ± 0.8
16-7N(G-C_6-K)-16	76 ± 1	0.22	21 ± 2
16-7N(G-C_{11}-K)-16	72 ± 2	0.11	19 ± 2
16-7N(G-C_6-K_3)-16	89 ± 2	0.25	32 ± 0.4
16-7N(G-C_{11}-K_3)-16	85 ± 1	0.26	29 ± 1
16-7N(C_6-K_3)-16	88 ± 2	0.20	29± 1
16-7N(C_{11}-K_3)-16	86 ± 0.8	0.19	34± 0.9
16-7N(C_6-K_7)-16	94 ± 0.4	0.23	42 ± 1
16-7N(C_{11}-K_7)-16	90 ± 0.5	0.22	39 ± 0.4

The incorporation of the hydrocarbon linker between the glycine and lysine residues or grafted directly into the spacer resulted in a decrease in the particle size (Table 3.2). This could be explained by the involvement of the hydrocarbon linker in the compaction of the DNA through hydrophobic interactions [49, 50]. This hypothesis is supported by the fact that smaller particle size was observed in lipoplexes formulated with gemini surfactants having an undecyl linker compared to an hexyl linker. For example, the presence of the undecyl linker in compound 16-7N(G-C_{11}-K)-16 reduced the particle size to 72 ± 2 nm from 80 ± 1 nm for the parent

compound 16-7N(G-K)-16 whereas the addition of the hexyl linker resulted in an intermediate particle size of 76 ± 1 nm (Table 3.2). Removing the glycine and conjugating the hydrocarbon linker directly into the spacer also resulted in minor changes in the particle size of 88 ± 2 nm for 16-7N(C_6-K_3)-16 compared to 89 ± 2 nm for 16-7N(G-C_6-K_3)-16 or 86 ± 0.8 nm for 16-7N(C_{11}-K_3)-16 compared to 85 ± 1 nm for16-7N(G-C_6-K_3)-16 (Table 3.2). While smaller particle size should result from the removal of the glycine moiety due to the less steric demand, this effect was offset by the weaker interactions with DNA caused by fewer hydrogen bond and van der Waals forces between the gemini surfactants and DNA [49]. Thus, there is interplay between the physical size of the head group of the gemini surfactant and potential interactions with the DNA molecule contributing to the overall size of the P/L/G lipoplexes.

Similar to the particle size, the P/L/G lipoplexes revealed a wide range of zeta potential values between +19 and +48 mV (Table 3.2). Increasing the number of lysine residues resulted in an increase in the zeta potential of nanoparticles. For instance, the zeta potential increased from 24 ± 2 mV to 38 ± 1 mV to 48 ± 1 mV upon increasing the number of lysine moieties from one to three to seven in 16-7N(G-K)-16, 16-7N(G-K_3)-16 and 16-7N(G-K_7)-16 molecules, respectively (Table 3.2). A higher number of lysine moieties implies more epsilon primary amines protonated at the intrinsic pH (≈ 6) of the formulation, leading to greater positively charged nanoparticles [51]. On the other hand, the insertion of the hydrocarbon linker resulted in a decrease in the zeta potential (Table 3.2). This effect could be a result of shielding of the charges with the hydrophobic linker. In fact, a longer linker rendered a lower zeta potential of 39 ± 1 mV in 16-7N(C_{11}-K_7)-16 compared to 16-7N(C_6-K_7)-16 that exhibited surface charge of 42 ± 1 mV (Table 3.2).

3.4.2.4. Determination of the lipid organization

The effect of structural differences of the peptide-modified gemini surfactants on the supramolecular assembly of the lipoplexes at three N/P ratios was evaluated using SAXS. Scattering profile of each individual constituent of the P/G/L nanoparticle was assessed separately as a reference. The plasmid DNA did not show any diffraction peaks, suggesting the absence of any crystalline structure. DOPE showed Bragg peaks at q values of 0.1039, 0.178 and 0.206 with ratio of 1:√3:√4 corresponding to the inverted hexagonal (H_{II}) phase [52]. In general, the gemini surfactants alone showed diffused scattering at low q values of 0.12-0.17 indicating micellar organization. Such a diffraction pattern resulted from the shell-like structure of the chloride counter-ion cloud around the micelles corresponding to a micellar diameter of 3.6-5.2 nm (Figure 3.5).

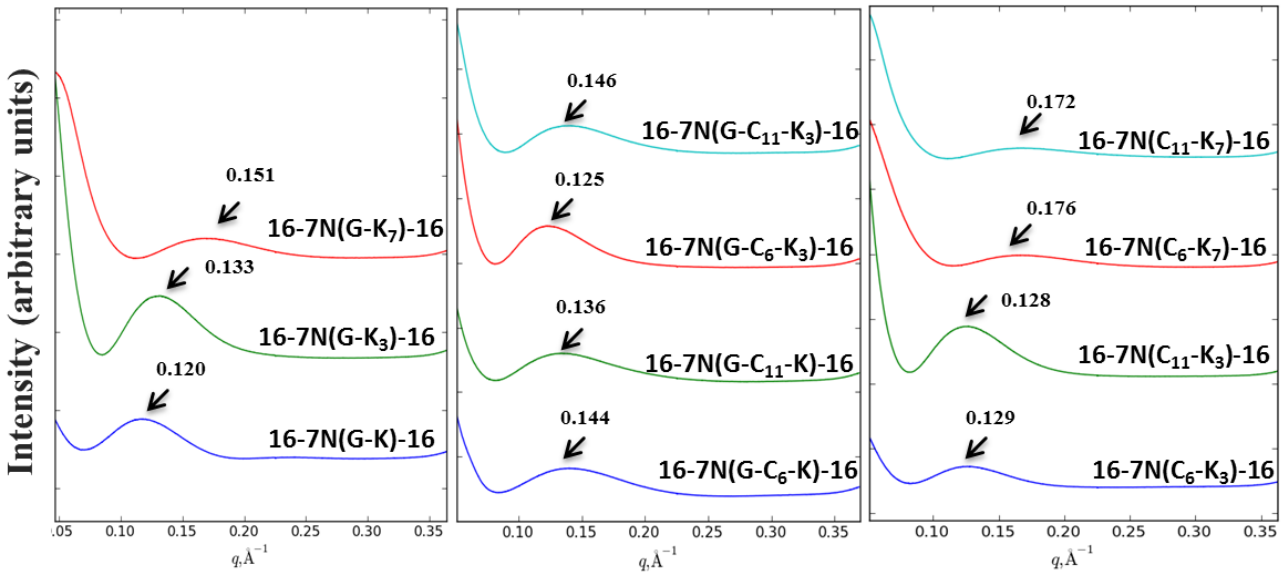

Figure 3.5. SAXS scattering profile of 30 mM solutions of the peptide modified gemini surfactants show a diffused scattering at low q values (~ 0.13) suggesting the formation of micellar structures.

The complexation of gemini surfactants with the DNA led to an increase of the intensity at q ~0.113 values with respect to plateau at higher q, indicative of larger scattering objects in the solution (Figure 3.6). Mixing DNA to 16-7N(G-K)-16 revealed the most prominent peak among tested compounds at q= 0.100 especially at N/P ratio of 10 (Figure 3.6A). However, the absence of a second peak prevented the identification of the phase. The incorporation of an hexyl linker between the glycine and lysine, 16-7N(G-C_6-K)-16, resulted in the formation of a small peak at q= 0. 110 and signs of a second diffraction peak at q= 0.22 at both N/P ratio of 2.5 and 5 (Figure 3.6D). This could be an indication of the presence of the multilamellar phase L_α^c; however, a third peak would have been necessary for confirmation. Moreover, both peak signals were weakened upon further increase in the amount of gemini surfactant, N/P =10 (Figure 3.6D). On the other hand, the incorporation of an undecyl linker gave rise to three diffraction peaks at q= 0.09, 0.180 and 0.268 in the ratio of 1:2:3 (Figure 3.6E), which correspond to peak positions of the multilamellar phase L_α^c [53]. However, the intensity of the peaks did not follow the conventional pattern of the previously reported multilamellar phases [53]. This could be due to the co-existence of another phase, albeit we were unable to assign this to the previously reported phases. Further increase in the ratio of gemini surfactants resulted in diffuse scattering that masked the second diffraction peak and minimized the intensity of the first and last peak.

P/G complexes of both 16-7N(G-K_3)-16 and 16-7N(G-K_7)-16 exhibited a small peak at q= 0.112 and 0.102, respectively, followed by diffuse scattering as indicated by the red arrows (Figure 3.6B and C). The diffused scattering was more intense in compound 16-7N(G-K_7)-16 which could be linked to its higher charge density compared to compounds with tri-lysine residues. In fact, the same effect was noticed upon increasing the N/P ratio (Figure 3.6B and C, at N/P = 10). Unlike compounds with mono lysine head groups, the addition of hydrocarbon linker with or

without the glycine moiety resulted in decreased intensity of both the smaller peak and the diffused scattering (Figure 3.6F-K). Overall, SAXS data revealed a complex behaviour of the P/G complex that is greatly affected by the molecular structure and valence of the spacer moieties.

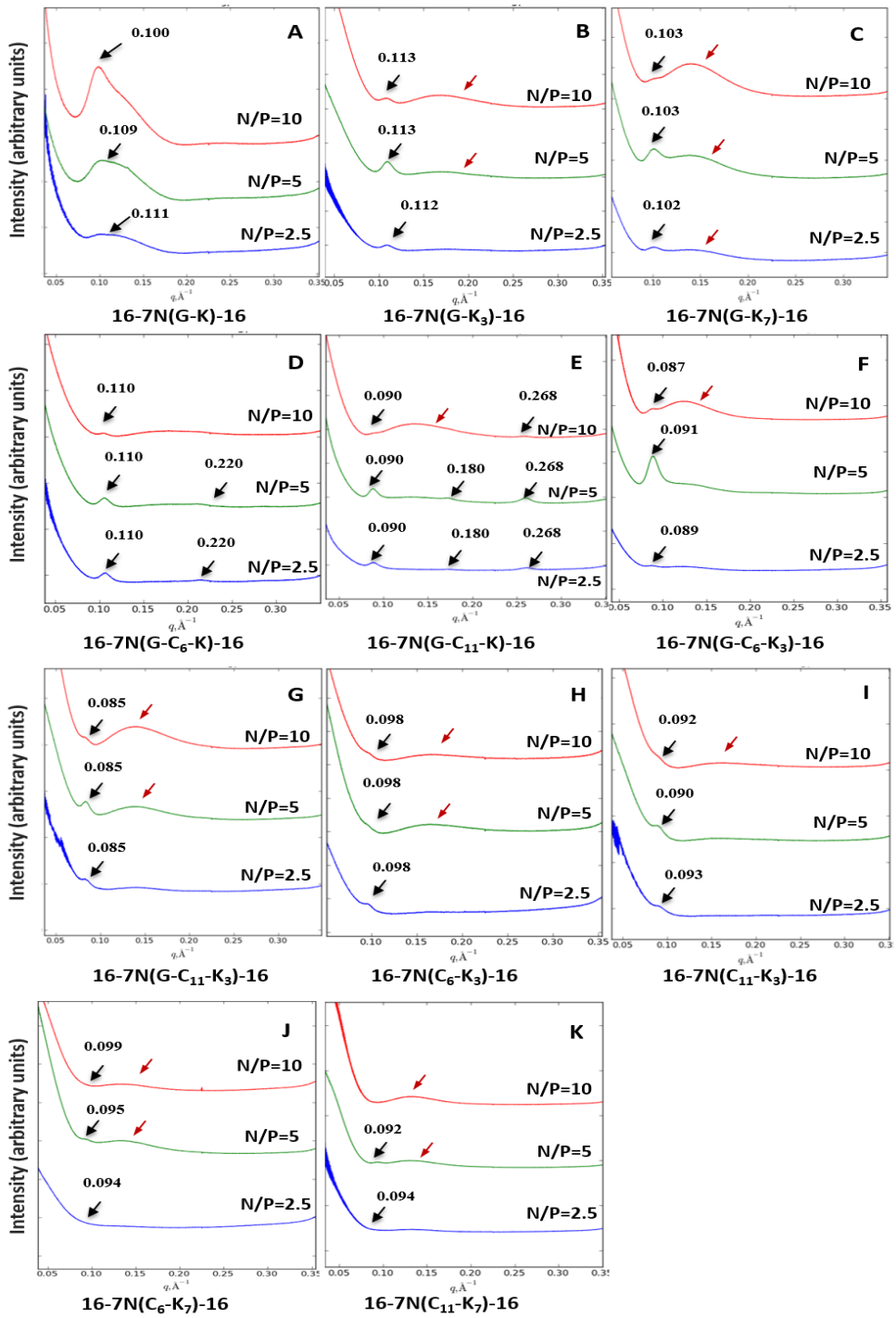

Figure 3.6. SAXS scattering profile of DNA and gemini surfactants (P/G) complexes of the peptide modified gemini surfactants at N/P ratios of 2.5, 5 and 10. Black arrows represent a sign of phase formation. A diffuse scattering peak (red arrows) indicate complexity of structures and might correspond to high charge density.

Combining the three components: DNA, gemini lipid and DOPE (P/G/L) led to a marked increase of the intensity at low q and the appearance of Bragg peaks at higher q values indicating internal ordering of the newly formed aggregates (Figure 3.7). An inverted hexagonal phase was adopted in all P/G/Ls at their optimal N/P ratios of 2.5. In cationic gene delivery systems, the inverted hexagonal phase (H_{II}) is known to be responsible for high transfection efficiency due to its ability to facilitate fusion with the cell membrane and cytoplasmic release of the DNA into the cytosol [54]. The position of the scattering peaks and the corresponding unit cell spacing ($a = 4\pi/\sqrt{3}\ q_{10}$, where q_{10} is the first Bragg peak) are listed in Table S1, Appendix II. At N/P ratio of 2.5, no significant differences were observed in the repeated distances and corresponding unit cell spacing despite the variation in the molecular structure among the compounds. This could be mainly attributed to the low molar ratio of the gemini surfactants to the DOPE (1:33) at this charge ratio. The effect of structural modifications became more prominent in lipoplexes with N/P ratios of 5 and 10 (Figure 3.7), corresponding to gemini surfactant to DOPE mole ratios of 1:16 and 1:8, respectively.

Lipoplexes of 16-7N(G-K)-16 maintained the H_{II} phase at N/P ratio of 2.5 and 5 (Figure 3.7A). Increasing the charge ratio of N/P to 10 resulted in diffuse scattering that overshadowed Bragg peaks. Such behaviour was reported by us and others and it is believed to be caused by the interaction of the excess gemini surfactants with the helper lipid [25, 55]. Both DOPE and 16-7N(G-K)-16 have an inverted truncated cone molecular shape which favour a negative membrane curvature giving raise to the H_{II} phase (Table 3.1) [56]. However, the difference in the molecular size between DOPE and 16-7N(G-K)-16 might cause the distortion of the H_{II} phase upon further increase in the amount of gemini surfactant at N/P of 10 (Figure 3.7A).

On the contrary, lipoplexes prepared from 16-7N(G-K_3)-16 or 16-7N(G-K_7)-16 exhibited the H_{II} phase only at an N/P ratio of 2.5 while a broad peak was observed at N/P ratios of 5 and 10 (Figure 3.7B and C). It is noteworthy that gemini surfactants 16-7N(G-K_3)-16 and 16-7N(G-K_7)-16 gave rise to truncated cone and cone molecular shapes which favour the formation of a positive spontaneous membrane curvature (Table 3.1). Therefore, it is possible that combining 16-7N(G-K_3)-16 or 16-7N(G-K_7)-16 with DOPE causes higher interference to the H_{II} phase than 16-7N(G-K)-16. Furthermore, 16-7N(G-K_3)-16 and 16-7N(G-K_7)-16 have a higher charge density than 16-7N(G-K)-16, hence they promote transitions towards less negatively curved phases than the H_{II} phase [57]. In fact, we think that the broad peak observed at N/P of 10 could be a sign of phase transition as previously reported in dendrimer like lipids [55].

The scattering pattern resulting from the incorporation of the hexyl linker into the compound with mono-lysine moiety (compound 16-7N(G-C_6-K)-16, Figure 3.7D) did not differ from the scattering pattern of compound 16-7N(G-K)-16 (Figure 3.7A). However, the incorporation of the undecyl linker caused a loss in the H_{II} phase at N/P =5 (compound 16-7N(G-C_{11}-K)-16, Figure 3.7E). A similar trend occurred upon the addition of hydrocarbon linkers to compounds with tri-lysine moieties in which lipoplexes of 16-7N(G-C_6-K_3)-16 maintained the H_{II} phase up to an N/P ratio of 5 while 16-7N(G-C_{11}-K_3)-16 lost the phase by N/P of 5 (Figure 3.7F and G). On the contrary, the length of the hydrocarbon linker in compounds modified with tri-lysine moieties without the presence of glycine residues, 16-7N(C_6-K_3)-16 and 16-7N(C_{11}-K_3)-16, did not interfere with the scattering profile of their lipoplexes (Figure 3.7H and I). In compounds with hepta-lysine residues the addition of an hexyl linker in 16-7N(C_6-K_7)-16 resulted in the formation of the diffuse scattering at an N/P ratio of 5 while the incorporation of an undecyl linker prompt the formation of the diffuse scattering at an N/P ratio of 10 (Figure 3.7J

and K). We believe that the scattering profile is affected by the overall geometrical shape of the molecules rather than the length of the hydrophobic linker. In particular, there is a tendency of the surfactant to support or disturb the formation of a liquid crystalline phase with negative curvature of H_{II} phase formed by DOPE. For example, all lipoplexes with cone-shaped gemini surfactants formed H_{II} phase only at an N/P ratio of 2.5 and diffuse scattering arose upon further increase in the amount of gemini surfactant (Table 3.1, Figure 3.7). On the other hand, compounds with truncated cone molecular structure caused less interference to the H_{II} phase, maintaining the phase up to N/P of 5 (Table 3.1, Figure 3.7). This was applicable to all truncated cone-shaped compounds except 16-7N(G-K_3)-16 (Figure 3.7B). We hypothesize that the interplay between the highly charged head of 16-7N(G-K_3)-16 and the lack of an hydrophobic linker to shield those charges could be the reason for the greater interference with the H_{II} phase formed by DOPE.

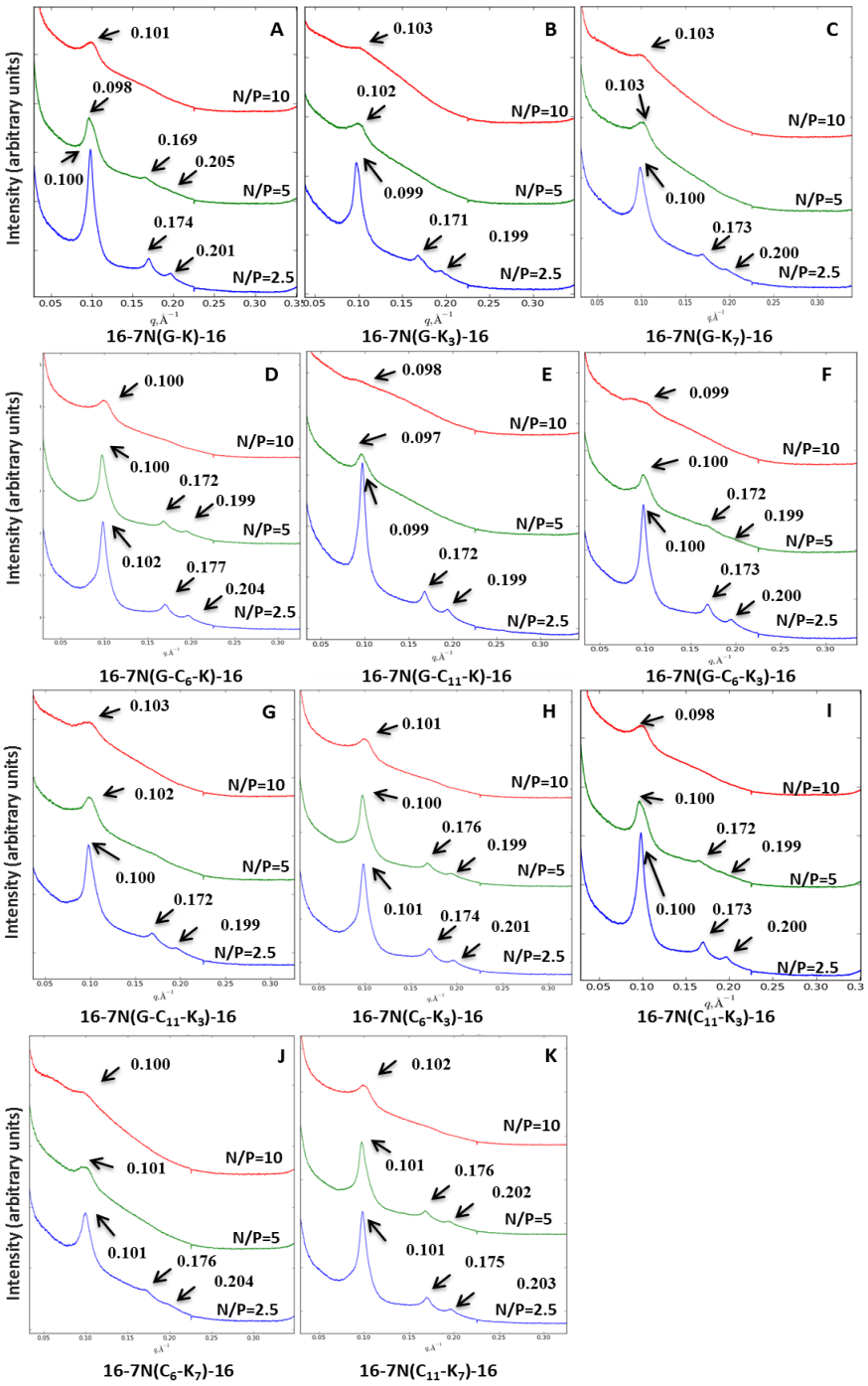

Figure 3.7. SAXS scattering profile of the P/G/L lipoplexes of the peptide modified gemini surfactants at N/P ratios of 2.5, 5 and 10. Black arrows indicate the position of Bragg peaks. q values with ratio of 1: √3: √4 correspond to the inverted hexagonal (H_{II}) phase.

3.4.3. Evaluation of the *in vitro* transfection activity

The transfection efficiency of the 22 peptide-modified gemini surfactants was evaluated in murine keratinocytes (PAM 212) since the ultimate goal of this research was to a develop topical gene delivery system that expands the treatment arsenal of fibrotic skin conditions (Figure S1, Appendix II). In addition, the compounds were evaluated in COS-7, a transfection cell-line commonly used to evaluate new transfection agents (Figure S2, Appendix II). Three N/P ratios of 2.5, 5 and 10 were assessed for all P/G/L lipoplexes. The most efficient N/P ratio was at 2.5 for all compounds in both cell lines (Figure S1 and S2, Appendix II). Increasing the N/P ratio above 2.5 was associated with a decreasing trend in the level of secreted protein. In PAM 212, this decrease was more prominent within the series that had seven terminal lysine moieties: m-7N(G-K_7)-m, m-7N(C_{11}-K_7)-m and m-7N(C_6-K_7)-m (Figure S1, Appendix II). In both cell lines, lipoplexes of gemini surfactants with hexadecyl tail; C16, showed the highest transfection efficiency compared to their analogs with dodecyl; C12, and oleyl chain; C18:1 (Figure S1 and S2, Appendix II). As such, in order to compare between the different subfamilies and assess the impact of various structural modifications into the spacer, the discussion will be mainly focused on compounds with a 16-carbon tail at the optimal charge ratio (N/P 2.5) (Figure 3.8).

P/G/Ls of gemini surfactant 16-7N(G-K)-16 exhibited the highest transfection efficiency among the tested compounds showing a protein level of 2.82± 0.2 ng INF-γ /15x10^3 cells in PAM 212 (Figure 3.8) and of 13.7± 0.8 ng INF-γ /10^4 cells in Cos-7 cell line (Figure S2, Appendix II). In fact, it showed more than 8-fold increase in the level of secreted protein, at four times lower concentration compared to the first-generation gemini surfactants [14]. Further increase in the number of terminal lysine moieties incorporated into the spacer of gemini

surfactants was associated with lower protein levels in both cell lines. P/G/Ls of gemini surfactants 16-7N(G-K_3)-16 and 16-7N(G-K_7)-16 showed about 2.5- and 3.5-fold reduction in the level of secreted protein, respectively, compared to 16-7N(G-K)-16 lipoplexes in PAM 212 (Figure 3.8). Such a drop was even more detrimental in the COS-7 cell line where it led to more that a 7-10 folds reduction in the level of secreted protein (Figure S2, Appendix II).

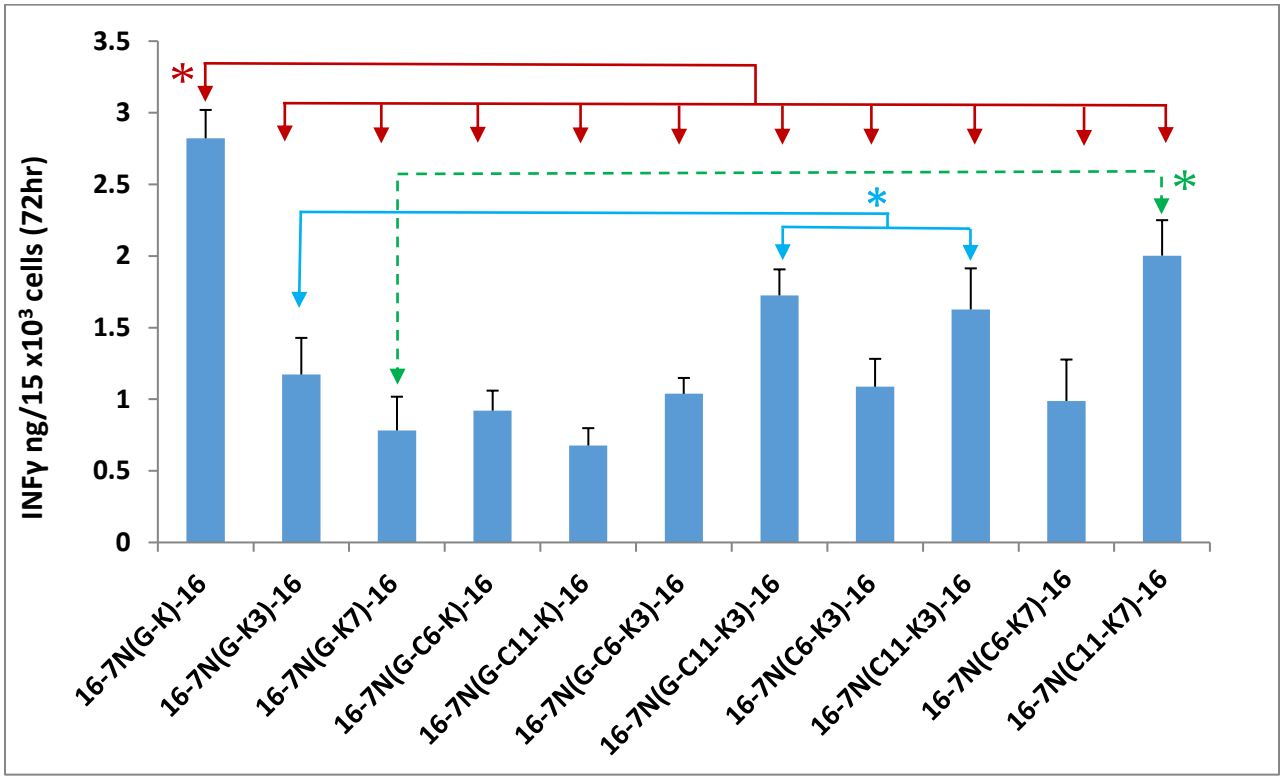

Figure 3.8. *In vitro* transfection of PAM 212 cells comparing the level of IFN-γ expression across the different subfamilies of the peptide-modified gemini surfactants. Results are the average of three plates of quadruplicate wells, error bars represent standard deviation. * Indicates significant at $p < 0.05$.

The reduction in transfection efficiency associated with increasing the number of lysine moieties could be attributed to several factors. First of all, 16-7N(G-K)-16 gemini surfactant had a packing parameter of 1.26 which favours the formation of inverted hexagonal phase (Table 3.1). On the contrary, 16-7N(G-K_3)-16 and 16-7N(G-K_7)-16 exhibited a packing parameter of 0.41 and 0.27, giving rise to truncated cone and cone-shaped molecules, respectively (Table 3.1). Such molecular shapes increase the preference for supramolecular assemblies with positive interfacial curvature. In fact, this was apparent in the SAXS data of the P/G/L lipoplexes where the H_{II} phase in 16-7N(G-K_3)-16 and 16-7N(G-K_7)-16 was only seen at a N/P ratio of 2.5. Conversely, 16-7N(G-K)-16 maintained the inverted hexagonal phase up to a N/P ratio of 5 (Figure 3.7A-C). Moreover, SAXS of the P/G of the lead compound 16-7N(G-K)-16 revealed the most prominent peak among all compounds suggesting a superior ability to form ordered structure even in the absence of the helper lipid, DOPE (Figure 3.6A-C). In addition, increasing the number of lysine moieties was associated with an increase in both the size and zeta potential which might hinder electrostatic attachment to the negatively charged cell surface and impede cellular uptake (Table 3.2). For example, D,L-lactide-coglycolide-based lipoplexes of 70 nm demonstrated a 27-fold higher transfection efficiency relative to larger-sized nanoparticles of 200 nm in COS-7 cells [45], indicating the importance of optimal particle size in the gene delivery process. As such, this could be, in part, the reasons for the higher transfection efficiency of 16-7N(G-K)-16 compared to 16-7N(G-K_3)-16 and 16-7N(G-K_7)-16 lipoplexes. Furthermore, 16-7N(G-K)-16 exhibited the lowest CMC value relative to 16-7N(G-K_3)-16 and 16-7N(G-K_7)-16 (Table 3.1), which could indicate a higher stability of the lipoplexes during the delivery process [34]. Higher charge density of compounds with tri- and hepta-lysine groups, 16-7N(G-K_3)-16 and 16-7N(G-K_7)-16, showed lower efficiency relative to 16-7N(G-K)-16. A high charge density

indicates a stronger interaction with the pDNA which hinder subsequent release, limiting nuclear localization of the genetic material [58].

The attachment of an hydrocarbon linker in compounds with the mono-lysine moiety led to a decrease in the level of secreted protein in both cell lines (Figure 3.8 and S2, Appendix II). In fact, a longer hydrophobic linker was associated with lower efficiency. For example, protein secretion of 16-7N(G-C_6-K)-16 and 16-7N(G-C_{11}-K)-16 based lipoplexes were 3-fold and 4-fold lower than the compound without the linker, respectively (Figure 3.8). This could be attributed to the higher hydrophobicity of compounds 16-7N(G-C_6-K)-16 and 16-7N(G-C_{11}-K)-16 relative to 16-7N(G-K)-16, resulting in stronger interaction with the pDNA which could hamper its subsequent release (Table 3.1). Manifestation of stronger pDNA-gemini surfactant interaction was also suggested by the smaller particle size of the lipoplexes formed with gemini surfactants with C6 and C11 linker (Table 3.2).

Unlike compounds with a mono lysine moiety, the incorporation of an hydrocarbon linker between the amino acids in compounds with tri-lysine residues resulted in an increase in their transfection efficiency (Figures 3.8 and S2, Appendix II). While the attachment of an hexyl linker (16-7N(G-C_6-K_3)-16) did not translate into significant elevation in the secreted protein in either cell lines, the addition of an undecyl linker (16-7N(G-C_{11}-K_3)-16) led to about 1.5-fold increase in the level of secreted INF-γ in PAM 212 and 2.3-fold in Cos-7 cell lines relative to compound 16-7N(G-K_3)-16 (Figures 3.8 and S2, Appendix II). The incorporation of the linker, especially the undecyl chain, gave rise to more hydrophobic compounds with lower CMC values which might confer a balanced binding with the plasmid DNA and better stability of the lipoplexes during the delivery process (Table 3.1). Although increasing the hydrophobicity in compounds with a mono-lysine moiety possibly hindered the release of the DNA, the higher

charge density of compounds with tri-lysine residues particularly upon acidification, might have balanced the DNA release process.

Eliminating the glycine moiety and connecting the hydrocarbon linker directly to the spacer as in compounds 16-7N(C_6-K_3)-16 and 16-7N(C_{11}-K_3)-16 did not cause any significant differences in the transfection efficiency compared to the corresponding analogues containing the glycine residues i.e., 16-7N(G-C_6-K_3)-16 and 16-7N(G-C_{11}-K_3)-16 in PAM 212 cell-line (Figure 3.8). However, it resulted in a decrease in the transfection efficiency in Cos-7 (Figure S2, Appendix II). Such a variation in the transfection efficiency was in agreement with the previously reported behaviour of mono- and di-amino acid-modified gemini surfactant. In particular, coupling lysine residue directly on the spacer in compound 12-7N(K)-12 reduced the transfection efficiency compared to the analogue containing the glycine moiety, 12-7N(G-K)-12, only in Cos-7 without showing any significant differences in PAM 212 cell-line [24].

In compounds with hepta-lysine moieties, incorporating the hydrocarbon linker resulted in significant increase in the transfection efficiency compared to compounds without the hydrocarbon linker in both cell-lines (Figures 3.8 and S2, Appendix II). While the addition of an hexyl linker increased the INF-γ secretion by 1.2-fold relative to 16-7N(G-K_7)-16, conjugating the undecyl linker resulted in 2.5-fold increase in the protein secretion (Figure 3.8). Similarly to compounds with tri-lysine groups, the addition of an hydrocarbon linker elevated the hydrophobicity ($_c$log P) and lowered CMC values (Table 3.1), contributing to balanced binding properties with the DNA.

3.4.4. Assessment of cell viability

The toxicity of the P/G/L nanoparticles prepared with peptide-modified gemini surfactants at N/P ratios of 2.5, 5 and 10 were evaluated in PAM 212 and COS-7 cell lines after 72 h and 48 h from the treatment, respectively (Figures 3.9 and S3, Appendix II). In both cell lines, P/G/Ls of the 16-7N(G-K)-16 exhibited the highest cell viability, 89% in PAM 212 and 83% in COS-7 cell line, demonstrating a 20% improvement in cell viability relative to first-generation unsubstituted gemini surfactants [14]. No significant differences were observed between the lead compounds at their optimal charge ratio (Figures 3.9 and S3, Appendix II). At the optimal ratio, P/G/Ls of all compounds showed a significantly lower toxicity compared to a commercially available transfection agent (approximately 50 % viability) in both PAM212 and Cos-7 cells [14, 25]. Increasing the N/P ratio in all compounds was accompanied by a dose-dependent cytotoxicity trend. However, the dose-dependent cytotoxicity was more prominent in m-7N(G-K_7)-m series (Figures 3.9 and S3, Appendix II). For example, increasing the N/P ratio from 2.5 to 10 in compound 16-7N(G-K_7)-16 resulted in about a 5-fold increase in the cytotoxicity (Figure 3.9). This could be attributed to their higher charge density caused by the high number of terminal amino groups that undergo protonation at the formulation intrinsic pH (≈ 6), leading to an increase in the overall positive charge of the lipoplexes as it was observed in the zeta potential measurements (Table 3.2). This was in agreement with a previously reported trend in literature where higher cationic charges were associated with higher tendency to rupture cell membrane, causing cell death [46].

The incorporation of the hydrophobic linkers, especially in compounds with tri- and hepta-lysine moieties, reduced the cytotoxicity of the lipoplexes. Such an increase in cell viability was more prominent upon the incorporation of the undecyl linker as in 16-7N(C_{11}-K_7)-

16 which has a cell viability of 62 % at an N/P ratio of 10 compared to the corresponding 15% for compound 16-7N(G-K_7)-16 (Figure 3.9). This supports our hypothesis that the hydrophobic linker in shielding the positive charges of the terminal lysine residues, which is also supported by the lower zeta potential of the lipoplexes (Table 3.2). On the other hand, the addition of the hydrophobic linker plays a role in compounds with mono-lysine residues caused an increase in the cytotoxicity. In particular, both compounds 16-7N(G-C_6-K)-16 and 16-7N(G-C_{11}-K)-16 showed a cell viability in the range of 75-78% while 16-7N(G-K)-16 exhibited cell viability of ≈ 89% (Figure 3.9). The addition of the hydrophobic linker in compounds with a mono-lysine moiety caused an unfavorable increase in their hydrophobicity, leading to a higher cytotoxicity [59].

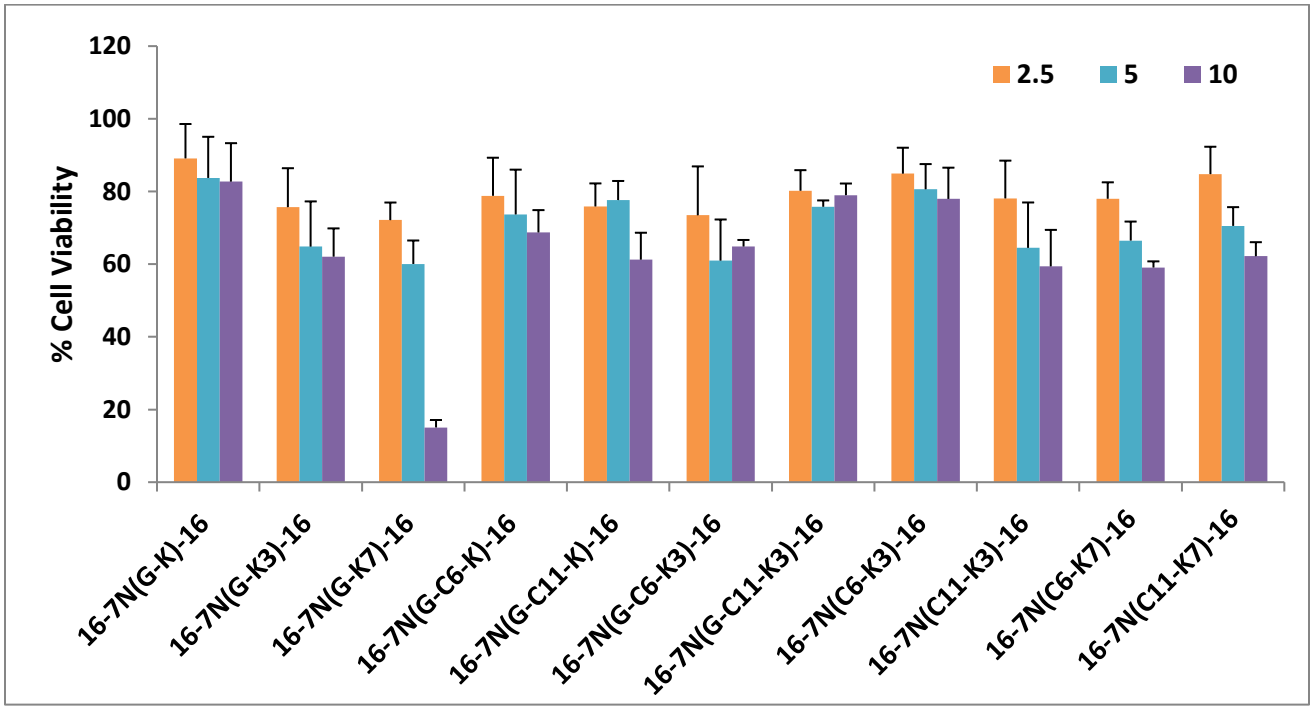

Figure 3.9. Evaluation of PAM 212 cell viability of the peptide-modified gemini surfactants at three N/P ratios. Results are the average of three plates of quadruplicate wells, error bars represent standard deviation.

3.5. Conclusions

In this work, a new series of peptide-modified gemini surfactants was introduced, reporting for the first time the design of dendrimers-like gemini surfactants. In addition, it evaluated the impact of incorporating a hydrocarbon linker of different length into the peptide chain. Our aim was to investigate the structure-activity relationship of the new compounds and identify the essential architectural requirements of efficient gene delivery system. The attachment of the peptide into the spacer region resulted in enhanced transfection efficiency and reduced cytotoxicity. In particular, lipoplexes composed of the lead compound, 16-7N(G-K)-16, demonstrated an 8-fold elevation in the level of protein secretion in PAM 212 and 20% increase in cell viability relative to the first-generation unsubstituted gemini surfactants. Such results suggest the potential of peptide-modified gemini surfactants as effective gene delivery systems for the treatment of fibrotic skin conditions. Further increase in the size of the incorporated peptide resulted in a decrease in the transfection efficiency. The impact of incorporating a hydrocarbon linker, on the other hand, was governed by the size of the peptide chain. In agreement with our recent report, peptide-modified gemini surfactants with hexadecyl alkyl tail exhibited the highest transfection efficiency compared to compounds with dodecyl and oleyl tails.

Assessment of physicochemical characteristics suggested that the molecular shape of the gemini surfactants plays an important role in determining the transfection efficiency of the compound. In particular, molecular shapes that support the formation of a negative interfacial curvature resulted in higher transfection efficiency due to the higher tendency to maintain the H_{II} assembly. Moreover, charge density of the gemini surfactants was associated with both transfection efficiency and cell viability wherein compounds with high charge density

demonstrated lower INF-γ secretion and higher cytotoxicity. Most importantly, a balance between the hydrophilic and hydrophobic characteristics of the gemini surfactants is an essential factor in determining the assembly, efficiency and safety profile of the peptide-modified gemini surfactants. Selected peptide-modified gemini surfactant-based gene delivery systems, including the lead compound will be further evaluated in animal models to assess the correlation between *in vitro* and *in vivo* gene delivery efficiency. The long-term goal is to develop a model that could be used to predict the *in vivo* efficiency of the gene delivery nanoparticles based on structural information.

3.6. Bibliography

1 Naldini L. Gene therapy returns to centre stage. Nature 2015; 526: 351-60.

2 Maeder ML, Gersbach CA. Genome-editing technologies for gene and cell therapy. Molecular Therapy 2016; 24: 430-46.

3 Ginn SL, Alexander IE, Edelstein ML, Abedi MR, Wixon J. Gene therapy clinical trials worldwide to 2012–an update. The journal of gene medicine 2013; 15: 65-77.

4 Oliveira C, Ribeiro AJ, Veiga F, Silveira I. Recent Advances in Nucleic Acid-Based Delivery: From Bench to Clinical Trials in Genetic Diseases. Journal of Biomedical Nanotechnology 2016; 12: 841-62.

5 Thomas CE, Ehrhardt A, Kay MA. Progress and problems with the use of viral vectors for gene therapy. Nature Reviews Genetics 2003; 4: 346-58.

6 Zhao Y, Huang L. Lipid nanoparticles for gene delivery. Advances in genetics 2014; 88: 13.

7 The Journal of Gene Medicine. Gene Therapy Clinical Trials Worldwide, <http://www.abedia.com/wiley/> Accesed January 2018.

8 Rosenzweig HS, Rakhmanova VA, MacDonald RC. Diquaternary ammonium compounds as transfection agents. Bioconjugate chemistry 2001; 12: 258-63.

9 Menger FM, Littau C. Gemini-surfactants: synthesis and properties. Journal of the American Chemical Society 1991; 113: 1451-2.

10 Ahmed T, Kamel AO, Wettig SD. Interactions between DNA and Gemini surfactant: impact on gene therapy: part I. Nanomedicine 2016; 11: 289-306.

11 Kumar V, Chatterjee A, Kumar N, Ganguly A, Chakraborty I, Banerjee M. d-Glucose derived novel gemini surfactants: synthesis and study of their surface properties, interaction with DNA, and cytotoxicity. Carbohydrate research 2014; 397: 37-45.

12 Biswas J, Mishra SK, Kondaiah P, Bhattacharya S. Syntheses, transfection efficacy and cell toxicity properties of novel cholesterol-based gemini lipids having hydroxyethyl head group. Organic & biomolecular chemistry 2011; 9: 4600-13.

13 Sharma VD, Lees J, Hoffman NE, Brailoiu E, Madesh M, Wunder SL, *et al*. Modulation of pyridinium cationic lipid–DNA complex properties by pyridinium gemini surfactants

and its impact on lipoplex transfection properties. Molecular pharmaceutics 2014; 11: 545-59.

14 Badea I, Verrall R, Baca-Estrada M, Tikoo S, Rosenberg A, Kumar P, *et al*. In vivo cutaneous interferon-γ gene delivery using novel dicationic (gemini) surfactant–plasmid complexes. The journal of gene medicine 2005; 7: 1200-14.

15 Badea I, Wettig S, Verrall R, Foldvari M. Topical non-invasive gene delivery using gemini nanoparticles in interferon-γ-deficient mice. European journal of pharmaceutics and biopharmaceutics 2007; 65: 414-22.

16 Badea I, Virtanen C, Verrall R, Rosenberg A, Foldvari M. Effect of topical interferon-γ gene therapy using gemini nanoparticles on pathophysiological markers of cutaneous scleroderma in Tsk/+ mice. Gene Therapy 2011; 19: 978-87.

17 Garcia MT, Kaczerewska O, Ribosa I, Brycki B, Materna P, Drgas M. Biodegradability and aquatic toxicity of quaternary ammonium-based gemini surfactants: Effect of the spacer on their ecological properties. Chemosphere 2016; 154: 155-60.

18 Pérez L, Pinazo A, Pons R, Infante M. Gemini surfactants from natural amino acids. Advances in colloid and interface science 2014; 205: 134-55.

19 Wasungu L, Scarzello M, van Dam G, Molema G, Wagenaar A, Engberts JB, *et al*. Transfection mediated by pH-sensitive sugar-based gemini surfactants; potential for in vivo gene therapy applications. Journal of molecular medicine 2006; 84: 774-84.

20 Scott E, Peter F, Sanders J. Biomass in the manufacture of industrial products—the use of proteins and amino acids. Applied microbiology and biotechnology 2007; 75: 751-62.

21 Pinazo A, Pons R, Pérez L, Infante MR. Amino acids as raw material for biocompatible surfactants. Industrial & Engineering Chemistry Research 2011; 50: 4805-17.

22 Wang F, Wang Y, Zhang X, Zhang W, Guo S, Jin F. Recent progress of cell-penetrating peptides as new carriers for intracellular cargo delivery. Journal of Controlled Release 2014; 174: 126-36.

23 Yang P, Singh J, Wettig S, Foldvari M, Verrall RE, Badea I. Enhanced gene expression in epithelial cells transfected with amino acid-substituted gemini nanoparticles. European Journal of Pharmaceutics and Biopharmaceutics 2010; 75: 311-20.

24 Singh J, Yang P, Michel D, E Verrall R, Foldvari M, Badea I. Amino Acid-Substituted Gemini Surfactant-Based Nanoparticles as Safe and Versatile Gene Delivery Agents. Current Drug Delivery 2011; 8: 299-306.

25 Al-Dulaymi MA, Chitanda JM, Mohammed-Saeid W, Araghi HY, Verrall RE, Grochulski P, *et al*. Di-Peptide-Modified Gemini Surfactants as Gene Delivery Vectors: Exploring the Role of the Alkyl Tail in Their Physicochemical Behavior and Biological Activity. The AAPS journal 2016; 18: 1168-81.

26 Singh J, Michel D, Getson HM, Chitanda JM, Verrall RE, Badea I. Development of amino acid substituted gemini surfactant-based mucoadhesive gene delivery systems for potential use as noninvasive vaginal genetic vaccination. Nanomedicine 2015; 10: 405-17.

27 Singh J, Michel D, Chitanda JM, Verrall RE, Badea I. Evaluation of cellular uptake and intracellular trafficking as determining factors of gene expression for amino acid-substituted gemini surfactant-based DNA nanoparticles. J Nanobiotechnology 2012; 10.

28 Foldvari M, Badea I, Wettig S, Verrall R, Bagonluri M. Structural characterization of novel gemini non-viral DNA delivery systems for cutaneous gene therapy. Journal of Experimental Nanoscience 2006; 1: 165-76.

29 Harkins WD, Jordan HF. A method for the determination of surface and interfacial tension from the maximum pull on a ring. Journal of the American Chemical Society 1930; 52: 1751-72.

30 Wettig S, Nowak P, Verrall R. Thermodynamic and aggregation properties of gemini surfactants with hydroxyl substituted spacers in aqueous solution. Langmuir 2002; 18: 5354-9.

31 Hanwell MD, Curtis DE, Lonie DC, Vandermeersch T, Zurek E, Hutchison GR. Avogadro: An advanced semantic chemical editor, visualization, and analysis platform. J. Cheminformatics 2012; 4: 17.

32 M. J. Frisch GWT, H. B. Schlegel, G. E., Scuseria MAR, J. R. Cheeseman, G. Scalmani, V. Barone, B. Mennucci,, G. A. Petersson HN, M. Caricato, X. Li, H. P. Hratchian,, A. F. Izmaylov JB, G. Zheng, J. L. Sonnenberg, M. Hada, M. Ehara,, K. Toyota RF, J. Hasegawa, M. Ishida, T. Nakajima, Y. Honda, O., Kitao HN, T. Vreven, J. A.

Montgomery, Jr., J. E. Peralta, F. Ogliaro,, *et al*. (Gaussian, Inc., Wallingford CT, 2013).

33 Advanced Chemistry Development I. ACD/Physchem Profiler 2016, <http://www.acdlabs.com/products/percepta/profilers.php> (2016).

34 Dauty E, Remy J-S, Blessing T, Behr J-P. Dimerizable cationic detergents with a low cmc condense plasmid DNA into nanometric particles and transfect cells in culture. Journal of the American Chemical Society 2001; 123: 9227-34.

35 Lombardo D, Kiselev MA, Magazù S, Calandra P. Amphiphiles self-assembly: basic concepts and future perspectives of supramolecular approaches. Advances in Condensed Matter Physics 2015; 2015.

36 Kopecky F, Fazekas T, Kopecka B, Kaclik P. Hydrophobicity and critical micelle concentration of some quaternary ammonium salts with one or two hydrophobic tails. Acta Fac Pharm 2007; 54: 84-94.

37 Buckingham SA, Garvey CJ, Warr GG. Effect of head-group size on micellization and phase behavior in quaternary ammonium surfactant systems. The Journal of Physical Chemistry 1993; 97: 10236-44.

38 Wang X, Wang J, Wang Y, Yan H, Li P, Thomas RK. Effect of the nature of the spacer on the aggregation properties of gemini surfactants in an aqueous solution. Langmuir 2004; 20: 53-6.

39 Smisterová J, Wagenaar A, Stuart MC, Polushkin E, ten Brinke G, Hulst R, *et al*. Molecular shape of the cationic lipid controls the structure of cationic lipid/dioleylphosphatidylethanolamine-DNA complexes and the efficiency of gene delivery. Journal of Biological Chemistry 2001; 276: 47615-22.

40 Israelachvili JN, Mitchell DJ, Ninham BW. Theory of self-assembly of hydrocarbon amphiphiles into micelles and bilayers. J. Chem. Soc., Faraday Trans. 2 1976; 72: 1525-68.

41 Kumar V. Complementary molecular shapes and additivity of the packing parameter of lipids. Proceedings of the National Academy of Sciences 1991; 88: 444-8.

42 Israelachvili JN. Special Interactions: Hydrogen-Bonding and Hydrophobic and Hydrophilic Interactions-8. 1992.

43 McIntosh TJ. Hydration properties of lamellar and non-lamellar phases of phosphatidylcholine and phosphatidylethanolamine. Chemistry and physics of lipids 1996; 81: 117-31.

44 Prabha S, Arya G, Chandra R, Ahmed B, Nimesh S. Effect of size on biological properties of nanoparticles employed in gene delivery. Artificial cells, nanomedicine, and biotechnology 2014: 1-9.

45 Prabha S, Zhou W-Z, Panyam J, Labhasetwar V. Size-dependency of nanoparticle-mediated gene transfection: studies with fractionated nanoparticles. International Journal of Pharmaceutics 2002; 244: 105-15.

46 Fröhlich E. The role of surface charge in cellular uptake and cytotoxicity of medical nanoparticles. International journal of nanomedicine 2012; 7: 5577.

47 Zhao Y, Piao Y, Zhang C, Jiang Y, Liu A, Cui S, *et al*. Replacement of quaternary ammonium headgroups by tri-ornithine in cationic lipids for the improvement of gene delivery in vitro and in vivo. Journal of Materials Chemistry B 2017; 5: 7963-73.

48 Sathyapriya R, Vishveshwara S. Interaction of DNA with clusters of amino acids in proteins. Nucleic acids research 2004; 32: 4109-18.

49 Dias R, Lindman B. DNA interactions with polymers and surfactants. (John Wiley & Sons, 2008).

50 Rosa M, Dias R, da Graça Miguel M, Lindman B. DNA− cationic surfactant interactions are different for double-and single-stranded DNA. Biomacromolecules 2005; 6: 2164-71.

51 Guillot-Nieckowski M, Joester D, Stöhr M, Losson M, Adrian M, Wagner B, *et al*. Self-assembly, DNA complexation, and pH response of amphiphilic dendrimers for gene transfection. Langmuir 2007; 23: 737-46.

52 Turner DC, Gruner SM. X-ray diffraction reconstruction of the inverted hexagonal (HII) phase in lipid-water systems. Biochemistry 1992; 31: 1340-55.

53 Rädler JO, Koltover I, Salditt T, Safinya CR. Structure of DNA-cationic liposome complexes: DNA intercalation in multilamellar membranes in distinct interhelical packing regimes. Science 1997; 275: 810-4.

54 Ma B, Zhang S, Jiang H, Zhao B, Lv H. Lipoplex morphologies and their influences on transfection efficiency in gene delivery. Journal of Controlled Release 2007; 123: 184-94.

55 Zidovska A, Evans HM, Ewert KK, Quispe J, Carragher B, Potter CS, *et al*. Liquid crystalline phases of dendritic lipid− DNA self-assemblies: lamellar, hexagonal, and DNA bundles. The Journal of Physical Chemistry B 2008; 113: 3694-703.

56 Fong C, Le T, Drummond CJ. Lyotropic liquid crystal engineering–ordered nanostructured small molecule amphiphile self-assembly materials by design. Chemical Society Reviews 2012; 41: 1297-322.

57 van't Hag L, Gras SL, Conn CE, Drummond CJ. Lyotropic liquid crystal engineering moving beyond binary compositional space–ordered nanostructured amphiphile self-assembly materials by design. Chemical Society Reviews 2017; 46: 2705-31.

58 Schaffer DV, Fidelman NA, Dan N, Lauffenburger DA. Vector unpacking as a potential barrier for receptor-mediated polyplex gene delivery. Biotechnology and bioengineering 2000; 67: 598-606.

59 Pinazo A, Petrizelli V, Bustelo M, Pons R, Vinardell M, Mitjans M, *et al*. New cationic vesicles prepared with double chain surfactants from arginine: Role of the hydrophobic group on the antimicrobial activity and cytotoxicity. Colloids and Surfaces B: Biointerfaces 2016; 141: 19-27.

CHAPTER 4

Tandem Mass Spectrometric Analysis of Novel Peptide-Modified Gemini Surfactants Used as Gene Delivery Vectors

Mays Al-Dulaymi [1], Anas El-Aneed [1*]

1. College of Pharmacy and Nutrition, University of Saskatchewan, Saskatoon, SK, Canada.

---

*This chapter is published in Journal of Mass Spectrometry, 2017, 52 (6):353–366.

Transitioning rationale:

The importance of structural modifications of the gene delivery vectors in enhancing their transfection efficiency and safety profile was established in the previous chapters (Chapters 2 and 3). The behavior of gemini surfactants in complex biological systems may ultimately determine their performance and the cytotoxicity. Accordingly, correlating the biodistribution and biological fate of the gemini surfactants to their chemical structure and physicochemical properties could provide insights into the rational design process, bridging the gap between empirical and rational design. As such, there is a need for an analytical approach to identify and quantify gemini surfactants in complex biological samples. Mass spectrometry (MS) was selected as the analytical technique of choice. This chapter aims at elucidating the tandem mass spectrometric (MS/MS) dissociation behaviour of peptides-modified gemini surfactants introduced in Chapter 3. The data from this study will be used for developing multiple reaction monitoring (MRM) quantification methods to probe the fate and the biodistribution of topically applied therapeutic gemini surfactant formulations (Chapter 5).

Contribution statement:

Mays Al-Dulaymi contributed to this manuscript by designing the study, performing experiments, data acquisition, data analysis and manuscript writing.

4.1. Abstract

Diquaternary ammonium gemini Surfactants have emerged as effective gene delivery vectors. A novel series of eleven peptide-modified compounds was synthesized, showing promising results in delivering genetic materials. The purpose of this work is to elucidate the tandem mass spectrometric (MS/MS) dissociation behaviour of these novel molecules establishing a generalized MS/MS fingerprint.

Exact mass measurements were achieved using a hybrid quadrupole orthogonal time-of-flight mass spectrometer (QqToF-MS) and a multi-stage tandem mass spectrometric analysis was conducted using a triple quadrupole-linear ion trap mass spectrometer (QqQLIT-MS). Both instruments were operated in the positive ionization mode and are equipped with electrospray ionization (ESI). Abundant triply charged $[M+H]^{3+}$ species were observed in the single stage analysis of all the evaluated compounds with mass accuracies of less than 8 ppm in mass error. MS/MS analysis showed that the evaluated gemini surfactants exhibited peptide-related dissociation characteristics due to the presence of amino acids within the compounds' spacer region. In particular, diagnostic product ions were originated from the neutral loss of ammonia from the amino acids' side chain resulting in the formation of pipecolic acid at the N-terminus part of the gemini surfactants. In addition, a charge directed amide bond cleavage was initiated by the amino acids' side chain producing a protonated α-amino-ε-caprolactam ion and its complimentary c-terminus ion that contains quaternary amines. MS/MS and MS^3 analysis revealed common fragmentation behaviour among all tested compounds, resulting in the production of a universal MS/MS fragmentation pathway.

4.2. Introduction

Gene therapy has emerged as a promising therapeutic approach for the treatment of inherited and acquired genetic disorders. The last few decades have witnessed unprecedented interest in developing efficient vectors able to compact, protect and deliver genetic material into targeted cells [1, 2]. One particular group is diquaternary ammonium gemini surfactants that have been extensively used as non-viral gene delivery vectors [3]. They have the ability to package and compact the negatively charged nucleic acids through electrostatic and hydrophobic interactions forming nano-sized lipoplexes [4]. Gemini surfactants are composed of two ionic head groups attached to their hydrocarbon tails and connected by a spacer (Figure 4.1A) [5]. The unique structure of gemini surfactants resulted in superior characteristics compared to their monomeric counterparts, such as their greater ability in reducing surface tension, lower critical micelle concentration (CMC) and lower Krafft temperature (critical micelle temperature) [6]. Owing to these enhanced characteristics, lower concentration of gemini surfactants is required for gene delivery compared to their monomeric counterparts, thus, they possess lower cytotoxicity profile [4]. In addition, gemini surfactants' distinctive structure offers virtually various possibilities for structural modification, allowing for the production of compounds specifically designed to overcome delivery barriers. For example, the insertion of pH-sensitive moieties resulted in the production of "intelligent" delivery vehicles that respond to the surrounding stimuli [7].

The most widely used group of gemini surfactants is the cationic N, N-bis(dimethylalkyl)-α,ω-alkane-diammonium surfactants (Figure 4.1). They were successfully utilized in delivering genetic materials both *in vitro* and *in vivo* [8, 9]. In fact, Badea *et al.* reported three-fold increase in topical transgene expression in animals treated with N,N'-bis(dimethylhexadecyl)-1,3-propanediammonium dibromide (designated as 16-3-16) gemini

surfactant-based nanoparticles compared to animals treated with naked DNA [9]. Despite the success of the traditional gemini surfactants, concerns regarding their toxicity have arisen [10]. Several approaches have been undertaken to address this problem, including the insertion of biocompatible and biodegradable moieties such as sugars, lipids, and amino acids [11-13]. For example, glycyl-lysine substituted gemini surfactants exhibited significantly higher gene expression *in vitro* and lower cytotoxicity compared to the unsubstituted parent compound [14-16]. Moreover, *in vivo* topical application of the glycyl-lysine substituted gemini surfactant-based lipoplexes into the rabbit vaginal cavities demonstrated higher transgene efficiency compared to the parent compound without visible toxicity [17].

Although extensive research was focused on the design of new gemini surfactants and optimizing their physicochemical properties to increase efficiency and reduce side effects [3, 16, 18], little is known about their post transfection fate. Many questions remain unanswered regarding the degradation profile of nanoparticles after releasing their therapeutic cargo including the formation of metabolic by-products, some of which can theoretically be toxic. Correlating the biodistribution and the biological fate of the nanoparticles to their chemical structure and physicochemical properties can provide insights into the rational design process to produce gene carriers with higher efficiency and reduced toxicity. Such knowledge will bridge the gap between empirical and rational design. As such, there is a need to develop analytical techniques that could identify and quantify gemini surfactants within complex biological samples.

Mass spectrometry (MS) is routinely used for both the quantitative and qualitative analysis of pharmaceuticals [19-22]. In our group, we investigated the fragmentation pathways of different structural families of gemini surfactants establishing collision induced dissociation-

tandem mass spectrometric (CID-MS/MS) fingerprints for accurate identification of gemini surfactants [23-26]. This data was subsequently utilized to develop MS-based methods for the quantification of conventional un-substituted gemini surfactants within cells to determine the rate of cellular uptake and removal [27-29]. Ongoing research, employs the use of these methods to investigate subcellular localization and to identify any potential metabolites.

Recently, a new generation of peptide modified gemini surfactants was introduced demonstrating a superior *in vitro* transfection efficiency compared to the traditional unsubstituted gemini surfactants (Figure 4.1B) [30]. Herein, we aim to evaluate the CID-MS/MS fragmentation behaviour of eleven novel peptide modified gemini surfactants. The peptides are attached to the spacer region via an amide bond with variable hydrocarbon linkages that may affect the efficiency of the developed nano-formulations. The data from this study will be needed for developing multiple reaction monitoring (MRM) quantification MS/MS methods to probe the fate and the biodistribution of topically applied therapeutic gemini surfactant formulations.

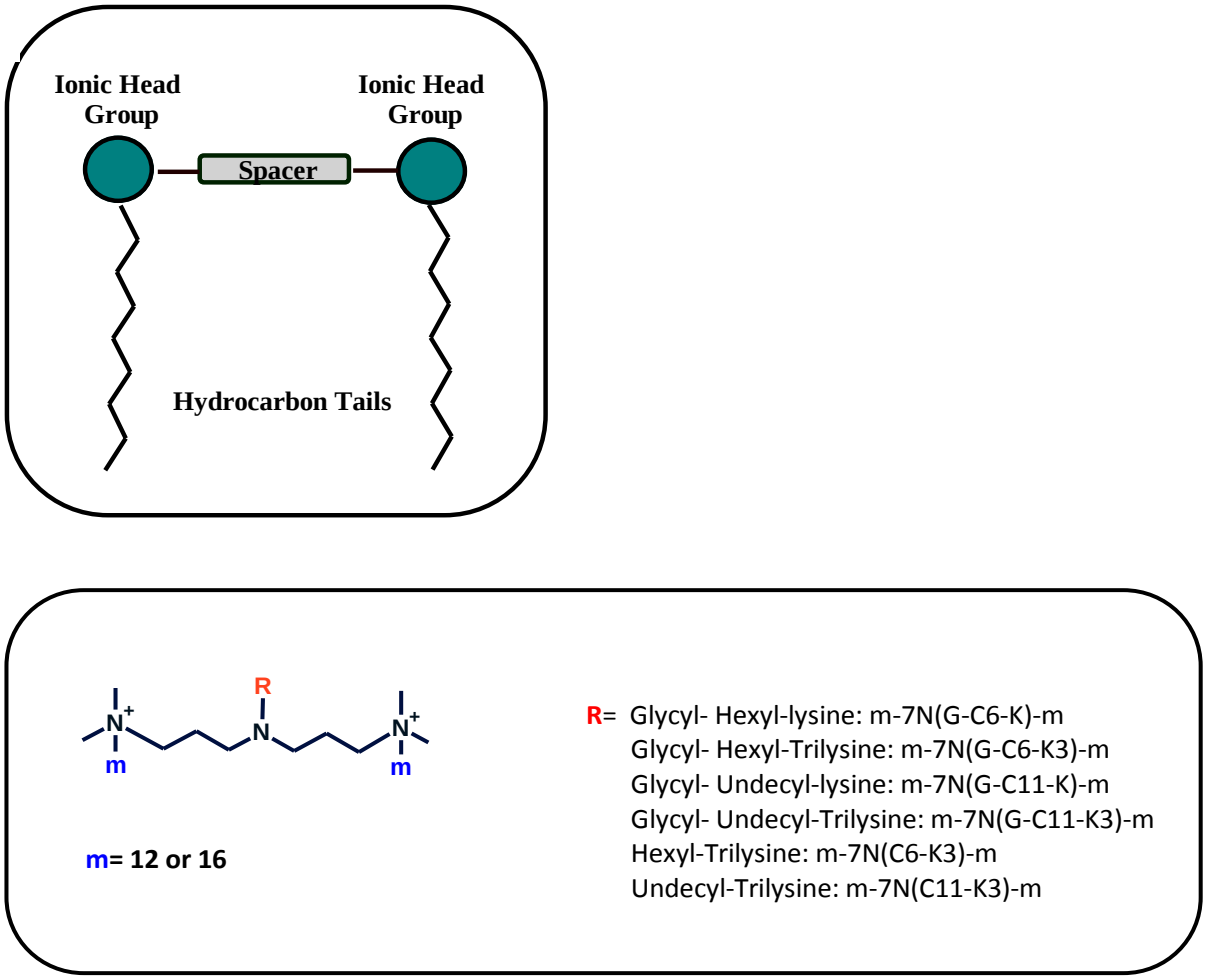

Figure 4.1. (A) Prototype of gemini surfactants showing the two ionic head groups, hydrocarbon tails and the spacer and (B) schematic representation of the general structure of the tested peptide modified gemini surfactants.

4.3. Material and methods

4.3.1. Material

Eleven novel peptide modified gemini surfactants were synthesized using previously reported synthetic methods [16]. Tested compounds were designated as m-7N(R)-m where m is the alkyl tail carbon chain length, m = 12 or 16 and R is a chain of hydrocarbon linkers attached to amino acids: R = Glycyl-Hexyl-lysine, Glycyl-Hexyl-Trilysine, Glycyl-Undecyl-lysine, Glycyl-Undecyl-Trilysine, Hexyl-Trilysine and Undecyl-Trilysine. The general chemical structure of these gemini surfactants is shown in Figure 4.1B. Methanol (HPLC grade purity, Fisher Scientific, Nepean, ON, Canada), Water (HPLC grade purity, Fisher Scientific, Nepean, ON, Canada), and formic acid (purity 90%, EMD Chemicals Inc., Merck KGaA, Darmstadt, Germany) were used as solvents.

4.3.2. Sample preparation

Stock solutions of 3 mM gemini surfactant were prepared in methanol/water (50:50 v: v) containing 0.1% formic acid and stored at −20 ◦C. Each sample was further diluted 1000 X at the time of analysis using the same solvent.

4.3.3. Mass spectrometric analysis

4.3.3.1.Single stage MS analysis

Gemini surfactants were analyzed using an AB SCIEX QSTAR® XL quadrupole orthogonal time of-flight hybrid mass spectrometer (QqToF-MS) equipped with an electrospray ionization (ESI) source (AB SCIEX, Redwood City, CA, USA). The instrument was operated in the positive ion mode with declustering potential of 100 V and focusing potential of 290 V. Sample aliquots were infused into the mass spectrometer at flow rate of 10 μL/min using an

integrated Harvard syringe pump through a Turbo Ionspray Source, having a needle voltage of 5500 V and a temperature of 80 °C. Nitrogen was used as the drying gas and ESI nebulizing gas. A two-point external calibration was performed prior to the analysis of gemini surfactants using two singly charged calibration standards: cesium iodide (CsI, *m/z* 132.9055, Sigma-Aldrich, Oakville, ON, Canada) and sex pheromone inhibitor (iPD1, *m/z* 829.5320, Bachem Bioscience Inc., PA, USA).

4.3.3.2.*Tandem mass spectrometric analysis*

Tandem mass spectrometric analysis of the tested gemini surfactants was performed using an AB SCIEX QTRAP® 4000 hybrid triple quadrupole–linear ion trap mass spectrometer (QqLIT-MS) equipped with a "Turbo V Ion Spray" ESI source (AB SCIEX, Redwood City, CA, USA). Collision-induced dissociation (CID) was conducted using nitrogen as the collision gas. The instrument was operated in the positive ion mode with declustering potential in the range of 45–100 (optimized for each compound). Collision energy (CE) was also optimized for the range 20–40 eV to induce fragmentation while maintaining the abundance of the precursor ion. Samples were infused into the instrument at flow rate of 10 μL/min by using a model 11 Plus syringe pump (Harvard Apparatus, Holliston, MA, USA). Ionspray voltage was set at 5500 V with source temperature of 300°C.

It is noteworthy that the MS/MS analysis of the all tested peptide-modified gemini surfactants was also conducted using the QSTAR®. It generated similar MS/MS spectra to that produced by the QTRAP®, confirming the elemental compositions of the projected product ions (Figure S1, Supplementary Material). However, MS/MS spectra acquired by the QTRAP® were

more informative due to the ability of the linear ion trap to accumulate ions when performing the enhanced product ion scan.

4.3.3.3.Multi-stage MS^3 analysis

MS^3 analysis of the selected second-generation ions was conducted on the AB SCIEX QTRAP® 4000 instrument under the same optimized conditions mentioned above. Excitation energy (AF2) was set at the range of 20–100 to obtain abundant fragments of the selected second-generation ions.

4.4. Results and discussion

4.4.1. Single-stage MS analysis

Full scan ESI-QqToF-MS analysis of all tested peptide-modified gemini surfactants showed an abundant triply charged $[M+H]^{3+}$ species (Table S1, Appendix III). In addition, some compounds with three terminal residues of amino acids showed a minor quadruply charged $[M+2H]^{4+}$ species. The exact masses were assessed showing mass accuracies of less than 8 parts per million (ppm) mass error confirming the projected molecular structure of the tested gemini surfactants (Table S1, Appendix III). This mass accuracy was achieved by employing two-point external calibration prior to the analysis of the gemini surfactants. In fact, the accuracy of these measurements was similar to a recent work by our group which utilized internal calibration to assess mono-amino acid and di-amino acids substituted gemini surfactants [25].

4.4.2. Tandem mass spectrometric analysis

The fragmentation behavior of peptide modified gemini surfactants was evaluated using low-energy CID-MS/MS employing ESI-QqLIT-MS instrument. Structural variation within the tested gemini surfactants, namely the number of amino acid residues, the length of the hydrocarbon tails and the length of the incorporated hydrocarbon linker drove the MS/MS dissociation behavior. In addition, MS/MS experiments yielded compound-specific product ions which authenticate the molecular structure of their precursor ions. Such product ions could be utilized as diagnostic ions for the qualitative and quantitative analysis of the evaluated gemini surfactants.

The MS/MS fragmentation behavior of peptide modified gemini surfactants showed remarkable differences compared to traditional gemini surfactants [23, 24]. This is mainly due to

the insertion of peptide segments within the gemini surfactant spacer region, resulting in the formation of peptide-related dissociation characteristics. The number of terminal amino acid residues in the spacer seems to play a major role in determining the MS/MS fragmentation pattern; hence, MS/MS analysis will be discussed based on the number of terminal amino acids residues. The following sections include detailed discussion of the fragmentation patterns of the 16-7N(C_{11}-K_3)-16 gemini surfactant as an illustrative example of compounds with the tri-terminal amino acids residues as it has the most complex MS/MS spectra among all tested compounds. In addition, the MS/MS dissociation behaviour of 16-7N(G-C_{11}-K)-16 is briefly discussed to highlight the fragmentation of gemini surfactants with a mono-terminal amino acid moiety. The major product ions for peptide modified gemini surfactants with tri-terminal amino acids residues and mono-terminal amino acid moiety are displayed in Tables 4.1 and 4.2 respectively.

4.4.2.1. MS/MS fragmentation pathway of the peptide modified gemini surfactants with tri-terminal lysine moieties

The fragmentation of the triply charged precursor ion of 16-7N(C11-K3)-16 gemini surfactant resulted in the formation of three initial diagnostic product ions that have their unique subsequent dissociation pathways (Figure 4.2, Table 4.1). Two initial product ions arise from the loss of one of the terminal lysine moieties producing either a doubly charged product ion (A) observed at *m/z* 538.54 or a triply charged product ion (B) observed at *m/z* 359.36. The third initial product ion results from the loss of a NH_3 moiety generating a triply charged product ion (C) observed at *m/z* 396.38. The coexistence of the three initial product ions suggests a competition between different fragmentation mechanisms. While both ions (A) and (B) are formed by losing one of the terminal lysine residues from the precursor ion, they have different

charge status implying the presence of different fragmentation mechanism for cleaving the amide bond.

As indicated earlier, the presence of peptides within the gemini surfactants offered the compound protonated peptide characteristics, unlike conventional gemini surfactants [23, 24]. The dissociation of protonated peptides can be explained by the 'mobile proton' model: a comprehensive model that suggests a competition between charge-remote and charge-directed reactions to predict the fragmentation process [31-33]. Under low-energy conditions such as CID, charge-directed reactions are believed to be the major pathway for peptide dissociation in which bond cleavage is initiated by active involvement of the ionizing proton [34]. Thus, the location of the ionizing proton on the peptide chain could determine the fragmentation mechanism [33]. As such, the composition of the amino acids (the presence or absence of a basic residue), the sequence, size and charge state of the investigated peptide will play a crucial role in determining the MS/MS fragmentation pattern.

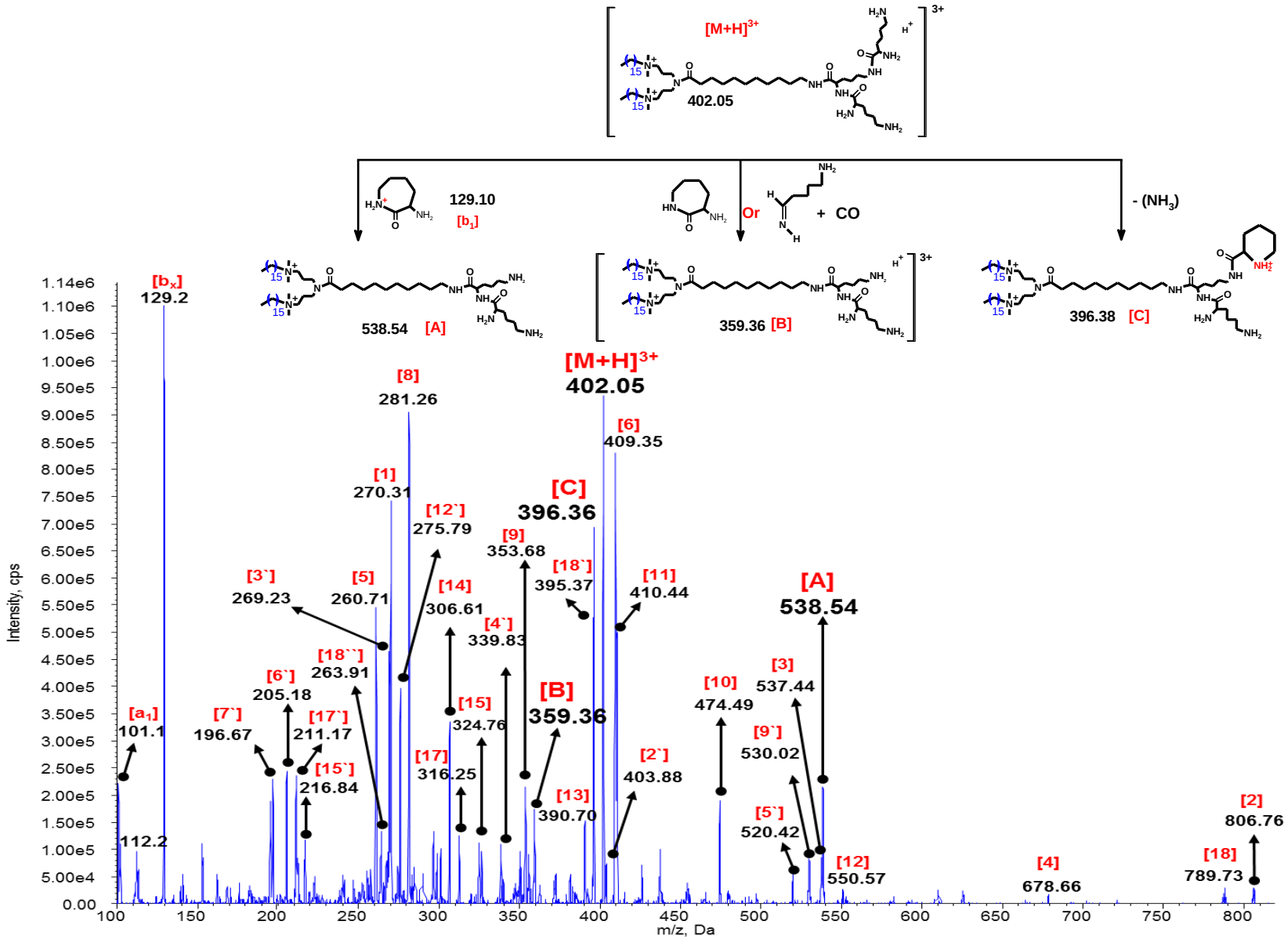

Figure 4.2. The ESI-QqLIT-MS/MS spectrum of 16-7N(C_{11}-K_3)-16 as a representative example of gemini surfactants with tri-terminal lysine moieties. Ions were labelled as designated in Figures 5-7. Strcture of the three initial product ions are shown as an insert (top).

Table 4.1. Product ions observed during MS/MS analysis of $[M+H]^{3+}$ ions of the peptide modified gemini surfactants with tri-terminal lysine moieties.

	Gemini surfactants	**12-7N(G-C_{11}-K_3)-12**	**16-7N(G-C_{11}-K_3)-16**	**12-7N(G-C_6-K_3)-12**	**16-7N(G-C_6-K_3)-16**	**12-7N(C_{11}-K_3)-12**	**16-7N(C_{11}-K_3)-16**	**12-7N(C_6-K_3)-12**	**16-7N(C_6-K_3)-16**
Ion #	**Product ions**	***m/z***	***m/z***	***m/z***	***m/z***	***m/z***	***m/z***	***m/z***	***m/z***
A	**$[M–C_6H_{13}N_2O]^{2+}$**	510.98	567.04	475.94	532.37	482.47	538.54	447.43	503.50
B (y_2)	**$[M–C_6H_{12}N_2O]^{3+}$**	340.99	378.37			321.98	359.36		
C	**$[M–NH_3]^{3+}$**	378.01	415.39	354.65	392.03	359.01	396.38	335.65	373.02
b_x	**$C_6H_{13}N_2O$**	129.10	129.10	129.10	129.10	129.10	129.10	129.10	129.10
a_1	**$C_5H_{13}N_2$**	101.10	101.10			101.10	101.10		
1	**Dimethylalkenaminium**	214.25	270.31	214.25	270.31	214.25	270.31	214.25	270.31
2	**$[M–(b_x)\text{-ion}(1)]^{2+}$**	404.36	432.39	369.32	397.35	375.85	403.88	340.81	368.84
2`	**$[M–(b_x)\text{-ion}(1)]^{+}$**	807.71	863.78	737.63	793.70	750.69	806.76	680.62	736.68
3	**$[M–(b_x)\text{-2 ion}(1)]^{+}$**	594.47	594.47	524.40	524.40	537.44	537.44	467.37	467.37
3`	**$[M–(b_x)\text{-2 ion}(1)]^{2+}$**	297.74	297.74	262.70	262.70	269.23	269.23	234.19	234.19
4	**$[M– 2(b_x)\text{-ion}(1)]^{+}$**	679.62	735.68	609.54	665.59	622.60	678.66	552.52	608.58
4`	**$[M– 2(b_x)\text{-ion}(1)]^{2+}$**	340.31	368.19	305.27	333.30	311.80	339.83	276.76	304.80
5	**$[M–(b_x)\text{-}(NH_3)\text{-2 ion}(1)]^{+}$**	577.44	577.44	507.36	507.36	520.42	520.42	450.34	450.34
5`	**$[M–(b_x)\text{-}(NH_3)\text{-2 ion}(1)]^{2+}$**	289.22	289.22	254.18	254.18	260.71	260.71	225.67	225.67
6	**$[M– 2(b_x)\text{-2 ion}(1)]^{+}$**	446.94	446.94	396.30	396.30	409.35	409.35	339.27	339.27
6`	**$[M– 2(b_x)\text{- 2 ion}(1)]^{2+}$**	233.69	233.69			205.18	205.18		

7	**[M–2(b_x)-(NH_3)-2ion(1)]** $^{2+}$	225.18	225.18	190.14	190.14	196.67	196.67	161.63	161.63
8	**[M–3(b_x)- 2 ion(1)]** $^{+}$	338.27	338.27	268.19	268.19	281.26	281.26	211.18	211.18
9	**[M–(b_x)-(NH3)]** $^{3+}$	335.31	372.69	311.96	349.33	316.31	353.68	292.95	330.32
9`	**[M–(b_x)-(NH3)]** $^{2+}$	502.47	558.53	467.43	523.49	473.96	530.02	438.92	494.98
10	**[M–2(b_x)]** $^{2+}$	446.94	503.00	411.90	467.96	418.43	474.49	383.39	439.45
11	**[M–3(b_x)]** $^{2+}$	382.89	438.95	347.85	403.91	354.38	410.44	319.34	375.40
12	**[M–3(b_x)- ion(1)]** $^{+}$	551.52	607.59	481.44	537.51	494.50	550.57	424.43	480.49
12`	**[M–3(b_x)- ion(1)]** $^{2+}$	276.27	304.30	241.23	269.26	247.75	275.79	212.71	240.75
13	**[M–2(NH_3)]** $^{3+}$	372.34	409.71	348.97	386.62	353.33	390.70	329.97	367.35
14	**[M–(NH_3)-ion(1)]** $^{3+}$	306.93	325.62	283.57	302.26	287.92	306.61	264.57	283.25
15	**[M–(NH_3)-2 ion(1)]**$^{2+}$	353.27	353.27	318.23	318.23	324.76	324.76	289.723	289.72
15`	**[M–(NH_3)-2 ion(1)]** $^{3+}$	235.85	235.85	212.49	212.49	216.84	216.84	193.48	193.48
16	**[M–2(NH_3)-ion(1)]** $^{3+}$	301.26	319.94	277.90	296.58	282.25	300.94	258.89	277.58
17	**[M–2(NH_3)-2 ion(1)]** $^{2+}$	344.76	344.76	309.72	309.72	316.25	316.25	281.21	281.21
17`	**[M–2(NH_3)-2 ion(1)]** $^{3+}$	230.17	230.17	206.82	206.82	211.17	211.17	187.81	187.81
18	**[M–(b_x)-(NH3)- ion(1)]** $^{+}$	790.69	846.75	720.61	776.67	733.67	789.73	663.59	719.65
18`	**[M–(b_x)-(NH3)- ion(1)]** $^{2+}$	395.85	423.87	360.81	388.84	367.33	395.37	332.30	360.33
18``	**[M–(b_x)-(NH3)- ion(1)]** $^{3+}$	264.23	282.92	240.87	259.56	245.23	263.91	221.87	240.55

The gemini surfactant 16-7N(C11-K3)-16 has a chain of three branched lysine moieties. Lysine is a basic amino acid that is most probably protonated at the ε-amino group of the side chain. Amide bond cleavage is initiated by nucleophilic attack by the lysine side chain on the amide bond [35, 36]. The first step of the reaction involves mobilization of the proton of the lysine side chain to the nitrogen of the C-terminal neighboring amide bond (Figure 4.3). Subsequently, nucleophilic attack by the lysine side chain on the carbon of the protonated amide bond leading to the cleavage of the amide bond and the formation of a protonated α-amino-ε-caprolactam ion observed at *m/z* 129.10 (b_1) (Figure 4.3). A complementary ion at *m/z* 538.5 (product ion A) is formed rather than a neutral species as in the case of peptides due to the presence of quaternary amines that exist within the structure of gemini surfactants (Figure 4.1B, Figure 4.3).

In fact, the formation of the product ion at *m/z* 129.10 is a characteristic of lysine containing peptides [35-37]. The loss of lysine through this mechanism explains the formation of product ion (A) the doubly charge compound, however, it does not explain the formation of product ion (B), the triply charged species of the same structure (Figure 4.2), suggesting the presence of alternative MS/MS dissociation mechanism.

Two mechanisms can be proposed for the formation of the product ion (B) observed at *m/z* 359.36. The first could be explained by the established fragmentation mechanism termed (a_x - y_x) which leads to integrated formation of a_x and y_x ions [38, 39]. This dissociation is focused on the cleavage of the amide bond and Cα –C_{amide} bond resulting in the formation of protonated imine, carbon monoxide and product ion B (i.e., protonated C-terminal fragment) (Figure 4.4) [38]. Following the expulsion of the weakly bound carbon monoxide, a proton-bound dimer between the N terminal and the C-terminal fragments is formed. Under low-energy CID conditions, the formed dimer has a long lifetime allowing for numerous proton transfers among

product ions to occur. As a result, the dimer is dissociated to form either product ion B (i.e., the y_2 ion based on Roepstorff nomenclature for peptide fragmentation[40]) or ion a_1 which is observed at *m/z* 101.10 (Figure 4.4). It should be noted that ions B and a_1 were only observed in gemini surfactants with longer hydrophobic linker chain (C_{11}) and not in shorter linker (C_6) (Table 4.1). This is in agreement with previously reported behavior of mono and di- amino acid substituted gemini surfactants in which no ion B analogues was observed [25].

Alternative mechanism that could lead to the formation of product ion (B) is simply the same as that of product ion (A) (Figure 4.3), however; a proton transfer from the amide-nitrogen of the protonated α-amino-ε-caprolactam to the ε-amino group of the remaining lysine (c-terminus) is required. Csonka *et al.* indicated the possibility of such a dissociation to occur especially when the c-terminal part of the compound has high enough proton affinity to compete with the α-amino-ε-caprolactam [36]. In the tested compound, the ε-amino group of the c-terminal has a higher *pKa* value than the amide-nitrogen, thus it has higher proton affinity raising the possibility for the ion transfer to take place. As such, it is possible that two mechanisms are simultaneously involved in the formation of product ion (B).

In addition to product ions A and B, Product ion (C) at *m/z* 396.38 results from the neutral loss of a (NH_3) moiety (Figure S1, Appendix III; Figure 4.2). This is expected as protonated peptides under low-energy CID conditions often undergo neutral losses of small molecules such as water or ammonia [34]. The loss of ammonia has been reported mainly in basic amino acid residues such as lysine, arginine, asparagine and glutamine [34]. A charge-directed fragmentation mechanism has been proposed for the elimination of ammonia from the lysine side chain [35]. As such, protonation of the side chain is required. Since ε-amino group is the most favored protonation site in lysine, mobilization of protons is not needed. Dookeran *et al.*

demonstrated utilizing an α-^{15}N protonated lysine that the loss of the NH_3 moiety involves in particular the nitrogen of the side chain [37]. When lysine is located at the peptide N-terminus, like in the tested gemini surfactants, the loss of ammonia occurs via nucleophilic attack by the N-terminal amino group resulting in the formation of pipecolic acid (Figure S2, Appendix III) [36]. It is noteworthy that the proposed fragmentation pathways forming the three initial product ions could involve either one of the two N-terminal lysine moieties, leading to identical product ions. In fact, the various observed ions could be a mixture of two species losing either lysine moiety terminal. Both losses will not affect the produced product ions that can still efficiently be used for both qualitative and quantitative applications.

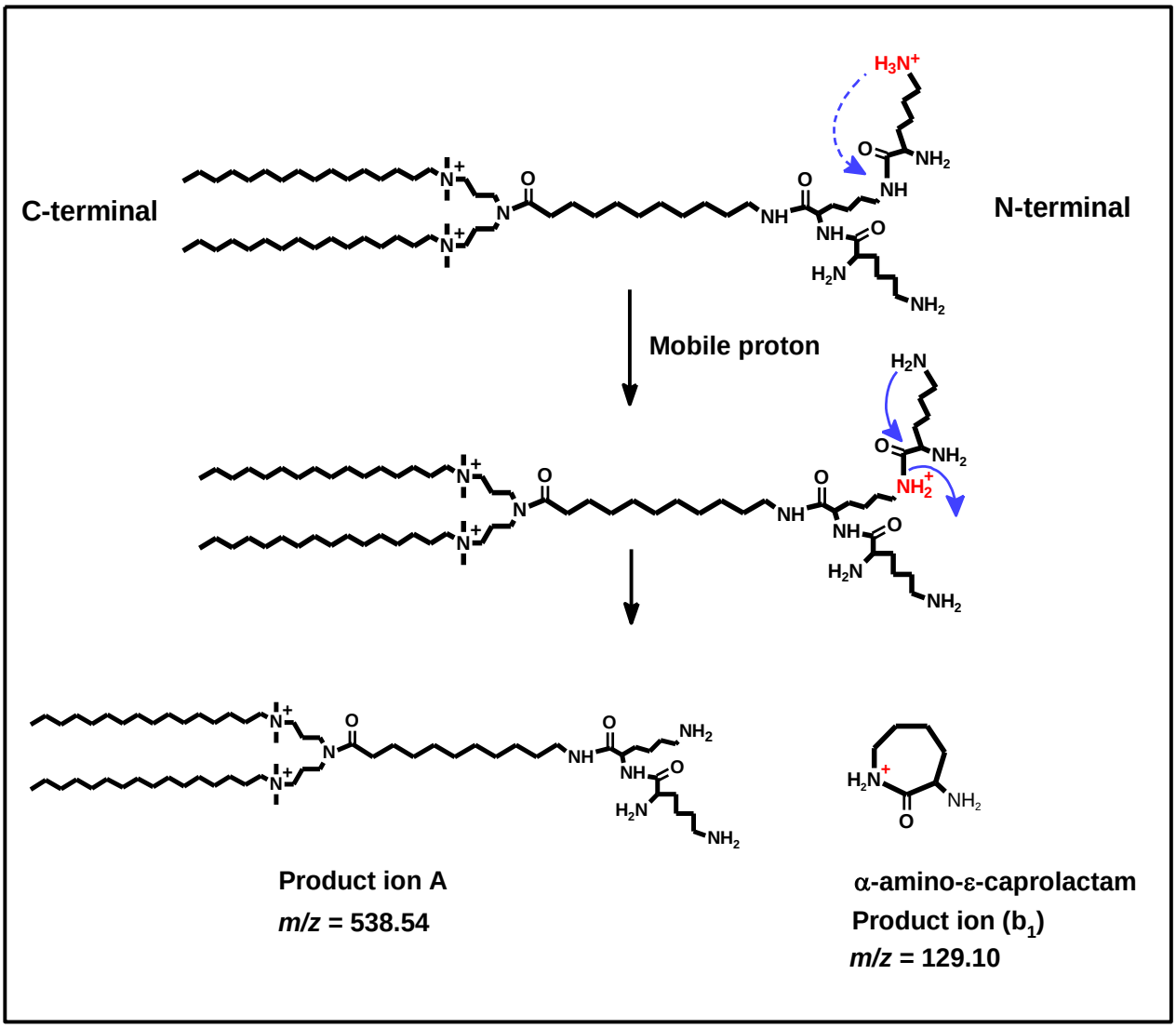

Figure 4.3. The proposed mechanism for the formation of product ion (A) and (b_1): amide bond cleavage initiated by lysine side chain. Dotted arrow indicates a mobile proton.

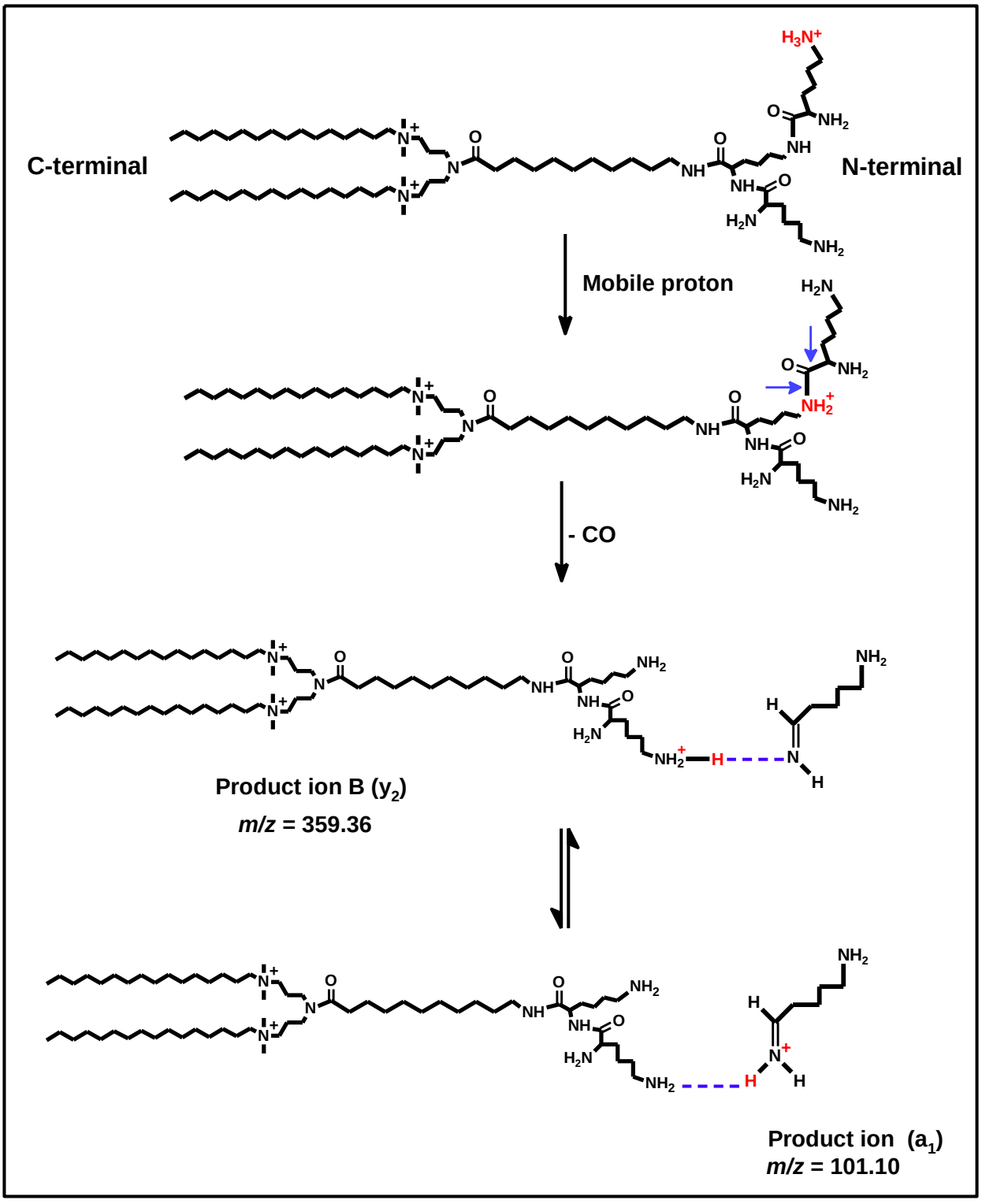

Figure 4.4. The proposed mechanism for the formation of product ion (B) and (a_1): cleavage of Cα –C $_{amide}$ bond through a_x - y_x fragmentation pathway.

Dissociation of product ion A

The dissociation of product ion (A) starts with the loss of the quaternary ammonium head group and the attached aliphatic tail resulting in the formation of two complementary ions: product ion (1) at *m/z* 270.31 a singly charged ion and a minor singly charged product ion (2) observed at *m/z* 806.76 (Figure 4.5, Table 4.1). In addition, a doubly charged species was observed at *m/z* 403.88 (2`) which shares the same molecular structure of product ion (2) albeit doubly charged. This suggests the existence of an alternative ion formation mechanism. It could be explained by a homolytic cleavage of the N-C bond between the quaternary ammonium head group and the hydrocarbon tail resulting in the neutral loss of the aliphatic tail (hexadec-1-ene) and the formation of a doubly charged minor product ion at *m/z* 426.41(2*) (Figure 4.5). In agreement with the previously observed behavior of mono and di- amino acid substituted gemini surfactants [25], the close proximity of the two positively charged head groups of ions such as (2*) could make the ion relatively unstable which easily fragments by the subsequent loss of a head group as dimethylamine leading to the formation of (2`) ion at *m/z* 403.88. Such a behavior was consistent among all the evaluated gemini surfactants. In fact, in some cases the intermediate ion (i.e., 2*) was abundant enough to enable for MS^3 analysis that supported the projected molecular structure of this ion (2*) (Table S2, Appendix III). The formation of such unstable intermediate ions and their subsequent stable product ions (i.e., ion 2` in this case) was commonly noticeable in the various tested gemini surfactants. It will be referenced frequently in the text as an intermediate ion.

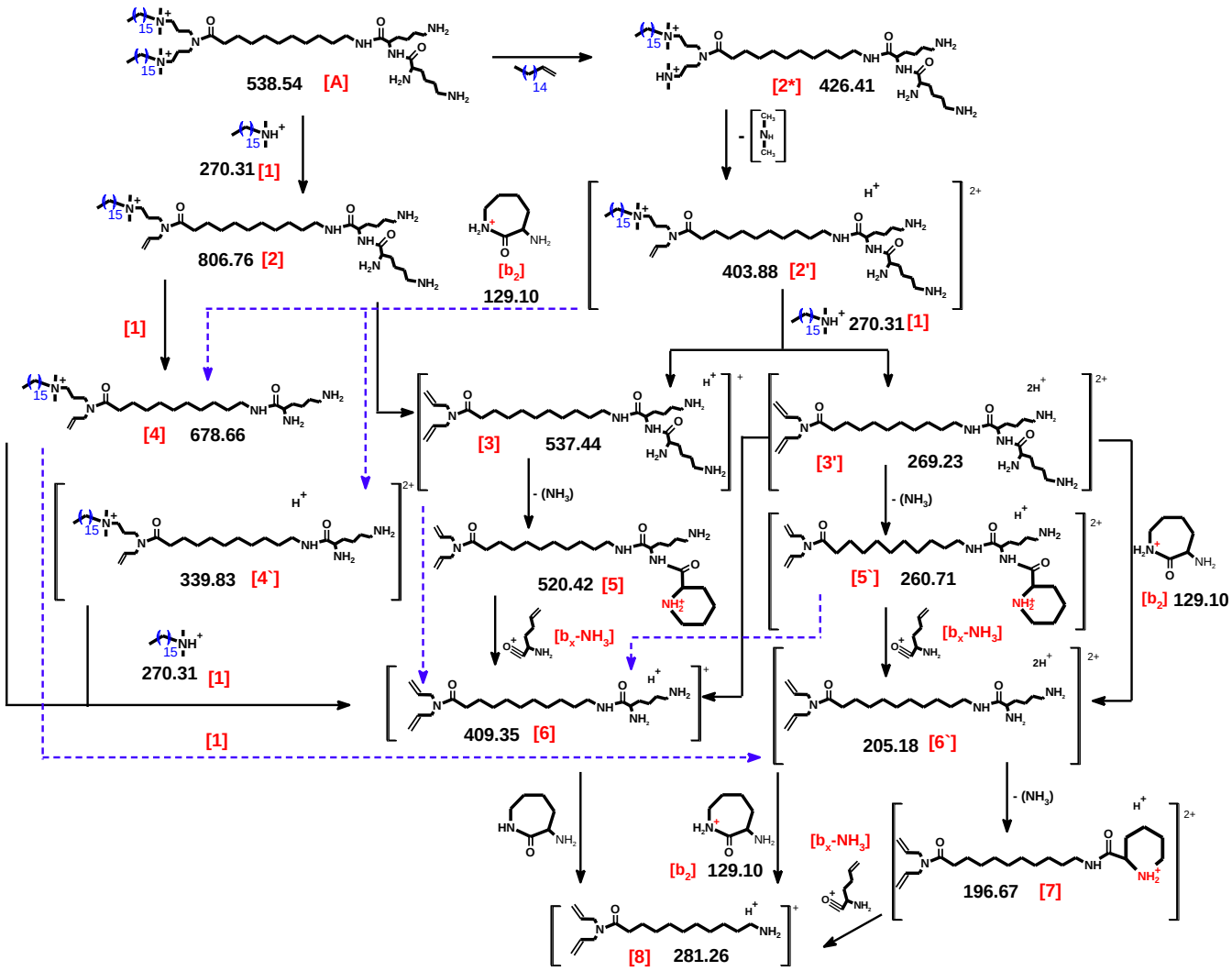

Figure 4.5. Proposed MS/MS product ions generated form product ion (A) at *m/z* 538.54 of 16-7N(C11-K3)-16 gemini surfactant. Product ion 2* is a transient ion.

Product ion (2`) subsequently yields the formation of four product ions (Figure 4.5). The first involves the loss of the head group and the attached aliphatic tail (ion 1) at *m/z* 270.31 producing a singly charged product ion (3) at *m/z* 537.44. A second ion is formed via the neutral loss of the aliphatic chain and the formation of intermediate doubly charged ion, as discussed above, at *m/z* 291.75 (ion structure is not shown) which easily loses the dimethylamine head group generating a doubly charged species (3`) at *m/z* 269.23. The third and fourth ions are

formed as a result of eliminating the terminal lysine moiety leading to the formation of a singly charged ion (4) at *m/z* 678.66 and the corresponding doubly charged ion (4`) at *m/z* 339.83 (dotted arrows originating from ion 403.8). As shown in Figure 4.3, this cleavage is usually initiated by nucleophilic attack of the lysine side chain on the amide bond releasing *m/z* 129.10 ion ($b_2$) as a protonated α-amino-ε-caprolactam and forming product ion (4). Ion (4`) on the other hand could either result from the same mechanism as ion (4) but it requires a proton transfer from the protonated α-amino-ε-caprolactam to the complementary c-terminal ion or through the (a_x - y_x) peptide fragmentation mechanism (Figure 4.4). Unlike product ion (2`), fragmentation of the singly charged ion (2) produces only two product ions: ions (3) and (4) (Figure 4.5).

Ion (3`) at *m/z* 269.23 undergoes neutral loss of ammonia forming pipecolic acid derivative compound at *m/z* 260.71 (5`) (Figure 4.5). Furthermore, (3`) loses another terminal lysine moiety forming a single-charged ion (6) at *m/z* 409.35 and a double-charged ion (6`) at *m/z* 205.18. Similar to ion (3`), ion (3) also eliminates an ammonia group producing ion (5) at *m/z* 520.42 and loses a lysine moiety to produce ion (6). Ion (6) can also be formed via the loss of alkyl tail from ion (4) as well as ion (4`); the latter can additionally yield ion (6`) as shown in Figure 4.5. Finally, ions (5) and (5`) can also yield the formation of product ion (6) through the loss of the pipecolic acid ring (Figure 4.5). It can be speculated that this loss occurred by the mobilization of the proton from the pipecolic acid ring to the nitrogen of the amide bond followed by nucleophilic attack either by the carbonyl group releasing pipecolic acid which was observed at *m/z* 112.07 or by the pipecolic acid ring's amine resulting in opening the ring and forming caprolactam ion which was also observed at *m/z* 114.09 (Figure 4.5).

Product ion (6`) experiences loss of ammonia group forming ion (7) at *m/z* 196.67 and eliminates the last lysine moiety forming ion (8) at *m/z* 281.26. It should be noted that ion (8) at

m/z 281.26 was also produced by ion (6); however, MS^3 analysis did not show any second generation product ions at *m/z* 129.10, which corresponds to the elimination of lysine as a protonated α-amino-ε-caprolactam (Table S2, Appendix III). This finding supports the theory of the proton transfer from the protonated α-amino-ε-caprolactam to the c-terminal fragment ion that we proposed earlier as a possible mechanism to justify the formation of product ion B.

Dissociation of product ion B

Product ion (B) dissociates via two fragmentation pathways; firstly by the loss of an NH_3 moiety from the terminal lysine producing pipecolic acid derivative, product ion (9) at *m/z* 353.68 (Figure 4.6, Table 4.1). The second product ion results from the loss of the terminal lysine amino acid residue (observed at *m/z* 129.10 [b2]) by amide bond cleavage forming a doubly charged product ion (10) at *m/z* 474.49. Elimination of the pipecolic acid part of ion (9) also leads to the formation of ion (10) which subsequently dissociates by eliminating the last terminal lysine, forming ion (11) observed at *m/z* 410.44. Furthermore, ion (10) loses the tail region and the attached head forming the previously mentioned singly and doubly charged ions designated as (4) and (4`). As it can be seen, the complexity of the MS/MS spectra supports the notion that some ions may be formed from various product ions as in the case of the product ions (4) and (4`). Such observation is supported by second generation MS^3 analysis (Table S2, Appendix III). Both of these ions further dissociate as shown in Figure 4.6. Ion (11) also loses the aliphatic tail and the attached head group yielding ion (12) and (12`) at *m/z* 550.57 and *m/z* 275.79 respectively supported by second generation MS^3 analysis (Table S2, Appendix III). Both ions subsequently eliminate the remaining dimethylalkenammonium ion forming the product ion (8) at *m/z* 281.26 (Figure 4.6).

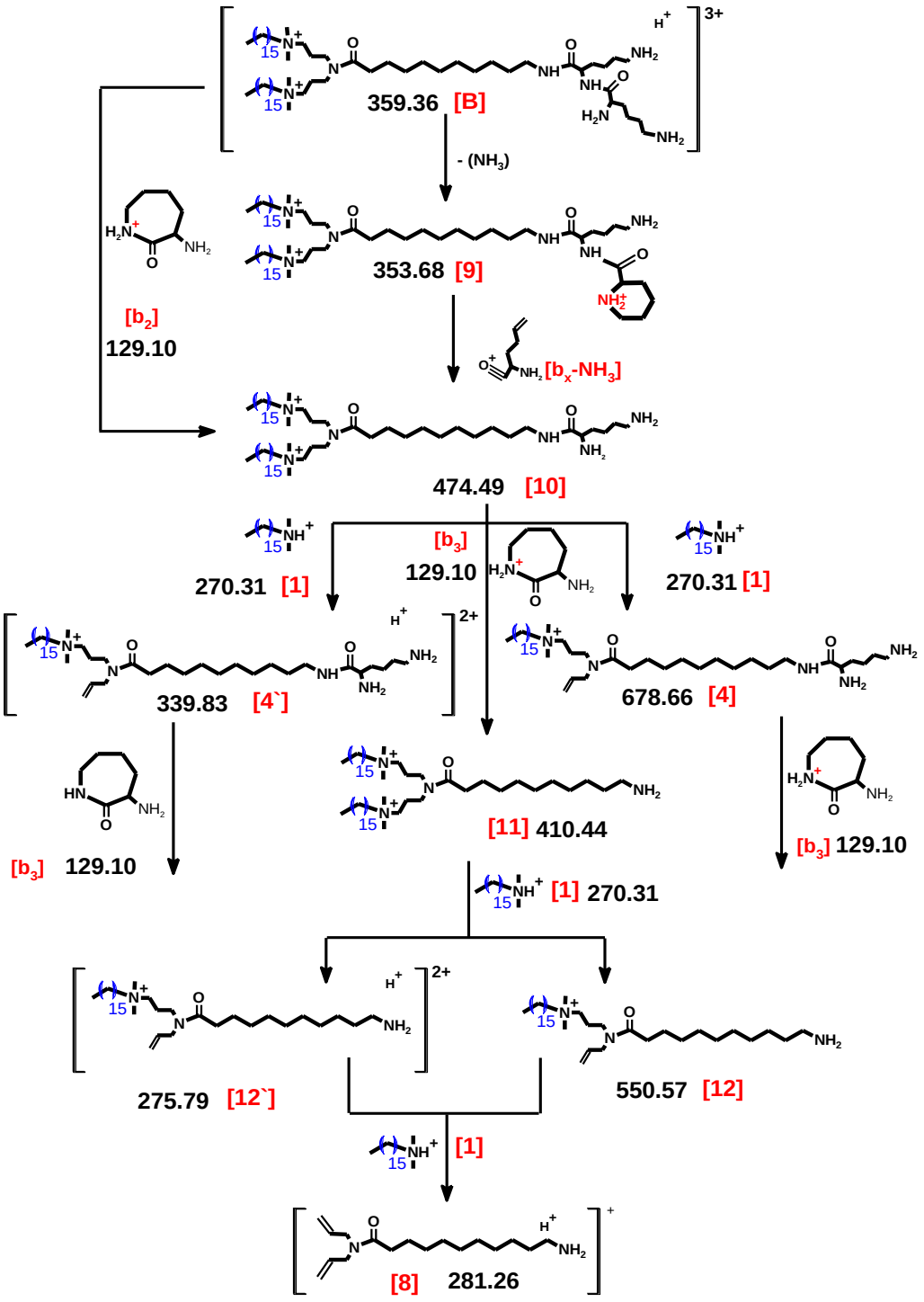

Figure 4.6. Proposed MS/MS product ions generated form product ion (B) at *m/z* 359.36 of 16-7N(C11-K3)-16 gemini surfactant.

Dissociation of product ion C

Product ion (C) was the source of six product ions (Figure 4.7) which is much more complex than product ions A or B. This is expected since product ion C retains the same structural backbone of the precursor ion with the simple loss of NH_3 moiety. The first two product ions arise from the loss of pipecolic acid re-forming product ions (A) or (B) which was confirmed by MS^3 analysis (Table S2, Figure S3, Appendix III). On the other hand, cleavage of the peptide bond of the lysine with intact side chain resulted in the formation of ions 9 and 9` observed at *m/z* 353.68 and *m/z* 530.02 (Figure 4.7, Table 4.1) respectively which differs only in the charge state due to variations in the formation mechanisms as disused earlier in details in the section entitled "Dissociation of product ion A". Interestingly, MS^3 analysis of ion (C) revealed that product ions (A) and (B) were of lower abundance than product ions 9 and 9` (Figure S3, Appendix III). This could be attributed to the ease of the cleavage of the amide bond linked to the lysine side chain ε-amino group in comparison to the loss of pipecolic acid.

Product ion (C) can also eliminates another ammonia group from the second terminal lysine producing a triply charge ion (13) observed at *m/z* at 390.70 (Figure 4.7, Table 4.1). Since the elimination of the ammonia is charge-directed, mobilization of the proton from the pipecolic acid ring to the lysine ε-amino group is required. Ion (13) subsequently loses one of the pipecolic acids yielding the previously mentioned ions (9) and (9`) which was confirmed by second generation MS^3 analysis (Table S2, Appendix III). Finally, product ion C undergoes a neutral loss of the aliphatic tail forming an unstable intermediate at *m/z* 321.63 (not shown) which easily loses dimethylamine group forming a triply charged ion (14) at *m/z* 306.61. Similar to past observation, such an intermediate ion was occasionally observed and its genesis was confirmed by MS^3 analysis.

Ion (14) eliminates the remaining ammonium head group and the associated aliphatic tail producing the product ion (15) at *m/z* 324.76. It also undergoes neutral loss of the tail through hemolytic cleavage of the N-C bond forming, as above, unstable intermediate at *m/z* 231.86 that subsequently losses the head group yielding ion (15`) at *m/z* 216.84. Ion (16) observed at *m/z* 300.94 is also produced from ion (13) after losing the dimethylalkenammonium ion and from ion (14) after the neutral loss of ammonia which was confirmed by MS^3 analysis (Figure 4.7, Table S2, Appendix III). Ion (16) follows same pathway as ion 14 forming ion (17) at *m/z* 316.25 and ion (17`) at *m/z* 211.17. Both ion 17 and 17` was generated by loss of ammonia from ions 15 and 15`. Ions 15, 15`, 17 and 17` further cleaved various amid bonds producing smaller structures product ions as illustrated in Figure 4.7.

Ions 9 and 9` follow similar fragmentation pattern as ion (13), firstly by losing one of the dimethylalkenammonium ions then by eliminating the second one (Figure 4.7, Table 4.1).The produced product ions later fragmented to smaller ions in a similar fashion by cleaving the amide bond and/or ejecting lysine moieties as illustrated in Figure 4.7.

In order to support the proposed fragmentation pathways of the peptide-modified gemini surfactants with tri-terminal lysine moieties, isotopically labeled analogues were evaluated. This include compounds 16-7N(G-C_{11}-K_D-K_2)-16 and 16-7N(G-C_6-K_D-K_2)-16 where K_D is a deuterated lysine moiety bearing four deuterium atoms. The MS/MS analysis revealed an increased *m/z* values in the product ions containing the deuterated lysine such as product ions (A), (B) and (C) (Figure S4, Appendix III). Moreover, fragment ions (8), (11), (12) and (12`) that bear no deuterated region showed identical *m/z* values, confirming the proposed fragmentation pathway (Figure S4, Appendix III).

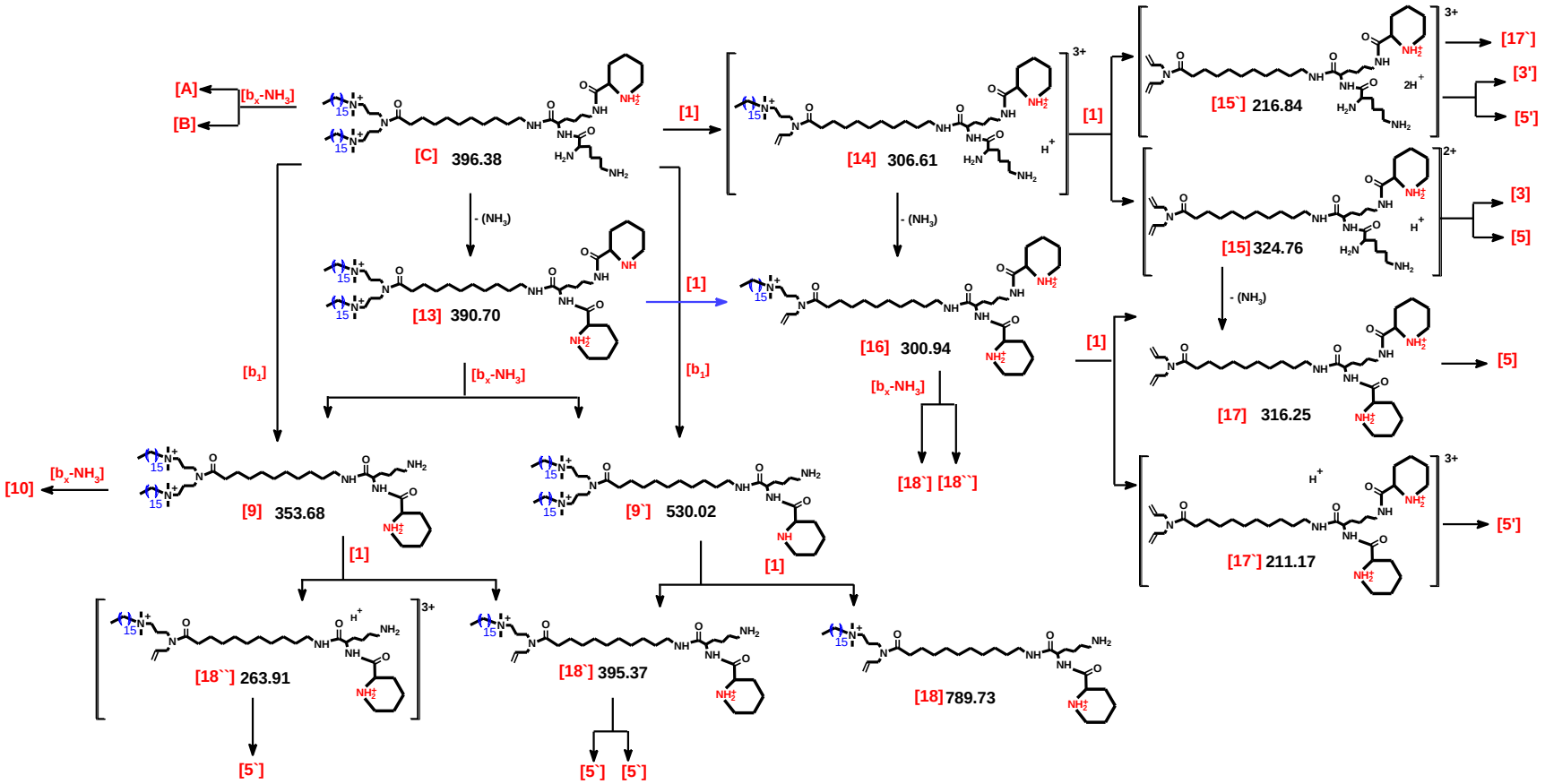

Figure 4.7. Proposed MS/MS product ions generated form product ion (C) at *m/z* 396.38 of 16-7N(C11-K3)-16 gemini surfactant.

4.4.2.2. MS/MS fragmentation pathway of the peptide modified gemini surfactants with mono-terminal lysine moiety

Gemini surfactant 16-7N(G-C_{11}-K)-16 is used as an illustrative example of peptide modified gemini surfactants functionalized with single terminal lysine moiety (Figure 4.8). Similar to the fragmentation pathway of 16-7N(C_{11}-K_3)-16 gemini surfactant, dissociation of 16-7N(G-C_{11}-K)-16 compound started with either the elimination of the lysine moiety and/or the neutral loss of amino group. Elimination of the lysine residue through the cleavage of the amide bond produced ion (A), a doubly charged product ion observed at *m/z* 438.95, and released its complimentary ion (b_1) at *m/z* 129.10 as a protonated α-amino-ε-caprolactam (Figure 4.8, Table 4.2). Unlike 16-7N(C_{11}-K_3)-16 gemini surfactants, the formation of a triply charged product ion after the elimination of the lysine residues from 16-7N(G-C_{11}-K)-16 was not observed. This is possibly due to the higher proton affinity of the α-amino-ε-caprolactam compared to the c-terminal product ions. A charge-directed loss of the lysine ε-amino group from the precursor ion resulted in the formation of pipecolic acid derivative product ion (B) at *m/z* 329.99 which can subsequently eradicate the pipecolic acid ring forming ion (A) (Figure 4.8).

As indicated earlier, product ion (A) undergoes the loss of the dimethylalkenammonium ion (1) generating both a single-charged product ion (2) at *m/z* 607.59 and a double-charged product ion (2`) at *m/z* 304.30 (Figure 4.8, Table 4.2). Both product ions experience a loss of the last dimethylalkenammonium ion producing product ion (3) at *m/z* 338.28. In addition, ion (2`) produced ion (3`), the doubly charged analog of ion (3).

Ion (B) also loses ion (1) producing ion (4) at *m/z* 240.22 which either eliminates the last dimethylalkenammonium ion generating ion (5) at *m/z* 225.18 and/or removes the pipecolic

acid ring resulting in the formation of ion (2`) (Figure 4.8, Table 4.2). Further dissociations of ion (5) are self-explanatory resulting in the production of ion (3) and (3`). Similar to other compounds, the genesis and structures of all ions observed in Figure 4.8 were confirmed by MS^3 analysis (data not shown).

Table 4.2. Product ions observed during MS/MS analysis of $[M+H]^{3+}$ ions of the peptide modified gemini surfactants with mono-terminal lysine moiety.

	Gemini surfactants	**16-7N(G-C_{11}-K)-16**	**12-7N(G-C_6-K)-12**	**16-7N(G-C_6-K)-16**
Ion #	**Product ions**	**m/z**	**m/z**	**m/z**
A	**$[M–C_6H_{13}N_2O]^{2+}$**	438.95	347.85	403.91
B	**$[M–NH_3]^{3+}$**	329.99	269.26	306.63
b_1	**$C_6H_{13}N_2O$**	129.1	129.1	129.1
1	**Dimethylalkenaminium**	270.31	214.25	270.31
2	**[M–(b_1)- ion(1)] $^+$**	607.59	481.44	537.51
2`	**[M–(b_1)- ion(1)] $^{2+}$**	304.3	241.23	269.26
3	**[M–(b_1)-2 ion(1)] $^+$**	338.28	268.2	268.2
3`	**[M–(b_1)-2 ion(1)] $^{2+}$**	169.64	134.6	134.6
4	**[M–(NH_3)- ion(1)] $^{3+}$**	240.22	198.18	216.86
5	**[M–(NH_3)- 2 ion(1)] $^{2+}$**	225.18	190.14	190.14

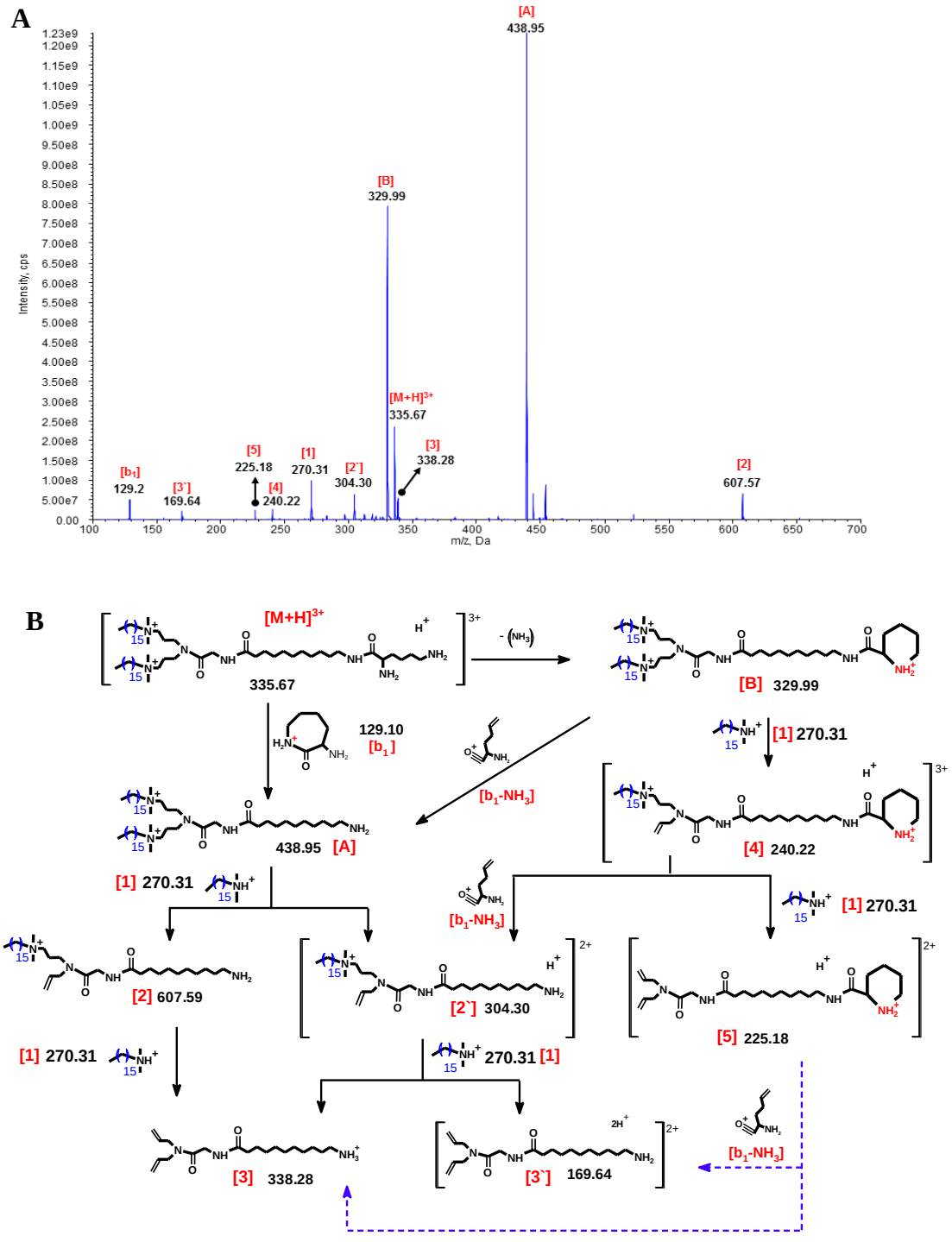

Figure 4.8. (A) The ESI-QqLIT MS/MS spectrum of 16-7N(G-C_{11}-k)-16 as a representative example of gemini surfactants with mono-terminal lysine moiety and (B) the proposed MS/MS fragmentation pattern.

4.4.2.3. Universal MS/MS fragmentation pattern of the novel peptide modified gemini surfactants

Similarities in the fragmentation behaviour of the peptide modified gemini surfactants resulted in the establishment of a universal MS/MS fragmentation pattern (Figure 4.9) that can be applied to any related structure. The universal fragmentation pathway begins with both the cleavage of the peptide bond forming a doubly charged product ion (A) and the neutral loss of the lysine's ε-amino group producing pipecolic acid derivative product ion (B).

Two dissociation pathways are proposed for product ion (A). First, a loss of one quaternary ammonium head group and the attached aliphatic tail producing two complimentary ions: dimethylalkenammonium product ion (1) and the singly charged product ion (2). The second pathway occurs via homolytic cleavage of the N-C bond between the quaternary ammonium headgroup and the hydrocarbon tail resulting in the neutral loss of the aliphatic tail and the production of a doubly charged intermediate ion that easily eradicates the dimethylamine head group, probably due to the close proximity of the two positively charged head groups, generating product ion (2`). In some cases, the intermediate ion was abundant enough to conduct $MS^3$ analysis to support proposition. Both ions (2) and (2`) also undergo subsequent loss of dimethylalkenammonium ion forming ions (3) and (3`) (Figure 4.9).

On the other hand, ion (B) dissociates by the loss of dimethylalkenammonium ion forming a triply charged ion (4) which subsequently eliminates another dimethylalken ammonium ion to produce ion (5). Product ions (B), (4) and (5) produced ions (A), (2`) and (3`) respectively through the removal of the pipecolic acid ring as illustrated in Figure 4.9.

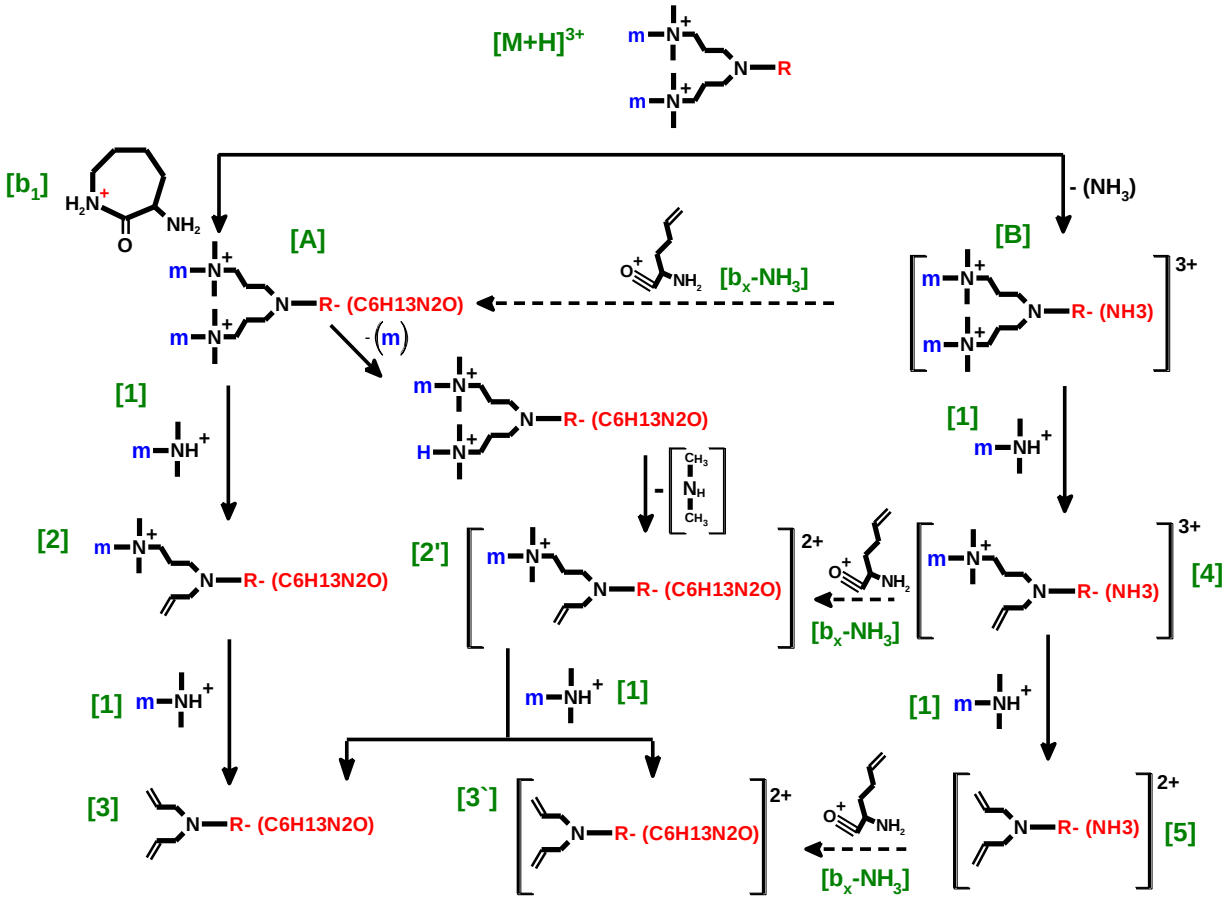

Figure 4.9. Universal MS/MS fragmentation pattern for peptide modified gemini surfactants.

4.5. Conclusion

In this work, we utilized ESI-QqToF-MS and ESI-QqLIT-MS to study the CID-MS/MS fragmentation behaviour of eleven novel peptide-modified gemini surfactants. Exact mass measurements confirmed the projected molecular composition of the evaluated compounds showing mass accuracies of less than 8 ppm. In addition, tandem mass spectrometric analysis generated compound-specific product ions authenticating the chemical structure of their precursor ions. The genesis of these product ions was further confirmed by MS^3 analysis (Table S2, Appendix III), allowing for the development of fragmentation pattern that could be used as a fingerprint for accurate identification of the tested compounds.

In general, the MS/MS dissociation was centered on the attached amino acids in which peptide bonds were cleaved for the generation of diagnostic product ions. Furthermore, neutral loss of an ammonia group from the amino acid side chain was dominant within the evaluated structures. Elimination of one or both of the quaternary ammonium head groups and the attached aliphatic tail was also observed. It should be noted that the number of terminal amino acid residues in the spacer and the length of the inserted hydrocarbon linker affected the dissociation behaviour. For example, the formation of the triply charged initial product ions after eliminating a terminal lysine residue was only observed in gemini surfactants with longer hydrophobic linker chain (C_{11}) and with tri-terminal amino acids residues. Nevertheless, similarities in the fragmentation behaviour among all the tested gemini surfactants resulted in the production of a universal fragmentation pattern as illustrated in Figure 4.9. This universal fragmentation pattern can be utilized to predict the dissociation behaviour of new compounds with similar general structural features. In addition, it will be utilized for the development of qualitative and

quantitative MS-based methods to probe the fate and biodistribution of topically applied therapeutic gemini surfactant formulations. We are currently quantitatively evaluating the distribution of lead gemini surfactants within skin tissues for therapeutic applications. This data will be reported upon completion.

4.6. Bibliography

1 Jin L, Zeng X, Liu M, Deng Y, He N. Current progress in gene delivery technology based on chemical methods and nano-carriers. Theranostics 2014; 4: 240-55.

2 Singh J, Mohammed-Saied W, Kaur R, Badea I. Nanoparticles in Gene Therapy: From Design to Clinical Applications. Reviews in Nanoscience and Nanotechnology 2013; 2: 275-99.

3 Ahmed T, Kamel AO, Wettig SD. Interactions between DNA and Gemini surfactant: impact on gene therapy: part I. Nanomedicine 2016.

4 Elsabahy M, Badea I, Verrall R, Donkuru M, Foldvari M. Dicationic gemini nanoparticle design for gene therapy. Organic nanomaterials. Wiley 2014: 509-28.

5 Menger FM, Littau C. Gemini-surfactants: synthesis and properties. Journal of the American Chemical Society 1991; 113: 1451-2.

6 Rosen MJ, Tracy DJ. Gemini surfactants. Journal of Surfactants and Detergents 1998; 1: 547-54.

7 Singh J, Michel D, Chitanda JM, Verrall RE, Badea I. Evaluation of cellular uptake and intracellular trafficking as determining factors of gene expression for amino acid-substituted gemini surfactant-based DNA nanoparticles. J Nanobiotechnology 2012; 10.

8 Badea I, Verrall R, Baca-Estrada M, Tikoo S, Rosenberg A, Kumar P, *et al*. In vivo cutaneous interferon-γ gene delivery using novel dicationic (gemini) surfactant–plasmid complexes. The journal of gene medicine 2005; 7: 1200-14.

9 Badea I, Wettig S, Verrall R, Foldvari M. Topical non-invasive gene delivery using gemini nanoparticles in interferon-γ-deficient mice. European journal of pharmaceutics and biopharmaceutics 2007; 65: 414-22.

10 Garcia MT, Kaczerewska O, Ribosa I, Brycki B, Materna P, Drgas M. Biodegradability and aquatic toxicity of quaternary ammonium-based gemini surfactants: Effect of the spacer on their ecological properties. Chemosphere 2016; 154: 155-60.

11 Wasungu L, Scarzello M, van Dam G, Molema G, Wagenaar A, Engberts JB, *et al*. Transfection mediated by pH-sensitive sugar-based gemini surfactants; potential for in vivo gene therapy applications. Journal of molecular medicine 2006; 84: 774-84.

12 Kim B-K, Doh K-O, Bae Y-U, Seu Y-B. Synthesis and optimization of cholesterol-based diquaternary ammonium gemini surfactant (chol-gs) as a new gene delivery vector. J. Microbiol. Biotechnol 2011; 21: 93-9.

13 Pérez L, Pinazo A, Pons R, Infante M. Gemini surfactants from natural amino acids. Advances in colloid and interface science 2014; 205: 134-55.

14 Yang P, Singh J, Wettig S, Foldvari M, Verrall RE, Badea I. Enhanced gene expression in epithelial cells transfected with amino acid-substituted gemini nanoparticles. European Journal of Pharmaceutics and Biopharmaceutics 2010; 75: 311-20.

15 Singh J, Yang P, Michel D, E Verrall R, Foldvari M, Badea I. Amino Acid-Substituted Gemini Surfactant-Based Nanoparticles as Safe and Versatile Gene Delivery Agents. Current Drug Delivery 2011; 8: 299-306.

16 Al-Dulaymi MA, Chitanda JM, Mohammed-Saeid W, Araghi HY, Verrall RE, Grochulski P, *et al*. Di-Peptide-Modified Gemini Surfactants as Gene Delivery Vectors: Exploring the Role of the Alkyl Tail in Their Physicochemical Behavior and Biological Activity. The AAPS Journal 2016: 1-14.

17 Singh J, Michel D, Getson HM, Chitanda JM, Verrall RE, Badea I. Development of amino acid substituted gemini surfactant-based mucoadhesive gene delivery systems for potential use as noninvasive vaginal genetic vaccination. Nanomedicine 2015; 10: 405-17.

18 Mohammed-Saeid W, Michel D, El-Aneed A, Verrall RE, Low NH, Badea I. Development of Lyophilized Gemini Surfactant-Based Gene Delivery Systems: Influence of Lyophilization on the Structure, Activity and Stability of the Lipoplexes. Journal of Pharmacy & Pharmaceutical Sciences 2012; 15: 548-67.

19 Aceña J, Stampachiacchiere S, Pérez S, Barceló D. Advances in liquid chromatography–high-resolution mass spectrometry for quantitative and qualitative environmental analysis. Analytical and bioanalytical chemistry 2015; 407: 6289-99.

20 Lyubarskaya Y, Kobayashi K, Swann P. Application of mass spectrometry to facilitate advanced process controls of biopharmaceutical manufacture. Pharmaceutical Bioprocessing 2015; 3: 313-21.

21 Lietz CB, Gemperline E, Li L. Qualitative and quantitative mass spectrometry imaging of drugs and metabolites. Advanced drug delivery reviews 2013; 65: 1074-85.

22 Pacholarz KJ, Garlish RA, Taylor RJ, Barran PE. Mass spectrometry based tools to investigate protein–ligand interactions for drug discovery. Chemical Society Reviews 2012; 41: 4335-55.

23 Buse J, Badea I, Verrall RE, El-Aneed A. Tandem mass spectrometric analysis of the novel gemini surfactant nanoparticle families G12-s and G18: 1-s. Spectroscopy Letters 2010; 43: 447-57.

24 Buse J, Badea I, Verrall RE, El-Aneed A. Tandem mass spectrometric analysis of novel diquaternary ammonium gemini surfactants and their bromide adducts in electrospray-positive ion mode ionization. Journal of Mass Spectrometry 2011; 46: 1060-70.

25 Mohammed-Saeid W, Buse J, Badea I, Verrall R, El-Aneed A. Mass spectrometric analysis of amino acid/di-peptide modified gemini surfactants used as gene delivery agents: Establishment of a universal mass spectrometric fingerprint. International Journal of Mass Spectrometry 2012; 309: 182-91.

26 Donkuru M, Chitanda JM, Verrall RE, El-Aneed A. Multi-stage tandem mass spectrometric analysis of novel β-cyclodextrin-substituted and novel bis-pyridinium gemini surfactants designed as nanomedical drug delivery agents. Rapid Communications in Mass Spectrometry 2014; 28: 757-72.

27 Buse J, Badea I, Verrall RE, El-Aneed A. A general liquid chromatography tandem mass spectrometry method for the quantitative determination of diquaternary ammonium gemini surfactant drug delivery agents in mouse keratinocytes' cellular lysate. Journal of Chromatography A 2013; 1294: 98-105.

28 Buse J PR, Verrall RE, Badea I, Zhang H, Mulligan CC, Peru KM, Bailey J, Headley JV, El-Aneed A.*. The Development and assessment of high-throughput mass spectrometry-based methods for the quantification of a nanoparticle drug delivery agent in cellular lysate. Journal of Mass Spectrometry. 2014.

29 Donkuru M, Michel D, Awad H, Katselis G, El-Aneed A. Hydrophilic interaction liquid chromatography–tandem mass spectrometry quantitative method for the cellular analysis of varying structures of gemini surfactants designed as nanomaterial drug carriers. Journal of Chromatography A 2016; 1446: 114-24.

30 Al-Dulaymi M, Michel D, Mohammed Saeid W, Chitanda J, Verrall R, Grochulski P, *et al*. Novel peptide-modified gemini surfactants as gene carriers structure activity

relashinship,physicochemical characterizations and mass spectrometric dissociation behaviour. In: AAPS Annual Meeting and Exhibition, Colorado, Denver, USA, 2016.

31 Boyd R, Somogyi Á. The mobile proton hypothesis in fragmentation of protonated peptides: a perspective. Journal of the American Society for Mass Spectrometry 2010; 21: 1275-8.

32 Wysocki VH, Tsaprailis G, Smith LL, Breci LA. Mobile and localized protons: a framework for understanding peptide dissociation. Journal of Mass Spectrometry 2000; 35: 1399-406.

33 Wysocki VH, Cheng G, Zhang Q, Herrmann KA, Beardsley RL, Hilderbrand AE. Peptide Fragmentation Overview. In: Principles of Mass Spectrometry Applied to Biomolecules. (2006), p 277-300.

34 Paizs B, Suhai S. Fragmentation pathways of protonated peptides. Mass spectrometry reviews 2005; 24: 508-48.

35 Yalcin T, Harrison AG. Ion chemistry of protonated lysine derivatives. Journal of mass spectrometry 1996; 31: 1237-43.

36 Csonka IP, Paizs B, Lendvay G, Suhai S. Proton mobility and main fragmentation pathways of protonated lysylglycine. Rapid Communications in Mass Spectrometry 2001; 15: 1457-72.

37 Dookeran NN, Yalcin T, Harrison AG. Fragmentation reactions of protonated-amino acids. Journal of mass spectrometry 1996; 31: 500-8.

38 Paizs B, Schnölzer M, Warnken U, Suhai S, Harrison AG. Cleavage of the amide bond of protonated dipeptides. Physical Chemistry Chemical Physics 2004; 6: 2691-9.

39 Paizs B, Suhai S. Theoretical study of the main fragmentation pathways for protonated glycylglycine. Rapid Communications in Mass Spectrometry 2001; 15: 651-63.

40 Roepstorff P, Fohlman J. Proposal for a Common Nomenclature for Sequence Ions in Mass-Spectra of Peptides. Biomed Mass Spectrom 1984; 11: 601.

CHAPTER 5

The Development of Simple Flow Injection Analysis Tandem Mass Spectrometric Methods for the Cutaneous Determination of Peptide-Modified Cationic Gemini Surfactants Used as Gene Delivery Vectors

Mays Al-Dulaymi[1], Deborah Michel[1], Jackson M. Chitanda, Ildiko Badea[1], Anas El-Aneed[1]

1. College of Pharmacy and Nutrition, University of Saskatchewan, Saskatoon, SK, Canada

---

*This chapter is published in Journal of Pharmaceutical and Biomedical Analysis, 2018, 159: 436-547.

Transitioning rationale:

Literature review provided evidence about the potential of gemini surfactants as a gene delivery carries for topical application. Peptide-modified gemini surfactants demonstrated promising results in transfecting keratinocytes (Chapter 3). The success of developing efficient and safe cutaneous gene delivery systems requires a thorough understanding of the vectors' skin deposition and penetration behaviour. In the previous chapter, we evaluated the MS/MS dissociation behaviours of peptide-modified gemini surfactants. Herein, we aim at developing flow injection analysis tandem mass spectrometric methods (FIA)-MS/MS to assess the skin deposition and penetration behaviour of topically applied therapeutic gemini surfactant formulations.

Contribution statement:

Mays Al-Dulaymi contributed to this manuscript by designing the study, performing experiments, data acquisition, data analysis and manuscript writing.

5.1. Abstract

Diquaternary ammonium gemini surfactants are a class of non-viral gene delivery vectors, primarily studied for their dermal applications. However, their biological fate has rarely been investigated. In this work, we developed simple flow injection analysis tandem mass spectrometric methods, (FIA)-MS/MS, to understand the fate and biodistribution of topically applied gemini surfactant-based therapeutics in an ex-vivo skin model.

Three peptide-modified gemini surfactants with varied structures and transfection efficiencies were evaluated. For each compound, two methods were developed to quantify their presence in skin tissue and in phosphate buffered saline (PBS). The methods were developed using single-point calibration mode. Skin penetration was assessed on CD1 mice dorsal skin tissue mounted in a Franz diffusion cell after extraction. Amongst the five evaluated liquid-liquid extraction protocols, the Folch method provides the highest extraction efficiency for all compounds. Weak cationic exchange solid phase extraction was also used to further isolate gemini surfactants from endogenous skin lipids. FIA–MS/MS analysis of the skin revealed that all compounds were detected in the skin with minimal partition into the PBS compartment, which represents circulation. Interestingly, the detected amounts of gemini lipids in the skin were correlated with their transfection efficiencies, where the lead compound exhibited the highest skin concentration. The developed methods will be used, in the close future, to investigate the fate of topically applied gemini surfactant-based formulation *in vivo.*

5.2. Introduction

Recent advances in discovering the genetic basis of many dermatological disorders have found cutaneous gene therapy to be a promising therapeutic option [1, 2]. Cutaneous delivery of genetic material offers numerous advantages over other routes of administration, such as minimizing systematic toxicity, bypassing first-pass metabolism, and avoiding rapid clearance from the systemic circulation [3]. Despite these advantages, skin is a formidable barrier to foreign materials, such as nanotechnology products [4]. Therefore, effective delivery systems capable of penetrating the cutaneous barrier and facilitating recombinant DNA uptake into the skin are needed to achieve gene expression – the ultimate goal of gene therapy.

Among topical delivery modalities currently being explored, lipid-based delivery vectors are at the forefront [5, 6]. They have the ability to encapsulate, protect, and compact negatively charged nucleic acids, whereby forming nano-sized lipoplexes. Furthermore, the chemical composition of lipid-based nanocarriers bears some similarity to skin lipids, which enables them to fuse with the lipids in the stratum corneum, the outer layer of the skin; destabilizing the lipid matrix and enhancing drug penetration [6]. Diquaternary ammonium gemini surfactants are a class of lipid-based delivery systems that are composed of dimeric surfactants with positively charged head groups and hydrocarbon tails linked by a spacer chain (Figure 5.1) [7],[8]. The structure of gemini surfactants can be tailored to overcome skin barrier functions [9]. The topical application of gemini surfactant-based nanoparticles demonstrated a promising potential in the treatment of localized cutaneous scleroderma [9-11]. Nanoparticles of N,N'-bis(dimethylhexadecyl)-1,3-propanediammonium dibromide gemini surfactant complexed with pDNA encoding for interferon gamma (INF-γ) showed a significant increase in the level of INF-γ in mice [9-11].

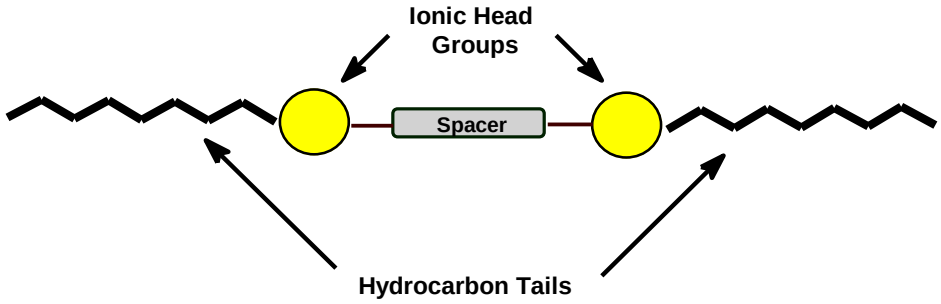

Figure 5.1. Schematic representation of gemini surfactants showing the two ionic head groups, hydrocarbon tails and the spacer.

Despite advances in the design of lipid-based nanocarriers, their biodistribution and biological fate have been less explored. Upon topical application, lipid-based nanoparticles distribute within various layers and cellular components. At present, the biodistribution, intracellular trafficking, and the ultimate fate of the lipid vector, after releasing its therapeutic cargo, are not fully understood. A fundamental understanding of the behavior of the lipid-based vectors in complex biological environments is essential in guiding the design of safer and more effective nanoparticles.

To track the fate and distribution of lipid-based nanoparticles, fluorescently labeled and radiolabeled carriers are the most commonly used strategies. However, labeling techniques have drawbacks, particularly their tendency to alter the physicochemical properties of the delivery system. These modifications, in turn, change the pharmacokinetic profile of the nanocarriers [12]. Furthermore, they are unable to distinguish between the localization of a labeled molecule and the metabolites that retain the fluorescent or radioactive probes [13]. Therefore, a more robust and

sensitive analytical technique should be employed to identify and quantify gene-based carriers in complex biological samples.

Mass spectrometry (MS) is an ideal technique to monitor the fate of gemini surfactants in the skin [14-16]. It is a label-free technique with a powerful chemical identification capability and is gaining popularity in pharmaceutical sciences due to its high selectivity and sensitivity [17, 18]. Coupling liquid chromatography to tandem mass spectrometry (LC–MS/MS) allows for reliable high throughput qualitative and quantitative analysis [19]. In fact, it is the gold standard technology for the quantification of pharmaceuticals in complex biological matrices [20, 21].

In our laboratory, we developed two LC–MS/MS methods for the quantification of unsubstituted diquaternary ammoniums gemini surfactants (N, N-bis(dimethylalkyl)-α,ω-alkane-diammonium), amine substituted diquaternary ammoniums compounds, and heterocyclic head group gemini surfactants (bis(alkyl-pyridinum) in epidermal keratinocytes [22, 23]. These methods provided essential information about the rate of cellular uptake and intracellular depletion of gemini surfactants [22, 23]. Currently, these methods are being employed to determine the subcellular localization of gemini surfactants and identify any potential metabolites. Recently, a new series of peptide modified diquaternary ammoniums gemini surfactants was found to exhibit superior transfection efficiency compared to previous generations of gemini surfactants [24]. Their collision-induced dissociation (CID)-MS/MS behaviour was evaluated, establishing a universal mass spectrometric fingerprint, essential for the development of targeted LC-MS qualitative and quantitative methods [14].

Herein, we resolved a significant analytical challenge, the efficient extraction of gemini surfactants from lipid rich skin tissues. Efficient analytical platforms are needed to guide the

development of effective pharmaceutical formulations. Three representative compounds were selected with high, low, and moderate transfection efficiencies. Subsequently, rapid and simple flow injection analysis (FIA)-MS/MS methods were developed to detect and quantify peptide-modified gemini surfactants in skin tissues as well as in phosphate buffered saline (PBS).

5.3. Materials and methods

5.3.1. Materials

The evaluated peptide-modified gemini surfactants, designated as 16-7N(R)-16 where 16 is the alkyl chain length and R is the peptide-containing moiety: R= glycyl-lysine, glycyl-hexyl-trilysine and glycyl-undecyl-trilysine (Figure 5.2), were synthesized using previously reported synthetic methods [24]. The corresponding internal standards were synthesized using the same synthetic procedure with the incorporation of deuterated lysine moiety bearing four deuterium atoms (Figure S1, Appendix IV). The plasmid pGThCMV.IFNGFP (pDNA), encoding for murine interferon gamma (IFN-γ) and green fluorescent protein (GFP) was utilized in this work [9].

The helper lipid 1,2-dioleoyl-snglycerol-3-phosphoethanolamine (DOPE) was purchased from Avanti Polar Lipids Inc. (Alabaster, AL, USA). Sucrose, used as a stabilizing agent, and phosphate buffered saline (PBS) were purchased from Sigma Aldrich (Oakville, ON, Canada). Mass spectrometry-grade methanol, water, and acetonitrile were purchased from Fisher Scientific (Nepean, ON, Canada). Formic acid (purity 90%) was obtained from EMD Chemicals Inc. (Merck KGaA, Darmstadt, Germany). Anhydrous chloroform and methyl tert-butyl ether (MTBE) used as extraction solvents were purchased from Sigma Aldrich (Oakville, ON, Canada). Solid phase extraction cartridges, Bond Elute® CBA, were obtained from Agilent Technologies (Mississauga, ON, Canada).

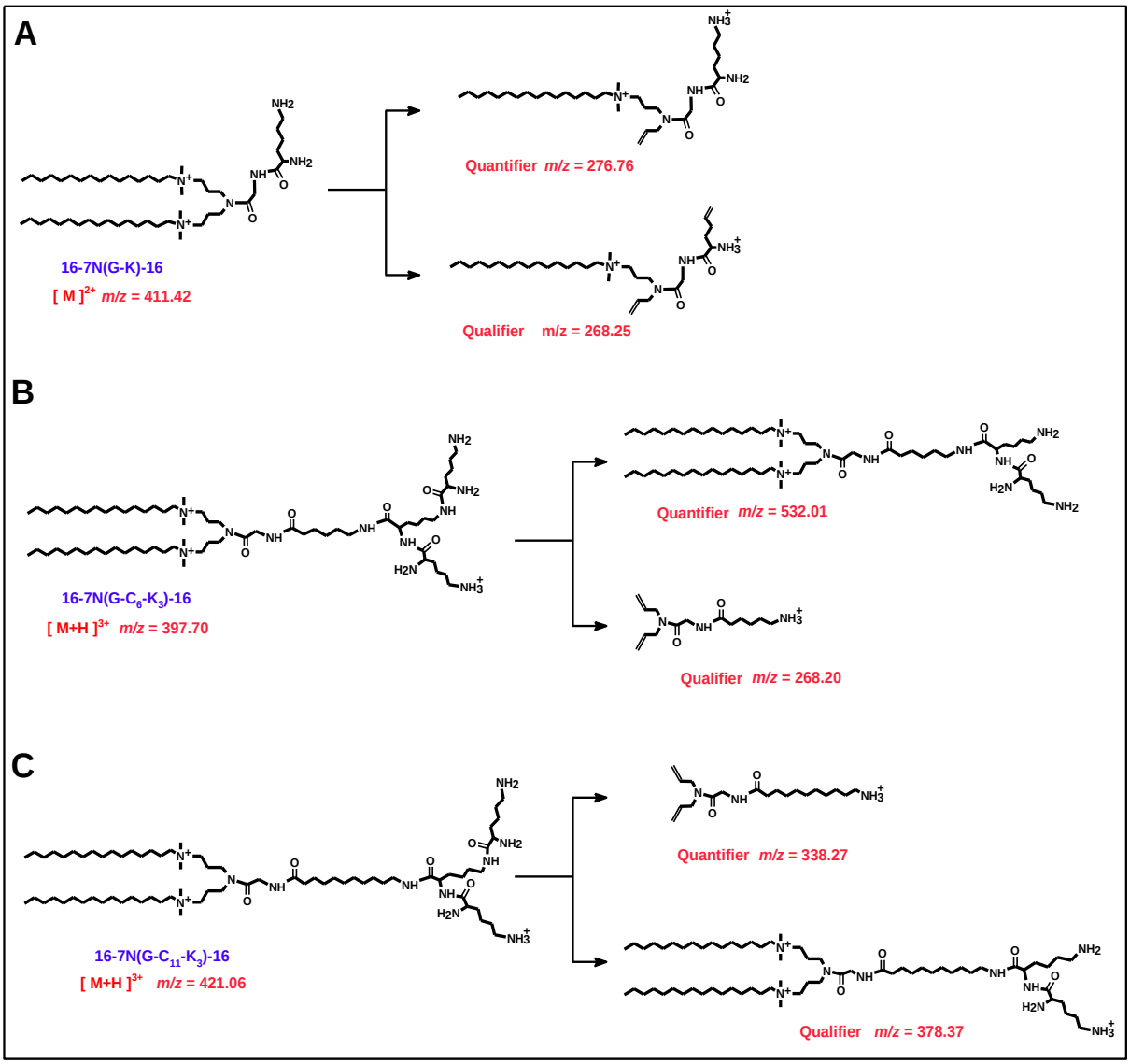

Figure 5.2. Chemical structure of gemini surfactants 16-7N(G-K)-16 (A), 16-7N(G-C_6-K_3)-16 (B) and 16-7N(G-C_{11}-K_3)-16 surfactants showing their precursor ion and the monitored product ions.

5.3.2. Preparation of topical formulations

Cationic gemini lipids were combined with pDNA at nitrogen (cationic) to phosphate (anionic) charge ratios (N/P) of 5 in the presence of a helper lipid DOPE to create pDNA/gemini lipid/helper lipid (P/G/L) nanoparticles. An appropriate amount of 30 mM aqueous solutions of gemini surfactant was added to 2 mg/mL pDNA solution and incubated for 20 minutes at room temperature (P/G complex). 2 mM DOPE was prepared as described previously [25] then concentrated to 10mM using Eppendorf concentrator 5301(Eppendorf, Hamburg, Germany). The concentrated DOPE was added to P/G complexes at a gemini surfactant to DOPE molar ratio of 1:16 to form the final nanoparticles (P/G/L) and incubated at room temperature for 20 minutes.

5.3.3. *Ex vivo* skin penetration study

Dorsal skin tissues were collected from female CD1 mice (Charles River Laboratories, Saint-Constant, QC, Canada) weighing around 22-24 g. Approval for this study was granted by the University of Saskatchewan's Animal Research Ethics Board in adherence to the Canadian Council on Animal Care guidelines for humane animal use (protocol # 20090081). The animals were shaved and the skin was collected and stored at -80 °C until use.

Skin penetration was evaluated using multi-station Franz diffusion cell system with 64 mm^2 surface area (PermeGear Inc., Hellertown, PA, USA). The skin tissue was mounted between the donor and receptor compartments of the Franz cell with the *stratum corneum* facing the donor compartment. The receiving chamber was filled with 5 mL PBS, avoiding any air bubbles between the skin and the solution. The skin tissues were allowed to equilibrate for 10 minutes before applying any formulation. A total 200 µL of peptide modified gemini surfactant-based lipoplexes containing 16 µg pDNA was placed in the donor compartment and the chamber was

covered with parafilm. Throughout the experiment, the PBS in the receptor compartment was continuously stirred at 700 rpm using a magnetic stirrer bar and temperature was maintained at 32 °C using a circulating water bath (Fisher Scientific, Nepean, ON, Canada).

Aliquots of 200 µL were withdrawn from the receptor compartment at fixed intervals (2, 4, 6, 8, 12, 18 and 24 h) and replaced with an equal volume of pre-warmed PBS. After 24 hours, any remaining formulation in the donor chamber was aspirated and the skin tissue was removed from the Franz cell. The skin was rinsed thoroughly with water, blotted with tissue paper, then stripped 10 times with Scotch adhesive tape. The collected skin tissues and PBS samples were stored at -80 °C prior to analyte extraction and FIA-MS/MS analysis.

5.3.4. Sample preparation for FIA-MS/MS analysis

Skin tissue (40 mg) was spiked with 200 µL of methanol containing 0.03 mM of the corresponding internal standards for 16-7N(G-K_{d4})-16 as well as 16-7N(G-C_{11}-K_{d4}-K_2)-16 and 0.015 mM of 16-7N(G-C_6-K_{d4}-K_2)-16. After adding the extraction solvent, the skin was homogenized using a probe homogenizer (PRO200 Homogenizer, PRO Scientific Inc., Oxford, Connecticut, USA). During homogenization, the sample was kept on ice to avoid overheating. Five extraction solvent protocols were evaluated as explained below.

5.3.4.1. *Liquid-liquid extraction protocols*

Modified Folch method

The analytes were extracted as described in the Folch protocol [26] with some modifications by the addition of 200 µL methanol containing the internal standards, followed by the addition of 400 µL chloroform. Then, the skin sample was homogenized in the presence of

ice to avoid overheating. High purity water (150 µL) was added to the homogenate to induce phase separation followed by pulse vortexing for a few seconds. The sample was centrifuged at 14,000 rpm for 10 min at room temperature to obtain separate aqueous and organic phases. The bottom organic phase was retrieved while the upper aqueous phase and the skin pellet were re-extracted by the addition of 400 µL chloroform as described above. The upper phase was discarded and both organic phases were combined, dried using a centrifugal evaporator, and stored at -80°C until analysis.

Modified Bligh and Dyer method (B&D)

The analytes were extracted by employing the Bligh and Dyer method with some modifications [27], by adding 80 µL high purity water, 200 µL methanol containing the internal standards and 100 µL chloroform to the skin tissue. Additional 100 µL chloroform was added, followed by 100 µL water while the sample was homogenized. Subsequently, the homogenate was centrifuged at 14,000 rpm for 10 min at room temperature. Similar to the modified Folch protocol, the lower organic layer was collected while the upper aqueous layer and the skin pellet were re-extracted with additional 200 µL chloroform. Finally, the organic layers were combined, dried with a centrifugal evaporator, and stored at -80°C.

Acidified/alkaline B&D method

The analytes and internal standards were extracted as described in the Bligh and Dyer protocol, except that either 2 µL of 3M hydrochloric acid [28] or 0.3% 12 M ammonium hydroxide [29] was added to the pre-homogenization mixture.

Modified methyl-tert-butyl ether (MTBE) method

The analytes were extracted as described [30], with modifications, by adding 200 µL methanol containing the internal standards, then 666 µL MTBE. Subsequently, the tissue sample was homogenized in the presence of ice to avoid overheating. Afterwards, phase separation was induced by adding 166 µL water followed by pulse vortexing for a few seconds. The homogenates were centrifuged for 10 min at 14,000 rpm then the upper organic layer was retrieved while the lower aqueous layer and the skin pellet were re-extracted by adding 666 µL MTBE. After final centrifugation, both organic phases were combined and dried before being stored at -80°C. Figure 5.3 summarizes the discussed liquid-liquid extraction protocols.

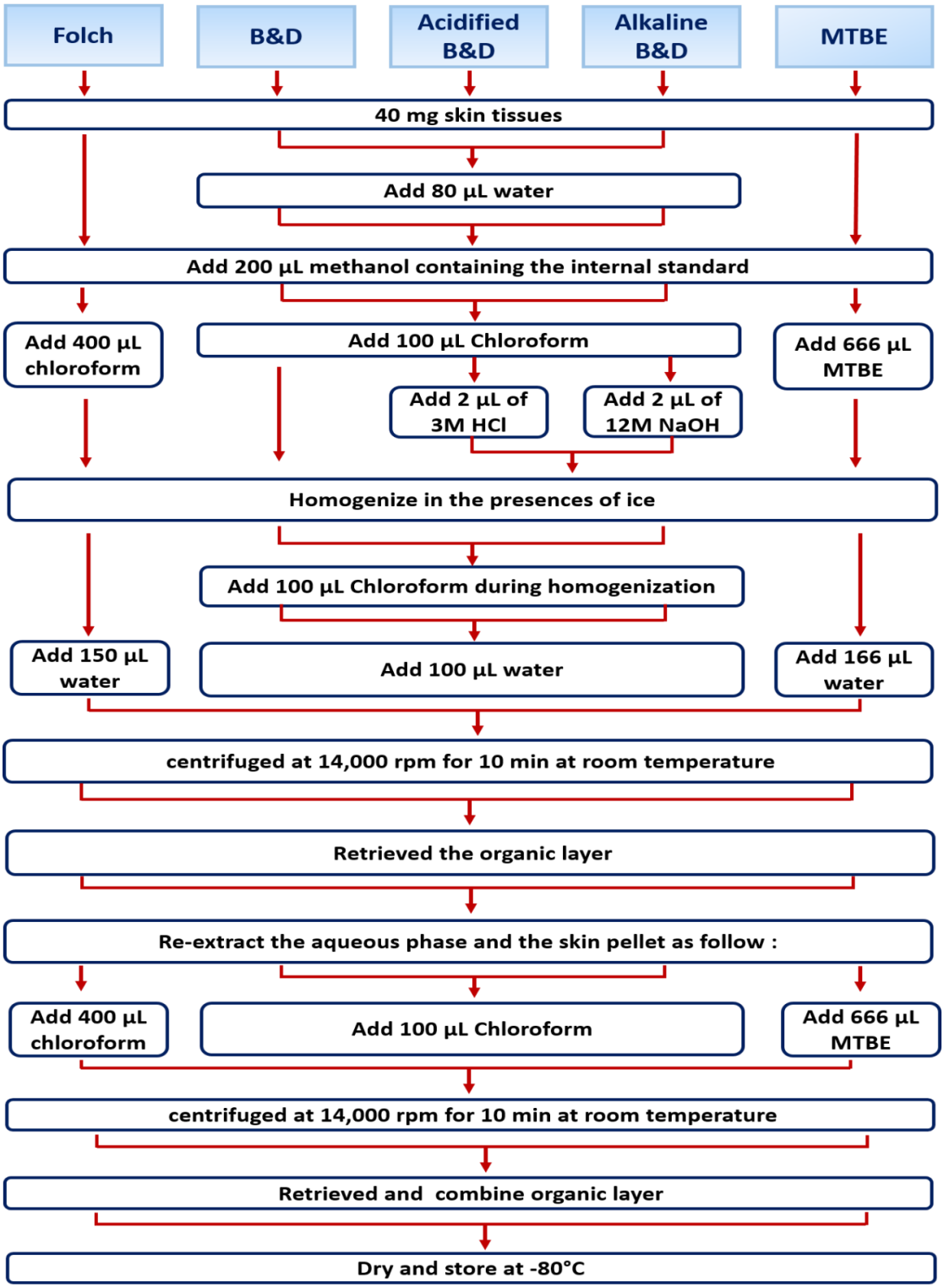

Figure 5.3. Flowchart summarizing the five evaluated liquid-liquid extraction methods.

5.3.4.2. *Solid phase extraction (SPE) protocol*

Extracts from each solvent system were solubilized in 3 mL methanol-water (50:50, v/v). The CBA cartridges were activated by successive additions of 3 mL methanol, 3 mL water, and 3mL methanol-water mixture (50:50, v/v). Subsequently, extracts were loaded into the cartridges followed by washing steps with 3 mL pure water and 3 mL methanol. Retained analytes and internal standards were eluted with 6 mL concentrated HCL-methanol (2:98, v/v). Finally, sample elutes were dried using a centrifugal evaporator and stored at -80°C.

Prior to MS analysis, extracted analytes were reconstituted in 3 mL methanol with 0.1% formic acid. Same procedure was followed to extract the analytes of interest from the PBS used in Franz cell's receptor compartment.

5.3.5. FIA-MS/MS instrumentation

FIA-MS/MS was performed on an Agilent 1290 infinity UHPLC (Agilent Technologies, Mississauga, ON, Canada) interfaced to an AB SCIEX QTRAP® 6500 triple quadrupole-linear ion trap mass spectrometer (QqLIT-MS) (AB SCIEX, Concord, ON, Canada). The mobile phase was optimized for each compound to achieve better ionization and peak shape. Isocratic mobile phase composed of acetonitrile/water mixture (50:50, v/v for 16-7N(G-K)-16 and 90:10, v/v for the rest of compounds) with 0.1% formic acid was delivered at a flow rate of 0.3 mL/min for a run time of 4 min. Sample aliquots of 1 µL were injected while maintaining the auto sampler temperature at 4 °C.

The AB SCIEX QTRAP® 6500 is equipped with a "Turbo V Ion Spray" ESI source, operated in the positive ion mode and set at 5500 V ionspray voltage. Optimal detection parameters for each analyte are listed in Table 5.1. The MS/MS data were obtained by low

energy collision-induced dissociation (CID) employing nitrogen as the collision gas. Multiple reaction monitoring (MRM) was selected as the scan mode to monitor the analytes and internal standards precursor ions to product ions transitions. Dwell time for all transitions was 150 ms at unit resolution. The monitored transitions and their MRM conditions are listed in Table 5.2. The structures of the monitored transitions are shown in Figure 5.2 as well as Figure S1, Appendix IV.

Table 5.1. Optimal detection parameters of the tested analytes on the AB SCIEX 6500 QTRAP® system.

Gemini Surfactants	**Curtain gas, CUR (psi)**	**Nebulizer gas, GS1 (psi)**	**Heater gas, GS2 (psi)**	**Collision gas, CAD (psi)**	**Source temperature (°C)**
16-7N(G-K)-16	45	50	80	10	700
16-7N(G-C_6-K_3)-16	45	60	60	11	700
16-7N(G-C_{11}-K_3)-16	45	70	90	10	600

Table 5.2. Conditions for MRM transitions of the gemini surfactants on AB SCIEX 6500 QTRAP® System.

Gemini surfactant	Transition (*m/z*)	DP (eV)	CE (eV)	CXE (eV)
16-7N(G-K)-16	411.4 → 276.9	151	27	10
	411.4→ 268.4	151	29	20
16-7N(G-K_{d4})-16	413.5 → 278.9	151	27	18
16-7N(G-C_6-K_3)-16	397.8 → 532.1	101	25	26
	397.8 → 268.2	101	33	10
16-7N(G-C_6-K_{d4}-K_2)-16	399.2 → 534.2	101	23	26
16-7N(G-C_{11}-K_3)-16	421.2 → 338.3	141	35	18
	421.2 → 378.4	141	23	18
16-7N(G-C_{11}-K_{d4}-K_2)-16	422.5 → 379.8	116	23	18

5.3.6. Preparation of standard solutions

In this work, two methods were developed for each gemini surfactant: *method A* to determine their presence in the skin tissues and *method B* to monitor their cumulative amount permeated into the PBS solution.

Method A:

Aqueous stock solutions of gemini surfactants and their internal standards were prepared at a concentration of 3mM and stored at -20 °C. Working stock solutions were prepared daily by serial dilution of the stock solutions in methanol to concentrations of 0.03 mM and 0.015 mM. One point calibration standards were prepared by adding 400 µL of 0.03 mM target analyte and

200 µL of 0.03 mM from the corresponding internal standards to 2.4 mL pooled blank skin tissue extract. The exception was with 16-7N(G-C_6-K_3)-16 gemini surfactants where 0.015 mM of the analyte and 0.015 mM IS were used, since the concentration of 16-7N(G-C_6-K_3)-16 in the skin was less than the other two compounds. The equivalent final mass concentration of the gemini surfactants and the corresponding internal standards are listed in Table S1, Supplementary Material.

Method B:

Aqueous stock solutions of gemini surfactants and their internal standards were prepared at a concentration of 3mM and stored at -20 °C. Working stock solutions were prepared daily by serial dilution of the stock solutions in methanol to concentrations of 3 µM and 1.5 µM. One point calibration standards were prepared by adding 60 µL of 3 µM target analyte (except for 16-7N(G-C6-K3)-16 gemini surfactants where 1.5 µM was used) and 40 µL of 3 µM from the corresponding internal standards (except for 16-7N(G-C_6-K_{d4}-K_2)-16 where 1.5 µM was used) to 200 µL blank PBS extract. The equivalent final mass concentration of the gemini surfactants and the corresponding internal standards are listed in Table S1, Appendix IV.

5.3.7. Method validation

The methods were partially validated with respect to selectivity, recovery, matrix effect, and process efficiency as recommended by the USFDA guidelines [31]. The performance of the methods was evaluated by statistically comparing the slope of the three-point calibration curves for three intra-run measurements.

5.3.8. Data analysis

Data processing for quantitative analysis was conducted using Analyst® software (Version 1.6.0). A sample concentration was obtained according to single point calibration mode using the following equation.

$$Conc\ (sample)\ = \frac{Peak\ Area\ Ratio\ (sample) \times Conc(Calibration\ Standard)}{Peak\ Area\ Ratio\ (Calibration\ Standard)} \quad (1)$$

The skin permeation parameters were calculated from the plot of cumulative amount of gemini surfactants permeated to the Franz diffusion cell's receptor compartment divided by 0.64 cm^2 to correct for the exposed skin area as a function of time. Steady-state flux (J_{ss}) was derived from the slope of the linear portion of the curve. The lag-time (t_{lag}) was estimated from the intercept of the tangent to the linear part of the absorption profile on the time axis. The permeability coefficient K_p was calculated using the following equation [32]:

$$K_p = \frac{J_{ss}}{C_{dose}} \quad (2)$$

where C_{dose} is the concentration of the applied dose.

Consequently, diffusion coefficient D_m and skin partition coefficient K_m could be calculated as follows:

$$D_m = \frac{d^2}{6 \times t_{lag}} \quad (3)$$

$$K_m = \frac{K_p \times d}{D_m} \quad (4)$$

where d is the measured skin thickness in cm.

5.3.9. Computational prediction

The gemini surfactants partition coefficient ($_c$log P), distribution coefficient ($_c$log D) at varying pH, and aqueous solubility ($_c$log S) were estimated using ACD/Physchem Profiler 2016 [33] (Advanced Chemistry Development, Inc., Toronto, ON, Canada).

5.3.10. Statistical analysis

Statistical analyses were performed using SPSS software (Version 24.0). One-way analysis of variance (ANOVA, Scheffé/Dunnett's post hoc tests) and Pearson's correlation were used for statistical analyses. Significant differences were considered at $p<0.05$ level.

5.4. Results and discussion

5.4.1. Method development

The major purpose of this work is to overcome an analytical challenge by developing simple and rapid MS-based methods for the detection and relative quantification of peptide-modified gemini surfactants in skin tissues as well as in PBS. Analytical strategies should meet the need of the experiment; in our work, a fit-for-the-purpose approach was adopted as it provides the needed data to drive future formulation decisions. The developed methods aim to track the distribution of topically applied gemini surfactant-based therapeutics and investigate the impact of structural variation on the efficiency of skin penetration.

LC-MS/MS is the most widely used platform for the quantification of pharmaceuticals in complex biological matrices, offering analyte separation and matrix effect reduction capabilities [20, 21]. Despite these advantages, LC-MS/MS significantly increases the overall analysis time and associated costs [34]. The sensitivity and selectivity of modern MS instruments and the evolution of efficient sample preparation techniques allow the development of simple analytical procedures [35, 36]. Direct introduction of the sample into the MS using FIA (i.e., loop injection) has emerged as an effective approach that offers a rapid sample possessing rate, low cost, and method simplicity [37]. It has been successfully applied in the quantitation of several analytes, including pharmaceuticals, environmental contaminants, and endogenous compounds [38-41]. Therefore, FIA-MS/MS methods were developed removing the need for chromatographic separation while relying on the MS separation capabilities. For each gemini surfactant, two methods were developed: *method A* to determine their presence in the skin and *method B* to monitor their cumulative amount permeated into the PBS.

To ensure adequate selectivity and specificity of the developed method, we capitalized on the QTRAP capability in the MRM scan mode. The MS operational parameters such as declustering potential (DP), collision energy (CE), and collision exit potential (CXP) were optimized as shown in Table 5.2 to maintain ion abundance and stability. Two diagnostic MRM transitions with relatively high abundance, listed in Table 5.2, were selected for each compound. To improve accuracy and precision, an isotopically labelled internal standard bearing four deuterium atoms was used for each compound. The use of 4 mass unit difference between the analyte and its corresponding internal standard prevents any cross talk. The proposed structure of the monitored product ions for each gemini surfactant and their internal standards are shown in Figures 5.2 and S1 (Appendix IV), respectively.

All tested compounds eluted before 0.8 min, as no column was used, with a total data acquisition time of 4 min (Figure 5.4A). No carryover was observed under the experimental conditions. This was significantly faster than the elution time in the recently developed HILIC-based LC-MS/MS quantification method in which second generation amine substituted gemini surfactants eluted at 7.12 min [30]. It is noteworthy that peptide-modified gemini surfactants are more polar than amine substituted gemini surfactants, hence, longer elution times are expected for peptide-modified gemini surfactants if the HILIC-MS/MS method was applied.

5.4.2. Selectivity

Selectivity of the developed methods was assessed by monitoring the existence of interfering peaks of the evaluated analytes and their internal standards in murine skin tissue extracts as well as in PBS solution from 6 different sources (data not shown). As shown in Figure 5.4 B and C, no interference from endogenous compounds against the selective bio-

determination of the gemini surfactants was observed in both double blank skin tissue extracts and PBS. The ratio of the quantifier to the identifier transition ions were also monitored showing less than 9% variations, indicating peak purity. The relative standard deviation (RSD) of the qualifier to the quantifier ratios was used as the acceptance criterion (less than 15%).

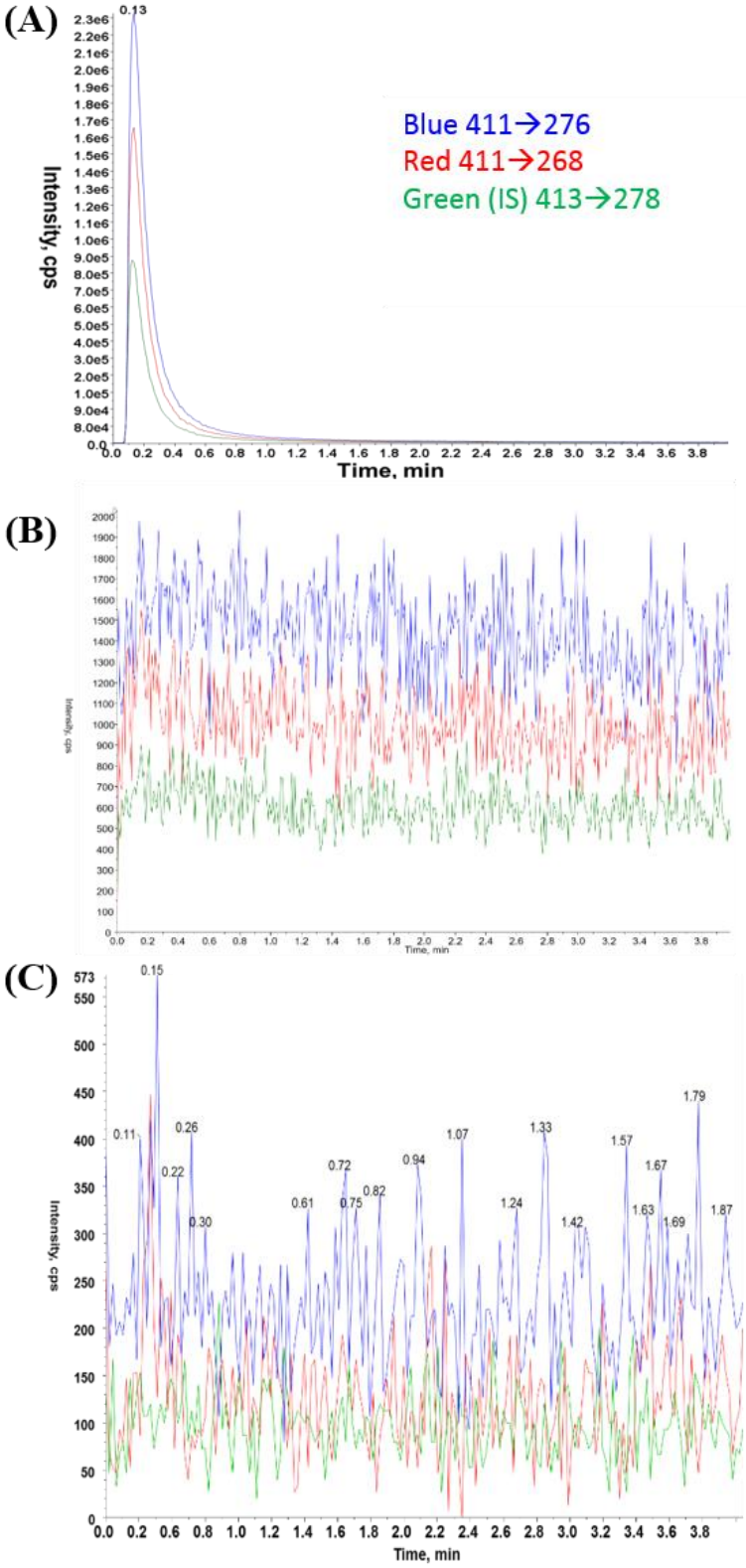

Figure 5.4. Representative FIA-MS/MS chromatograms of (A) skin tissue extract of 16-7N(G-K)-16 gemini surfactants, (B) double blank skin tissue extract, and (C) double blank PBS extract.

5.4.3. Sample preparation

Sample preparation represents one of the most critical steps for obtaining reliable and sensitive quantitative data [42]. As such, the ability to extract gemini surfactants from skin tissues was thoroughly assessed in this work using five common liquid-liquid extraction protocols, namely Folch [26], B&D [27], Acidified B&D [28], Alkaline B&D [29], and MTBE [30]. Extraction of gemini surfactants from skin tissues posed an analytical challenge due to the complexity of the skin matrix and the presence of a wide variety of interfering substances such as proteins, salts, and lipids [43]. In fact, the main challenge was the lipid-rich nature of skin tissues that caused significant matrix effects (data not shown) due to the high affinity of the endogenous lipids to the organic phase, similar to the target analyte, i.e., the gemini surfactants. Therefore, further purification was necessary to isolate gemini surfactants from the skin's endogenous lipids.

Since the skin is composed of a wide variety of lipid classes ranging from highly non-polar to polar lipids [44]; we capitalized on the gemini surfactants' unique feature, namely the two permanently charged quaternary amines to efficiently isolate them. Therefore, Bond Elute® CBA weak cationic exchange solid phase extraction (SPE) was used to purify extracts obtained from the liquid-liquid extractions. Bond Elute® CBA is a silica-based sorbent with a weak anion, carboxylic acid group, bonded to the surface. The carboxylic acid functional group has a *pKa* of 4.8 that is negatively charged at pH 6.8 and higher, allowing for strong ionic interaction with the positively charged nitrogen atoms of the gemini surfactants. Washing of the cartridges with non-acidic methanol and water was used to remove non-bonded skin lipids and other interfering substances. Finally, elution of the gemini surfactants was achieved by neutralizing the carboxylic acid functional group using acidified methanol (pH 2.8 and lower).

Recovery, matrix effect, and process efficiency were evaluated across the five extraction protocol according to Matuszewski *et al*. [45] equations as follow:

$$\%\ Recovery = \frac{Response\ \ pre-extraction\ spiked\ sample}{Response\ post-extraction\ spiked\ sample} \times 100 \quad (5)$$

$$\%\ Matrix\ effect = \frac{Response\ post-extraction\ spiked\ sample}{Response\ non-extracted\ neat\ sample} \times 100 \quad (6)$$

$$\%\ Process\ efficiency = \frac{Response\ \ pre-extraction\ spiked\ sample}{Response\ non-extracted\ neat\ sample} \times 100 \quad (7)$$

where the pre-extraction spiked sample refers to gemini surfactant standards added to the skin tissue before extraction and where samples were processed according to each liquid-liquid extraction procedure followed by purification with SPE. Response from the post-extraction spiked sample contains gemini surfactant standards added to the extracted blank tissues after passing through the SPE. The non-extracted neat sample contains the gemini surfactants added to the final reconstitution solvent (methanol with 0.1% formic acid). The determined value is the average for a set of triplicates.

Table 5.3 displays the effect of the extraction protocols on the recovery, matrix effect, and process efficiency. The Folch method resulted in the highest extraction efficiency in all gemini surfactants while MTBE displayed the lowest efficiency. The higher extraction efficiency of Folch compared to B&D methods was in agreement with the notion that the Folch protocol is more suited for extracting lipids from tissues, whereas B&D is more successful for biological fluids [46, 47]. Although both Folch and B&D methods are based on the biphasic chloroform-methanol-water mixtures, the Folch method uses a higher percentage of chloroform over methanol (Folch maintains the chloroform-methanol-water mixture at 8:4:3 while the B&D ratio is 2:2:1.8) [26, 27]. Chloroform is a widely used extraction reagent for analytes with intermediate

polarity such as gemini surfactants, while methanol is not an ideal extraction solvent since it is miscible with water. In fact, methanol is incorporated into the extraction mixture to disturb the interaction of the target analyte with the cellular biopolymers such as proteins, owing to its polarity and high dielectric constant [46]. Although methanol has recently been used as a monophasic extraction system for phospholipids in blood and polar lipids in the upper layer of human skin [48, 49], in our experiments, it showed no success in extracting gemini surfactants from the skin tissues (data not shown).

Adjustment of the pH in the B&D method is viewed as an effective way to optimize the extraction efficiency of specific classes of lipids [28, 29, 50]. In the case of gemini surfactants, higher recovery and less ion suppression were reported with alkaline B&D compared to conventional B&D, however the differences were not statistically significant (Table 5.3). Alkaline medium caused an increase in logD values and a decrease in logS values of the tested gemini surfactants (Table 5.4), resulting in their higher partition into the organic layer. In addition, the alkaline medium increases the polarity of the phosphate moiety of the skin natural lipids, which might increase their partition into the aqueous layer, minimizing interference with gemini surfactants.

Acidified B&D was the least effective method among the B&D methods; it exhibited the highest ion suppression. This could be attributed to the higher affinity of the endogenous lipids to the organic phase under acidic conditions resulting in significant ion suppression. The addition of HCl neutralizes the negatively charged skin lipids resulting in increased hydrophobicity, hence, higher unfavorable partition into the organic phase.

Extraction with MTBE was significantly the least effective among the evaluated extraction protocols (Table 5.3). This could be attributed to the lower polarity index of MTBE of 2.5 compared to chloroform of 4.1 [51]. MTBE was introduced as an alternative solvent system to chloroform that offered simplified sample handling [30]. It has a lower density than water and methanol, thus, it forms the upper layer during the extraction allowing for easier analyte collection. While it was suggested that extraction with MTBE is effective for most major classes of lipids, including polar and neutral lipids [30, 52], contradictory reports indicate that MBTE was only able to extract 10% of major polar lipids [53].

Comparison of the extraction efficiency among the three gemini surfactants revealed that 16-7N(G-C_{11}-K_3)-16 exhibited the highest recovery in all extraction methods, followed by 16-7N(G-K)-16, then 16-7N(G-C_6-K_3)-16 (Table 5.3). This trend was in accordance with the $_c$log P values of the gemini surfactants in which the higher the compound hydrophobicity, the higher its affinity into the organic phase, hence the higher the extraction efficiency (Table 5.4). However, while there is a major difference in the $_c$log P values between compound 16-7N(G-C_{11}-K_3)-16 and 16-7N(G-K)-16 (3.27 and 2.8 respectively), the differences in the extraction efficiency is not as dramatic. This could be explained by the higher number of terminal lysine moieties in compound 16-7N(G-C_{11}-K_3)-16 compared to 16-7N(G-K)-16 which exhibit higher affinity to bind to the negatively charged constituents of the skin. In fact, such speculation could explain the substantially low extraction efficiency of compound 16-7N(G-C_6-K_3)-16, which has three polar lysine residues and shorter hydrophobic spacer, conferring low lipophilicity to the molecule.

Since the modified Folch method demonstrated the highest process efficiency, it was selected as the liquid-liquid extraction method for the bioanalysis.

Table 5.3. Recovery, matrix effect, and process efficiency of the evaluated-peptide modified gemini surfactants using different liquid-liquid extraction protocol.

	Gemini surfactants								
	16-7N(G-K)-16			**16-7N(G-C_6-K_3)-16**			**16-7N(G-C_{11}-K_3)-16**		
Extraction Method	% Recovery	%Matrix effects	%Process efficiency	% Recovery	%Matrix effects	%Process efficiency	% Recovery	%Matrix effects	%Process efficiency
MTBE	51.80 ± 2	89.75± 6	56.67 ± 1	21.9 ± 3	75.29 ± 7	23.1 ± 5	53.98 ± 1	83.66±4	45.86 ± 0.8
Folch	85.32 ± 7	71.48 ±6	75.06 ± 5	46.04 ± 7	71.8 ± 1	38.28 ± 0.3	93.82 ± 5	74.63 ±5	77.09 ± 3
Blight&Dyer	74.18 ± 3	77.92± 4	69.01 ± 0.5	30.7 ± 1	53.44 ± 3	30.1 ± 0.8	76.57 ± 0.8	62.71± 2	60.88 ± 4
Acidify B&D	60.17 ± 3	67.7 ± 6	60.81 ±5	28.37 ± 2	46.09 ± 0.9	29.64 ± 1	63.65 ± 5	53.91 ± 8	55.97 ± 4
Alkaline B&D	77.60 ± 2	88 ± 1	73.18 ± 2	39.9 ± 1	68.49 ± 4	31.2 ± 1	80.7 ± 6	67.24 ± 4	60.77 ± 0.5

Table 5.4. Physicochemical properties of the evaluated gemini surfactants estimated using ACD/Physchem Profiler.

Physicochemical properties	Gemini surfactants		
	16-7N(G-K)-16	**16-7N(G-C_6-K_3)-16**	**16-7N(G-C_{11}-K_3)-16**
$_c$log P	2.80	1.28	3.27
$_c$log D at pH= 4	0.8	-2.7	-0.7
$_c$log D at pH= 6	1.0	-2.6	-0.6
$_c$log D at pH= 10	2.3	0.3	2.3
$_c$log S at pH= 4	-9.2	-7.6	-9.1
$_c$log S at pH= 6	-9.4	-7.7	-9.2
$_c$log S at pH= 10	-10.7	-10.6	-12.1

5.4.4. Single point calibration

Fully validated quantification methods are usually needed for preclinical and clinical analysis, however, they require considerable time, workload, and resources [54, 55]. In the case where full validation is not required, a "fit-for-the-purpose" approach is a more suited analytical strategy to obtain the needed data and is frequently used to answer predefined research questions [54], [56, 57]. One common quantification strategy is single-point calibration; considered a compromise between the rigor of the analytical method and the workload without sacrificing the accuracy of the results. In fact, several studies compared single point to conventional multi-point calibration showing the usefulness of single-point calibration in providing quantitative data with accuracy and precision that meet regulatory guidelines [58-60]. Since the scope of this work is to conduct a relative comparison among three gemini surfactants with varying transfection efficiencies; a one-point calibration quantitative strategy is deemed adequate to provide relative quantification data with acceptable accuracy and precision, effectively reducing the required time, resources, and cost of analysis.

In single point calibration, one reference concentration is employed for the quantification of the analyte of interest. However, two conditions must be fulfilled: (i) the concentration-response function is linear and (ii) the y-intercept is negligibly small [61]. In this work, a single concentration of gemini surfactants was selected to serve as a calibration standard for each method: *method A* and *method B* (Table S1, Appendix IV). The calibration standard was prepared in triplicate and the average response was used for quantification. The RSD values (i.e., precision) in all cases did not exceed 11%. The concentrations of selected calibration standards were relatively close to the concentration of the analytes in the skin tissue samples for *method A* and in the mid-range of the sample concentrations in the PBS solution (Table S1, Appendix IV).

The selection of each point was extrapolated from previous knowledge about the penetration behaviour of similar delivery vectors, which was then adjusted experimentally to best suit the method [62]. Although some studies suggest that the linearity condition for single point calibration can be avoided if the analyte amount in the evaluated samples is close to its amount in the calibration standard [61], the linearity over the samples' concentrations range was verified by developing a three-point calibration curve in the range of 1 µg/mL to 7 µg/mL for *method A* and of 50 ng/mL to 3000 ng/mL for *method B.* In order to assess the reliability and reproducibility of the methods, the slope of the three-point calibration curve for each method was statistically compared across at least three intra-run measurements. One-way analysis of variance comparison suggested that the variations between the evaluated slopes were not significantly different (p<0.05), indicating the reproducibility and reliability of the generated quantitative data.

5.4.5. Skin penetration study

The developed methods were used to assess the cutaneous deposition and penetration behaviour of the three peptide-modified gemini surfactants after the topical application of P/G/L nanoparticles. The selection of gemini surfactants was based on: (i) the variation in their molecular structure and (ii) their differences in transfection efficiency profiles. Namely, 16-7N(G-K)-16 was the lead compound with the highest transfection efficiency showing protein expression of 2.82 ±0.2 ng/ $15*10^3$ in PAM 212 murine keratinocytes. On the other hand, 16-7N(G-C_{11}-K_3)-16 demonstrated moderate transfection efficacy with protein expression of 1.73 ±0.2, while 16-7N(G-C_6-K_3)-16 had a low transfection ability of 1.09 ±0.1. The choice of the three compounds was based on a comprehensive evaluation of over 20 compounds (data not shown, manuscript in preparation). Table 5.5 displays the skin disposition and penetration parameters of the gemini surfactants obtained in accordance with the Organisation for Economic

Co-operation and Development (OECD) guideline for determining the dermal penetration of chemicals [32].

Table 5.5. Skin disposition and penetration parameters of the evaluated peptide-modified gemini surfactants. Results are the average of five measurements. Abbreviations: J_{ss}: the steady-state flux, t_{lag}: the lag-time, K_p: the skin permeability coefficient, D_m: diffusion coefficient and K_m: partition coefficient.

		Skin tissues		**Skin penetration parameter (receptor compartment)**						
Gemini Surfactants	**Applied dose (μg/cm²)**	**Amount in skin (μg/cm²) ± RSD (%)**	**% Deposit-ed in skin**	**Total amount penetrated across skin (μg/cm²) ± RSD (%)**	**% Penetrate-d across skin**	**J_{ss} (ng/cm²/h)**	**t_{lag} (h)**	**K*p* (cm/h)**	**D*m* (cm²/h)**	**K*m***
16-7N(G-K)-16	181.36	20.30± 4	11.19	0.99± 0.01	0.55	50.59	5.0	2.79×10^{-4}	2.70×10^{-4}	0.93
16-7N(G-C_6-K_3)-16	264.31	10.45± 3	3.95	0.28±0.02	0.11	13.67	5.5	0.52×10^{-4}	2.45×10^{-4}	0.19
16-7N(G-C_{11}-K_3)-16	277.46	22.25 ± 5	8.02	0.86± 0.02	0.31	43.48	5.3	1.57×10^{-4}	2.55×10^{-4}	0.55

After 24 h of topical application, FIA–MS/MS analysis of the skin tissues revealed that 3.95-11.19% of the applied dose of the three evaluated gemini surfactants was retained in the skin (Table 5.5). It is noteworthy that the detected amounts of gemini surfactants in the skin correlated with their transfection efficiency, where the lead compound 16-7N(G-K)-16 exhibited the highest skin deposition (11.19%) followed by 16-7N(G-C_{11}-K_3)-16 (8.02%) and the least performing compound 16-7N(G-K)-16 (3.95%). This could be explained by the gemini surfactants physicochemical properties, particularly lipophilicity and molecular size. In fact, it has been established in the literature that molecular size and hydrophobicity are the main determinants of dermal penetration suggesting that small hydrophobic compounds have a higher tendency to pass through the different layers of the skin [63, 64]. In the evaluated model compounds, the lead compound, 16-7N(G-K)-16, with the highest skin deposition had the smallest molecular size (M.Wt. 967.24 g/mol) among the tested compounds; in addition, it showed the highest lipophilicity ($_c$log D= 1.0) at the intrinsic pH of the formulation (pH=6, Table 5.4). However, while compound 16-7N(G-C_6-K_3)-16 has a smaller molecular size than 16-7N(G-C_{11}-K_3)-16, it exhibited significantly less residence in the skin tissues (Table 5.5). This could be attributed to the significantly lower $_c$log D value of the former (-2.7) compared to the latter (-0.6) at the formulation intrinsic pH of 6 (Table 5.4). This is in agreement with the reported trend in the literature where lower skin penetration is expected for compounds with higher molecular weight unless they have higher lipophilicity [65].

In addition to the lipophilicity and molecular size, several other parameters such as solubility might play a role in determining skin penetration ability. In the evaluated model compounds, skin penetration correlated negatively with the compounds' aqueous solubility ($_c$log

S at pH 6, Table 5.4). Lower aqueous solubility is usually associated with a higher ability to penetrate through the lipid-rich *stratum corneum* [66].

Finally, the physicochemical parameters of the P/G/L nanoparticles could also affect the dermal delivery. For example, small particle size and lower surface charge usually translate into higher skin penetration due to their superior ability to move through the complex skin matrix [67, 68]. Evaluation of the size and zeta potential of the P/G/L nanoparticles revealed that the lead compound, 16-7N(G-K)-16, exhibited the smallest particle size (85 ± 2 nm) and lowest zeta potential (34 ± 2 mV) among the tested compounds. On the other hand, compound 16-7N(G-C_{11}-K_3)-16 had a particle size of 96 ± 1 nm and a zeta potential of 44± 1 mV while 16-7N(G-C_6-K_3)-16 with the least skin disposition demonstrated the largest particle size and zeta potential, i.e., 107 ± 3 nm and 52 mV, respectively.

The cumulative amount of gemini surfactants that permeated across the skin into the receptor compartment increased progressively with time (Figure 5.5). After 24 h, only 0.11-0.55% of the applied dose was found in the Franz cell diffusion receptor compartment. This is an indication that the gemini surfactant-based gene delivery system could be suitable for the treatment of localized skin conditions like scleroderma or melanoma with minimum passing into the systematic circulation.

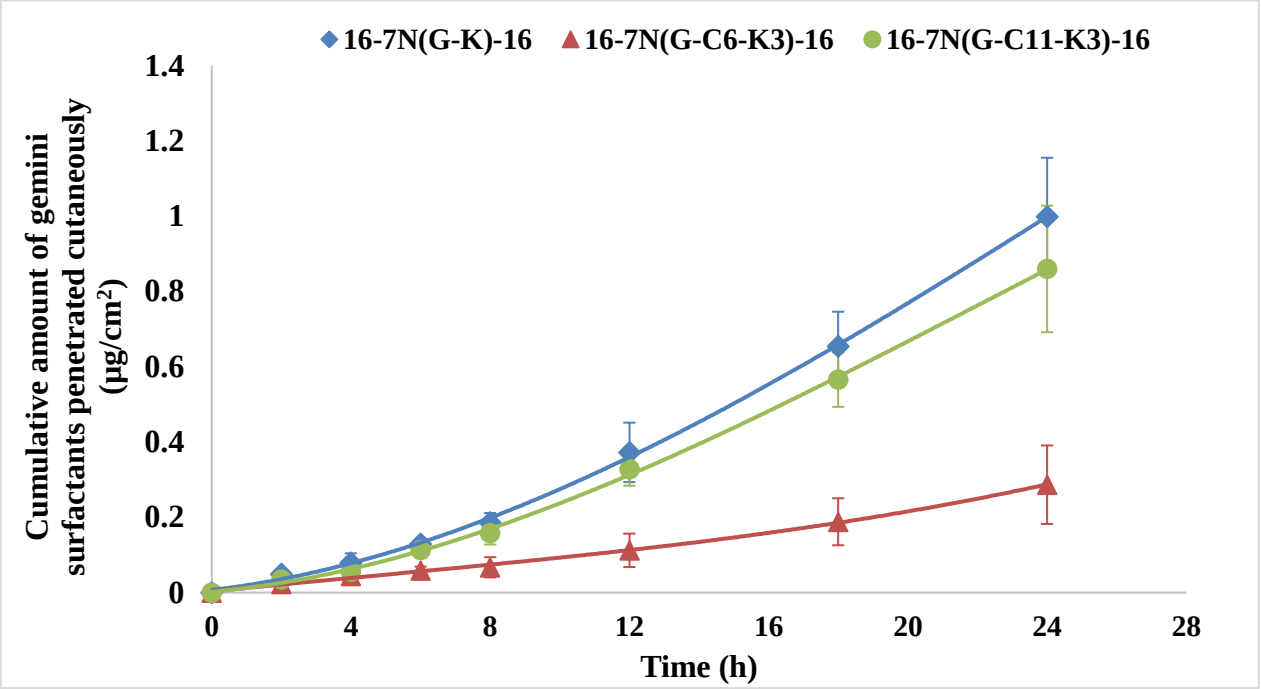

Figure 5.5: Cumulative amount of gemini surfactants (µg/cm^2) penetrated across the skin into the Franz cell diffusion receptor compartment versus time curves. Results are the average of five measurements, error bars represent standard deviation.

From the linear part of the curves plotted in Figure 5.5, the steady-state flux (J_{ss}), the lag-time (t_{lag}), the skin permeability coefficient (K_p), diffusion coefficient (D_m) and partition coefficient (K_m) were calculated (Table 5.5). The time required before the steady state absorption occurs denoted as t_{lag} was around 5 - 5.5 h for all compounds. The compound with the highest skin penetration 16-7N(G-K)-16 demonstrated the shortest t_{lag} of 5.0 h, followed by 16-7N(G-C_{11}-K_3)-16 (t_{lag} =5.3 h), and 16-7N(G-C_6-K_3)-16, with t_{lag}= 5.5 h (Table 5.5). Lag time is a reflection of the efficiency of the compound to pass through the different layers of the skin. Therefore, it is mainly influenced by the same parameters that determine skin permeability, namely lipophilicity, solubility, and molecular size [69]. While t_{lag} inversely correlated with the $_c$log D values at the formulation intrinsic pH, it directly correlated with $_c$log S values (Table 5.4). The gemini surfactants' net rate of transport, once equilibrium conditions have been reached, is

described by the steady-state flux (J_{ss}). Similar to t_{lag}, J_{ss} is a representation of the efficiency of the compounds to penetrate the skin. As such, J_{ss} is directly related to the total amount of gemini surfactants found in the Franz cell receptor compartment (Table 5.5).

The permeability coefficient (K_p), which depicts the rate at which gemini surfactants penetrate the skin, diffusion coefficient (D_m), and partition coefficient (K_m), are extracted from t_{lag} and Jss (equations 2-4), thereby showing a direct relationship with the compounds' hydrophobicity at the intrinsic pH, lipid solubility, and skin penetration ability (Table 5.4 and 5.5). Reporting these parameters is not only valuable for drug delivery but it is also of significant interest for assessing the toxicity and occupational risk of the gemini surfactants [70].

5.5 Conclusion

In this work, rapid and simple FIA-MS/MS methods were developed for the relative quantification of three peptide-modified gemini surfactants in skin tissues as well as PBS solution. Combining the Folch liquid-liquid extraction protocol with weak cationic exchange SPE enhanced the extraction efficiency of gemini surfactants from the complex lipid-rich skin tissues. As such, proper sample preparation (i.e., clean extracts) eliminated the need for HPLC column, resulting in fast analysis in which all compounds eluted before 0.8 min with a total acquisition time of merely 4 min. In addition, single-point calibration was successfully employed, resulting in a significant reduction in the required time and resources for method development and sample analysis.

The developed methods were applied to assess the skin deposition and skin penetration behavior of the evaluated gemini surfactants, generating data that could help in the design of more effective cutaneous lipid-based gene delivery vectors. The skin disposition and penetration

behavior of gemini surfactants heavily relied on their physicochemical properties, particularly their lipophilicity. Furthermore, it correlated with the transfection efficiency of the gemini surfactants. A favorable deposition in the skin with minimum escape into the PBS compartment (representing circulation) was observed, suggesting the feasibility of the delivery system in a topical application. The developed methods will be further utilized to probe the biodistribution and fate of topically applied therapeutic gemini surfactant formulations in animal models. Such knowledge is fundamental before any translation from laboratory to clinical evaluation.

5.6. Bibliography

1 DeStefano GM, Christiano AM. The genetics of human skin disease. Cold Spring Harbor perspectives in medicine 2014; 4: a015172.

2 Gorell E, Nguyen N, Lane A, Siprashvili Z. Gene therapy for skin diseases. Cold Spring Harbor perspectives in medicine 2014; 4: a015149.

3 Greenhalgh DA, Rothnagel JA, Roop DR. Epidermis: an attractive target tissue for gene therapy. Journal of investigative dermatology 1994; 103: 63S-9S.

4 Baroli B. Penetration of nanoparticles and nanomaterials in the skin: fiction or reality? Journal of pharmaceutical sciences 2010; 99: 21-50.

5 Geusens B, Strobbe T, Bracke S, Dynoodt P, Sanders N, Gele MV, *et al*. Lipid-mediated gene delivery to the skin. European Journal of Pharmaceutical Sciences 2011; 43: 199-211.

6 Hua S. Lipid-based nano-delivery systems for skin delivery of drugs and bioactives. Frontiers in pharmacology 2015; 6.

7 Rosenzweig HS, Rakhmanova VA, MacDonald RC. Diquaternary ammonium compounds as transfection agents. Bioconjugate chemistry 2001; 12: 258-63.

8 Menger FM, Littau C. Gemini-surfactants: synthesis and properties. Journal of the American Chemical Society 1991; 113: 1451-2.

9 Badea I, Verrall R, Baca-Estrada M, Tikoo S, Rosenberg A, Kumar P, *et al*. In vivo cutaneous interferon-γ gene delivery using novel dicationic (gemini) surfactant–plasmid complexes. The journal of gene medicine 2005; 7: 1200-14.

10 Badea I, Wettig S, Verrall R, Foldvari M. Topical non-invasive gene delivery using gemini nanoparticles in interferon-γ-deficient mice. European journal of pharmaceutics and biopharmaceutics 2007; 65: 414-22.

11 Badea I, Virtanen C, Verrall R, Rosenberg A, Foldvari M. Effect of topical interferon-γ gene therapy using gemini nanoparticles on pathophysiological markers of cutaneous scleroderma in Tsk/+ mice. Gene Therapy 2011; 19: 978-87.

12 Beloqui A, Solinís MA, Delgado A, Evora C, del Pozo-Rodríguez A, Rodríguez-Gascón A. Biodistribution of nanostructured lipid carriers (NLCs) after intravenous

administration to rats: influence of technological factors. European Journal of Pharmaceutics and Biopharmaceutics 2013; 84: 309-14.

13 James ML, Gambhir SS. A molecular imaging primer: modalities, imaging agents, and applications. Physiological reviews 2012; 92: 897-965.

14 Al-Dulaymi M, El-Aneed A. Tandem Mass Spectrometric Analysis of Novel Peptide-Modified Gemini Surfactants Used as Gene Delivery Vectors. Journal of Mass Spectrometry 2017.

15 Mohammed-Saeid W, Buse J, Badea I, Verrall R, El-Aneed A. Mass spectrometric analysis of amino acid/di-peptide modified gemini surfactants used as gene delivery agents: Establishment of a universal mass spectrometric fingerprint. International Journal of Mass Spectrometry 2012; 309: 182-91.

16 Donkuru M, Chitanda JM, Verrall RE, El-Aneed A. Multi-stage tandem mass spectrometric analysis of novel β-cyclodextrin-substituted and novel bis-pyridinium gemini surfactants designed as nanomedical drug delivery agents. Rapid Communications in Mass Spectrometry 2014; 28: 757-72.

17 Nilsson A, Goodwin RJ, Shariatgorji M, Vallianatou T, Webborn PJ, Andrén PE. Mass spectrometry imaging in drug development. Analytical chemistry 2015; 87: 1437-55.

18 Crotti S, Posocco B, Marangon E, Nitti D, Toffoli G, Agostini M. Mass spectrometry in the pharmacokinetic studies of anticancer natural products. Mass spectrometry reviews 2017; 36: 213-51.

19 Xu RN, Fan L, Rieser MJ, El-Shourbagy TA. Recent advances in high-throughput quantitative bioanalysis by LC–MS/MS. Journal of pharmaceutical and biomedical analysis 2007; 44: 342-55.

20 Korfmacher WA. Foundation review: principles and applications of LC-MS in new drug discovery. Drug discovery today 2005; 10: 1357-67.

21 Bakhtiar R, Majumdar TK, Tse FL. The Role of Liquid Chromatography–Mass Spectrometry in Pharmacokinetics and Drug Metabolism. HPLC for Pharmaceutical Scientists 2007: 605-40.

22 Buse J, Badea I, Verrall RE, El-Aneed A. A general liquid chromatography tandem mass spectrometry method for the quantitative determination of diquaternary ammonium

gemini surfactant drug delivery agents in mouse keratinocytes' cellular lysate. Journal of Chromatography A 2013; 1294: 98-105.

23 Donkuru M, Michel D, Awad H, Katselis G, El-Aneed A. Hydrophilic interaction liquid chromatography–tandem mass spectrometry quantitative method for the cellular analysis of varying structures of gemini surfactants designed as nanomaterial drug carriers. Journal of Chromatography A 2016; 1446: 114-24.

24 Al-Dulaymi MA, Chitanda JM, Mohammed-Saeid W, Araghi HY, Verrall RE, Grochulski P, *et al*. Di-Peptide-Modified Gemini Surfactants as Gene Delivery Vectors: Exploring the Role of the Alkyl Tail in Their Physicochemical Behavior and Biological Activity. The AAPS journal 2016; 18: 1168-81.

25 Foldvari M, Badea I, Wettig S, Verrall R, Bagonluri M. Structural characterization of novel gemini non-viral DNA delivery systems for cutaneous gene therapy. Journal of Experimental Nanoscience 2006; 1: 165-76.

26 Folch J, Lees M, Sloane Stanley G. A simple method for the isolation and purification of total lipids from animal tissues. J biol Chem 1957; 226: 497-509.

27 Bligh EG, Dyer WJ. A rapid method of total lipid extraction and purification. Canadian journal of biochemistry and physiology 1959; 37: 911-7.

28 Retra K, Bleijerveld OB, van Gestel RA, Tielens AG, van Hellemond JJ, Brouwers JF. A simple and universal method for the separation and identification of phospholipid molecular species. Rapid Communications in Mass Spectrometry 2008; 22: 1853-62.

29 Yatomi Y, Ohmori T, Rile G, Kazama F, Okamoto H, Sano T, *et al*. Sphingosine 1-phosphate as a major bioactive lysophospholipid that is released from platelets and interacts with endothelial cells. Blood 2000; 96: 3431-8.

30 Matyash V, Liebisch G, Kurzchalia TV, Shevchenko A, Schwudke D. Lipid extraction by methyl-tert-butyl ether for high-throughput lipidomics. Journal of lipid research 2008; 49: 1137-46.

31 Food U. Drug Administration FDA Guidance for Industry: Bioanalytical Method Validation. US Department of Health and Human, Services Food and Drug Administration. and Center for Drug Evaluation and Research 2001.

32 Jones A, Dick I, Cherrie J, Cronin M, Van de Sandt J, Esdaile D, *et al*. CEFIC workshop on methods to determine dermal permeation for human risk assessment. European Chemical Industry Council 2004: 1-86.

33 Advanced Chemistry Development I. ACD/Physchem Profiler 2016, <http://www.acdlabs.com/products/percepta/profilers.php> (2016).

34 Habchi B, Alves S, Paris A, Rutledge DN, Rathahao-Paris E. How to really perform high throughput metabolomic analyses efficiently? Trends in Analytical Chemistry 2016: 128-39.

35 Thomson B. Driving high sensitivity in biomolecular MS. 2012.

36 Bylda C, Thiele R, Kobold U, Volmer DA. Recent advances in sample preparation techniques to overcome difficulties encountered during quantitative analysis of small molecules from biofluids using LC-MS/MS. Analyst 2014; 139: 2265-76.

37 Nanita SC, Kaldon LG. Emerging flow injection mass spectrometry methods for high-throughput quantitative analysis. Analytical and bioanalytical chemistry 2016; 408: 23-33.

38 Mohammed-Saeid W, Michel D, Badea I, El-Aneed A. Rapid and Simple Flow Injection Analysis-Tandem Mass Spectrometric (FIA-MS/MS) Method for the Quantification of Melphalan in Lipid-Based Drug Delivery System. Rapid Communications in Mass Spectrometry 2017.

39 Nanita SC. High-throughput chemical residue analysis by fast extraction and dilution flow injection mass spectrometry. Analyst 2011; 136: 285-7.

40 Heux S, Fuchs TJ, Buhmann J, Zamboni N, Sauer U. A high-throughput metabolomics method to predict high concentration cytotoxicity of drugs from low concentration profiles. Metabolomics 2012; 8: 433-43.

41 Michel D, Gaunt MC, Arnason T, El-Aneed A. Development and validation of fast and simple flow injection analysis–tandem mass spectrometry (FIA–MS/MS) for the determination of metformin in dog serum. Journal of pharmaceutical and biomedical analysis 2015; 107: 229-35.

42 Clark KD, Zhang C, Anderson JL. Sample preparation for bioanalytical and pharmaceutical analysis . Analytical Chemistry 2016; 88: 11262-11270 ACS.

43 Freinkel RK, Woodley DT. The Biology of the Skin. (Taylor & Francis, 2001).

44 Nicolaides N. Skin Lipids: Their Biochemical Uniqueness. Science 1974; 186: 19-26.

45 Matuszewski B, Constanzer M, Chavez-Eng C. Strategies for the assessment of matrix effect in quantitative bioanalytical methods based on HPLC− MS/MS. Analytical chemistry 2003; 75: 3019-30.

46 Pati S, Nie B, Arnold RD, Cummings BS. Extraction, chromatographic and mass spectrometric methods for lipid analysis. Biomedical Chromatography 2016; 30: 695-709.

47 Schiller J, Süß R, Arnhold J, Fuchs B, Leßig J, Müller M, *et al*. Matrix-assisted laser desorption and ionization time-of-flight (MALDI-TOF) mass spectrometry in lipid and phospholipid research. Progress in Lipid Research 2004; 5: 449-88.

48 Zhao Z, Xu Y. An extremely simple method for extraction of lysophospholipids and phospholipids from blood samples. Journal of lipid research 2010; 51: 652-9.

49 Kindt R, Jorge L, Dumont E, Couturon P, David F, Sandra P, *et al*. Profiling and characterizing skin ceramides using reversed-phase liquid chromatography–quadrupole time-of-flight mass spectrometry. Analytical chemistry 2011; 84: 403-11.

50 Nishihara M, Koga Y. Extraction and composition of polar lipids from the archaebacterium, Methanobacterium thermoautotrophicum: effective extraction of tetraether lipids by an acidified solvent. The Journal of Biochemistry 1987; 101: 997-1005.

51 Solvent Polarity Index, <http://macro.lsu.edu/HowTo/solvents/Polarity%20index.htm>. Accessed January 2018

52 Chen S, Hoene M, Li J, Li Y, Zhao X, Häring H-U, *et al*. Simultaneous extraction of metabolome and lipidome with methyl tert-butyl ether from a single small tissue sample for ultra-high performance liquid chromatography/mass spectrometry. Journal of Chromatography A 2013; 1298: 9-16.

53 Kuyukina MS, Ivshina IB, Philp JC, Christofi N, Dunbar SA, Ritchkova MI. Recovery of Rhodococcus biosurfactants using methyl tertiary-butyl ether extraction. Journal of Microbiological Methods 2001; 46: 149-56.

54 Tan A, Awaiye K, Trabelsi F. Some unnecessary or inadequate common practices in regulated LC–MS bioanalysis. Bioanalysis 2014; 6: 2751-65.

55 Lang J, Bolton S. A comprehensive method validation strategy for bioanalytical applications in the pharmaceutical industry—1. Experimental considerations. Journal of pharmaceutical and biomedical analysis 1991; 9: 357-61.

56 Lee JW, Devanarayan V, Barrett YC, Weiner R, Allinson J, Fountain S, *et al*. Fit-for-purpose method development and validation for successful biomarker measurement. Pharmaceutical research 2006; 23: 312-28.

57 Cummings J, Raynaud F, Jones L, Sugar R, Dive C. Fit-for-purpose biomarker method validation for application in clinical trials of anticancer drugs. British journal of cancer 2010; 103: 1313.

58 Peters FT, Maurer HH. Systematic comparison of bias and precision data obtained with multiple-point and one-point calibration in six validated multianalyte assays for quantification of drugs in human plasma. Analytical chemistry 2007; 79: 4967-76.

59 Fornal E, Stachniuk A. Application of a truly one-point calibration for pesticide residue control by liquid chromatography–mass spectrometry. Journal of Chromatography B 2012; 901: 107-14.

60 Bjørk MK, Nielsen MK, Markussen LØ, Klinke HB, Linnet K. Determination of 19 drugs of abuse and metabolites in whole blood by high-performance liquid chromatography–tandem mass spectrometry. Analytical and bioanalytical chemistry 2010; 396: 2393-401.

61 Cuadros-Rodríguez L, Bagur-González MG, Sánchez-Vinas M, González-Casado A, Gómez-Sáez AM. Principles of analytical calibration/quantification for the separation sciences. Journal of Chromatography A 2007; 1158: 33-46.

62 Foldvari M, Baca-Estrada ME, He Z, Hu J, Attah-Poku S, King M. Dermal and transdermal delivery of protein pharmaceuticals: lipid-based delivery systems for interferon α. Biotechnology and applied biochemistry 1999; 30: 129-37.

63 Cross SE, Magnusson BM, Winckle G, Anissimov Y, Roberts MS. Determination of the effect of lipophilicity on the in vitro permeability and tissue reservoir characteristics of topically applied solutes in human skin layers. Journal of Investigative Dermatology 2003; 120: 759-64.

64 Potts RO, Guy RH. Predicting skin permeability. Pharmaceutical research 1992; 9: 663-9.

65 Moss GP, Dearden JC, Patel H, Cronin MT. Quantitative structure–permeability relationships (QSPRs) for percutaneous absorption. Toxicology in Vitro 2002; 16: 299-317.

66 Kasting GB, Smith RL, Cooper E. Effect of lipid solubility and molecular size on percutaneous absorption. Pharmacol Skin 1987; 1: 138-53.

67 Verma DD, Verma S, Blume G, Fahr A. Particle size of liposomes influences dermal delivery of substances into skin. International journal of pharmaceutics 2003; 258: 141-51.

68 Gillet A, Compère P, Lecomte F, Hubert P, Ducat E, Evrard B, *et al*. Liposome surface charge influence on skin penetration behaviour. International journal of pharmaceutics 2011; 411: 223-31.

69 Bo Nielsen J, Ahm S⊘ rensen J, Nielsen F. The usual suspects—influence of physicochemical properties on lag time, skin deposition, and percutaneous penetration of nine model compounds. Journal of Toxicology and Environmental Health, Part A 2009; 72: 315-23.

70 Cronin MT, Jaworska JS, Walker JD, Comber MH, Watts CD, Worth AP. Use of QSARs in international decision-making frameworks to predict health effects of chemical substances. Environmental Health Perspectives 2003; 111: 1391.

CHAPTER 6

General Discussions

6.1. General discussion

Gene therapy has emerged as a promising biotherapeutic approach aimed at improving health and combating diseases. In order to realize the full benefit of gene therapy, an effective gene delivery vector must overcome complex tissue and cellular barriers to deliver the therapeutic DNA into the targeted site efficiently without toxic side effects [1]. Gemini surfactants are entering the mainstream as an effective class of non-viral gene delivery carriers [2-4]. Their unique molecular structure offer enhanced nucleic acid packaging abilities, promoting the assembly into nano-sized lipoplexes that favour cellular internalization [5]. Research efforts capitalized on bottom-up design flexibility of gemini surfactants to produce new compounds capable of conquering numerous biological barriers. Over the past two decades, several structural designs of gemini surfactants have emerged and were successfully utilized in the delivery of genetic materials both *in vitro* and *in vivo* [6-9].

Despite their promising results [8-10], the transfection efficiency of gemini surfactants is still insufficient to encourage their translation into clinical applications. Moreover, concerns regarding the biocompatibility and biodegradability of gemini surfactants have recently been expressed [11]. Therefore, there is a need to design novel compounds capable of driving proficient expression of therapeutic genes without disrupting normal cell functions; such tasks can be achieved through rational modification of the basic structure of gemini surfactants. As such, my research evaluated, for the first time, a series of 22 peptide-modified gemini surfactants and conducted a systematic investigation of their physicochemical properties, cytotoxicity, transfection efficiencies, and tissue localization. My main goal was to assess the structure-

activity relationship of the new compounds and to identify the fundamental architectural characteristics required for efficient and safe gene delivery.

Cutaneous gene delivery is an attractive approach for treating various dermatological disorders with minimal systemic side effects [12]. The potential of gemini surfactant-based lipoplexes in delivering genetic material into the skin was previously evaluated, demonstrating their feasibility in overcoming skin barrier functions [6, 7, 13]. Upon topical application, gemini surfactants distribute within various skin layers and cellular compartments. While many studies focused on the development of new DNA carriers monitoring gene expression and overall toxicity, the fate and distribution of the delivery agent per se in the biological system has not been fully explored. In-depth understanding of the behavior of gemini surfactants in complex biological environments is essential for developing efficient and safe gene delivery systems. Therefore, my research also evaluated the skin deposition and penetration behaviour of three representative examples of the peptide-modified gemini surfactants. The selection of the representative compounds was based on variation in their chemical structure as well as differences in their transfection efficiency profiles. The purpose was to correlate the skin penetration efficiency to the compounds' architectural characteristics, physicochemical properties and transfection efficiency profiles.

In order to determine the skin deposition and penetration behaviour of the peptide-modified gemini surfactants, a robust and sensitive bioanalytical method is required. The lack of any chromophore or fluorophore on the gemini surfactants and the existence of two permanently charged quaternary amine groups made mass spectrometry (MS) an ideal technique for the detection and quantification of gemini surfactants in complex biological matrices [14-17]. Therefore, understanding the collision induced dissociation-tandem mass spectrometric

behaviour (CID-MS/MS) of peptide-modified gemini surfactants is needed to ensure selective and specific identification of the gemini surfactants in the complex lipid-rich skin tissues. It also allows for the development of targeted quantification methods by choosing suitable diagnostic product ions. Accordingly, my research project assessed the MS/MS fragmentation behaviour of eleven compounds of the peptide-modified gemini surfactants. The generated data was later utilized to develop a multiple reaction monitoring (MRM) quantification method to assess the skin deposition and penetration behaviour of topically applied therapeutic gemini surfactant formulations.

6.1.1. Molecular engineering of peptide-modified gemini surfactants

The design of a new generation of peptide-modified gemini surfactants was motivated by the good transfection efficiency and relatively low cell toxicity of the previously developed amino acid-substituted gemini surfactant-based lipoplexes [18, 19]. Strategic modifications to the conjugated amino acid sequence grafted onto the spacer were carried out (Figure 3.2). Notably, we evaluated the impact of increasing the number of the terminal lysine moieties (Figure 3.2, compounds 1-3), considering the previous research findings that suggest the importance of terminal lysine moiety positioned on the spacer of gemini surfactant-based lipoplexes [19, 20]. To the best of our knowledge, such compounds represent the first dendrimer-like gemini surfactants. In addition, we evaluated the impact of altering the distance between the terminal lysine moieties and the quaternary ammonium head groups by incorporating a hydrocarbon linker of either a hexyl or undecyl chain (Figure 3.2, compounds 4-7). Finally, the effects of removing the glycine moiety grafted on the spacer while conjugating the hydrocarbon linker directly onto the spacer was investigated (Figure 3.2, compounds 8-11).

In general, the incorporation of peptides into the gemini surfactants spacer region improved transfection efficiency and reduced cytotoxicity. In particular, lipoplexes of the lead compound, 16-7N(G-K)-16, exhibited an 8-fold increase in the level of protein secretion in PAM 212 and a 20% increase in cell viability compared to the first-generation unsubstituted gemini surfactants (Figures 3.8 and 3.9) [6]. Peptides are biocompatible and biodegradable structural motifs that render conformational flexibility to the gemini surfactants. They allow for a balanced binding properties with the nucleic acid which mediate both DNA compaction and subsequent release [19]. Moreover, the addition of peptides induced a pH-dependent increase in particle size and zeta potential (Figure 2.5), producing "intelligent" nanoparticles that respond to endosomal acidification to avoid lysosomal degradation [20]. Finally, the presence of terminal amino groups in the peptide backbone imparted a higher positive charge to the modified compounds, hence fewer gemini surfactant molecules are required to neutralize and compact the DNA. This was manifested by the lower optimal N/P ratio of 2.5 for peptide-modified gemini surfactants relative to N/P of 10 for first-generation unmodified gemini surfactants (Figure 2.2) [6].

Contrary to the theoretical expectations, increasing the number of terminal lysine moieties added into the spacer from mono- to tri- then to hepta-lysine residues resulted in reduction in the transfection efficiency and cell viability (Figure 3.8 and 3.9). Such observations are attributed to the collective effect of (i) increasing charge density, (ii) decreasing hydrophobicity and (iii) changing the compounds' geometry. Both charge density and hydrophobicity play a role in the interaction with the DNA through the electrostatic and cooperative hydrophobic interactions [21]. Therefore, a balance between optimal charge density and hydrophobicity is needed to compact the DNA, maintain the stability of the complex during the delivery process, and facilitate the release of the DNA from the endosomal compartments. In

addition, a higher charge density of the compounds resulted in a higher zeta potential of the P/G/L nanoparticles (Table 3.2). Higher cationic charge is associated with greater tendency of rupturing the cell membrane and causing cell death [22].

With the increase in the number of amino acids in the peptide, the geometry of the gemini surfactants' molecular shape transformed from compounds that prefer negative membrane curvature to compounds that favor positive curvature (Figure 3.3). This is mainly due to increasing the bulkiness of the functional groups incorporated into the spacer that caused an enlargement in the head group area of the compounds, altering their molecular packing parameter (Table 3.1). The supramolecular assembly of the lipoplexes is highly dependent on the molecular packing parameter of its lipid components. In particular, compounds with molecular shapes that support the formation of a negative interfacial curvature exhibited greater tendency of maintaining the inverted hexagonal phase (H_{II}) assembly (Figure 3.7), resulting in higher transfection efficiency (Figure 3.8). On the other hand, compounds that favor the formation of positive interfacial curvature distorted the H_{II} phase at lower concentration of the gemini surfactants ($N/P \geq 5$) and demonstrated lower transfection efficiency (Figures 3.7 and 3.8).

The impact of incorporating a hydrocarbon linker into the peptide chain on the transfection efficiency and cytotoxicity profile was dependant on the number of amino acids in the peptide chain. While the addition of a hydrocarbon linker reduced the transfection efficiency of compounds with di-peptides, it enhanced the transfection of those with greater number of amino acids (Figure 3.8). Furthermore, the incorporation of the hydrocarbon linker increased the cytotoxicity of compounds with di-peptides; however, the reverse was observed for compounds with hepta-lysine residues (Figure 3.9). Coupling hydrophobic linkers to compounds with a

mono-lysine moiety caused an unfavorable increase in their hydrophobicity, which resulted in higher cytotoxicity [23]. Vectors with high hydrophobicity could also cause a stronger interaction with the pDNA, hindering its subsequent release. On the contrary, the incorporation of a hydrocarbon linker to compounds with hepta-lysine residues resulted in favorable increases in hydrophobicity that prompted a balanced binding with the pDNA and better stability of the lipoplexes during the delivery process (Table 3.1). The decrease in cell toxicity is also attributed to the role of the hydrophobic linker in shielding the excess positive charges of the terminal lysine residues as attested by the lower zeta potential of the lipoplexes (Table 3.2). Removing the glycine moiety while incorporating a hydrocarbon linker directly into the spacer did not result in any obvious changes (Figure 3.8). This was in agreement with previously reported behaviors of mono- and di-amino acid-modified gemini surfactant-based lipoplexes [19].

The introduced series of peptide-modified gemini surfactants also examined the role of the alkyl tails on transfection efficiency. In particular, three hydrophobic tails that differ in their length and degree of unsaturation were evaluated; namely dodecyl, hexadecyl and oleyl (Figures 2.1A and 3.2). *In vitro* evaluation revealed that the highest transgene activity was observed in compounds with hexadecyl tails (Figures 3.8). In fact, it showed a 5-10 fold increase in the level of reporter protein in compounds with di-peptides compared to its analogues with dodecyl and oleyl carbon-tail evaluated in a COS-7 cell-line (Figures 2.2). These observations are linked to the: (i) hydrophobicity of the compounds' and (ii) geometry of the compounds' tails relative to that of the helper lipid. Firstly, hexadecyl tails are more hydrophobic than dodecyl ones, rendering a lower CMC value that will increase the stability of the lipoplexes during the delivery process [24]. Secondly, the geometry of the alkyl tail controls the membrane fluidity of the nanoparticle, which impacts critical steps such as membrane fusion and endosomal escape [25].

The geometry of unsaturated hydrophobic tails hampers the packing of lipids at the molecular level, conferring a higher membrane fluidity relative to saturated tails [151, 152]. Therefore, mixing unsaturated lipids with the helper lipid, DOPE, which is also composed of an unsaturated hydrophobic tail, might result in a loose packing arrangement of the P/G/L lipoplexes. Accordingly, formulations prepared by mixing a saturated and unsaturated lipid together resulted in the highest transfection efficiency compared to formulations prepared from mixing either two saturated or two unsaturated lipids [26].

In summary, a balance between the hydrophilic and hydrophobic features of the peptide-modified gemini surfactants lead to parameters conducive to the gene delivery process. My work lays a foundation for the advancement of peptide-based gemini surfactants towards clinical applications.

6.1.2. Mass spectrometric analysis of peptide-modified gemini surfactants

Mass spectrometric analysis of the peptide-modified gemini surfactants was conducted to (i) confirm their projected molecular composition, (ii) assess their MS/MS dissociation behaviour and (iii) identify unique diagnostic product ions for each compound. This was achieved by using a combination of high-resolution single-stage (MS), tandem (MS/MS) and multi-stage (MS^3) analysis. While a hybrid quadrupole orthogonal time-of-flight mass spectrometer (QqToF-MS) was used to conduct single-stage MS analysis, a triple quadrupole-linear ion trap mass spectrometer (QqQLIT-MS) was used to perform tandem and multi-stage MS analysis. Both instruments were operated in the positive ionization mode and were equipped with electrospray ionization (ESI).

High-resolution single-stage MS analysis confirmed the projected molecular structure of the 11 evaluated peptide-modified gemini surfactants by assessing their exact masses (Table S1, Appendix III). Two-point external calibration prior to the analysis of the peptide-modified gemini surfactants produced mass accuracies of less than 8 ppm, which were comparable to those attained using internal calibration in a previous work by our group that assessed mono-amino acid and di-amino acid-substituted gemini surfactants [27]. The generation of compound-specific product ions upon MS/MS analysis authenticated the chemical structure of their precursor ions (Tables 4.1 and 4.2). Further confirmation of the genesis of the produced product ions was achieved by MS^3 analysis (Table S2, Appendix III). Such a comprehensive analysis allowed for the development of compound-specific CID-MS/MS fingerprint for rapid and accurate identification of these compounds in complex matrices (Figure 4.2).

MS/MS analysis of the peptide-modified gemini surfactants revealed that the presence of amino acids on the compounds structure defined peptide-related dissociation characteristics, which was remarkably different compared to traditional gemini surfactants [14, 28]. In particular, the formation of pipecolic acid at the N-terminus part of the gemini surfactants was a unique observation for these structural family. It resulted from the neutral loss of ammonia on the amino acids' side chain (Figure S1, Appendix III). Furthermore, a protonated α-amino-ε-caprolactam ion and its complimentary c-terminus ion was generated as a result of an amide bond cleavage initiated by a nucleophilic attack of the lysine side chain (Figure 4.3). The compounds also demonstrated a typical gemini surfactants dissociation pattern such as the elimination of one or both of the quaternary aminium head groups and the attached aliphatic tail (Figures 4.5- 4.7).

Structural features such as the length of the inserted hydrocarbon linker and the number of terminal amino acid residues determined the dissociation behaviour. For instance, gemini surfactants with a longer hydrophobic linker chain (C_{11}) and with tri-terminal amino acids residues were the only compounds that produced the triply charged initial product ions after the elimination of a terminal lysine moiety (Figure 4.4). However, similarities in the dissociation behaviour of peptide-modified gemini surfactants allowed for the establishment of a universal MS/MS fragmentation pathway (Figure 4.9). Such a pathway could be applied to predict the dissociation behaviour of new families of compounds with similar general structural features. The generated MS/MS data was utilized for the development of targeted MRM quantification methods to probe the skin deposition and penetration behaviour of topically applied gemini surfactant-based formulations.

6.1.3. Cutaneous distribution of peptide-modified gemini surfactants

The success of developing efficient and safe gemini surfactant-based gene delivery systems for cutaneous application requires a thorough understanding of their skin deposition and penetration behaviour. Furthermore, correlating the behaviour of gemini surfactants in complex biological environments to their structural features and transfection efficiency is an essential aspect in guiding the design of future gemini surfactants. Therefore, skin penetration and deposition behaviour of three structurally distinct peptide-modified gemini surfactants (Figure 5.2) with varying transfection efficiency profiles were evaluated on CD1 mice dorsal skin tissue mounted in a Franz diffusion cell. After 24 h of topical application, the remaining gemini surfactant-based formulation in the Franz cell's donor chamber were discarded, while the skin

tissues and the PBS in the receptor compartment (mimicking blood circulation) were collected for MS analysis.

The first step in the analysis process is the selection of an appropriate sample preparation approach to extract gemini surfactants from the skin tissues as well as the PBS. Skin as a matrix posed an analytical challenge due to the presence of a wide variety of interfering substances such as proteins, salts and skin endogenous lipids. The latter group, in particular, required careful consideration owing to the resemblance in their structure and physicochemical properties to the gemini surfactants. Such a challenge emphasized the importance of optimizing sample preparation to obtain reliable and reproducible data. Accordingly, extraction of the gemini surfactants from the skin followed three steps: (i) tissue homogenization, (ii) liquid-liquid extraction and (iii) purification using solid phase extraction (SPE).

I conducted systematic evaluation of extraction procedures for the gemini surfactants using five liquid-liquid extraction protocols (Figure 5.3): Folch [29], B&D [30], Acidified B&D [31], Alkaline B&D [32] and MTBE [33]. The Folch method achieved the highest extraction efficiency for all compounds (Table 5.3). This was attributed to the presence of a higher ratio of chloroform in the Folch method that has an intermediate polarity (polarity index of 4.1), making it suitable to extract the gemini surfactants [34]. Extraction with MTBE was the least effective in all compounds (Table 5.3), probably due to its low polarity index of 2.5 [34]. Finally, weak cationic exchange SPE was efficient in isolating the positively charged gemini surfactants from endogenous skin lipids, minimizing matrix effects. The same SPE procedure was used to extract gemini surfactants from the PBS solution.

The development of an efficient sample preparation strategy eliminated the need for chromatographic separation, allowing direct introduction of the sample into the MS using flow injection analysis (FIA). This offered simplicity and rapid sample processing in which the total acquisition time was merely 4 min (Figure 5.4A). The elution time at 0.8 min was about 9 times faster than even less polar compounds (amine substituted gemini surfactants) in the recently developed HILIC-based LC-MS/MS quantification method [17]. By selecting two diagnostic product ions with relatively high abundance (Table 5.2), we capitalized on the QTRAP capability in the MRM scan mode to achieve adequate selectivity and specificity (Figure 5.4 B and C). Furthermore, the use of an isotopically labelled internal standard bearing four deuterium atoms for each compound prevented any cross talk, improving accuracy and precision. Since the aim of this work is to conduct a relative comparison among three gemini surfactants, a single point calibration technique was selected to develop the quantitative approach. Such a strategy also reduced the required time and cost of analysis compared to the traditional multi-point calibration [35]. For each compound, two methods were developed for their detection and relative quantification in skin tissue and in PBS solution.

FIA-MS/MS analysis revealed that the three assessed peptide-modified gemini surfactants were detected in the skin with minimal partition into the PBS compartment, suggesting the suitability of the delivery system to be used for topical application. (Table 5.5). Their skin deposition and penetration behaviour was dependent on the lipophilicity and molecular weight of the compounds. Furthermore, the physicochemical parameters of the P/G/L nanoparticle such as size and zeta potential affected the dermal penetration where smaller particle size and low zeta potential resulted in higher penetration.

6.2. Conclusion

Peptide-modified gemini surfactants showed a potential as an effective gene delivery system for the treatment of fibrotic skin conditions. A balance between the hydrophilic and hydrophobic characteristics of the gemini surfactants is essential since it produces physicochemical parameters conducive to the gene delivery process. Furthermore, geometrical consideration of the compounds controls their transfection efficiency. The number of terminal amino acids and the length of the hydrocarbon linker drove the MS/MS dissociation behavior of the compounds. The lipophilicity and molecular weight of the compounds were the main determinants of their skin deposition and penetration behavior. My results indicated a direct correlation between the skin penetration ability and the transfection efficiency profile. This work identifies some of the fundamental structural requirements (mono lysine residue and absence of hydrocarbon linker) needed for efficient gene delivery vehicle, providing a framework for future development of peptide-modified gemini surfactant-based gene delivery system.

6.3. Future directions

The ultimate goal of my research is to develop a more efficient and less toxic gemini surfactant-based gene delivery system with potential application in the treatment of fibrotic skin conditions. The introduced peptide-modified gemini surfactant-based lipoplexes demonstrated an enhanced transfection efficiency and reduced cytotoxicity. In addition, gemini surfactants showed a favorable deposition in the skin with minimum penetration into the receptor chamber (representing circulation), suggesting the feasibility of the delivery system to be used for topical application. The promising results of my research lay a foundation for future research directions

to focus on translating the gemini surfactant-based gene delivery system into clinical applications.

The extensive physicochemical characterization of the 22 peptide-modified gemini surfactant-based lipoplexes conducted in my research provided information about the fundamental requirements for efficient gene delivery system. However, further characterization could allow for the determination of other essential characteristics. This includes the use of circular dichroism and atomic force microscopy to assess the interaction of gemini surfactants with the pDNA and the shape of the lipoplexes. In addition, the use of grazing-incidence small-angle scattering (GISAS) will evaluate the effects of structural variations on the interaction of the delivery system with a cell membrane model. The effect of structural variation of the peptide-modified gene delivery system on the method of cellular entry should also be evaluated.

Evaluation of the transfection efficiency of the gene delivery system *in vitro* represents an excellent start for the screening of novel vectors. However, it does not account for the complications associated with the *in vivo* environment. Therefore, the developed peptide-modified gemini surfactant-based gene delivery systems should be further evaluated in an animal model to assess the correlation between *in vitro* and *in vivo* data. The long-term goal is to develop a structure-activity relationship model that could be used to predict the *in vivo* efficiency of the gene delivery nanoparticles based on structural information and physicochemical parameters.

The next step is to evaluate the delivery system in a diseased animal model such as scleroderma to assess clinical relevance. Optimization of the treatment regimen should be

conducted to assess optimal dose, dose frequency and duration of the treatments. Toxicological studies should also be performed to evaluate the safety of the delivery system.

The ex-vivo assessment of skin deposition and penetration behaviour conducted in my research provides basic evidence about the favorable deposition of gemini surfactants in skin tissues. However, tracking the fate and biodistribution of topically applied gemini surfactant-based gene delivery systems in animal models is essential before any translation into clinical applications. Correlating the tissue distribution and degradation profile of gemini surfactants to their chemical structure and physicochemical characteristics will provide insights into the rational design process to produce compounds with higher efficiency and reduced toxicity. This will benefit from the extraction protocols and the FIA-MS/MS methods developed in my work (Chapter 5).

6.4. Bibliography

1 Yin H, Kanasty RL, Eltoukhy AA, Vegas AJ, Dorkin JR, Anderson DG. Non-viral vectors for gene-based therapy. Nature Reviews Genetics 2014; 15: 541-55.

2 Rosenzweig HS, Rakhmanova VA, MacDonald RC. Diquaternary ammonium compounds as transfection agents. Bioconjugate chemistry 2001; 12: 258-63.

3 Wettig SD, Verrall RE, Foldvari M. Gemini surfactants: a new family of building blocks for non-viral gene delivery systems. Current gene therapy 2008; 8: 9-23.

4 Donkuru M, Wettig SD, Verrall RE, Badea I, Foldvari M. Designing pH-sensitive gemini nanoparticles for non-viral gene delivery into keratinocytes. Journal of Materials Chemistry 2012; 22: 6232-44.

5 Ahmed T, Kamel AO, Wettig SD. Interactions between DNA and Gemini surfactant: impact on gene therapy: part I. Nanomedicine 2016; 11: 289-306.

6 Badea I, Verrall R, Baca-Estrada M, Tikoo S, Rosenberg A, Kumar P, *et al*. In vivo cutaneous interferon-γ gene delivery using novel dicationic (gemini) surfactant–plasmid complexes. The journal of gene medicine 2005; 7: 1200-14.

7 Badea I, Wettig S, Verrall R, Foldvari M. Topical non-invasive gene delivery using gemini nanoparticles in interferon-γ-deficient mice. European journal of pharmaceutics and biopharmaceutics 2007; 65: 414-22.

8 Singh J, Michel D, Getson HM, Chitanda JM, Verrall RE, Badea I. Development of amino acid substituted gemini surfactant-based mucoadhesive gene delivery systems for potential use as noninvasive vaginal genetic vaccination. Nanomedicine 2015; 10: 405-17.

9 Alqawlaq S, Sivak JM, Huzil JT, Ivanova MV, Flanagan JG, Beazely MA, *et al*. Preclinical development and ocular biodistribution of gemini-DNA nanoparticles after intravitreal and topical administration: towards non-invasive glaucoma gene therapy. Nanomedicine: Nanotechnology, Biology and Medicine 2014; 10: 1637-47.

10 Badea I, Virtanen C, Verrall R, Rosenberg A, Foldvari M. Effect of topical interferon-γ gene therapy using gemini nanoparticles on pathophysiological markers of cutaneous scleroderma in Tsk/+ mice. Gene Therapy 2011; 19: 978-87.

11 Garcia MT, Kaczerewska O, Ribosa I, Brycki B, Materna P, Drgas M. Biodegradability and aquatic toxicity of quaternary ammonium-based gemini surfactants: Effect of the spacer on their ecological properties. Chemosphere 2016; 154: 155-60.

12 Gorell E, Nguyen N, Lane A, Siprashvili Z. Gene therapy for skin diseases. Cold Spring Harbor perspectives in medicine 2014; 4: a015149.

13 Badea I, Virtanen C, Verrall R, Rosenberg A, Foldvari M. Effect of topical interferon-γ gene therapy using gemini nanoparticles on pathophysiological markers of cutaneous scleroderma in Tsk/+ mice. Gene Therapy 2011; 19: 978-87.

14 Buse J, Badea I, Verrall RE, El-Aneed A. Tandem mass spectrometric analysis of the novel gemini surfactant nanoparticle families G12-s and G18: 1-s. Spectroscopy Letters 2010; 43: 447-57.

15 Buse J, Badea I, Verrall RE, El-Aneed A. A general liquid chromatography tandem mass spectrometry method for the quantitative determination of diquaternary ammonium gemini surfactant drug delivery agents in mouse keratinocytes' cellular lysate. Journal of Chromatography A 2013; 1294: 98-105.

16 Donkuru M, Chitanda JM, Verrall RE, El-Aneed A. Multi-stage tandem mass spectrometric analysis of novel β-cyclodextrin-substituted and novel bis-pyridinium gemini surfactants designed as nanomedical drug delivery agents. Rapid Communications in Mass Spectrometry 2014; 28: 757-72.

17 Donkuru M, Michel D, Awad H, Katselis G, El-Aneed A. Hydrophilic interaction liquid chromatography–tandem mass spectrometry quantitative method for the cellular analysis of varying structures of gemini surfactants designed as nanomaterial drug carriers. Journal of Chromatography A 2016; 1446: 114-24.

18 Yang P, Singh J, Wettig S, Foldvari M, Verrall RE, Badea I. Enhanced gene expression in epithelial cells transfected with amino acid-substituted gemini nanoparticles. European Journal of Pharmaceutics and Biopharmaceutics 2010; 75: 311-20.

19 Singh J, Yang P, Michel D, E Verrall R, Foldvari M, Badea I. Amino Acid-Substituted Gemini Surfactant-Based Nanoparticles as Safe and Versatile Gene Delivery Agents. Current Drug Delivery 2011; 8: 299-306.

20 Singh J, Michel D, Chitanda JM, Verrall RE, Badea I. Evaluation of cellular uptake and intracellular trafficking as determining factors of gene expression for amino acid-substituted gemini surfactant-based DNA nanoparticles. J Nanobiotechnology 2012; 10.

21 Matulis D, Rouzina I, Bloomfield VA. Thermodynamics of cationic lipid binding to DNA and DNA condensation: roles of electrostatics and hydrophobicity. Journal of the American Chemical Society 2002; 124: 7331-42.

22 Fröhlich E. The role of surface charge in cellular uptake and cytotoxicity of medical nanoparticles. International journal of nanomedicine 2012; 7: 5577.

23 Pinazo A, Petrizelli V, Bustelo M, Pons R, Vinardell M, Mitjans M, *et al*. New cationic vesicles prepared with double chain surfactants from arginine: Role of the hydrophobic group on the antimicrobial activity and cytotoxicity. Colloids and Surfaces B: Biointerfaces 2016; 141: 19-27.

24 Dauty E, Remy J-S, Blessing T, Behr J-P. Dimerizable cationic detergents with a low cmc condense plasmid DNA into nanometric particles and transfect cells in culture. Journal of the American Chemical Society 2001; 123: 9227-34.

25 Ramezani M, Khoshhamdam M, Dehshahri A, Malaekeh-Nikouei B. The influence of size, lipid composition and bilayer fluidity of cationic liposomes on the transfection efficiency of nanolipoplexes. Colloids and Surfaces B: Biointerfaces 2009; 72: 1-5.

26 Moghaddam B, McNeil SE, Zheng Q, Mohammed AR, Perrie Y. Exploring the correlation between lipid packaging in lipoplexes and their transfection efficacy. Pharmaceutics 2011; 3: 848-64.

27 Mohammed-Saeid W, Buse J, Badea I, Verrall R, El-Aneed A. Mass spectrometric analysis of amino acid/di-peptide modified gemini surfactants used as gene delivery agents: Establishment of a universal mass spectrometric fingerprint. International Journal of Mass Spectrometry 2012; 309: 182-91.

28 Buse J, Badea I, Verrall RE, El-Aneed A. Tandem mass spectrometric analysis of novel diquaternary ammonium gemini surfactants and their bromide adducts in electrospray-positive ion mode ionization. Journal of Mass Spectrometry 2011; 46: 1060-70.

29 Folch J, Lees M, Sloane Stanley G. A simple method for the isolation and purification of total lipids from animal tissues. J biol Chem 1957; 226: 497-509.

30 Bligh EG, Dyer WJ. A rapid method of total lipid extraction and purification. Canadian journal of biochemistry and physiology 1959; 37: 911-7.

31 Retra K, Bleijerveld OB, van Gestel RA, Tielens AG, van Hellemond JJ, Brouwers JF. A simple and universal method for the separation and identification of phospholipid molecular species. Rapid Communications in Mass Spectrometry 2008; 22: 1853-62.

32 Yatomi Y, Ohmori T, Rile G, Kazama F, Okamoto H, Sano T, *et al*. Sphingosine 1-phosphate as a major bioactive lysophospholipid that is released from platelets and interacts with endothelial cells. Blood 2000; 96: 3431-8.

33 Matyash V, Liebisch G, Kurzchalia TV, Shevchenko A, Schwudke D. Lipid extraction by methyl-tert-butyl ether for high-throughput lipidomics. Journal of lipid research 2008; 49: 1137-46.

34 Solvent Polarity Index, <http://macro.lsu.edu/HowTo/solvents/Polarity%20index.htm> Accessed January 2018.

35 Tan A, Awaiye K, Trabelsi F. Some unnecessary or inadequate common practices in regulated LC–MS bioanalysis. Bioanalysis 2014; 6: 2751-65.

APPENDICES

Appendix I

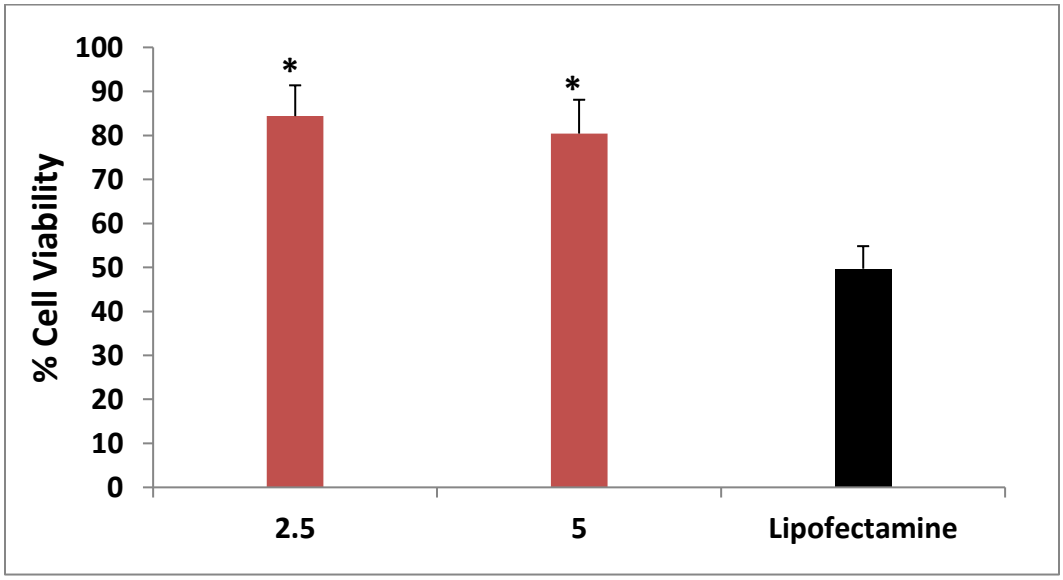

Figure S1. Evaluation of COS-7 cell viability of P/G/Ls formulated with 16-7N(G-K)-16 at N/P ratios of 2.5 and 5 using MTT assay after 48 h of treatment compared to commercial transfection agent (lipofectamine). Results are the average of three plates of quadruplicate wells, error bars represent standard deviation. * Indicates significant at $p < 0.05$.

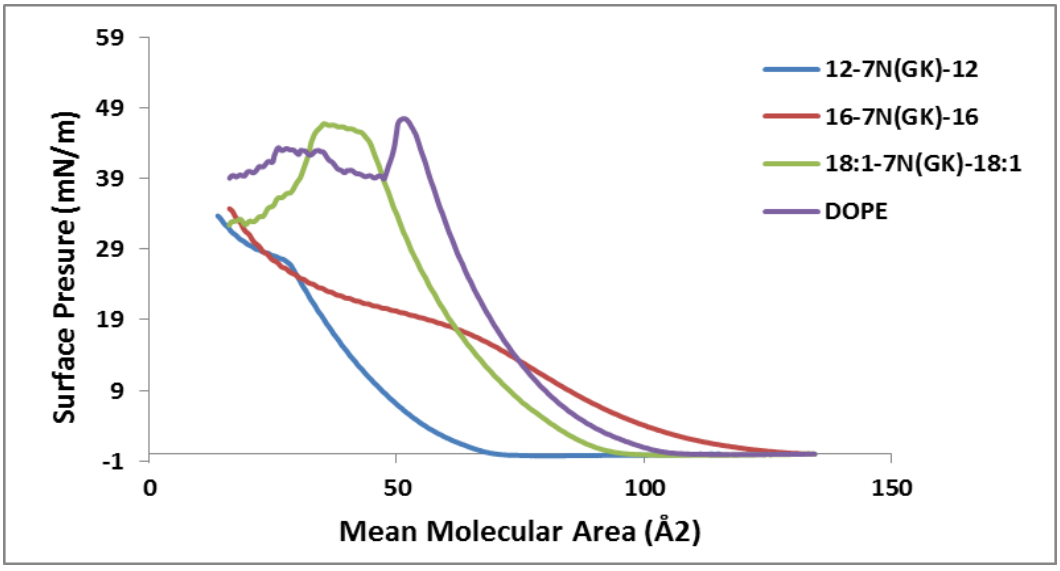

Figure S2. Pressure-area isotherms of the gemini surfactants and DOPE at 22°C, pH= 6.6.

Table SI. Scattering peak position and the corresponding a spacing for nanoparticles containing DNA/ gemini surfactants/ DOPE, where gemini were either 12-7N(G-K)-12 or 16-7N(G-K)-16 or 18:1-7N(G-K)-18:1 at six N/P ratios each.

Gemini type	N/P Ratio	q10 (Å $^{-1}$)	q11 (Å $^{-1}$)	q20 (Å $^{-1}$)	a (Å)
12-7N(G-K)-12	1	0.102	0.177	0.204	71.130
	2.5	0.101	0.174	0.200	71.833
	5	0.097	0.167	0.192	74.795
	10	0.101			NA
	15	0.100			NA
	20	0.099			NA
16-7N(G-K)-16	1	0.103	0.179	0.205	70.438
	2.5	0.102	0.177	0.203	71.129
	5	0.098	0.167	0.193	74.032
	10	0.100			NA
	15	0.099			NA
	20	0.099			NA
18:1-7N(G-K)-18:1	1	0.104	0.180	0.208	69.761
	2.5	0.102	0.177	0.205	71.129
	5	0.100	0.174	0.201	72.551
	10	0.098	0.169	0.194	74.03
	15	0.097	0.168	0.194	74.795
	20	0.097	0.167	0.193	74.795

Appendix II

Table S1: Scattering peak position and the corresponding a spacing for P/L/G lipoplexes at three N/P ratios.

Gemini type	N/P Ratio	q10 (Å $^{-1}$)	q11 (Å $^{-1}$)	q20 (Å $^{-1}$)	a (Å)
16-7N(G-K)-16	2.5	0.100	0.174	0.201	72.552
	5	0.098	0.169	0.205	74.033
	10	0.101			
16-7N(G-K$_3$)-16	2.5	0.099	0.171	0.199	73.285
	5	0.102			
	10	0.103			
16-7N(G-K$_7$)-16	2.5	0.100	0.173	0.200	72.552
	5	0.103			
	10	0.103			
16-7N(G-C$_6$-K)-16	2.5	0.102	0.177	0.204	71.130
	5	0.100	0.172	0.199	72.552
	10	0.100			
16-7N(G-C$_{11}$-K)-16	2.5	0.099	0.172	0.199	73.285
	5	0.097			
	10	0.098			
16-7N(G-C$_6$-K$_3$)-16	2.5	0.100	0.173	0.200	72.552
	5	0.100	0.172	0.199	72.552
	10	0.099			
16-7N(G-C$_{11}$-K$_3$)-16	2.5	0.100	0.172	0.199	72.552
	5	0.102			
	10	0.103			
16-7N(C$_6$-K$_3$)-16	2.5	0.101	0.174	0.201	71.834
	5	0.100	0.176	0.199	72.552
	10	0.101			
16-7N(C$_{11}$-K$_3$)-16	2.5	0.100	0.173	0.200	72.552
	5	0.100	0.172	0.199	72.552
	10	0.098			
16-7N(C$_6$-K$_7$)-16	2.5	0.101	0.176	0.204	71.834
	5	0.101			
	10	0.100			
16-7N(C$_{11}$-K$_7$)-16	2.5	0.101	0.175	0.203	71.834
	5	0.101	0.176	0.202	71.834
	10	0.102			

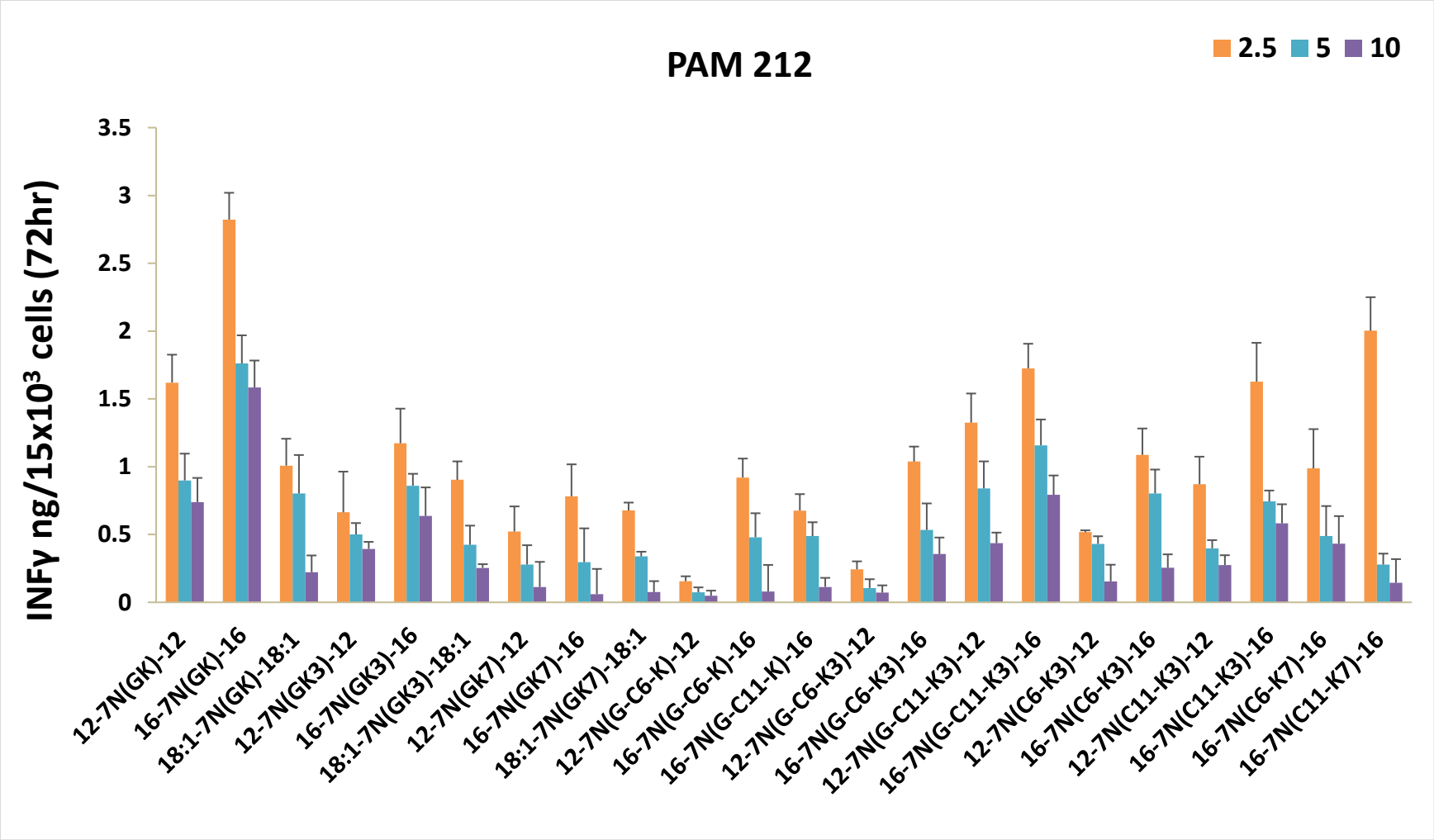

Figure S1: *In vitro* transfection of PAM 212 cells comparing the level of IFN-γ expression of the peptide-modified gemini surfactants after 72 h of treatment. Results are the average of three plates of quadruplicate wells, error bars represent standard deviation.

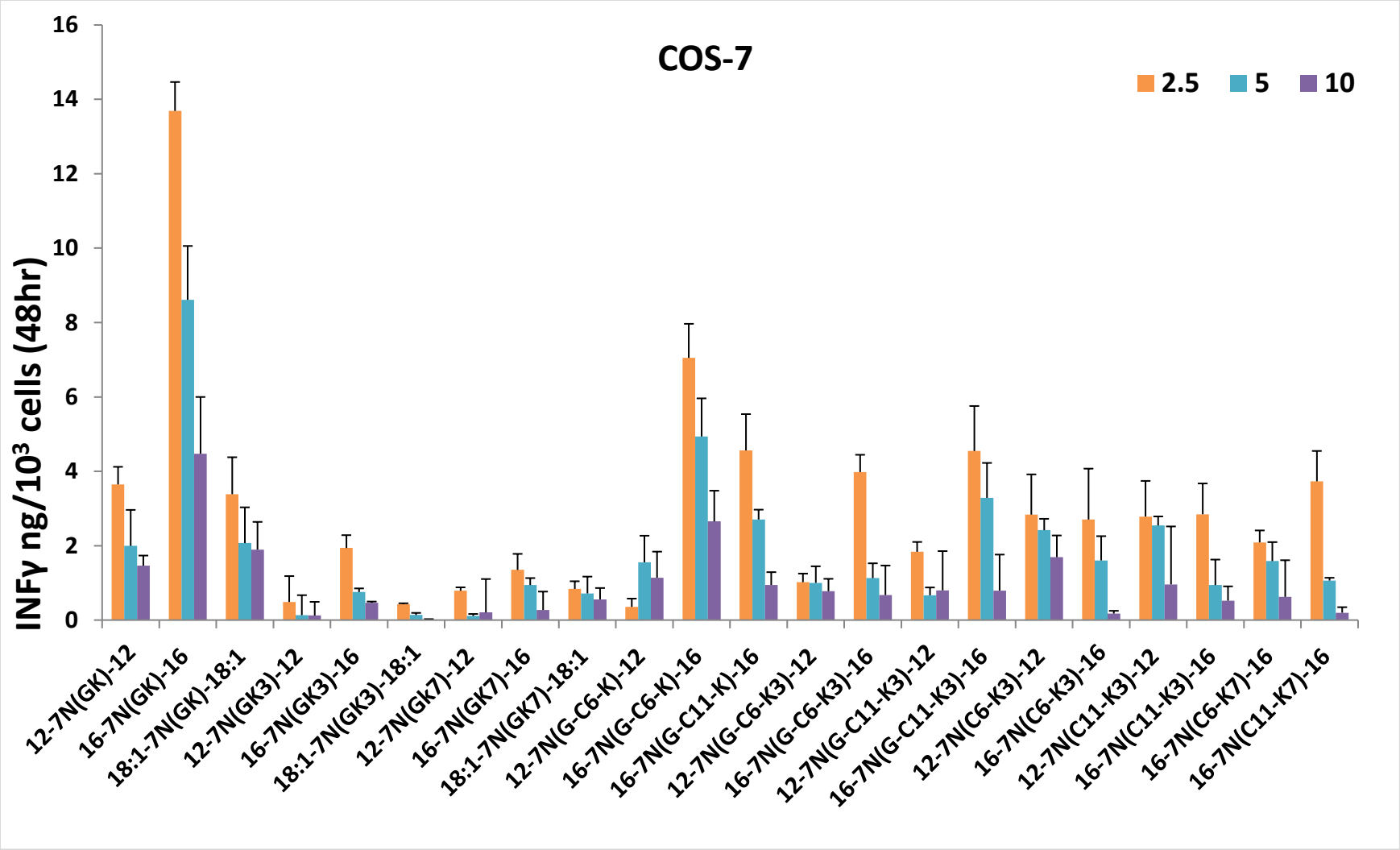

Figure S2: *In vitro* transfection of COS-7 cells comparing the level of IFN-γ expression of the three gemini surfactants after 48 h of treatment. Results are the average of three plates of quadruplicate wells, error bars represent standard deviation.

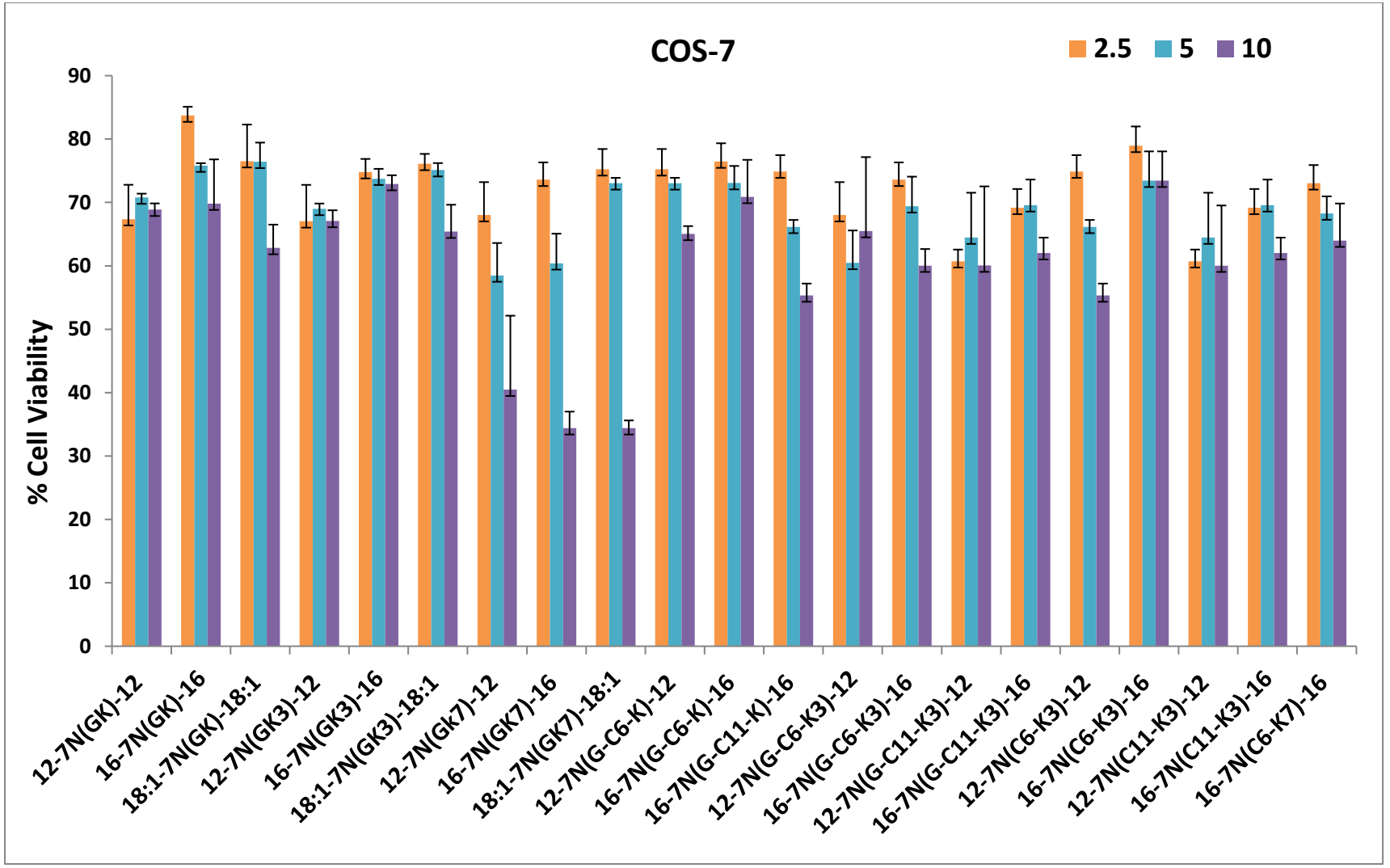

Figure S3: Evaluation of COS-7 cell viability at three different N/P ratios of the tested gemini surfactants using MTT assay after 48 h of treatment. Results are the average of three plates of quadruplicate wells, error bars represent standard deviation.

Appendix III

Table S1. Mass accuracies of the triply charged ions $[M+H]^{3+}$ obtained during single stage ESI-QqToF-MS.

Gemini surfactants	Molecular formula	Theoretical, *m/z*	Observed, *m/z*	Mass accuracy (ppm)
12-7N(G-C_{11}-K_3)-12	$C_{65}H_{136}N_{11}O_5$	383.6903	383.6895	2.124
16-7N(G-C_{11}-K_3)-16	$C_{73}H_{152}N_{11}O_5$	421.0653	421.0633	4.945
16-7N(G-C_{11}-K)-16	$C_{61}H_{128}N_7O_3$	335.6687	335.6693	1.668
12-7N(G-C_6-K_3)-12	$C_{60}H_{126}N_{11}O_5$	360.3308	360.3344	5.555
16-7N(G-C_6-K_3)-16	$C_{68}H_{142}N_{11}O_5$	397.7059	397.7076	4.11
12-7N(G-C_6-K)-12	$C_{48}H_{101}N_7O_3$	274.9342	274.9356	4.887
16-7N(G-C_6-K)-16	$C_{56}H_{118}N_7O_3$	312.3093	312.3098	1.526
12-7N(C_{11}-K_3)-12	$C_{63}H_{133}N_{10}O_4$	364.6831	364.6828	0.988
16-7N(C_{11}-K_3)-16	$C_{71}H_{149}N_{10}O_4$	402.0582	402.0593	2.667
12-7N(C_6-K_3)-12	$C_{58}H_{123}N_{10}O_4$	341.3237	341.3257	5.73
16-7N(C_6-K_3)-16	$C_{66}H_{139}N_{10}O_4$	378.6988	378.7015	7.101

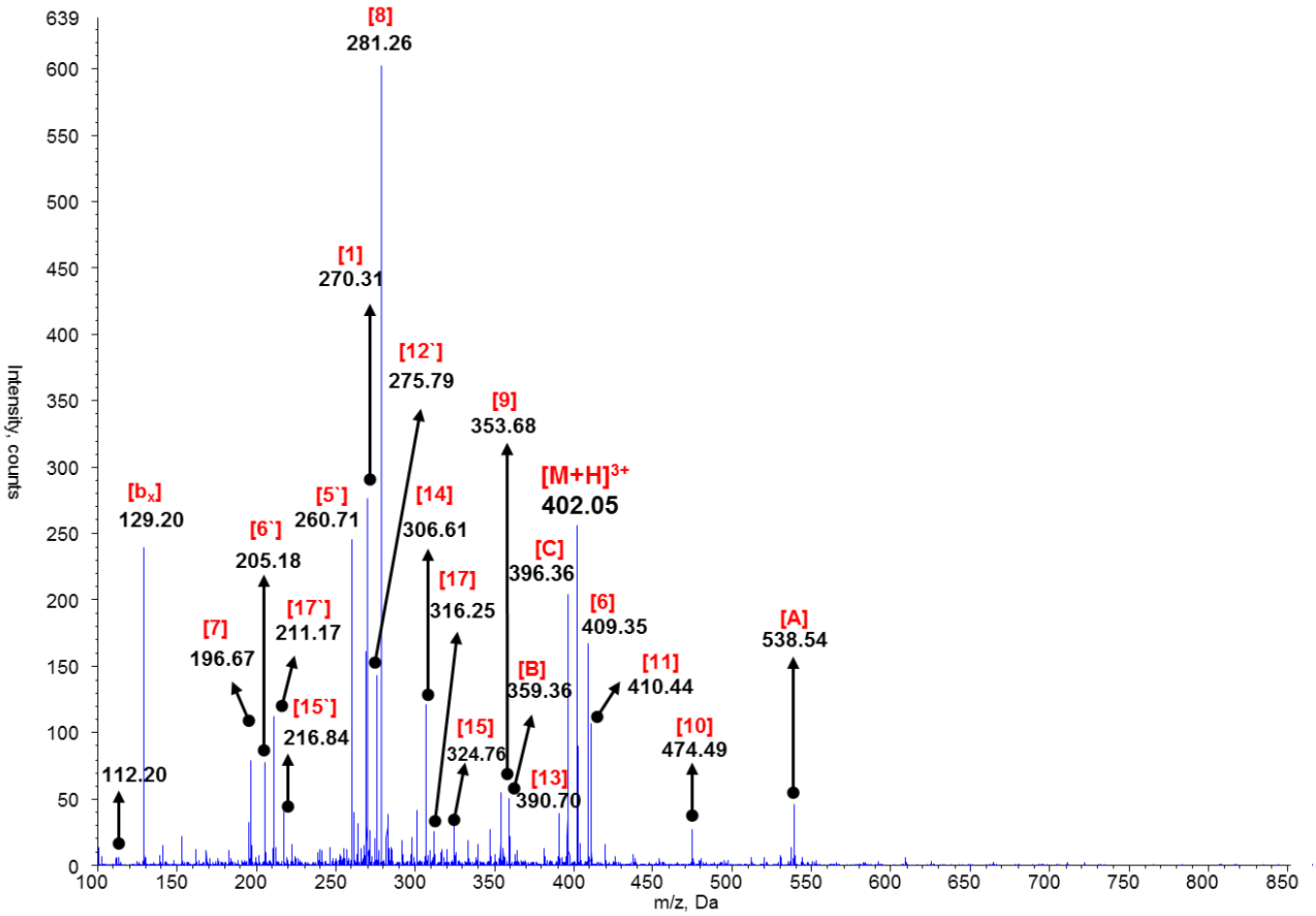

Figure S1. The ESI-QqToF MS/MS spectrum of 16-7N(C_{11}-K_3)-16 as a representative example of gemini surfactants with tri-terminal lysine moieties. Ions were labelled as designated in Figures 5-7.

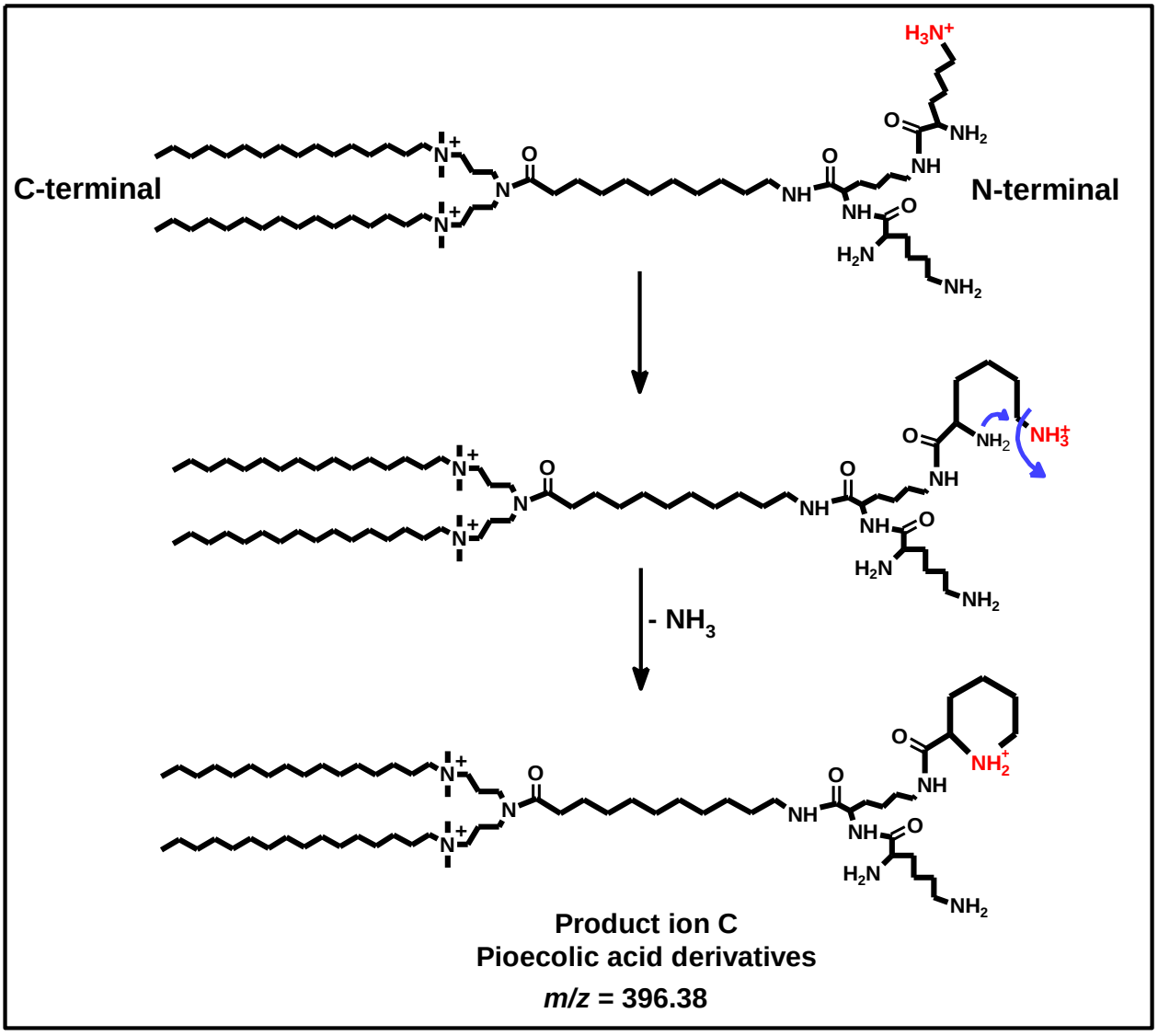

Figure S2. The proposed mechanism for the formation of product ion (C): loss of ammonia group from the lysine side chain.

Table S2. Summary of MS^3 analysis for 16-7N(C_{11}-K_3)-16 gemini surfactants.

Precursor ion	MS/MS product ions	Ms^3 product ions
402.05	538.54 [A]	806.76 [2], 403.88 [2`], 270.31 [1], 537.44 [3], 269.23 [3`], 129.10 [b_1], 678.66 [4], 339.83 [4`], 520.42 [5], 260.71 [5`], 409.35 [6], 205.18 [6`], 196.67 [7], 281.26 [8]
	359.36 [B]	353.68 [9], 474.49 [10], 129.10 [b_1], 678.66 [4], 339.83 [4`], 270.31 [1], 410.44 [11], 550.57 [12], 275.79 [12`], 281.26 [8] , 270.31 [1]
	396.38 [C]	538.54 [A], 359.36 [B], 390.70 [13], 306.61 [14], 216.84 [15`], 324.76 [15], 300.94 [16], 316.25 [17], 211.17 [17`], 353.68 [9], 530.02 [9`], 789.73 [18], 395.37 [18`], 263.91 [18``], 474.49 [10], 537.44 [3], 269.23 [3`], 520.42 [5], 260.71 [5`], 270.31 [1], 129.10 [b_1]
	129.10 [b_1]	
	270.31 [1]	
	806.76 [2]	537.44 [3], 678.66 [4], 129.10 [b_1], 270.31 [1], 520.42 [5], 409.35 [6], 281.26 [8]
	403.88 [2`]	537.44 [3], 269.23 [3`],129.10 [$b_1$], 678.66 [4], 339.83 [4`], 270.31 [1], 520.42 [5], 260.71 [5`], 409.35 [6], 205.18 [6`], 196.67 [7], 281.26 [8]
	537.44 [3]	520.42 [5], 409.35 [6], 281.26 [8]
	269.23 [3`]	260.71 [5`], 409.35 [6], 205.18 [6`], 196.67 [7], 281.26 [8], 129.10 [b_1]
	678.66 [4]	409.35 [6], 281.26 [8], 129.10 [b_1], 270.31 [1]
	339.83 [4`]	409.35 [6], 205.18 [6`], 196.67 [7], 281.26 [8], 129.10 [b_1], 270.31 [1]
	520.42 [5]	409.35 [6], 281.26 [8]
	260.71 [5`]	409.35 [6], 205.18 [6`], 196.67 [7], 281.26 [8], 129.10 [b_1]
	409.35 [6]	281.26 [8]
	205.18 [6`]	196.67 [7], 281.26 [8], 129.10 [b_1]
	196.67 [7]	281.26 [8]
	281.26 [8]	
	353.68 [9]	474.49 [10], 678.66 [4], 339.83 [4`], 474.49 [10], 409.35 [6], 205.18 [6`], 129.10 [b_1], 270.31 [1], 196.67 [7], 281.26 [8], 395.37 [18`], 263.91 [18``], 520.42 [5], 260.71 [5`]
	530.02 [9`]	789.73 [18], 395.37 [18`], 520.42 [5], 260.71 [5`], 409.35 [6], 205.18 [6`], 196.67 [7], 281.26 [8]
	474.49 [10]	678.66 [4], 339.83 [4`], 270.31 [1], 410.44 [11] , 409.35 [6], 205.18 [6`], 129.10 [b_1], 550.57 [12], 275.79 [12`], 281.26 [8]

	410.44 [11]	550.57 [12], 275.79 [12`], 270.31 [1], 281.26 [8]
	550.57 [12]	281.26 [8]
	275.79 [12`]	281.26 [8]
	390.70 [13]	300.94 [16], 316.25 [17], 211.17 [17`], 353.68 [9], 530.02 [9`], 789.73 [18], 395.37 [18`], 263.91 [18``], 474.49 [10], 520.42 [5], 260.71 [5`], 409.35 [6], 205.18 [6`], 196.67 [7], 281.26 [8], 129.10 [b_1], 270.31 [1]
	306.61 [14]	216.84 [15`], 324.76 [15], 300.94 [16], 316.25 [17], 211.17 [17`], 395.37 [18`], 263.91 [18``], 520.42 [5], 260.71 [5`], 537.44 [3], 269.23 [3`],129.10 [b_1], 270.31 [1]
	324.76 [15]	316.25 [17], 537.44 [3], 520.42 [5], 409.35 [6], 281.26 [8] ,129.10 [b_1]
	216.84 [15`]	211.17 [17`],269.23 [3`], 260.71 [5`], 129.10 [b_1]
	300.94 [16]	395.37 [18`], 263.91 [18``], 520.42 [5], 260.71 [5`], 409.35 [6], 205.18 [6`], 196.67 [7], 281.26 [8], 129.10 [b_1], 270.31 [1]
	316.25 [17]	520.42 [5], 409.35 [6], 281.26 [8]
	211.17 [17`]	260.71 [5`], 409.35 [6], 205.18 [6`], 196.67 [7], 281.26 [8], 129.10 [b_1]
	789.73 [18]	520.42 [5], 409.35 [6], 281.26 [8],
	395.37 [18`]	520.42 [5], 260.71 [5`], 409.35 [6], 205.18 [6`], 196.67 [7], 281.26 [8], 129.10 [b_1]
	263.91 [18``]	260.71 [5`], 205.18 [6`], 196.67 [7], 281.26 [8], 129.10 [b_1]

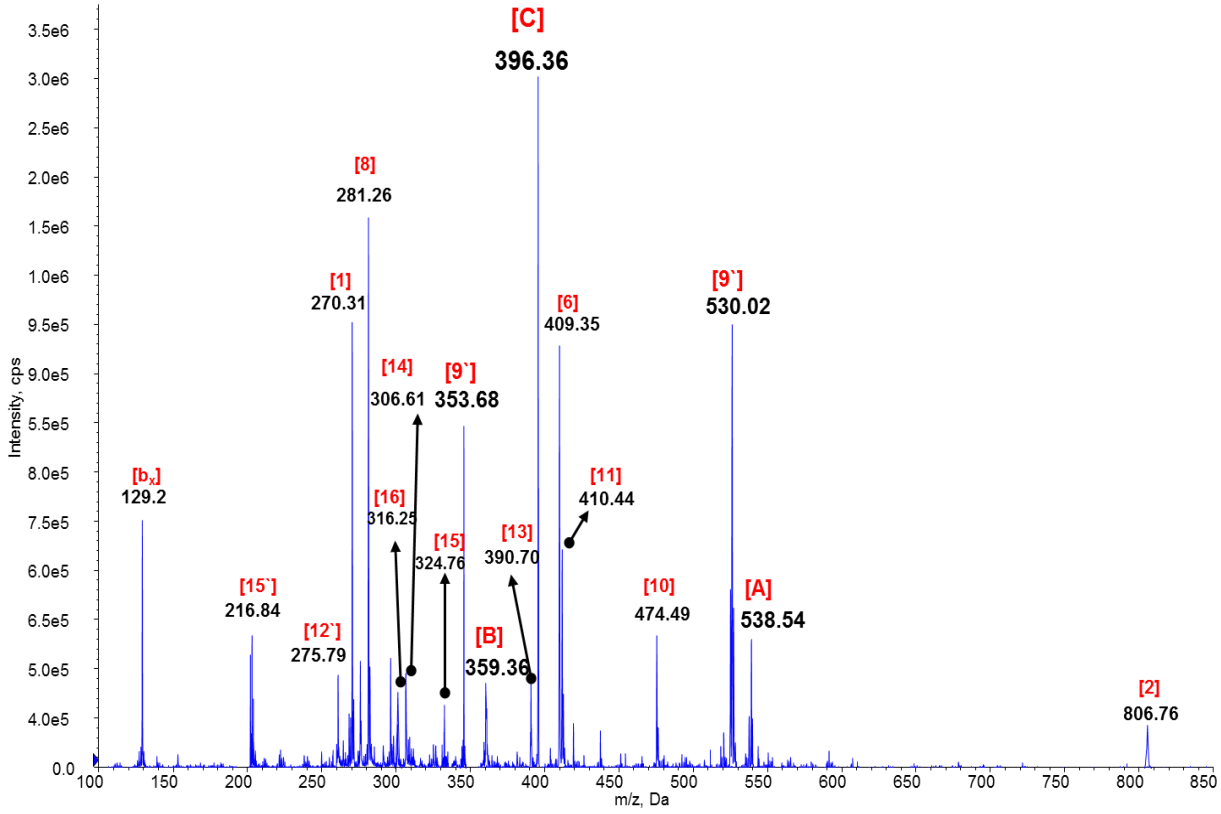

Figure S3. The ESI-QqLIT-MS^3 spectrum of product ion (C) at *m/z* 396.38 of 16-7N(C11-K3)-16 gemini surfactant. Ions were labelled as designated in Figures 7.

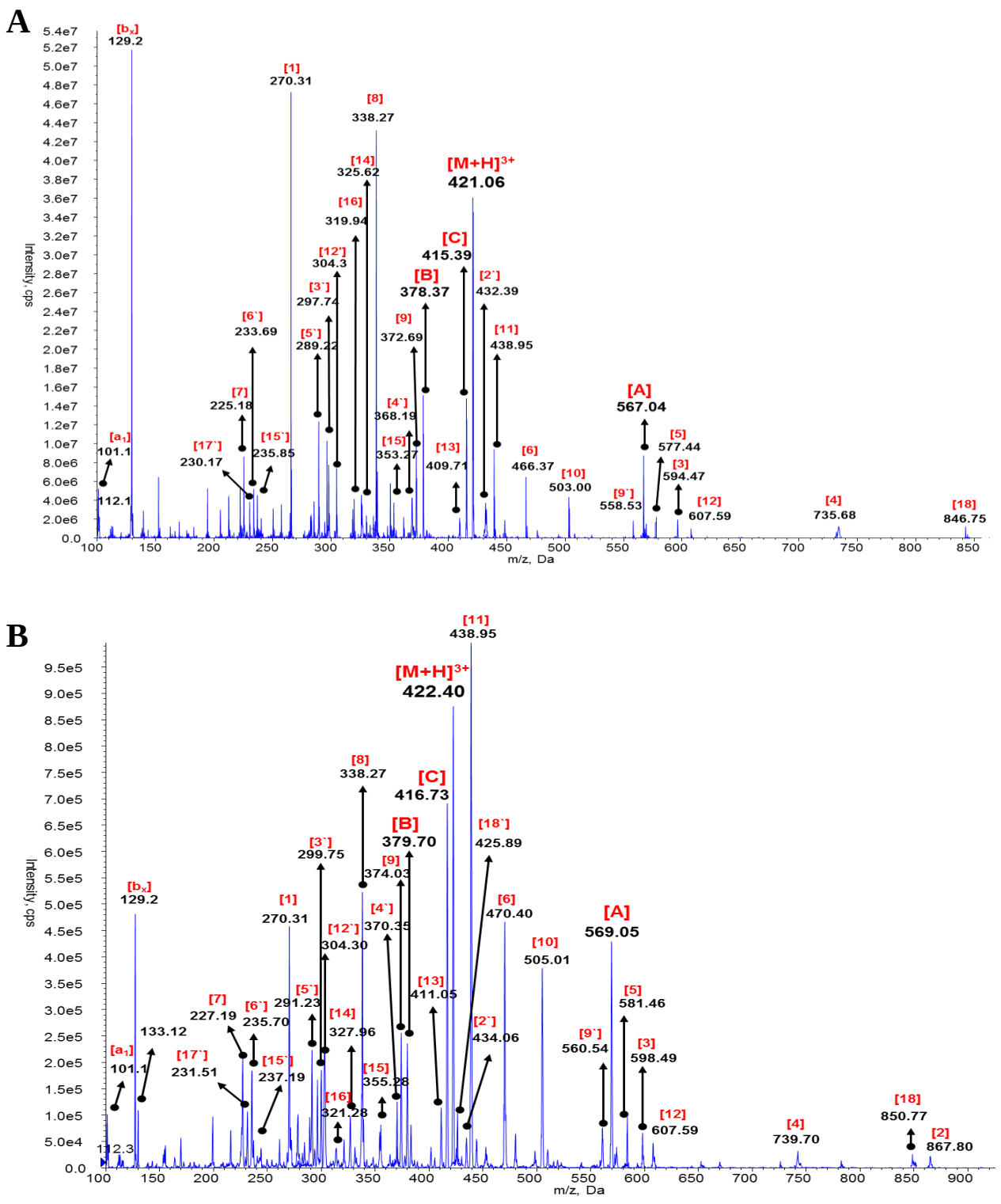

Figure S4. The ESI-QqLIT-MS/MS spectrum of (A) 16-7N(G-C_{11}-K_3)-16 and (B) its deuterated version 16-7N(G-C_{11}-K_D-K_2)-16 showing the similarities in the fragmentation patterns. Ions were labelled as designated in Figures 5-7.

Appendix IV

Table S1. Equivalent analytes final mass concentrations in the single point calibration standards.

	Calibration standard final mass concentration	
Gemini surfactant	**Methods A's (µg/mL)**	**Methods B's (ng/mL)**
16-7N(G-K)-16	3.86	580.34
16-7N(G-C_6-K_3)-16	2.81	422.90
16-7N(G-C_{11}-K_3)-16	5.91	887.87
16-7N(G-K_{d4})-16	1.94	388.47
16-7N(G-C_6-K_{d4}-K_2)-16	1.4137	282.73
16-7N(G-C_{11}-K_{d4}-K_2)-16	2.9676	593.52

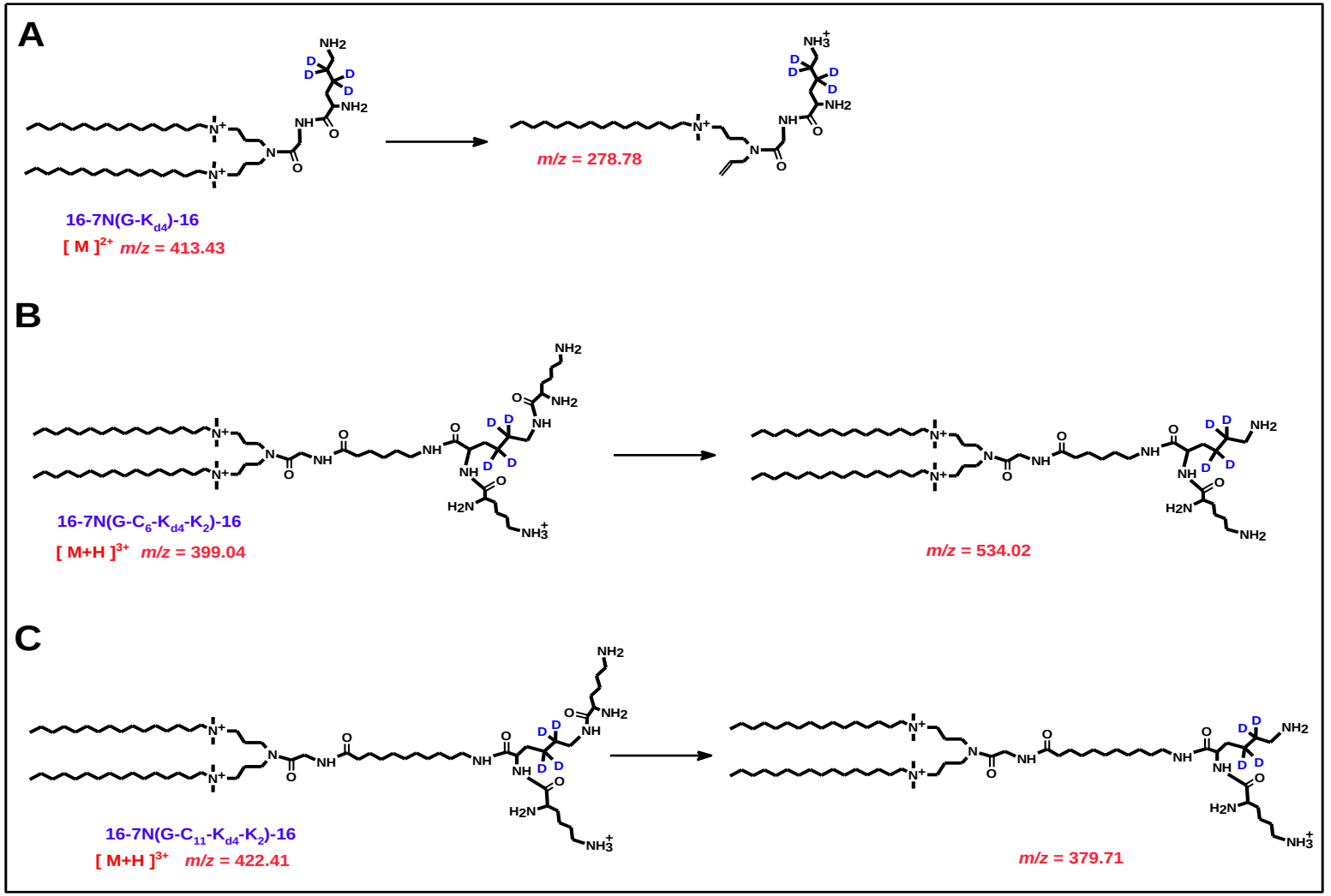

Figure S1. Chemical structure of the internal standards' precursor ion and the monitored product ion of 16-7N(G-K_{d4})-16 (A), 16-7N(G-C_6-K_{d4}-K_3)-16 (B) and 16-7N(G-C_{11}-K_{d4}-K_3)-16.